

The effect of Hydrogen Sulphide on TNF- α -induced Endothelial Dysfunction.

Lorena Diaz Sanchez

Doctor of Philosophy

Aston University

September 2022

© Lorena Diaz Sanchez, 2022

Lorena Diaz Sanchez, 2022 asserts her moral right to be identified as the author of this thesis.

This copy of the thesis has been supplied on condition that anyone who consults it is understood to recognise that its copyright rests with its author and that no quotation from the thesis and no information derived from it may be published without proper acknowledgement.

Aston University

THE EFFECT OF HYDROGEN SULPHIDE ON TNF- α -INDUCED ENDOTHELIAL
DYSFUNCTION

Lorena Diaz Sanchez

Doctor of Philosophy

September 2022

Thesis Summary

Cardiovascular disease is the leading cause of morbidity and mortality globally. Endothelial dysfunction (ED) is implicated in the development and aggravation of cardiovascular complications. There is growing interest in understanding the pathophysiological mechanisms underlying ED and identifying therapeutic strategies that may prevent or reduce the risk of vascular complications and associated diseases. Hydrogen sulphide (H₂S) is an endogenous gasotransmitter that can act as an essential biological mediator. In the vasculature, H₂S can mediate beneficial effects through anti-inflammatory and redox-modulating regulatory mechanisms. Reduced H₂S bioavailability is reported in chronic diseases such as atherosclerosis, diabetes, hypertension and preeclampsia, suggesting the possible value of investigating H₂S as a therapeutic strategy for vascular-related conditions.

The study aimed to examine the cytoprotective roles of H₂S against TNF- α -mediated ED. Human umbilical vein endothelial cells (HUVECs) were stimulated with TNF- α (1 ng/ml) followed by a slow H₂S-releasing donor, GYY4137, post-treatment (100 μ M). TNF- α proved to be an efficient agent enabling ED as evidence enhanced oxidising redox state, inflammation and apoptosis via mitochondrial-dependent downstream signalling pathway. Confocal microscopy and gene-transcriptional expression analysis revealed that TNF- α affects mitochondrial dynamics, characterised as well by fragmentation of the organelle. GYY4137 post-treatment balances the redox state that alleviates endothelial inflammation, mitochondrial dysfunction, and pro-apoptotic signalling. In addition, GYY4137 enhanced protein S-sulphydration of Keap1 and caspase 3, stimulating Nrf2-downstream response and inhibiting caspase 3/7 activity, respectively.

In conclusion, the findings of this research contribute to expanding the understanding of the overall role H₂S underlying mechanisms and indicate that the slow-releasing H₂S donor may have putative therapeutic applications in inflammation-associated ED.

Key words: Endothelial dysfunction, hydrogen sulphide, mitochondria, S-sulphydration.

Acknowledgements

This thesis is dedicated to my family, my love and friends, whose unconditional love and encouragement allowed me to complete this journey.

I would first and foremost like to thank my supervisor, Dr Irundika Dias, for initially providing the opportunity to do a PhD, for her guidance through the PhD journey, for her patience with me and for the valuable amount of knowledge and advice imparted that has enabled me to grow as a more confident researcher. Thank you to Dr. Corinne M Spickett, Dr Keqing Wang and Dr. Helen R Griffiths for their support and guidance in encouraging me to overcome my insecurities.

To my parents, Noraida, Pablo and Carlos; and to my siblings, Lena and Marcell, who have been a constant source of motivation and support during the difficult and desolation moments. These past years would have been impossible without all of you in my life. I am forever thankful. A special thank you to the light of my eyes, Dr Adam Lynes, who has grown during this journey to my side, making my life happier. Thank you for your humour, support and love. I would also like to point out the wonderful people who have cared for me since day one, Kay, Peter, Sophie and Brenda.

The time spent with the group has helped me become more comfortable taking responsibility and trying new approaches. I have met wonderful people during my PhD and wish them all the best in their futures. A special thank you to Sophie, Lissette, Hala, Re Ea Tay, Mandeep, Yolanda, Milda and May for listening when I complained about life and helping to believe in myself as a scientific researcher. Unfortunately, there is not enough coffee in the world to compensate for all the hours you have to listen to me.

Finally, I would like to thank my old and new friends, who, although they have not been with me in the laboratory, have given me extraordinary moments full of laughter and love. A special thank you to Patri, Angela, Beatriz, Marta, Patricia EG, Carmen, Natalia, Sara, Patricia ZG, Fatima, Irene, Leticia, Karla and Daniel. All of you already know, but still, you are just the light in the darkness. Thank you.

Table of Contents

1	General Introduction.....	21
1.1	The Cardiovascular System	22
1.1.1	Blood Vessel Anatomy	22
1.2	The Vascular Endothelium	23
1.2.1	The endothelium functions	25
1.3	Endothelial Dysfunction.....	27
1.3.1	Redox Biology and Endothelial dysfunction.....	28
1.3.2	Inflammation and Endothelial dysfunction	37
1.3.3	Apoptosis and Endothelial dysfunction.....	38
1.3.4	Assessment and prevention of Endothelial dysfunction	40
1.4	Gasotransmitters.....	42
1.4.1	Nitric Oxide	43
1.4.2	Carbon monoxide.....	44
1.5	Hydrogen sulphide	45
1.5.1	Physiochemical properties of H ₂ S	45
1.5.2	Methods for H ₂ S measurement	46
1.5.3	Endogenous Synthesis and Oxidation of H ₂ S.....	49
1.5.4	Biogenesis of H ₂ S	50
1.5.5	Oxidation of H ₂ S.....	52
1.6	H ₂ S Donors and Inhibitors	54
1.6.1	Natural Donors.....	55
1.6.2	Sulfide Salts	55
1.6.3	Synthetic H ₂ S donors	56
1.6.4	Other H ₂ S donors.....	58
1.6.5	Inhibitors of H ₂ S	59

1.7	Physiological Effects of H ₂ S	59
1.7.1	H ₂ S and metal centres interaction	59
1.7.2	Interaction of H ₂ S with oxidants.....	60
1.8	Protein S-Sulfhydration	60
1.9	Properties of Sulfhydration	61
1.10	Involvement of H ₂ S in vascular diseases.....	63
1.11	Research Hypothesis and Aims	66
2	Materials and Methods	67
2.1	Materials	68
2.2	Cell Culture	68
2.2.1	Cell Lines	68
2.2.2	Cell culture media and solutions.....	68
2.2.3	Cell culture maintenance.....	70
2.2.4	Cell counting	70
2.2.5	Freezing the cells.....	71
2.2.6	Thawing the cells	71
2.2.7	Cell Treatment settings	72
2.2.8	Cell culture experimental settings.....	72
2.3	Metabolic capacity assay	74
2.4	In situ cellular H ₂ S measurement	74
2.5	Assessment of ROS formation	75
2.5.1	Detection of Hydrogen peroxide production.....	75
2.5.2	Detection of mitochondrial superoxide production	76
2.6	Flow Cytometry analysis	76
2.6.1	Assessment of cell adhesion molecules expression.....	77
2.6.2	Assessment of apoptosis using Annexin V-PI	78

2.7	Caspase 3/7 activity assay	80
2.8	GSH: GSSG ratio assay	81
2.9	Immunofluorescence microscopy	81
2.9.1	Endothelial phenotype fluorescent microscopy.....	82
2.9.2	Cellular localisation of Nrf2.....	82
2.9.3	Mitochondrial network fluorescence analysis.....	83
2.9.4	Phalloidin F-actin staining	84
2.10	Senescence (SA- β -gal) staining	85
2.11	ELISA assay	86
2.12	Tube formation assay.....	86
2.13	Isolation of Nuclear and Cytoplasmic protein fractions	87
2.14	Characterisation of Mitochondrial $\Delta\psi_m$	88
2.15	Characterisation of Bioenergetic profile	88
2.15.1	Seahorse Mito Stress test	88
2.15.2	Seahorse Glycolytic Test assay	91
2.16	Bradford assay	94
2.17	Western Blot analysis.....	94
2.17.1	Protein extraction	94
2.17.2	BCA protein quantification.....	95
2.17.3	Sample preparation and gel electrophoresis	95
2.17.4	Protein transfer to the membrane [Semi-dry transfer].....	96
2.17.5	Blocking of membrane	97
2.17.6	Primary and Secondary antibodies.....	97
2.17.7	Detection of proteins	98
2.18	Total RNA extraction and RT- qPCR analysis	98
2.18.1	RNA extraction and quantification	98

2.18.2	Reverse transcription	99
2.18.3	Real-time PCR	99
2.18.4	Quantification (Relative quantification method)	101
2.18.5	Primers	102
2.19	Maleimide Red assay	103
2.20	Modified Biotin Switch assay	104
2.20.1	Experimental design conditions:.....	104
2.20.2	Biotin Switch protocol.....	105
2.21	Statistical Analysis	109
3	Assessment of endothelial in vitro model using TNF- α and GYY4137 compounds	110
3.1	Introduction	111
3.2	Aims.....	113
3.3	Materials and Methods	113
3.3.1	Endothelial cell culture	113
3.3.2	Fluorescence microscopy.....	114
3.3.3	ELISA.....	114
3.3.4	RT-qPCR	114
3.3.5	Flow cytometry	114
3.3.6	Statistical Analysis	114
3.4	Results.....	116
3.4.1	Characterisation of EA.hy926 cells as <i>in vitro</i> endothelial model.....	116
3.4.2	Titration of the optimum GYY4137 dose and assessing intracellular H ₂ S content in EA.hy926 cells.	117
3.4.3	Characterisation of TNF- α as an agent to alter endothelial functions in EA.hy926 cells.	119
3.4.4	Establishing an in vitro experimental model using TNF- α and GYY4137 compounds in EA.hy926 cells.	120

3.4.5	Assessment of the optimum and non-toxic dose of GYY4137 for HUVECs.	124
3.4.6	Establishing TNF- α as an agent to induce endothelial activation in HUVECs.....	127
3.5	Discussion.....	130
4	Investigation of the effect of H ₂ S on TNF- α -induced ED	135
4.1	Introduction	136
4.2	Aims.....	138
4.3	Materials and Methods.....	138
4.3.1	Endothelial cell culture.	138
4.3.2	Fluorescence microscopy.....	138
4.3.3	RT-qPCR	139
4.3.4	Flow cytometry.....	139
4.3.5	Western blot.....	139
4.3.6	ELISA.....	139
4.3.7	GSH: GSSG ratio assay.....	139
4.3.8	Statistical analysis.....	140
4.4	Results.....	141
4.4.1	Intracellular H ₂ O ₂ content in TNF- α -treated HUVECs with GYY4137 post-treatment.....	141
4.4.2	Antioxidant effect of GYY4137 post-treatment in TNF- α -treated HUVECs.	143
4.4.3	Thioredoxin and GSH systems in TNF- α and GYY4137 post-treated HUVECs.....	144
4.4.4	Assessing modulatory effects of TNF- α and GYY4137 on cell adhesion molecules surface expression.	146
4.4.5	Monitoring inflammation and apoptosis in HUVECs subjected to TNF- α and GYY4137 post-treatment.....	151
4.5	Discussion.....	154
5	Assessment of the effect of H ₂ S and TNF- α in mitochondria	159

5.1	Introduction	160
5.2	Aims.....	163
5.3	Materials and Methods.....	163
5.3.1	Endothelial cell culture.....	163
5.3.2	Fluorescence microscopy.....	164
5.3.3	RT-QPCR	164
5.3.4	Extracellular Flux analyser (Seahorse technology).....	164
5.3.5	Western blot.....	164
5.4	Statistical analysis.....	164
5.5	Results.....	166
5.5.1	Evaluation of the mitochondrial-mediated redox state in TNF- α and GYY4137 post-treated cells.....	166
5.5.2	Analysis of mitochondrial bioenergetics in HUVECs.....	168
5.5.3	Analysis of glycolysis in HUVECs.....	172
5.5.4	Uncoupling proteins in TNF- α and GYY4137-treated HUVECs.	174
5.5.5	Analysis of $\Delta\psi_m$ in HUVECs.....	176
5.5.6	Mitochondrial morphology and dynamic machinery in HUVECs.	178
5.5.7	Regulation of TNF- α and GYY4137 on apoptotic-related proteins in HUVECs.....	181
5.6	Discussion.....	183
6	Preliminary assessment and quantification of protein S-sulfhydration in HUVECs 192	
6.1	Introduction	193
6.2	Aims.....	197
6.3	Material and Methods.....	197
6.3.1	Endothelial cell culture	197
6.3.2	Maleimide Red assay.....	198
6.3.3	Modified Biotin switch assay	198

6.3.4	Fluorescence microscopy.....	198
6.3.5	Western blot.....	198
6.3.6	Caspase 3/7 activity assay.....	198
6.3.7	Statistical analysis.....	198
6.4	Results.....	199
6.4.1	Preliminary analysis of S-sulfhydrated proteins using Maleimide assay. 199	
6.4.2	Preliminary Detection of S-sulfhydrated proteins using Modified Biotin Switch assay.	200
6.4.3	Assessment of S-sulfhydrated Keap1 in TNF- α and GYY4137-treated HUVECs.....	202
6.4.4	Relation between GYY4137 and Nrf2 nuclear translocation.	204
6.4.5	Impact of GYY4137 on the mRNA levels of Nrf2 targets.	207
6.4.6	Analysis of S-sulfhydrated Caspase 3 in TNF- α and GYY4137-treated HUVECs.....	209
6.5	Discussion.....	213
7	General Conclusions & Limitations.....	219
7.1	Summary of findings	220
7.1.1	Characterisation of ED and H ₂ S experimental setting.....	220
7.1.2	The role of H ₂ S in TNF- α -mediate impaired redox state.	222
7.1.3	The role of H ₂ S in TNF- α -mediated inflammation and apoptosis.	224
7.1.4	The role of H ₂ S and TNF- α on mitochondria.....	226
7.1.5	S-sulfhydration as an H ₂ S underlying signalling mechanism.	229
7.2	Future work.....	232
7.2.1	Optimising experimental approach.....	232
7.2.2	Protein S-sulfhydration in vascular cells.....	232
7.2.3	Increasing the number of replicates	233
7.3	Final conclusions.....	233
8	References.....	234

9	Appendices	276
9.1	Appendix a. Consumables	277
9.2	Appendix b. Supplementary material.....	284
9.3	Appendix c. Uncropped western blot images.....	288
10	Publications.....	293
10.1	Published study 1.....	294
10.2	Published study 2.....	295
10.3	Published study 3.....	296

List of Figures

Figure 1.1. Schematic diagram displaying the cross-section of an artery.	23
Figure 1.2 Schematic diagram of blood vessel diameter influences.....	24
Figure 1.3 Endothelial dysfunction and associated pathological conditions.	28
Figure 1.4 Biochemical reactions of critical endothelial ROS and RNS formation.	30
Figure 1.5 Schematic diagram indicating reversible and irreversible ROS-induced redox modifications of cysteine residues on target proteins.	32
Figure 1.6 Schematic diagram of ROS-generating sources in the endothelium.....	34
Figure 1.7 Redox triangle model.	36
Figure 1.8 Schematic diagram of the extrinsic and intrinsic apoptosis pathways.....	39
Figure 1.9 Gasotransmitters.....	42
Figure 1.10 H ₂ S biosynthesis by enzymatic and non-enzymatic pathways.....	49
Figure 1.11 Schematic representation of H ₂ S oxidation and metabolism.....	54
Figure 1.12 Chemical structures of several H ₂ S donors.	56
Figure 1.13 Reversible Post-translational modifications of cysteine.....	61
Figure 1.14 Properties of persulfide sulfur atoms in cysteine.	62
Figure 1.15 Proposed reactions for S-sulfhydrated proteins by H ₂ S.	63
Figure 2.1. Timeline of experimental settings in ECs.....	73
Figure 2.2 Representative flow cytometer histogram showing adhesion molecule (CD54)- positive and IgG cells.	78
Figure 2.3 Representative diagram of annexin V staining quadrants.	80
Figure 2.4 Representative graph of the Mito Stress test in the Seahorse instrument.	89
Figure 2.5 Representative graph of the Glycolysis Stress test in the Seahorse instrument.	92
Figure 2.6. Representative Melting curves in the RT-qPCR.....	100
	12

Figure 2.7 Comparative mRNA expression of different housekeeping genes.	101
Figure 2.8 Illustration of Maleimide assay used to detect S-sulphydration in cells.	104
Figure 2.9 Schematic diagram of Modified Biotin switch assay.	107
Figure 3.1 Expression of endothelial markers by EA.hy926 cells.	116
Figure 3.2 Titration of non-toxic GYY4137 dose and analysis of intracellular H ₂ S content in EA.hy926 cells.	118
Figure 3.3 Assessing TNF- α effect on endothelial activation in EA.hy926 cells.	120
Figure 3.4 Comparison between three experimental settings on the IL-6 secretion in EA.hy926 cells.	123
Figure 3.5 Characterisation of optimal non-toxic GYY4137 dose in HUVECs.	125
Figure 3.6 Intracellular H ₂ S content in the presence of GYY4137 in HUVECs.	127
Figure 3.7 Effect of TNF- α increasing doses on endothelial activation in HUVECs.	129
Figure 4.1 Effect of TNF- α and GYY4137 on H ₂ O ₂ levels in HUVECs.	142
Figure 4.2 Effects of TNF- α and GYY4137 post-treatment on antioxidant genes.	143
Figure 4.3 Effects of TNF- α and GYY4137 post-treatment on Trx antioxidant system in HUVECs.	145
Figure 4.4 Glutathione role on the redox signalling state in treated HUVECs.	146
Figure 4.5 Flow cytometric primary plots analysis and quantification of ICAM-1 MFI (%) in ECs following TNF- α and GYY4137 treatment.	148
Figure 4.6 Flow cytometric primary plots analysis and quantification of E-selectin MFI (%) in ECs following TNF- α and GYY4137 treatment.	149
Figure 4.7 Flow cytometric primary plots analysis and quantification of VCAM-1 MFI (%) in ECs following TNF- α and GYY4137 treatment.	150
Figure 4.8 Secretion of pro-inflammatory cytokines in response to TNF- α and GYY4137 stimulation in ECs.	151

Figure 4.9 Flow cytometric primary plots analysis and quantification of apoptosis rate on ECs following TNF- α and GYY4137 treatment.	153
Figure 5.1. Effect of TNF- α and GYY4137 post-treatment on O ₂ ⁻ levels.	167
Figure 5.2. RT-qPCR mRNA levels in TNF- α and GYY4137 stimulated HUVECs.....	168
Figure 5.3. Mitochondrial OCR profile upon TNF- α and GYY4137 post-treatment.	169
Figure 5.4. Comparison of mitochondrial respiration parameters of untreated and treated HUVECs.	171
Figure 5.5. ECAR rate in TNF- α and GYY4137-cultured HUVECs.	173
Figure 5.6. Comparison of glycolytic parameters in untreated and treated-HUVECs.	174
Figure 5.7. TNF- α and GYY4137 post-treatment effect on UCP2 mRNA levels in HUVECs...	175
Figure 5.8. Effects of TNF- α and GYY4137 on $\Delta\psi_m$ in HUVECs.....	177
Figure 5.9. Mitochondrial network parameters in HUVECs.	179
Figure 5.10 Disruption of the mitochondrial fission/fusion balance machinery in HUVECs.....	180
Figure 5.11 TNF- α and GYY4137 modulated apoptotic-associated proteins in HUVECs.....	182
Figure 6.1 Schematic overview of the redox sensor Keap1-Nrf2 system.	196
Figure 6.2 Preliminary analysis of S-sulfhydration using the Maleimide assay in EA.hy926 cells.	200
Figure 6.3 Preliminary analysis of the Modified Biotin Switch assay in EA.hy926 cells.	202
Figure 6.4 Total protein staining of S-sulfhydrated and total load proteins in the presence of TNF- α and GYY4137 post-treatment setting via Biotin Switch Assay.	203
Figure 6.5 Analysis of Keap1 S-sulfhydratrion in HUVECs.....	204
Figure 6.6 Preliminary analysis of Nrf2 localisation in HUVECs treated with TNF- α and GYY4137 post-treatment.....	206
Figure 6.7 Analysis of Nrf2 protein accumulation in the nucleus in HUVECs.	207
Figure 6.8 Analysis of GYY4137 and TNF- α effect in Nrf2-downstream target proteins.	209

Figure 6.9 Analysis of S-sulfhydration of caspase 3 in HUVECs.....	211
Figure 6.10 Activity of caspase 3/7 upon TNF- α and GYY4137 treatments in HUVECs.	212
Figure 6.11 Proposed labelling mechanism of persulfide groups during Modified Biotin switch assay.	216
Figure 7.1 Hypothetical model proposed for cell ED triggered by TNF- α and rescue model mediated by H ₂ S.....	231

List of Tables

Table 1-1 Enzymatic antioxidants and their catalytic reactions.	35
Table 1-2 Summary of techniques in the measurement of ED.	41
Table 1-3 Biological features of NO and CO in the vasculature.	44
Table 1-4 Overview of Methods for detection of H ₂ S.....	48
Table 2-1. Cell culture media	69
Table 2-2. Cell culture seeding numbers.	71
Table 2-3. Antibody used for flow cytometry.....	77
Table 2-4. Primary antibodies used during immunofluorescence with their specific dilutions, host and supplier details.	84
Table 2-6. Secondary conjugated antibodies with their specific dilutions, host and supplier details.	84
Table 2-7. Components of staining mixture for SA-β-gal staining	85
Table 2-8. Injection Mito Stress test compounds on the XF24 Seahorse instrument.....	90
Table 2-9. Mitochondrial bioenergetic parameters for Mito Stress test.	90
Table 2-10. Injection of Glycolysis Stress test compounds on the XF24 Seahorse instrument .	93
Table 2-11. Glycolytic bioenergetic parameters for the Glycolysis Stress test.	93
Table 2-12. Reagents for resolving and stacking gels	96
Table 2-13. Primary antibody used for immunoblotting	97
Table 2-14 Secondary fluorescence-conjugated antibodies used for immunoblotting	98
Table 2-15. Thermal cycle settings for reverse transcription from mRNA to cDNA.....	99
Table 2-16. Real-time qPCR thermal profile.	100
Table 2-17. List of forward and reverse primers sequences used in RT-qPCR experiments...	102
Table 2-18. Reagents used for Modified Biotin Switch assay.....	108

Table 9-1. Laboratory equipment and software	277
Table 9-2. Laboratory Reagents and Chemicals	278
Table 9-3. Assays Kits.....	281
Table 9-4. Cell Culture Reagents	282
Table 9-5. H ₂ S donors	283

List of Abbreviations

$\Delta\psi_m$	Mitochondrial membrane potential
Δp	Protonmotive force
ΔpH	Mitochondrial pH gradient
ACADM	Medium-chain specific acyl-CoA dehydrogenase, mitochondrial
ALDOA	Aldolase, fructose-biphosphate A
AMPK	AMP-activated protein kinase
APC	Activated protein
ARE	Antioxidant response element
AT-III	Antithrombin III
APC	Allophycocyanin
fluorophore	
ATP	Adenosine triphosphate
Bcl-2	B-cell lymphoma
BH4	Tetrahydrobiopterin
BTB	Bric-a-brac
CAT	Catalase
CATf	Cystathionine β -synthase
CBS	Cystathionine β -synthase
CKD	Chronic kidney disease
CO	Carbon monoxide
CoQ	Coenzyme Q
COX	Cyclooxygenase
CSE	Cystathionine β -synthase
CVD	Cardiovascular disease
Cys	Cysteine
Cyto c	Cytochrome c
cEGM	Endothelial growth media used for maintenance and treatment in HUVECs
cDMEM	DMEM media used for cell culture growth in EA.hy926 cells
cM199	Media 199 used for culture treatment in EA.hy926 cells
DADS	Diallyl disulfide
DAO	Diallyl trisulfide
DAS	Diallyl trisulfide
DATS	Diallyl trisulfide
DRP1	Dynamin-related protein 1
DMSO	Dimethyl sulfoxide
DRP1	Dynamin-related protein 1
DCF	2',7'-dichlorofluorescein
ECs	Endothelial cell
ED	Endothelial dysfunction
EDHF	Endothelium-derived hyperpolarising factor
EDRF	endothelium-derived hyperpolarising factor
eNOS	Endothelial nitric oxide synthase
E-selectin	Endothelial selectin
EA.hy926	Immortalised endothelial cell line
ET	Endothelin
ETC	Electron transport chain
ETHE1	Ethylmalonic encephalopathy 1
FMD	Flow-mediated vasodilation
FOXO	Forkhead box O
FBS	Feta bovine serum
FITC	Fluorescein isothiocyanate
fluorophore	
GcLC	Glutamate-Cysteine Ligase Catalytic Subunit
GMP	Guanosine monophosphate
GP	Glycoprotein
GPX	Glutathione peroxidase

GR	Glutathione reductase
GSH	Glutathione
GSSG	Oxidised GSH
GY4137	4-methoxyphenyl-morpholin-4-yl-sulfanylidene-sulfido- λ 5-phosphane;morpholin-4-ium
H ₂ O ₂	Hydrogen peroxide
H ₂ S	Hydrogen sulphide
HEK 293	Human embryonic kidney cells
HIF1 α	Hypoxia Inducible Factor 1 Subunit Alpha
HO	Heme-oxygenase
HOCl	Hypochlorous acid
HPLC	High Performance Liquid Chromatography
HUVECs	Human umbilical vein endothelial cell
I/R	Ischaemia reperfusion
IAPs	Inhibitor of apoptosis
ICAM	Intracellular cell adhesion molecule 1
IgSF	Immunoglobulin super family
IL	Interleukin
IFN- γ	Interferon gamma
JAMs	Junctional adhesion molecule
Keap1	Kelch-like ECH-associated protein1
LDL	Low density lipoprotein
L-selectin	Leukocyte-selectin
3-MST	3-mercaptopyruvate sulfurtransferase
3-MP	3-mercaptopyruvate
MAPK	Mitogen-activated protein kinases
MFI	Mean fluorescence intensity
MitoQ	Mitoquinone
MPO	Myeloperoxidase
MPTP	Mitochondrial permeability transition pore
MFNs	Mitofusin
NAC	N-acetyl cysteine
Na ₂ S	Disodium sulfide
NaHS	Hydrogen sulfide
NF- κ B	Nuclear factor kappa B
NO	Nitric oxide
NOX	NADPH oxidase
Nrf2	Nuclear factor erythroid 2-related factor 2
NSAIDs	Human embryonic kidney cells
NQO1	NAD(P)H Quinone Dehydrogenase 1
OXPPOS	Oxidative phosphorylation
PAF	Platelet-activating factor
PAR1	Protease-activated receptor 1
PECAM-1	Platelet endothelial cell adhesion molecule-1
PE	Phycocerythrin
fluorophore	
PerCP-Cy5.5	Peridinin chlorophyll protein-Cyanine 5.5
fluorophore	
PGI ₂	Prostacyclin
PJ-34	Poly-(ADP-ribose) polymerase inhibitor
PKC	Protein kinase C
PLP	Pyridoxal-5'-phosphate
PON	Paraoxonase
Prx	Peroxiredoxin
PI	Propidium iodide
P-selectin	Platelet-selectin
PTMs	Post-translational modification
PBS	Phosphate-buffered saline
RNS	Reactive nitrogen species
ROS	Reactive oxygen species

RSS	Reactive sulfur species
RSSG	S-glutathionylated
SAM	S-adenosylmethionine
SARS-CoV-2	Severe acute respiratory syndrome coronavirus 2
sFit-1	Soluble Fms-like tyrosine kinase 1
sGC	Soluble guanylate cyclase
SGL	Glycoprotein ligands
sMaf	Small musculoaponeurotic fibrosarcoma
SMAC	mitochondria-derived activator of caspases
SNO	S-nitrosylation
SO	Sulfite oxidase
SOD	Sodium dismutase
SQR	Sulfide quinone oxidoreductase
STEL	Short-term exposure limit
UCPs	Uncoupling proteins
TFP1	Tissue factor pathway inhibitor
TLV-STEL	Threshold limit value-Short Term exposure limit
TM	Thrombomodulin
TPP+	Triphenylphosphonium cation
Trx	Thioredoxin
TrxRD	Thioredoxin reductase
TRP	Transient receptor potential
TSMT	S-methyltransferase enzyme
TST	Thiosulfate sulfurtransferase
TNF- α	Tumour necrosis factor-alpha
VCAM-1	Vascular cell adhesion molecule 1
VEGF	Vascular endothelial growth factor
VEGFRs	Vascular endothelial growth factor receptors
VSMc	Vascular smooth muscle cells
vWf	Von Willebrand factor
XDH	Xanthine dehydrogenase
XO	Xanthine oxidase
XOR	Xanthine oxidoreductase

1 General Introduction

1.1 The Cardiovascular System

The cardiovascular system consists of the heart, blood vessels and blood. Its primary function is transporting nutrients, hormones, and oxygen-rich blood through the body and carrying deoxygenated blood back to the lungs. It also facilitates the removal of waste products from the body. The heart pumps blood through the vasculature, maintaining an appropriate cardiac output. The delivery and return of blood in the systemic vasculature are through a network of blood vessels (Sherwood, 1997).

1.1.1 Blood Vessel Anatomy

Blood vessels are the body's highway that allows blood to flow quickly and efficiently from the heart through the body and back again. All blood vessels contain a hollow area called lumen through which blood can flow; surrounding the lumen is the wall of the vessel (Chaudhry, Miao and Rehman, 2021).

There are three major types of blood vessels: arteries, capillaries and veins. In arteries, vessels exhibit a thicker and elastic walls to withstand high blood pressure levels. While capillaries are the smallest and thinnest of blood vessels, veins are the large return vessels of the body (Fishman, 1982).

Arteries and veins are structurally layered into three distinct regions (Figure 1.1). The outer layer of blood vessels is called the tunica adventitia and comprises collagen, elastic fibres and connective tissue. Elastic fibres allow blood vessels to expand when experiencing blood flow pressure on the walls of the vessels.

The middle layer, known as the tunica media, occupies the greatest area of the vessel wall and is composed of vascular smooth muscle (VSMC) cells, collagen and elastic fibres. This middle layer is responsible for most of the mechanical properties of the vessel, where VSMCs regulate constriction and dilation; elastic fibres help to maintain blood flow, and collagen ensures that excessive expansion and dilation of vessels are prevented. Finally, the tunica intima (inner layer) lines the luminal surface of the vessel and is composed of a monolayer of cells referred to as the vascular endothelium. Capillaries are composed of a single layer of endothelial cells (ECs), allowing the exchange of molecules between blood and the surrounding tissue (Vito and Dixon, 2003).

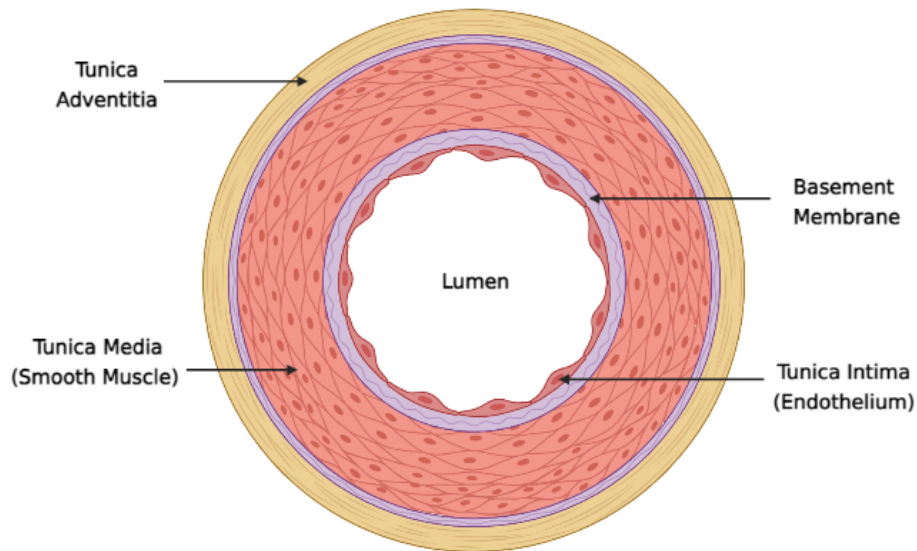


Figure 1.1. Schematic diagram displaying the cross-section of an artery.

The interior of the vessel (lumen) is surrounded by the wall of the vessel composed of three layers: Tunica Intima, Media and Adventitia. The endothelium lines the luminal surface. Created with Bio-render.com.

1.2 The Vascular Endothelium

The endothelium comprises a monolayer of individual endothelial cells that collectively lines the entire vascular system. Initially, it was viewed as the inert cell barrier that facilitated the nutrient exchange across itself. However, early studies in the '50s and electron microscopic reports of lymphocyte-endothelium interaction paved the way for subsequent research on the endothelium's multiple vital roles (Gowans, 1959; Fishman, 1982).

Currently, the endothelium is viewed as a dynamic organ with inducible synthetic and metabolic functions, partly due to its unique position at the interface between blood and surrounding tissue. Blood vessel diameter can be controlled by intrinsic signalling such as metabolic, mechanical, endothelial and paracrine (Meininger and Davis, 1992; Korthuis, 2011). Extrinsically, remote processes such as neuronal and hormonal mechanisms can also modulate vessel diameter (Sherwood, 1997; Korthuis, 2011) (Figure 1.2).

The functional capacity of the endothelium is elicited by its ability to secrete and respond to several molecules along with membrane-bound receptors and cell-to-cell interactions (Krüger-Genge *et al.*, 2019).

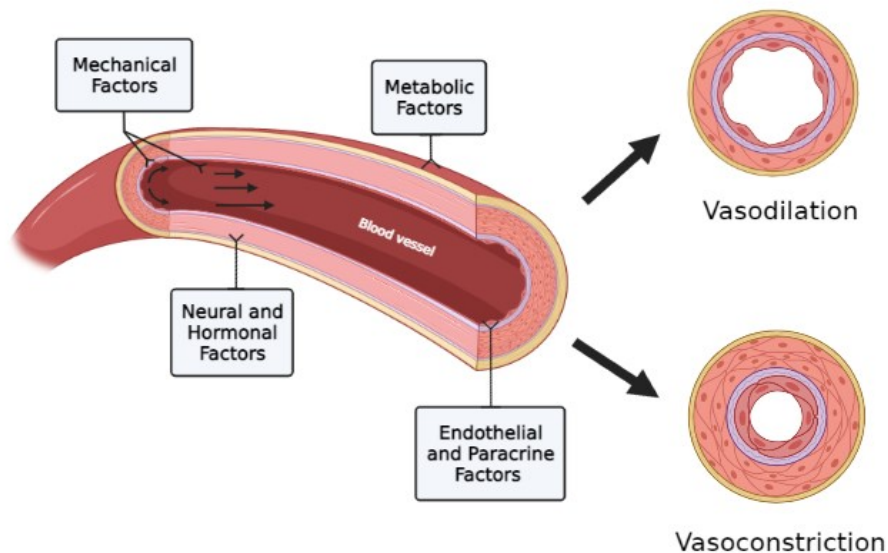


Figure 1.2 Schematic diagram of blood vessel diameter influences.

Vasomotor control mechanisms operant in endothelium and vascular smooth muscle cells in the walls of small arteries and arterioles. Intrinsic and extrinsic factors modify blood vessels diameter (constriction or dilation) and thus can influence blood flow in vascular beds. (Created with Bio-render.com. Modified from (Onyewu, Coombs and Kromah, 2021).

Like other organs, the numerous functions of the endothelium are mediated by differentiated ECs, and their heterogeneity depends on the vascular bed in which it is situated (Aird, 2003). Vascular-bed heterogeneity also covers surface protein expression and endothelial phenotype; for instance, the endothelial biomarker von Willebrand factor (vWf) varies within vessel type (Aird, 2007).

The endothelium plays a fundamental role in regulating several homeostatic vascular processes in its quiescent state. The most widely studied and well-established functions are cell barrier, vascular development, control of vascular tone, coagulation, fibrinolysis, and interaction with blood cells (Michiels, 2003).

1.2.1 The endothelium functions

The interface between blood and tissue is surrounded by ECs, interacting with circulatory cells on one hand and vascular wall cells on the other. This privileged location allows ECs to respond primarily to vascular changes and exhibit various functions. Detailed literature reviews have been published regarding ECs functions (Michiels, 2003; Galley and Webster, 2004; Krüger-Genge *et al.*, 2019). Nevertheless, the most widely studied processes are briefly reviewed in this project.

1.2.1.1 Vascular tone

The simple, early acknowledgement of the endothelium as a structural barrier between circulation and surrounding tissue was challenged by Furchgott and Zawadzki's research report. The group found that rat VSMc relaxation in response to acetylcholine was endothelium-dependent (Furchgott and Zawadzki, 1980). Although the authors demonstrated the presence of an endothelium-derived relaxing factor (EDRF), the nature of the EDRF itself was not determined. Identification of EDRF as nitric oxide (NO) was later reported (Palmer, Ferrige and Moncada, 1987). To date, it is known that the vascular endothelium produces vasodilator agents modulating blood flow, which is fundamental in permitting individual tissues and organs to meet their changing metabolic demands at rest and under stress conditions. Additional regulation of the vasomotor tone relies on the production of vasoactive molecules such as prostacyclin (PGI₂) and platelet-activating factor (PAF) (Meade *et al.*, 1996; Walterscheid, Ullrich and Nghiem, 2002).

The representation of vasoconstrictor molecules began with the isolation of endothelin (ET) in 1989 (Inoue *et al.*, 1989). Although there are three types of ET, vascular ECs only produce ET-1. In VSMc, vasoconstrictor actions emerge after binding to the endothelin_A (ET_A) receptor and later phospholipase C. Binding to ET_B receptor on ECs results in vasoconstriction of some blood vessels (Gardiner *et al.*, 1994; Mazzuca and Khalil, 2012).

1.2.1.2 Cell proliferation and Angiogenesis

The vascular network development requires complex and coordinated communication between different cell types. De novo vascularisation involves mesodermal-derived ECs forming a primitive vessel network (Conway, Collen and Carmeliet, 2001). On the other hand, new blood vessels created from pre-existing is referred to as angiogenesis,

resulting in the expansion of the vascular network (Ribatti and Crivellato, 2012). Vascular endothelial growth factor (VEGF), a well-known potent angiogenic factor, was first described as an essential growth factor for vascular endothelial cells. VEGF regulates several ECs functions, including proliferation, migration, differentiation and survival (Cross and Claesson-Welsh, 2001; Hoeben *et al.*, 2004).

In addition, VEGF exhibits its angiogenic processes through the interaction with cell-surface family receptors, including VEGFR1, VEGFR2 (both expressed in the vascular endothelium), and VEGFR3 (only in lymphatic endothelium) (Carmeliet and Jain, 2011). Recently, a family of growth factors known as angiopoietins and their ligands (tie-1 and tie-2) have been associated with vascular effects, including vascular tree expansion and vascular wall formation (Rajendran *et al.*, 2013).

1.2.1.3 Interaction with circulatory cells

As the interface between blood flow and subendothelial tissue, the endothelium can respond quickly to local changes by expressing cell surface molecules (Pober and Sessa, 2007). Upon stimulation, ECs become activated and change phenotype by expressing cell-associated molecules that contribute to directing the migration of platelets and leukocytes to specific regions of the endothelium (Videm and Albrigtsen, 2008). Recruitment of circulating cells from blood to the inflamed tissue involves a multistep process dependent on specific adhesion receptors family and in response to chemical stimulus on the surface of ECs, including platelet-selectin (P-selectin), leukocyte-selectin (L-selectin), endothelial-selectin (E-selectin), immunoglobulin superfamilies (IgSF) members such as intracellular cell adhesion molecule 1 (ICAM-1) and vascular cell adhesion molecule 1 (VCAM-1) (Zhang *et al.*, 2011; Nourshargh and Alon, 2014).

1.3 Endothelial Dysfunction

Abnormality related to individual normal functions of the vascular endothelium predisposes a dysfunctional endothelial phenotype characterised, but not limited, by compromised cell barrier, increased leukocyte adhesion, oxidative stress, impaired processing of vasodilator substances, inflammation, altered metabolism, cell death, and senescence (Rajendran *et al.*, 2013). However, the transition between ECs function and endothelial dysfunction (ED) is not always clear, but ED usually arises from otherwise adaptive responses that are excessive, sustained or temporally misplaced (Favero *et al.*, 2014).

An early description of ED was focused on structural changes or loss of anatomical integrity in the context of atherosclerosis, in which authors employed the term EC dysfunction to describe the hyperadhesiveness of the endothelium to platelets (Bevilacqua *et al.*, 1987). Moreover, ED cannot simply include all interruptions in regular functions, as endothelium serves different roles in different organ systems, conferring a heterogeneous response to physiopathological stimuli (Aird, 2007). The endothelium shift towards, but is not limited to, vasoconstriction, inflammation, oxidative stress, leukocyte adhesion, altered metabolism, eNOS uncoupling, and cell death upon ED phenotype (Xu *et al.*, 2021). Several classical and non-classical risk factors have been reported to induce ED, which precedes the progression of the underlying pathogenesis. Risk factors include hypercholesterolaemia, hyperlipidaemia, hypertension, chronic smoking, diabetes mellitus, chronic inflammatory disease, psoriasis, ageing or environmental factors (Nadar, Blann and Lip, 2004; Camici *et al.*, 2007; Gagat *et al.*, 2014; Steyers *et al.*, 2014). ED is thought to represent crucial steps in the initiation and progression of cardiovascular diseases (CVD) and vascular-related complications conditions such as atherosclerosis, hypertension, diabetes, peripheral arterial disease, metabolic syndrome, chronic kidney disease (CKD), neurodegeneration, cancer and more recently SARS-CoV-2 virus-induced COVID-19 condition (Rajendran *et al.*, 2013; Al-Jameil *et al.*, 2014; Tong *et al.*, 2020). Thus, ED exhibits prognostic implications as a predictor of cardiovascular events and patients with risk factors, conceiving relevant implications for pathophysiological, diagnostic and therapy (Figure 1.3).

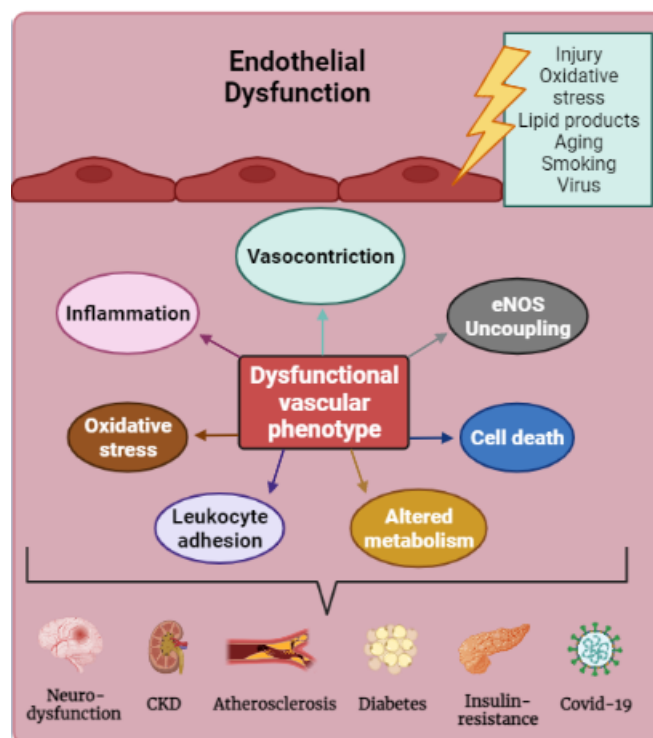


Figure 1.3 Endothelial dysfunction and associated pathological conditions.

There are different factors that can trigger ED such as excess of pro-oxidants, modified LDL, aging, cell and tissue injury, and virus such as SARS-CoV-2. These factors can induce a shift from executing physiologic functions to impaired dysfunctional vascular endothelium characterised by 1) vasoconstriction of vessels; 2) eNOS uncoupling and less NO production; 3) apoptosis; 4) impaired ATP production and metabolic routes; 5) enhanced of leukocyte adhesion and migration; 6) excessive pro-oxidants formation and decreased antioxidant defense; 7) release of pro-inflammatory cytokines and reduction of anti-inflammatory mediators. ED is more a composite of these dysfunctional aspects that emerges as a hallmark in the initiation and progression of neurodegeneration, CKD, atherosclerosis, diabetes, insulin-resistance, and viral infections such as Covid-19.

1.3.1 Redox Biology and Endothelial dysfunction

The evolution of aerobic organisms that utilise oxygen for their energetic needs has led to a considerable diversification in the forms of life that have subsequently developed. In biological systems, redox reactions, which involve electron exchange (redox) processes between two chemical species with oxidation (loss of electrons) and reduction (gain of electrons), are essential to basic cellular functions, including metabolism and respiration. Cellular redox systems include cooperative and interconnect components grouped into small metabolites, often derived from oxygen, that may exhibit second messenger roles.

In redox biology, one of the main essential components includes chemically reactive, oxidant molecules, potentially deleterious, defined as reactive oxygen species (ROS). Traditionally, ROS has been described as toxic by-products of metabolism with the potential to cause damage to lipids, proteins and DNA (Finkel, 1998). Nowadays, ROS—along with reactive nitrogen species (RNS) and recently reactive sulfur species (RSS)—are thought to be essential in cellular processes and may even act as second messengers, "redox signalling" (Sies, 2015).

In the endothelium, various types of ROS that can be formed include superoxide anion ($O_2^{\cdot-}$), H_2O_2 , hydroxyl radicals ($\cdot OH$) and hypochlorous acid (HOCl) (Figure 1.4). Among the different ROS species, chemical properties such as half-life or lipid solubility characterised its ability as an efficient signalling mediator. For instance, $O_2^{\cdot-}$ has a short half-life and is membrane impermeable; $O_2^{\cdot-}$ can rapidly form H_2O_2 via superoxide dismutase (SOD). As a more stable molecule, H_2O_2 has a longer half-life compared to $O_2^{\cdot-}$ and the ability to cross the membrane. In the presence of reduced transition metals (e.g. ferrous or cuprous ions) or to oxidise chloride (Cl^-), highly reactive $\cdot OH$ or HOCl species can be formed. Alternatively, H_2O_2 is ultimately converted to water by antioxidant enzymes such as catalase (CAT) or glutathione peroxidase (GPX) (Thannickal and Fanburg, 2000). Furthermore, the reaction of oxygen with nitrogen results in RNS formation, such as nitric oxide (NO) and the reaction between NO and $O_2^{\cdot-}$ forms one of the most potent oxidants, peroxynitrite anion ($ONOO^-$) (Song and Zou, 2014).

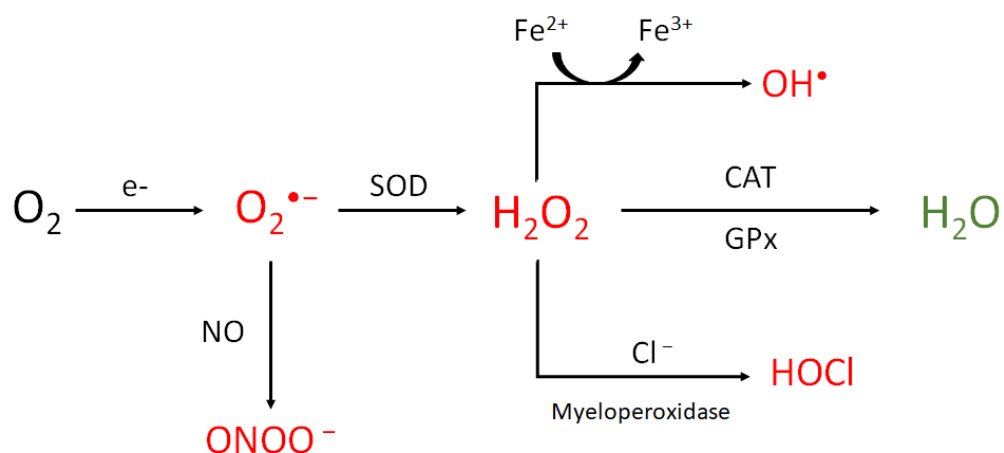


Figure 1.4 Biochemical reactions of critical endothelial ROS and RNS formation.

The univalent reaction of molecular oxygen (O_2) formed superoxide ($O_2^{\bullet-}$) that, upon dismutation reaction, is converted to H_2O_2 . In transition metals or chloride presence, H_2O_2 can be converted to hydroxyl radical ($\bullet OH$) or hypochlorous acid (HOCl). Ultimately, enzymatic reactions lead to converting H_2O_2 to water. Peroxynitrite ($ONOO^-$) is formed from the non-enzymatic reaction between $O_2^{\bullet-}$ and nitric oxide (NO).

A large part of ROS-mediated signal transduction relies on oxidative modifications of proteins (Figure 1.5). The sulfur-containing group (thiol) amino acids, especially cysteine (Cys), is believed to be primarily responsible for transmitting these redox cues. It is now known that ROS cannot mediate the oxidation of all Cys residues but only target Cys thiol groups displaying low pKa thiolate anions (Winterbourn, 2008). Specific properties such as susceptibility to ROS/RNS, selectivity in different local environments and flexibility by its reversible modifications; allow thiols in Cys residues to act as redox signal switches (Ferrer-Sueta *et al.*, 2011). ROS-mediated modification of the sulfhydryl or thiol group (-SH) of a single Cys can be described as a sequential oxidation reaction from sulfenic (-SOH) to sulfinic (-SO₂H), sulphonic (-SO₃H) or S-glutathionylated (-SSG) derivatives (Figure 1.5) (Finkel, 2011).

Sulfenic acid can be reversible and reduced via the cell's intrinsic antioxidant systems and exhibit physiological effects. In addition, sulfinic and sulfonic acids occur under high pro-oxidant levels and are in irreversible oxidation states (Benhar, 2020). If the critical Cys is located within the catalytic domain, these alterations can modify the functional activity of a protein or transcription factor.

Furthermore, transcription factors such as nuclear factor erythroid 2-related factor 2 (Nrf2), nuclear factor kappa B (NF- κ B) and forkhead box O (FOXO) are redox-sensitive factors acting as redox sensors that pleiotropically reprogram cell's redox state (Song and Zou, 2014). One of the most potent transcription factors is Nrf2. Its complex, alongside Kelch-like ECH-associated protein1 (Keap1), plays a vital role as an oxidant sensor and regulator of redox homeostasis in ECs (Deshmukh *et al.*, 2017). Exposure to ROS can enhance Keap1 inhibition, which subsequently promotes the nuclear translocation of Nrf2 and triggers the transcription of genes that encode antioxidant molecules (Ooi, Goh and Yap, 2017).

In addition, the localisation of cysteine residues within a protein tertiary or quaternary structure can result in ROS-induced covalent intra- and inter-disulphide bond formation that elicits a conformation change. The transcription factor p53 displays oxidative-reductive conformational modification at Cys near the DNA interface, regulating its transcriptional activation (Rainwater *et al.*, 1995). Both antioxidant intracellular thiol redox systems thioredoxin (Trx) and glutathione (GSH), and their system components, including NADPH, thioredoxin reductase (TrxRD), oxidised GSH (GSSG) and glutathione reductase (GR), play a significant role in reversing thiol modifications (Ahsan *et al.*, 2009). In addition, ROS and RNS catabolism depend on both Trx and GSH, and the crosstalk within both redox systems appears to be selective rather than a general manner and is involved in the modulation of several cell survival and death pathways (Figure 1.5) (Go *et al.*, 2013; Ren *et al.*, 2017).

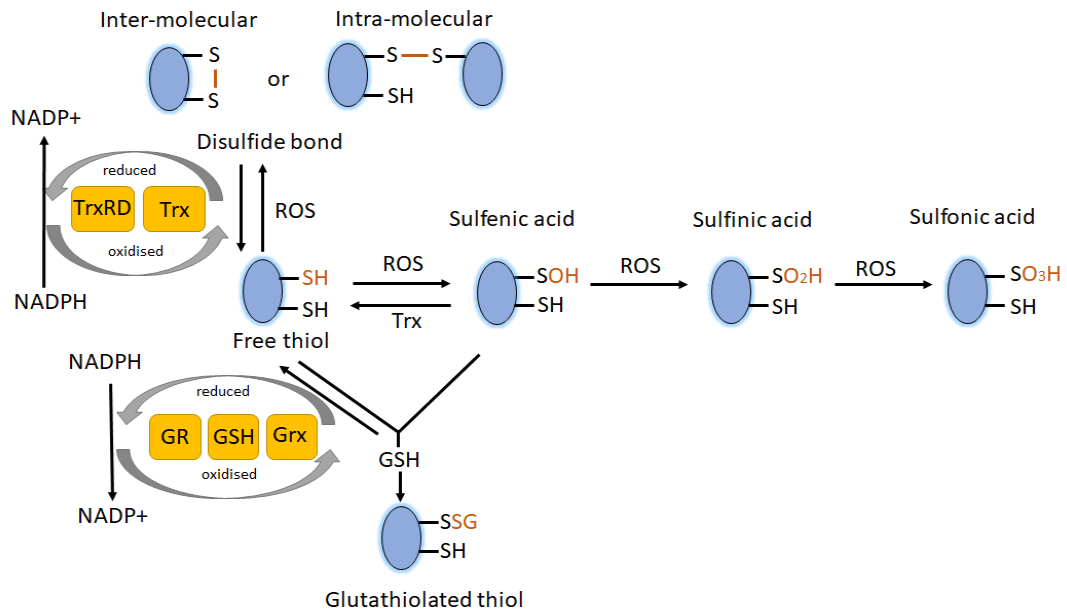


Figure 1.5 Schematic diagram indicating reversible and irreversible ROS-induced redox modifications of cysteine residues on target proteins.

Oxidation of cysteine thiol (RSH) by ROS or RNS leads to the generation of inter – and intra-molecular disulfide bonds (RSSR) or reaction with glutathione (GSH) to become S-glutathionylated (SSG). These oxidative modifications are reversible, and reduction is catalysed by thiol redox systems thioredoxin (Trx) and GSH. Glutaredoxin (Grx) and Trx themselves result in oxidised forms, which are reduced by GSH and Trx reductase (TrxRD), respectively. Oxidised GSH (GSSG) is diminished by GSH reductase (GR). Both thiol redox systems received electrons from NADPH. Sequential oxidation of sulfenic (RSOH) to sulfinic (RSO₂H) and sulfonic acid (RSO₃H) are generally irreversible modifications. Adapted from (Abo and Weerapana, 2019).

1.3.1.1 Source of ROS

Cellular ROS-producing systems within the endothelium include reduced nicotinamide adenine dinucleotide phosphate (NADPH) oxidase (NOX), xanthine oxidase and uncoupled eNOS and mitochondria (Meo *et al.*, 2016; Abo and Weerapana, 2019).

Mitochondrial ROS generation: The aerobic metabolic processes in the mitochondria, referred to as oxidative phosphorylation (OXPHOS), ultimately result in the condensation of the inorganic phosphate and adenosine diphosphate (ADP) to produce adenosine triphosphate (ATP), a valuable energy source. The process involves an electron transport chain (ETC) form of multi-subunit complexes (I to IV) alongside coenzyme Q (CoQ) and cytochrome c (cyto c); and the transport of electrons throughout the complexes and flux of protons into the intermembrane space that creates a gradient across the mitochondrial inner membrane, which drives the production of ATP by the

ATP synthase (complex V). During mitochondria respiration activity, most of the molecular oxygen is reduced to water, but around 1-2% of the oxygen, mainly by complexes I and III, is reduced to $O_2^{\cdot-}$, which is rapidly converted to H_2O_2 by the manganese-dependent SOD (MnSOD or SOD2) (Turrens, 2003) (Figure 1.6 A).

Xanthine oxidase system: Xanthine oxidoreductase (XOR) catalyses hypoxanthine oxidation to xanthine and subsequently to uric acid, which are the final steps in the purine degradation pathway. The enzyme can be found in two interconvertible forms, xanthine oxidase (XO) and xanthine dehydrogenase (XDH) (McNally *et al.*, 2003). The most common form, XDH, can be reversibly converted to XO by sulfhydryl oxidation at Cys⁵³⁵ and Cys⁹⁹² (Berry and Hare, 2004). In contrast, proteolysis results in irreversible oxidation to XO. Moreover, XDH reduces both NAD^+ and O_2 , whereas XO does not interact with NAD^+ and will form $O_2^{\cdot-}$ and H_2O_2 by reduction of O_2 (Figure 1.6 B) (Enroth *et al.*, 2000).

NADPH oxidase system: NADPH oxidase enzymes constitute a family of enzymes (1-5 isoforms) whose function is to catalyse the transfer of electrons to O_2 , generating $O_2^{\cdot-}$ or H_2O_2 using NADPH as an electron donor. The enzyme is composed of two membrane subunits, NOX and transmembrane protein p22^{phox}, alongside cytosolic subunits (Figure 1.6 C) (Bedard and Krause, 2007; Gavazzi and Faury, 2021).

Endothelial NOS: In mammals, three NOS isoforms are present, including inducible NOS (iNOS), neuronal NOS (nNOS) and endothelial NOS (eNOS), which is the predominant form in ECs (Balligand *et al.*, 1995; Taddei *et al.*, 1996; Zakhary *et al.*, 1997). In the endothelium, eNOS produces NO during the oxidation of L-arginine to L-citrulline using cofactors such as BH₄, FAD and NADPH (Govers and Rabelink, 2001). Mechanistically, deficiency of BH₄ or L-arginine causes eNOS uncoupling, in which the reduction of O_2 by NADPH becomes uncoupled from L-arginine oxidation and NO synthesis; therefore, the NOS enzyme generates $O_2^{\cdot-}$ instead of NO (Figure 1.6 D) (Moncada and Higgs, 2006).

Additionally, S-glutathionylation of eNOS results in its inactivation, uncoupling of eNOS and excessive formation of $O_2^{\cdot-}$ (Chen *et al.*, 2010). In addition, the production of ROS by uncoupled eNOS has been shown to enhance the development of cardiovascular-related conditions such as diabetes mellitus and hypertension (Stroes *et al.*, 1997; Dikalova *et al.*, 2016).

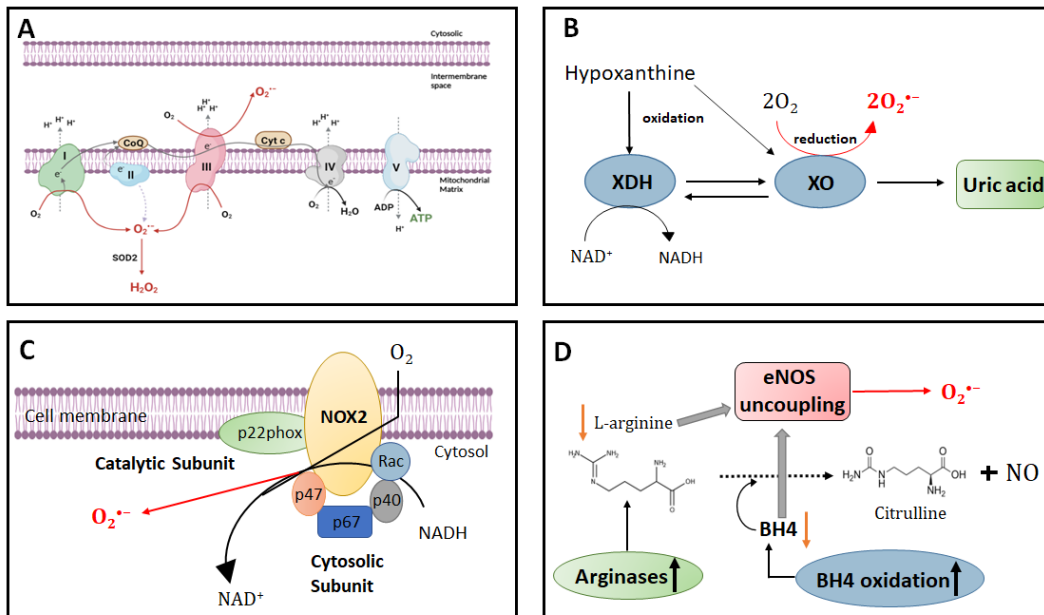


Figure 1.6 Schematic diagram of ROS-generating sources in the endothelium.

(A) Electron transport chain during oxidative phosphorylation in mitochondria and the production of $O_2^{\bullet-}$ as by-products by complex I, II and III, which through dismutation formed H_2O_2 . (B) Xanthine oxidoreductases exist in two interconvertible isoforms. Xanthine dehydrogenase (XDH) uses NAD^+ as an electron acceptor and does not produce ROS. In contrast, xanthine oxidase (XO) uses oxygen (O_2) as an electron acceptor and, thus, can form $O_2^{\bullet-}$. (C) NADPH oxidase enzymes comprised by membrane subunits (NOX and P22phox) in the endothelium promote the formation of $O_2^{\bullet-}$ using NADPH as an electron donor. (D) The endothelial NO synthase (eNOS) can become uncoupled mainly through deficiency of cofactor BH4 or of the substrate L-arginine. Uncoupled eNOS produces $O_2^{\bullet-}$. Created with Bio-render.com.

1.3.1.2 Antioxidant systems

Redox homeostasis involves maintaining a balance between the production and removal of ROS. As mentioned, optimal levels are modified for normal cell function of physiological processes, and enzymatic and non-enzymatic antioxidant systems maintain the optimal balance to avoid an excessive production of ROS (Münzel *et al.*, 2017). The antioxidant enzymes include SOD, CAT, GPx, peroxiredoxin (Prx) and paraoxonase (PON) (Table 1-1).

Table 1-1 Enzymatic antioxidants and their catalytic reactions.

Enzyme systems	
	Reaction / Function
Superoxide dismutase	$O_2^{\cdot-} \longrightarrow H_2O_2 + O_2$
Catalase	$H_2O_2 \longrightarrow H_2O + O_2$
Peroxidase	$GSH + H_2O_2 \longrightarrow GSSG + H_2O$
Peroxiredoxin	$H_2O_2 \longrightarrow H_2O$ (Trx as e^- donor)
Paraoxonase	Inhibition of mitochondrial-ROS and myeloperoxidase activity

In mammalian tissues, three isoforms of SOD can be found. Copper/zinc-SOD, SOD1, is in the cytoplasm and mitochondrial intermembrane space. SOD2 is located in the mitochondrial matrix, whereas copper/zinc-SOD (SOD3) is mostly extracellular. All three SOD forms catalysed the dismutation of $O_2^{\cdot-}$ via the inactivation of iron-sulfur centres containing mitochondrial enzymes (Fukai and Ushio-Fukai, 2011). Once generated, H_2O_2 can be decomposed to molecular oxygen and water by antioxidant enzymes, including CAT and peroxidases (Ighodaro and Akinloye, 2018). Although CAT is mainly located in the peroxisome, evidence of mitochondrial locations has been reported (Csiszar *et al.*, 2019).

Another predominant antioxidant enzyme is GPx, which catalyses the decomposition of H_2O_2 using the monomeric GSH as an electron donor. In mammals, of the four different GPx isoforms, GPx-1 is the most abundant, which in ECs can be found in the cytoplasm and mitochondria (Handy *et al.*, 2009; Ighodaro and Akinloye, 2018). Furthermore, Prx proteins are thiol specific-enzymes that catalyse the degradation of H_2O_2 using active cysteine residues and electron donors such as Trx (Rhee, 2016). Six isoforms of Prx in mammals have been identified, with differences in the number of cysteine residues required for the catalytic activity (Sue, Ho and Kim, 2005). The PON family consists of three antioxidant isoenzymes. PON1 and PON3 are expressed mainly in the liver and kidneys and function as inhibitors of lipid peroxidation of the LDL and HDL particles in plasma. PON1 secreted by the liver exerts its antioxidative effects through the activity of myeloperoxidase (MPO) (Huang *et al.*, 2013). PON2 is a more ubiquitous membrane-bound form that exerts ROS-scavenging effects by interacting with coenzyme Q10

(Altenhöfer *et al.*, 2010). An additional contribution to the antioxidant systems emerges from non-enzymatic compounds such as uric acid, bilirubin, GSH and vitamin (C and E) (Münzel *et al.*, 2017). GSH is present at millimolar concentrations in the cell and scavenges ROS through GSSG formation. The ratio of GSSG:GSH can be used as a readout of the intracellular redox state. Indeed, when the intrinsic antioxidant system is overwhelmed by excessive ROS production, oxidative stress is induced, which manifests in cellular damage and disease (Shaito *et al.*, 2022).

1.3.1.3 Oxidative stress

The term "oxidative stress" is broadly used to refer to imbalances in redox couples (reduced to oxidised), an imbalance between oxidant and antioxidant activity, or failure of the antioxidant system leading to excessive ROS/RNS/RSS. This imbalance alters normal cellular function, eventually causing cell dysfunction (Incalza *et al.*, 2018). Although the "redox triangle model" is the most common representation of the oxidative stress design, the misleading and simplicity of the model have been recently questioned (Figure 1.7) (Held, 2020).

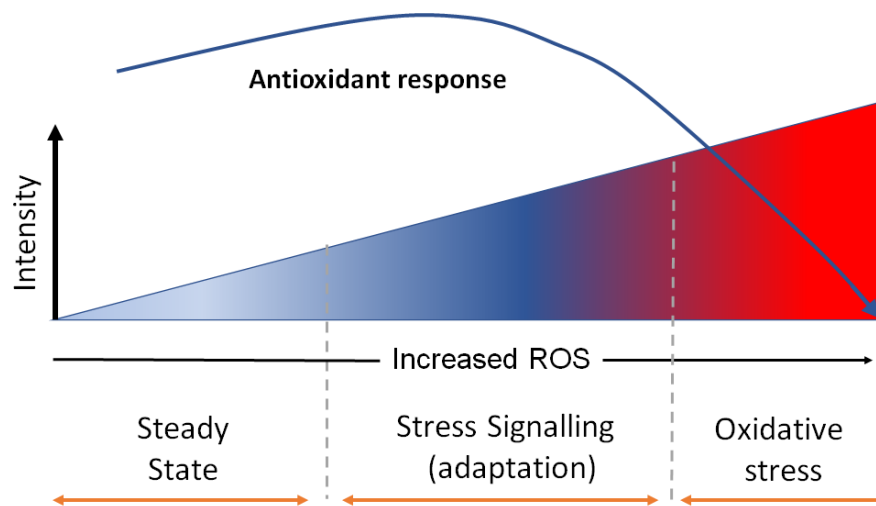


Figure 1.7 Redox triangle model.

A typical representation of the redox state and progression from homeostatic to signalling adaptation towards oxidative stress, in which generation and excessive ROS levels are associated with inadequate antioxidant defence systems. Adapted from (Held, 2020).

Nevertheless, the implications of oxidative stress in the pathogenesis of CVDs and other vascular conditions are undeniable, as exemplified by the regulation of blood pressure in ECs and VSMCs (Gage *et al.*, 2013). In addition, oxidative stress-related research is constantly growing, focusing on unmasking underlying mechanisms. Several mechanisms have been reported, such as eNOS uncoupling, activation of NF- κ B, mitochondrial DNA damage and lipid peroxidation (Landmesser *et al.*, 2003; Romagnoli *et al.*, 2010; Ivanova and Perkins, 2019; Nunes *et al.*, 2021). Excessive lipid peroxidation is associated with the risk of thrombotic, hypertensive and diabetic patients (Ito, Sono and Ito, 2019). In rodent-aged models, measurement of ONOO⁻ in serum offers a quantitative marker for oxidative stress-associated NO (Ma *et al.*, 2014).

1.3.2 Inflammation and Endothelial dysfunction

Pro-inflammatory mediators such as TNF- α , interleukin-1 β (IL-1 β) and lipopolysaccharide (LPS) can stimulate ECs. Upon activation, ECs secrete pro-inflammatory cytokines, including IL-6, IL-8, and interferon- β (IFN- β), to contribute to the inflammatory response (Griffin *et al.*, 2012; Libby, 2017; Tucureanu *et al.*, 2017). Furthermore, anti-inflammatory cytokines such as IL-10 and IL-35 can block endothelial activation by reducing oxidative stress (Xinyuan Li *et al.*, 2020). Interestingly, crosstalk between oxidative stress and inflammation has been reported (Hajjar and Gotto, 2013); through the interaction between oxidants, NF- κ B and C-Jun N-terminal kinase (JNK) (Nakano *et al.*, 2006).

Multiple studies suggest that oxidative stress regulates the extravasation of leukocytes in response to inflammatory stimuli via the activation of cellular adhesion molecules (JIANG *et al.*, 2020, Liu *et al.*, 2017, Zhao *et al.*, 2017). H₂O₂ has been reported to induce inflammation in culture ECs by activating the transcription factor NF- κ B (JIANG *et al.*, 2020). The NF- κ B represents a master regulator of vascular inflammation by regulating many pro-inflammatory genes, such as IL-6 and IL-1 β , in response to TNF- α (T. Liu *et al.*, 2017). Inhibition of endothelium inflammation has emerged as a novel therapeutic strategy to reverse ED. For instance, a derivative of Danshen, a traditional herb that can reduce TNF- α -induced ED via ICAM-1 surface expression, is currently under clinical trial (Zhao *et al.*, 2017).

1.3.3 Apoptosis and Endothelial dysfunction

Following endothelial damage, programmed cell death or apoptosis may be initiated. Genetically determined morphological changes and energy-dependent biochemical mechanisms characterise apoptosis (Onyewu, Coombs and Kromah, 2021). Under homeostatic conditions, apoptosis maintains tissue cell population as a defence mechanism. Light and electron microscopy has identified apoptotic development stages: the early process involves cell shrinkage, pyknosis (irreversible condensation of chromatin in the nucleus) and smaller size. Subsequently, extensive plasma membrane blebbing occurs, destructive fragmentation of the nucleus and fragmented apoptotic bodies emerge within intact plasma membrane that macrophages can phagocytose (Obeng, 2021). The uncontrolled degradative process after cell death is called necrosis (an energy-independent type of death).

Research indicates two main apoptotic pathways involving a cascade of molecular events, the extrinsic and intrinsic pathways. First, the extrinsic pathway involves a transmembrane receptor-mediated interaction involving death receptors members of the TNF receptor gene superfamily. The sequence of events that defines this model requires receptor-ligand binding followed by the recruitment of cytoplasmic adapter proteins, leading to the activation of procaspase 8 . Once caspase 8 is activated, the execution phase of apoptosis is triggered by the proteolytic cascade, in which one activated caspase can further activate other pro-caspases (Obeng, 2021). Interestingly, evidence of crosstalk between intrinsic and extrinsic pathways has been reported, involving the pro-death B-cell lymphoma (Bcl-2) family protein, Bid. Extrinsic-derived caspase 8 truncated Bid commonly exhibits anti-apoptotic signalling in the intrinsic pathway, triggering the intrinsic cascade signalling (Figure 1.8) (Roy and Nicholson, 2000).

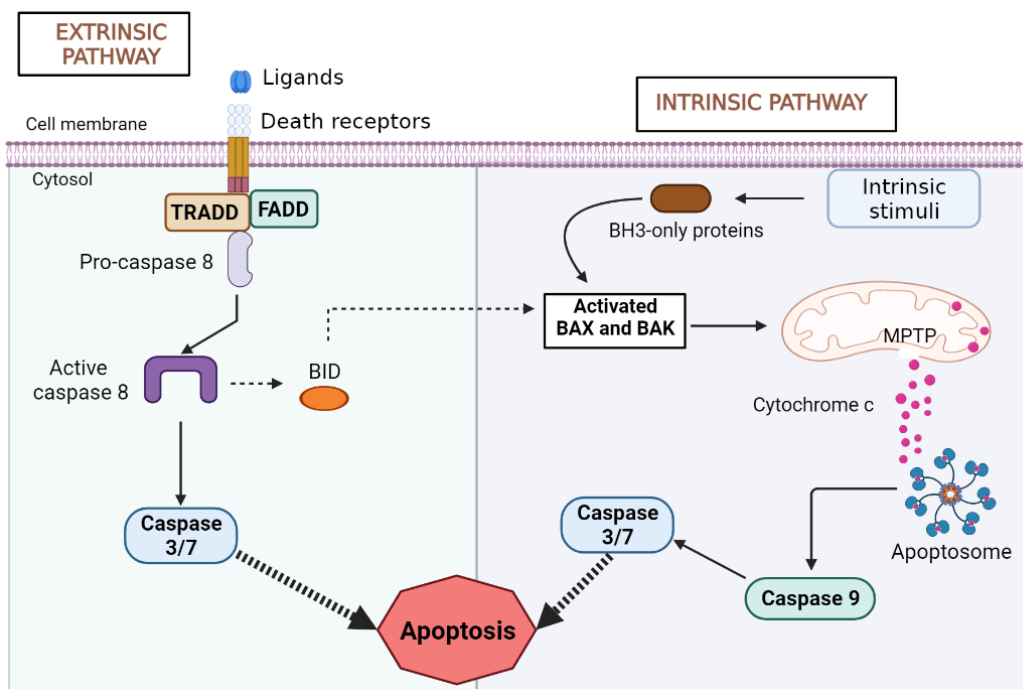


Figure 1.8 Schematic diagram of the extrinsic and intrinsic apoptosis pathways.

Binding ligand-death receptors can initiate the extrinsic pathway, activating caspase 8 and downstream proteins. In the intrinsic route, cellular stressors activate BAX and BAK proteins that trigger mitochondrial permeabilisation transition pore opening and release of pro-apoptotic molecules such as cytochrome c. After apoptosome formation, downstream caspase cascade signalling occurs, with caspase 3 as the primary effector. Crosstalk between both pathways has been associated with truncated BID protein by caspase 8. Created with Bio-render.com.

Secondly, the intrinsic signalling pathway commonly occurs upon non-receptor-mediated stimuli that produce intracellular signals within the cell and are mitochondria-initiated events. The intrinsic cascade signalling might be stimulated by positive stimulation of the pathway or by the absence of inhibition of the path, thereby triggering apoptosis (Figure 1.8) (Obeng, 2021). All these factors activate Bax and Bak, members of the Bcl-2 family and core regulators, by starting the opening of the mitochondrial permeability transition pore (MPTP) and releasing pro-apoptotic proteins into the cytosol (Peña-Blanco and García-Sáez, 2018). These pro-apoptotic mediators consist of cyto c, which binds and activates apoptotic protease-activating factor 1 and pro-caspase 9, forming an apoptosome complex. The apoptosome cleaves the pro-caspase form into the active form, caspase 9, which further stimulates the downstream caspase cascade signalling.

Caspase 3 emerges as the most crucial executor, which can be activated by any initiator (caspase 8, caspase 9, caspase 10). Moreover, additional pro-apoptotic proteins such as HtrA2/Omi and second mitochondria-derived activator of caspases (SMAC) can promote the intrinsic apoptosis pathway by inhibiting inhibitors of apoptosis proteins (IAPs) (Qin *et al.*, 2015). Notably, there is evidence of crosstalk between both routes upon stimulation of TNF superfamily members in ECs (Chandrasekar *et al.*, 2004).

The ability to modulate cell survival exerts an immense therapeutic potential, reflected by the rapid research rate in the cell cycle machinery (Circu and Aw, 2008; Suen, Norris and Youle, 2008; Galimov, 2010). High circulating concentrations of low-density lipoprotein (LDL), disturbed blood flow, smoking, elevated levels of Ang-II, oxidative stress, and irradiation can induce endothelial cell apoptosis (Elmore, 2007). Atherosclerosis, a common cardiovascular condition with plaque formation inside arteries, is coupled with apoptosis of vascular cells where cell-derived extracellular vesicles contribute to the condition's progression (Paone *et al.*, 2018). According to previous reports, TNF- α -induced apoptotic intracellular signalling *in vitro* and *in vivo* models (Jiang *et al.*, 2016; J.-X. Chen *et al.*, 2021). Further elucidation of these signalling pathways should offer relevant implications in anti-apoptotic therapy.

1.3.4 Assessment and prevention of Endothelial dysfunction

In some domains, analysis of dysfunctional vascular-related conditions has drifted from the research environment into the clinical field. Functional assessment of the endothelium includes *in vivo*, *ex-vivo* and *in vitro* techniques (Chia, Teo and Yeo, 2020). Table 1-2 describes some of these techniques.

Despite the vast array of techniques available and the continued development of new strategies, our understanding of the human endothelium system is still incomplete (Musz *et al.*, 2021). Various pharmacological therapies have been designed to reduce the development and progression of vascular conditions, with ED as an underlying mechanism (Favero *et al.*, 2014).

Table 1-2 Summary of techniques in the measurement of ED.

Technique	Function	Invasiveness	Experiment type	Limitations	References
Intra-arterial or intra-venous infusion	Vascular tone	Invasive	In vivo	Interference of other cell functions and time-consuming	(Newby <i>et al.</i> , 1999; Lind, 2006)
Flow-mediated dilation	Artery diameter and dilation	Non-invasive	In vivo	High cost and a high degree of operator skill.	(Corretti <i>et al.</i> , 2002)
Laser-based technique	Skin microvascular	Non-invasive	In vivo	Elevated cost and strict protocol required	(Debbabi <i>et al.</i> , 2010)
Myograph	Arteries stiffness	Invasive	Ex vivo	Depending on opportunistic samples	(Myers <i>et al.</i> , 2005)
Transendothelial electrical resistance	Ion permeability	N.A	Ex vivo and In vitro	Important in vivo features may be affected	(Mahajan <i>et al.</i> , 2015; Srinivasan <i>et al.</i> , 2015)
Venous inclusion technique	Coagulation and fibrinolysis	Invasive	In vivo	N.A	(Oliver, Webb and Newby, 2005)
ELISA, molecular assay and MS	ED biomarkers	Non-invasive	Ex vivo and In vitro	Kinetics may not be well-known, and in vivo functions may be a lost.	(Paulus, Jennewein and Zacharowski, 2011; Lertkiatmongkol <i>et al.</i> , 2016)

1.4 Gasotransmitters

Signalling molecules come in all sizes and chemical structures, from large proteins, peptides, and amino acids to gaseous molecules. Gasotransmitter is a gaseous messenger molecule that participates in cell signalling. The discovery and characterisation of this family have altered the conventional paradigm of intercellular signalling. Unlike classical molecules, gasotransmitters are synthesised enzymatically on demand. As lipophilic molecules, gasotransmitters can freely cross cell membranes and do not require cell-bound receptors to amplify signal cascade. The most important unique feature relies on its capacity to chemically modify intracellular proteins, thus directly affecting cellular signalling and acting as second messengers (Mustafa, Gadalla and Snyder, 2009). Gaseous signalling molecules exert various effects within various cell types, leading to pleiotropic consequences.

The endogenously generated gasotransmitter NO was the first to be categorised in this family. In addition to NO being identified as a gasotransmitter, carbon monoxide (CO) is endogenously produced and exhibits biological effects. Recently, hydrogen sulphide (H₂S) has been the latest member to join the gasotransmitters family (Figure 1.9). More recently, these novel signalling molecules have been the subject of growing research, with H₂S as the leader molecule (Mustafa, Gadalla and Snyder, 2009).

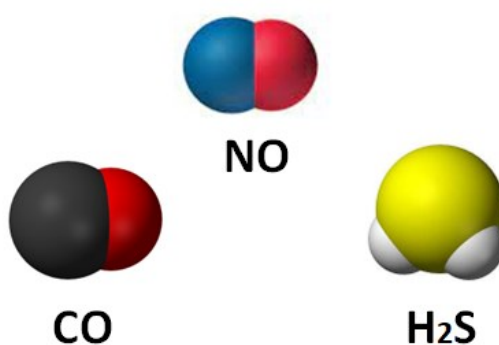


Figure 1.9 Gasotransmitters.

A representative illustration represents major endogenous gaseous signalling molecules. NO: nitric oxide, CO: carbon monoxide and H₂S: hydrogen sulphide.

1.4.1 Nitric Oxide

Since the 1700s, NO was identified as a gasotransmitter. Still, its importance in biology and medicine as a physiological mediator has not fully appreciated until 1988 its role in vascular (Taylor and Weston, 1988). As described in section 1.3.1.1, three isoforms of NO synthase can generate; NO, eNOS being the predominant isoform in the endothelium. A large part of the ubiquitous influence of NO on cellular signalling and mediation of redox-based physiological reactions relies on its post-translational modification capability, referred to as S-nitrosylation (SNO) (Foster, Hess and Stamler, 2009). Generally, post-translational modification is the covalent modification of amino acid side chains on proteins by modifying an existing functional group or introducing a new one. For example, phosphorylation is known to be precisely controlled by activities of kinase and phosphatase families that serve to add and remove phosphate groups, respectively (Ardito *et al.*, 2017a).

Specifically, SNO is the covalent attachment of a nitrogen monoxide group to the thiol side chain of Cys. In tissues and biofluids, SNO concentrations have been measured in the low nM - μ M range. S-nitrosylation regulates several cellular underlying mechanisms, including apoptosis, metabolism, and enzyme activities. The impact of the dysregulation of this post-translational modification has been observed in pathophysiological vascular conditions (Hess *et al.*, 2005). For example, stimulation of NOS in neurons or macrophages triggers glyceraldehyde-3-phosphate dehydrogenase (GAPDH) S-nitrosylation at Cys¹⁴⁵, which enhances GAPDH-SNO nuclear accumulation and promotion of downstream cytotoxicity during apoptosis (Hara *et al.*, 2005). A primary mechanism for S-nitrosylation *in vivo* is the reversible transnitrosylation of protein thiol to GSH, yielding GSNO and protein Cys-SH as co-products (Foster, McMahon and Stamler, 2003). Accumulated GSNO can undergo denitrosylation enzymatic reaction by a GSNO reductase, acting as an indirect regulator for controlled SNO-protein levels (Table 1-3) (Lu *et al.*, 2013).

1.4.2 Carbon monoxide

Similar in molecular size and structure to NO, CO is a diatomic, relatively non-radical stable gas due to weak chemical reactivity (Table 1-3) (Hartsfield, 2002). CO is physiologically generated via heme catalysis by a family of enzymes known as heme-oxygenase (HO). This family comprises three isoenzymes; HO-1, HO-2 and HO-3, of which HO-1 and HO-2 are catalytically active proteins. While HO-1 becomes active upon stress stimuli such as inflammation or oxidative stress, HO-2 is constitutively expressed and is responsible for basal CO production in the brain and cardiovascular system (Sharma and Magde, 1999). CO exhibit anti-inflammatory, anti-apoptotic, anti-coagulant, vasodilation and antiviral. CO signalling shares similarities with NO via increased cGMP stimulation, resulting in v vessel vasorelaxation. However, the NO-cGMP effects exhibit a 5-fold growth compared to CO-mediate signalling (Wu and Wang, 2005).

Dysregulation in CO levels or deficiency in HO-1 enzymes has been associated, for instance, with hypertension and impaired placenta development during pregnancy (Zhang *et al.*, 2001; Zhao *et al.*, 2009). To note, CO may also exert biological actions by inducing direct carbonylation of amino acids such as Cys, lysine, histidine, or arginine residues in target proteins. Carbonylation is irreversible and non-enzymatic, forming carbonyl derivates (e.g., aldehydes) and leading to protein damage (Wong *et al.*, 2008). However, the role of CO and the oxidative-mediated signal transduction of this process remains contradictory and not fully understood, as no involvement of CO in the carbonylation has been reported (Suzuki, Carini and Butterfield, 2010). Despite the current observations, the complete biochemical mechanisms and underlying signalling through which CO acts are not fully known.

Table 1-3 Biological features of NO and CO in the vasculature.

	VASCULATURE SYSTEM	
	Nitric Oxide	Carbon Monoxide
Discovery of physiological functions	1988	1991
Enzymatic Production	nNOS, iNOS, eNOS	HO-1 and HO-2
Second messenger target(s)	sGC-cGMP	sGC-cGMP
Blood concentrations	Low nM	nM to μ M
Chemical modification of proteins	S-nitrosylation	Carbonylation?

1.5 Hydrogen sulphide

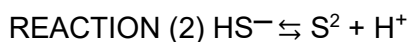
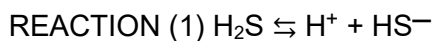
H₂S is a small colourless, flammable gas and sulfur analogue of the water molecule, which exhibits lipophilic characteristics allowing high permeability across biological membranes. The historical reputation of H₂S as a highly toxic gas has been associated with inhibiting mitochondrial respiration via cytochrome c oxidase (mitochondrial Complex IV) (Szabo, 2018). As H₂S is gas, inhalation can be the primary route for H₂S-associated pathology. According to the American Council of Government Industrial Hygienists (ACGIH), the newly proposed Threshold limit value-Short Term exposure limit (TLV-STEL) and Short-term exposure limit (STEL) for H₂S stand for 1 *part per million* (ppm) and 5ppm, respectively. Inhalation of H₂S at high concentrations (30 and 80 ppm) significantly increased nasal lesions and neuron loss in adult male rats (Brenneman *et al.*, 2000). In humans, exposure to 10 ppm of H₂S leads to eye soreness and respiratory difficulty, and death occurs at ≥ 500 ppm (Poda, 1966; Beauchamp *et al.*, 1984; Malone Rubright, Pearce and Peterson, 2017).

However, the re-appreciation of H₂S from a toxic molecule to a physiological mediator began with the discovery of its endogenous production and neurological regulation ability (Abe and Kimura, 1996). This breakthrough initiated a wave of research with H₂S as the primary research core in different systems, such as cardiovascular, immunological and nervous systems (Kimura and Hideo, 2014). At a cellular level, H₂S can be synthesised in the vascular wall by both ECs and VSMCs. The production of H₂S is shown to be 100-1000 fold higher in smooth muscle (nanomolar) compared to EC lines (picomolar), allowing H₂S to act as a smooth muscle relaxant (Scrivner *et al.*, 2021).

1.5.1 Physiochemical properties of H₂S

H₂S is a flammable gas with a characteristic smell of rotten eggs. As a water-soluble gas remains in equilibrium with its gas phase when dissolved in a solvent, it is soluble in up to 120 mM at 20°C and 80 mM at 37°C in water. The combination of high solubility, inability to form hydrogen bonds, and slightly hydrophobic nature allows freely permeate migration across biological membranes, acting as a paracrine signalling molecule (Cuevasanta *et al.*, 2012). Notably, mathematical models demonstrated that biological membranes might exhibit resistance partially to the diffusion of H₂S, resulting in an elevated presence within the compartments (Cuevasanta *et al.*, 2012).

As a weak acid [$P_{Ka1} \sim 6.76$ and $P_{Ka2} \sim 11.96$], under physiological conditions, it is dissociated to hydrosulfide anion (HS^-) and sulfide anion (S^{2-}) in an aqueous solution as described in reactions (1) and (2) (Cuevasanta, Möller and Alvarez, 2017).



In biological systems, at a physiological pH of 7.4 and 37°C, H_2S is in fast equilibrium and primarily exists in its anionic deprotonated form, HS^- , while the level of S^{2-} is nearly inexistent. The HS^- ratio observed in biological fluids is three-fold higher compared to the undissociated H_2S form, with a trace of S^{2-} (Li, Lancaster and Jr., 2013). Moreover, sulfur exhibits a range of oxidation from -2 to +6 due to its six valence electrons and empty 3p orbital (Lau and Pluth, 2019). Characteristics of sulfur, including nucleophilicity, high polarizability and low electronegativity, defined the ability of HS^- to donate a pair of electrons and form a covalent bond. H_2S can be a strong reductant with a two-electron reduction potential E° of -0.23 V at pH 7.0, similar to main redox couples. Under aerobic conditions, H_2S has a propensity for autoxidation, which enables the unfavourable thermodynamic reaction of H_2S and HS^- with O_2 . The oxidation of H_2S by O_2 can generate several sulfur species products and intermediates, in part, through the use of transition metal ions as catalysts. These sulfur species include, and are not limited to, polysulfide ions, sulfite (SO_3^{2-}), sulfate (SO_4^{2-}), thiosulfate ($S_2O_3^{2-}$), polysulfides (S_n^{2-} , $R-n \geq 2$) and elemental sulfur. Notably, inorganic polysulfides generated during H_2S oxidation could have biological effects (Filipovic *et al.*, 2018).

The term “ H_2S ” in this thesis denotes the gas and the mixture of species (H_2S and HS^-) in an aqueous solution unless otherwise specified.

1.5.2 Methods for H_2S measurement

As part of the growing interest in H_2S biological roles, the development of H_2S detection tools has rapidly expanded. In pure solutions, H_2S solutions can be diluted in buffer at pH ~ 9.6 , where the deprotonated and predominant form HS^- can be determined by absorbance at 230 nm (Filipovic *et al.*, 2018). However, in complex biological samples and mixtures, oxidation and other components such as labile sulfur compounds, iron-

sulfur clusters, acid-labile sulfur pools or sulfur-containing species can interfere in the estimation of H₂S concentration, with a variation from undetectable to >500 μM (Nagy *et al.*, 2014). An overview of the most widely used methods for H₂S detection is provided in Table 1-4.

Detection techniques such as gas chromatography and chemiluminescence have revealed relatively organ-dependent low basal levels of H₂S. In murine liver and brain, basal levels of H₂S were estimated between ~10-15 nM (Furne, Saeed and Levitt, 2008). Notably, H₂S levels in the aorta are significantly higher, ~1.5 μM (Levitt, Abdel-Rehim and Furne, 2011). The tissue-dependent concentration of H₂S is evident in vascular beds, where the endogenous production in rat aorta and mesenteric artery are inferior compared to the rat tail artery and ileum (Zhao, 2001). In healthy humans, plasma levels were found between 70-125 μM using a microfluidic technique described by Karunya and collaborators (Karunya *et al.*, 2019). The low steady-state tissue concentrations are primarily due to high rates of H₂S oxidation, as suggested by the significantly faster decay rates under aerobic conditions and dramatically decrease under hypoxic conditions in murine liver and brain (Vitvitsky, Kabil and Banerjee, 2012).

Table 1-4 Overview of Methods for detection of H₂S

Method	Detection Technique	Fundamental	Drawbacks	Reference
Methylene Blue method	The blue dye is detectable by spectrophotometric, chromatography or mass spectrometry (MS)	H ₂ S reacts with <i>N, N</i> -dimethyl- <i>p</i> -phenylenediamine and Fe ³⁺ in acidic conditions.	Low sensitivity, lack of specificity and cross-reactivity with other sulfur species.	(Mylon and Benoit, 2001; Small and Hintelmann, 2007)
Electrochemical Sensors	Ion-Selective electrodes measurement against a glass pH electrode	Silver sulfide membrane with S ²⁻ interaction results in potential change across the membrane.	Require long equilibrium time, presence of artefacts and high pH	(Searcy and Peterson, 2004)
	Polarographic sensors offering real-time monitoring by respirometer chamber	H ₂ S diffuses through the membrane, reducing potassium ferricyanide to ferrocyanide in an alkaline solution.	Easy leakage, presence of impurities.	(Doeller <i>et al.</i> , 2005)
Monobromobimane (MBB) Derivatization	Fluorogenic sulfide dibimane thiol measured by reversed-phase fluorescence HPLC or MS	Nucleophilic attack of H ₂ S on MBB to form substituted thiol	The relatively slow reaction rate	(Shen <i>et al.</i> , 2014)
Fluorescent Probes	Fluorogenic scaffold: rhodamine, dansyl or naphthalimide by microscopy, spectrophotometrically	H ₂ S-mediated reduction of an azide or nitro group to amines	Slow reaction rates and possible interferences of other thiols species	(Lin, Lippert and Chang, 2013; Lippert, 2014)
	Fluorogenic scaffold with bis-electrophilic centres: aldehyde and benzodithiolone or metal centres.	H ₂ S reaction with aldehyde and acrylate group. H ₂ S react with disulfide and attacks ester forming benzodithiolone. Copper-centred probes with H ₂ S affinity	Possibility of interferences	(C. Liu <i>et al.</i> , 2011; Sasakura <i>et al.</i> , 2011)
Gas Chromatography	Ion chromatography, chemiluminescence or through silver particles	With or without derivatisation of H ₂ S to bis(pentafluorobenzyl) sulfide into organic phase and analysis. Absorption of H ₂ S as Ag ₂ S through silver particles.	It required specialised and expensive equipment.	(Ishigami <i>et al.</i> , 2009; Islam <i>et al.</i> , 2021)

1.5.3 Endogenous Synthesis and Oxidation of H₂S

The intracellular H₂S concentration is maintained at a low steady-state through a balance between biogenesis and metabolism (Kabil and Banerjee, 2010). While enzymatic and non-enzymatic routes can form H₂S, the later pathway is underappreciated and involves less research (Kimura, 2014). The non-enzymatic routes, described in section 1.5.4.4, occur via the reduction of equivalents such as thiol-containing molecules from oxidative processes like oxidation of glucose or conversion of elemental sulfur (Figure 1.10) (Kolluru *et al.*, 2013; Yang *et al.*, 2019).

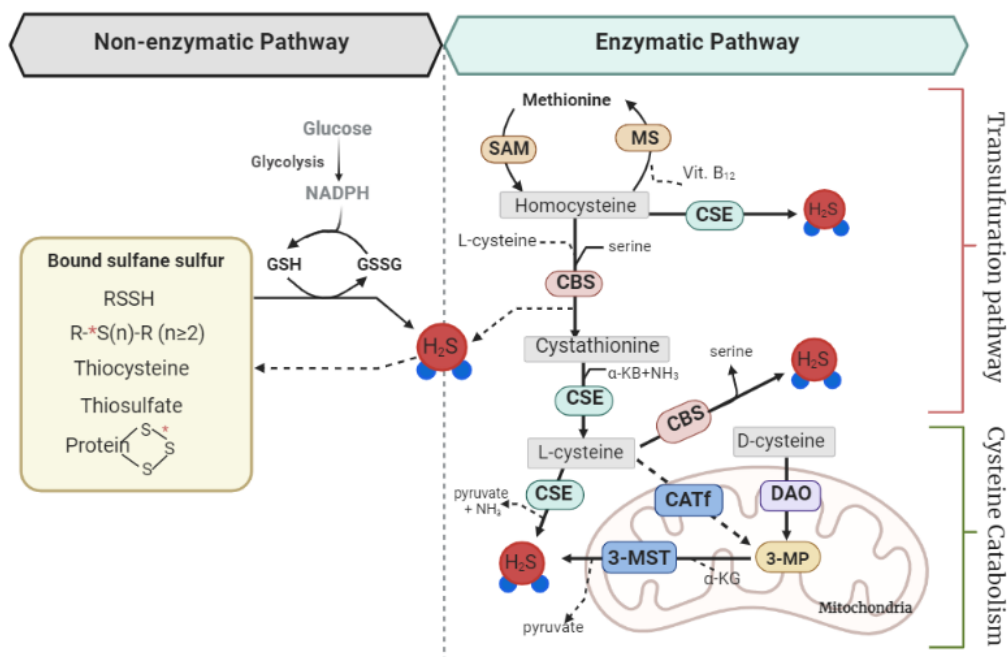


Figure 1.10 H₂S biosynthesis by enzymatic and non-enzymatic pathways.

The abbreviated enzymes involved in H₂S production are CBS, cystathionine β- synthase; CSE, cystathionine γ-lyase; 3-MST, 3-mercaptopyruvate sulfurtransferase; CATf, cysteine aminotransferase; DAO, D-amino acid oxidase; SAM, S-adenosylmethionine; MS, methionine synthase. Transsulfuration pathway and cysteine catabolism cofactors abbreviations: α-kB, α-ketoglutarate; 3-MP, 3-mercaptopyruvate; NH₃, ammonia. Created with Bio-render.com. Adapted from (Predmore, Lefer and Gojon, 2012).

1.5.4 Biogenesis of H₂S

In mammals, three enzymes have been found to have the capacity to synthesize H₂S, including cystathionine β-synthase (CBS), cystathionine γ-lyase (CSE, also known as CTH) and 3-mercaptopyruvate sulfurtransferase (3-MST, also known as MPST) (Wang, 2012; Bełtowski, 2019). The pyridoxal-5'-phosphate (PLP, metabolically active form of Vitamin B6)-dependent enzymes, CBS and CSE, form the transsulfuration pathways (canonical and reverse) and are mainly located in the cytosol (Kabil and Banerjee, 2010). The critical role of the transsulfuration pathway is the synthesis of cysteine (canonical pathway), which in turn results in a wide range of metabolic conversion, by-products and H₂S (Kabil and Banerjee, 2010). The third enzyme is the PLP-independent 3-MST which resides in both mitochondria and cytoplasm compartments and utilizes different enzymatic reactions to produce H₂S (Rudolph and Freeman, 2009).

1.5.4.1 Cystathionine β-synthase (CBS)

CBS was the first H₂S-producing enzyme to be identified and provided sulfur for the synthesis and catabolism of cysteine from the methionine cycle. (Munke *et al.*, 1988). The reaction cycle of CBS comprises the conversion of homocysteine and serine to cystathionine in a reaction subject to regulation by its allosteric binding activator, S-adenosylmethionine (SAM). Subsequently cleaved into cysteine and α-ketobutyrate by CSE activity. In addition, CBS can accept cysteine as a substrate to produce H₂S (Figure 1.10) (Renga, 2011). Regulation of CBS, like CSE, is based on substrate affinity and concentration, such as deficiency of vitamin B6 and homocysteine concentration (Gregory *et al.*, 2016). In mammals, the activity of CBS is mainly found in the brain and central nervous system (Robert *et al.*, 2003; Jhee and Kruger, 2005), preferentially expressed in the glia and astrocytes (Enokido *et al.*, 2005). Nevertheless, CBS can be expressed in other tissues, such as the liver, kidneys and lungs, but it might be rare and low (Kabil *et al.*, 2011; Madurga *et al.*, 2015).

1.5.4.2 Cystathionine γ-lyase (CSE)

CSE is considered the main H₂S-producing enzyme within the cardiovascular system, with high expression in the heart, vascular endothelium, liver, kidney, uterus, placenta and pancreatic islets (Kabil, Motl and Banerjee, 2014). The cytosolic location of CSE allows an array of catalytic reactions within the transsulfuration pathway, some of which

result in the generation of H₂S (Figure 1.10) (Yadav *et al.*, 2016). Notably, compartment-translocation of CSE depending on cellular needs has been reported. For instance, CSE can be translocated to the mitochondria under the regulation of Tom20, a mitochondrial protein import, in the mitochondrial membrane. Since the cysteine level inside mitochondria is about three times higher than in the cytosol, mitochondrial translocation of CSE elevates the production of H₂S (Fu *et al.*, 2012). The possible regulation of its activity appears from its ability to accommodate different substrates and thus habilitation for competition. The relevance of the CSE/H₂S pathway in the vasculature was described by using the CSE-null mice model. Firstly, the homozygous CSE model results in H₂S dropping by 80% in the aorta and heart and 50% in serum levels. Secondly, the CSE deficiency mutant developed age-dependent hypertension, and intravenously injection of an H₂S-releasing donor showed a reduction in systolic blood pressure (Yang *et al.*, 2008a). Impaired CSE expression and activity lead to impaired H₂S-mediated vasodilation and oxidative stress and contribute to the progression of cardiovascular conditions (Yang *et al.*, 2008b).

1.5.4.3 3-mercaptopyruvate sulfurtransferase (3-MST)

The third H₂S-producing enzyme is 3-MST, with predominant expression in the mitochondria. Unlike CBS and CSE, 3-MST H₂S formation comprises the cysteine catabolism pathway. 3-MST generates H₂S combined with cysteine aminotransferase (CATf) using L-cysteine and α -ketoglutarate as substrates in a 2-step manner. CATf converts these substrates into the intermediate 3-mercaptopyruvate (3-MP), creating a persulfidated form of 3-MST and pyruvate. The second half-reaction involves the reduction of persulfidated 3-MST in reductants such as Trx, which can subsequently liberate H₂S (Figure 1.10) (Coletta *et al.*, 2015). Unlike CBS and CSE, 3-MST is redox-state-dependent rather than transcriptional-dependent (Shibuya *et al.*, 2009). The active site cysteine (Cys²⁴⁸, Cys¹⁵⁴ and Cys²⁶³) is redox-sensitive and modified to cysteine sulfenate, which can lead to activity loss under oxidative stress (Nagahara and Katayama, 2005; Nagahara, 2013). The combined role of 3-MST and CATf has a growing interest in the CATf: MST axis for H₂S synthesis and cell metabolic rewiring (Predmore, Lefer and Gojon, 2012). Especially, H₂S synthesis through this pathway is highly dependent on GSH levels, interconnecting cysteine bioavailability for protein synthesis and cellular redox status (Bełtowski and Jamroz-Wiśniewska, 2014). The potential role of the 3-MST: CATf axis on ECs bioenergetics and metabolism has been recently reported through a 3-MST inhibition study (Abdollahi Govar *et al.*, 2020).

In addition, an alternative route for forming 3-MP has been recently reported, including a catalytic activity of a fourth enzyme, D-amino acid oxidase, using D-cysteine (DAO) and oxidation of D-cysteine. The location of this route is in peroxisomes inside mitochondrial fractions that generate 3-MP, which ultimately is yielded to H₂S through 3-MST activity in neurons and kidneys (Shibuya *et al.*, 2013) (Figure 1.10). This enzymatic pathway could offer some advantages in brain-conditions studies, as D-cysteine is a better substrate in the cerebellum than L-cysteine (Seki *et al.*, 2018). However, the regulation of the synthesis of H₂S via the DAO pathway is limited, except for a possible regulation involving Ca²⁺ flux (Filipovic *et al.*, 2018). Nevertheless, D-cysteine administration has been suggested as a therapeutic approach to delivering H₂S to specific tissues (Kimura, 2015).

1.5.4.4 Non-enzymatic generation of H₂S

Finally, the concentration of H₂S biogenesis is also determined by intracellular sulfur stores, representing a minor but relevant pool generation (Figure 1.10). In the mitochondria, the acid-labile sulfur pool releases H₂S under acidic conditions and usually forms iron-sulfur complexes (Fe-S) (Kolluru *et al.*, 2013). The second endogenous H₂S sulfur pool, bound sulfide, is localized in the external nuclear membrane and contributes to H₂S generation under reducing reaction (Wang, 2012). The existing forms of bound sulfide include polysulfides (RSSH), thiosulfate (S₂O₃²⁻), elemental sulfur (S⁰) or polysulfides (RS(Sn)SR) (Kimura, 2015). A well-known process for H₂S generation involves thiosulfate via glutathione-dependent reduction, which mediates signalling mechanisms in vascular cells (Leskova *et al.*, 2017).

1.5.5 Oxidation of H₂S

As a toxic molecule at high concentrations, accumulation of H₂S would harm the cell, tissue, and organs (through its inhibition of Complex IV in the mitochondria); thus, tightly regulated oxidation is required (Abou-Hamdan *et al.*, 2015). Therefore, the intracellular H₂S rate is maintained at a low steady state by balancing biogenesis and catabolism. The most efficient known mechanisms of H₂S within mammalian cells comprise mitochondria, where H₂S is oxidised to thiosulfate (S₂O₃²⁻) or sulfate (SO₄²⁻) (Picton *et al.*, 2002). The clearance of H₂S begins in the mitochondrial matrix and is completed in the inter-mitochondrial membrane space (Figure 1.11 A) (Picton *et al.*, 2002; Caliendo *et al.*, 2010a).

In the mitochondrial matrix, oxidation involves a cluster of mitochondrial enzymes, otherwise known as sulfide oxidation unit (SOU), that consists of sulfide quinone oxidoreductase (SQR), ethylmalonic encephalopathy 1 (ETHE1) thiosulfate sulfurtransferase (TST, also known as Rhodanese, (Rho)) and sulfite oxidase (SO). SQR mediates the first step of H₂S oxidation to either a sulfane sulfur (S⁰) or by forming a persulfide (R-SSH) (Szabo *et al.*, 2014; Marutani and Ichinose, 2020). SQR is a membrane-bound protein expressed on mitochondrial matrix, with two redox centres, an active site trisulfide and a FAD cofactor, which allow it to fuel two-electrons transport to CoQ and into the ETC via complex III and complex IV (Cherney *et al.*, 2010; Abou-Hamdan *et al.*, 2015). The sulfur-bound persulfide is then transferred to an endogenous sulfur acceptor such as GSH or sulfite (SO₃²⁻) (Picton *et al.*, 2002). Depending on which acceptor is employed, GSSH or thiosulfate can be yielded (Hildebrandt and Grieshaber, 2008). The formed GSSH can be further oxidised to sulfite by mitochondrial matrix ETHE1. Subsequently, in the mitochondrial intermembrane space, sulfite can either be oxidized to form sulfate or reduced to generate thiosulfate by sulfite oxidase SO and TST, respectively (Kabil and Banerjee, 2014). Thus, most H₂S is finally excreted as sulfate or is metabolised through the urine (Benchoam *et al.*, 2019).

Apart from oxidation, H₂S can also be catabolized through methylation. This cytosolic process yields methanethiol that can be further methylated to dimethyl sulfide (non-toxic compound) via thiol S-methyltransferase enzyme (TSMT) (Donnarumma, Trivedi and Lefer, 2017). Metabolically, dimethyl sulfide is a substrate for TST forming thiocyanate (SCN⁻) and sulfate, the major end-product of H₂S clearance (Levitt *et al.*, 1999).

Alternative H₂S catabolism pathways include H₂S scavenging by metalloproteins such as methemoglobin, forming sulfhemoglobin or disulfides such as GSSG (Figure 1.11 B) (Kimura, 2013), as evidence of the abolished antiproliferative effect of exogenous H₂S in HEK-293 cells in the presence of methemoglobin treatment (Yang *et al.*, 2004).

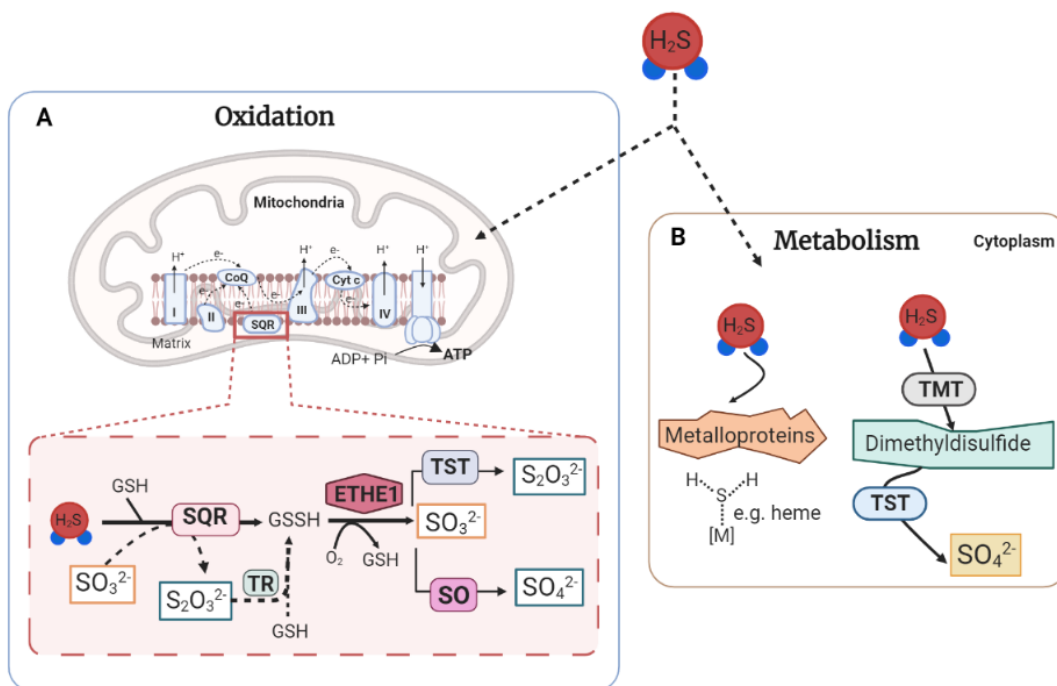


Figure 1.11 Schematic representation of H₂S oxidation and metabolism.

(A) The mitochondrial electron transport chain comprises four complexes designated I through V and transport e⁻. It creates a proton motive force, which is used by ATP synthase to ATP as an energetic outcome. Mitochondrial oxidation of H₂S via electron donation occurs at the CoQ level, forming thiosulfate (S₂O₃²⁻), sulfite (SO₃²⁻) and sulfate (SO₄²⁻). In the mitochondrial matrix, SQR oxidizes H₂S using sulfite and GSH as electron acceptors, forming thiosulfate or GSSH. The enzymatic action of TR can convert thiosulfate to GSSH. Moreover, ETHE1 oxidizes GSSH to sulfite, which is further oxidized to sulfate and thiosulfate by SO and TST, respectively. **(B)** Cytoplasmic H₂S metabolism can also occur via methylation or reaction with metalloproteins (e.g. containing heme centre). H₂S is converted into dimethylidissulfide via TMT. TST further metabolizes Dimethylidissulfide to generate sulfate, which is excreted through urine. Created with Bio-render.com. (Adapted from Murphy et al, 2019).

1.6 H₂S Donors and Inhibitors

As part of the growing interest in H₂S and its biological functions, a wide range of subtype donors have been designed and have become increasingly important in understanding the underlying mechanisms of actions and tasks of H₂S. On the other hand, due to this wide variability of available donors and the different releasing mechanisms mediated, conflicting results have arisen in the literature. In addition, this section provided a brief overview of the types and subtypes of H₂S-releasing compounds and some characteristic features (Y. Zheng *et al.*, 2015).

1.6.1 Natural Donors

Allium vegetables, such as garlic and onion, have been recognized for years as natural products with beneficial effects. To date, organosulfur compounds from garlic release H₂S upon thiol or GSH reaction, generating low molecular weight persulfides. Garlic contains γ -glutamyl-S-allyl-L-cysteine and S-allyl-L-cysteine sulfoxides. Some of the subtypes of organosulfur agents include diallyl sulfide (DAS) (Ho *et al.*, 2012) and diallyl disulfide (DADS) (Caro *et al.*, 2012), and diallyl trisulfide (DATS) (Figure 1.12 A) (Hayashida *et al.*, 2017). However, DADS have been reported to induce mitochondrial dysfunction in mouse liver via impaired mitochondrial membrane potential ($\Delta\psi_m$) and depletion of GSH (Caro *et al.*, 2012). In contrast, DATS administration inhibited apoptosis in high-glucose-induced ED via decreased mitochondrial ROS (Caro *et al.*, 2012). Shift toward sulfane sulfur compounds (e.g., polysulfides and persulfides) derived from H₂S have been proposed as crucial modulators of garlic-derived compounds' effects (Benchoam *et al.*, 2019).

1.6.2 Sulfide Salts

Sulfide-containing salts such as sodium hydrogen sulfide (NaHS) and disodium sulfide (Na₂S) are the standard options for exogenous H₂S-releasing agents. In their hydrated forms, these salts have been used for decades as H₂S equivalents to investigate the therapeutic potential of exogenous H₂S delivery (Figure 1.12 C). These sulfide salts are immediately hydrolysed to give H₂S (Chen *et al.*, 2009). These donors have displayed cytoprotective actions in vascular models through direct modulation of mitochondrial biogenesis and function (Elrod *et al.*, 2007; Suzuki *et al.*, 2011; Untereiner *et al.*, 2016). However, using these H₂S-releasing agents can carry certain disadvantages, from inaccurate concentration to the inability to mimic low endogenous concentrations of H₂S. Notably, these agents can be helpful for proof-of-concept signalling studies (Y. Zheng *et al.*, 2015).

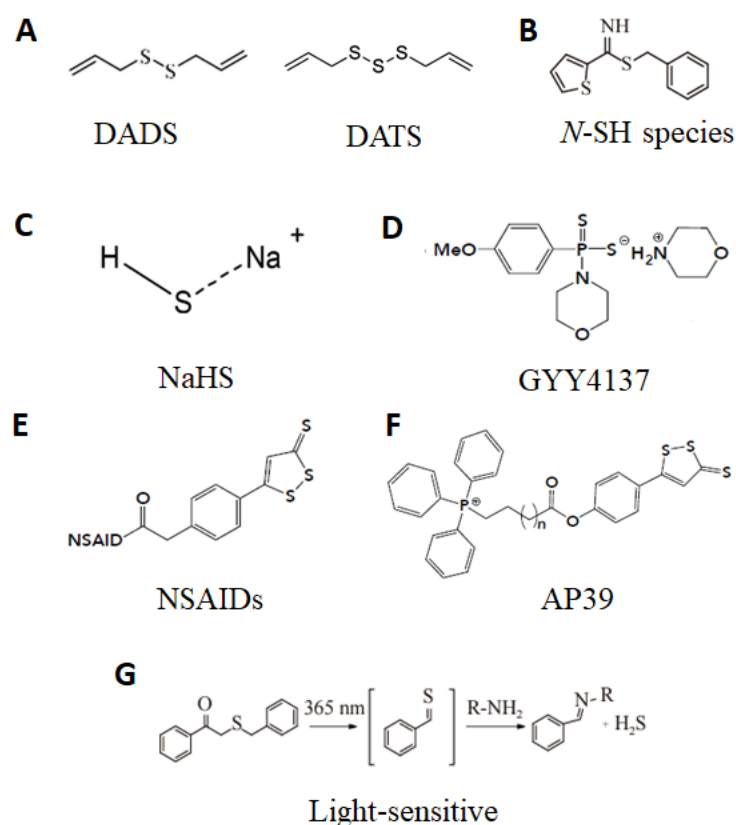


Figure 1.12 Chemical structures of several H₂S donors.

(A) Garlic-derived molecules such as diallyl disulfide (DADS) and diallyl trisulfide (DATS) generate H₂S upon reaction with GSH. (B) Thiol-activated donors release controlled H₂S rates such as N-(benzoylthiol) benzamides. (C) Sulfide salts, in their hydrated forms, including hydrogen sulfide (NaSH·xH₂O), are among the most common types of H₂S donors. (D) A water-soluble derivate of Lawesson's reagent, GYY4137, releases H₂S hydrolysis. (E, F) Hydrolysis-triggered H₂S donors, dithiolethiones can be conjugated to non-steroidal anti-inflammatory drugs (NSAIDs) or mitochondrial anchors, AP39. (G) Light-sensitive triggered compounds also release H₂S.

1.6.3 Synthetic H₂S donors

The creation of synthetic H₂S donors appears due to the demand to recreate physiological H₂S production. In contrast to sulfide salts, artificial donors can exhibit a slow(er)-release rate of H₂S. This type of agent can be subdivided into (i) thiol-triggered release, (ii) hydrolysis-triggered release, and (iii) alternative-releasing agents (Y. Zheng *et al.*, 2015).

1.6.3.1 Thiol-triggered H₂S release

The elevated presence of thiols within the cells makes possible the design of thiol-triggered agents that release H₂S through thiol exchange following nucleophilic addition. For instance, one of the first donors was N-(benzoylthio)benzamides with an N-mercapto template with the release of the gasotransmitters in the presence of thiols such as GSH (Figure 1.12 B). In addition, perthiol-based donors with an acyl group enhance stability and H₂S-release capacity. Notably, both donors may create mixed disulfides, which can interfere with cell signalling (Filipovic *et al.*, 2018).

1.6.3.2 Hydrolysis-triggered H₂S release

Compounds such as Lawesson's reagent (2,4-bis(4-methoxyphenyl)-1,3,2,4-dithiadiphosphetane-2,4-disulfide) are known to reach H₂S release by spontaneous hydrolysis in aqueous solutions. However, the insolubility of the agent and uncontrolled hydrolysis limits its applications. On the contrary, one of the most commonly used commercially available H₂S donors is a derivative of Lawesson's reagent, known as morpholin-4-ium 4-methoxyphenyl(morpholino) phosphine-dithioate (GYY4137) (Figure 1.12 D). This easy-handling H₂S-releasing agent is a water-soluble donor that offers a slow release (pH- and temperature-dependent), mimicking endogenous H₂S content (Wei Lee *et al.*, 2011). In the vascular endothelium, GYY4137 can protect against ED and mitochondrial dysfunction in a wide range of *in vitro* and *in vivo* models, including ischaemia/reperfusion (I/R) (Qiu *et al.*, 2018), atherosclerosis (Liu *et al.*, 2013), lung injury (Vadivel *et al.*, 2014) and hypertension (Al-Magableh *et al.*, 2014).

Furthermore, dithiolethiones are another subtype of hydrolysis-releasing H₂S donor, in which the H₂S-releasing moiety is conjugated to pharmacologically active components such as non-steroidal anti-inflammatory drugs (NSAIDs) (Figure 1.12 E). ADTOH or triphenylphosphonium cation (TPP⁺) as mitochondrial anchors (Caliendo *et al.*, 2010b). One of the most common and well-known mitochondrial-targeted H₂S donors is AP39, which exhibits release content at a nanomolar level and organelle specificity (Figure 1.12 F) (Geró *et al.*, 2016). AP39 improved mitochondrial function in glucose oxidase-induced oxidative stress in ECs and restored vascular homeostasis (Szczesny *et al.*, 2014).

Both donors have been observed to decrease hyperpolarization of the $\Delta\psi_m$ and inhibit mitochondrial oxidant production whilst increasing the electron transport at complex III, thus improving cellular metabolism (Gerő *et al.*, 2016). Recently, the CSE-generating H₂S pathway in endothelial mitochondrial bioenergetic was restored by MZe786, an ADTOH H₂S donor linked with aspirin in mice with increased expression of soluble Fms-like tyrosine kinase 1 (sFlt-1) (Sanchez-Aranguren, Ahmad, *et al.*, 2020). Dithiolethiones can be conjugated to diclofenac to create HS-NSAID-hybrid ATB-337 and analogous such as ATP-429 and ATB-346. Notably, the latter compound is currently under phase 2 clinical trial for gastrointestinal conditions as an anti-inflammatory drug (Wallace *et al.*, 2020).

1.6.4 Other H₂S donors

In addition to those widely used subtypes, several prodrugs that can release H₂S in the presence of triggers, such as enzymes, pH, and UV light, have been designed. For instance, Xian and colleagues identified a gem-dithiol with a phot-cleavable structure added, and these molecules release H₂S under UV irradiation (365 nm) (Figure 1.12 G) (Xiao *et al.*, 2017). A novel prodrug, SG-1002, a polysulfur mixture, has been shown to release H₂S and promote H₂S bioavailability in heart failure patients (Polhemus *et al.*, 2015). In a murine model with induced transverse aortic constriction, SG1002 preserved cardiac function following the activation of VEGF-Akt-eNOS-NO-cGMP signalling pathways (Kondo *et al.*, 2013). However, although several studies have reported the protective effects of SG-1002 as an H₂S-releasing drug, the release mechanism has not been described (Polhemus *et al.*, 2015). In addition, elimination-based ROS-sensitive, esterase-sensitive or cysteine-sensitive prodrugs have been developed to allow more specific mechanisms (Zhao and Pluth, 2016; Zhao, Steiger and Pluth, 2018; Bakalarz *et al.*, 2021). Interestingly, the organosulfur compound methylsulfonylmethane (MSM)-releasing H₂S compound has been used as a dietary supplement (Butawan, Benjamin and Bloomer, 2017).

1.6.5 Inhibitors of H₂S

The enzymatic production of H₂S has encouraged the development of specific blockers for H₂S-producing enzymes. This category includes propargylglycine (PPG), an antibiotic which inhibits CSE irreversibly (Yang, Sun and Wang, 2004). The activity of CBS can be suppressed by hydroxylamine and aminooxyacetate (AOA) (Kimura, 2002). In addition, currently available, there are endogenous inducers of H₂S-generating enzymes, including SAM, epidermal growth factors, s-nitroso-N-acetylpenicillamine (SNAP) or microRNAs-21 (Enokido *et al.*, 2005; Jhee and Kruger, 2005; Patel *et al.*, 2009; Yang *et al.*, 2011). Recently, it was reported that the administration of SAM could potentially inhibit vascular endothelial growth factor-A-related diseases induced by adverse effects of long-term treatment of levodopa (L-dopa) (Yan *et al.*, 2020).

1.7 Physiological Effects of H₂S

Since its discovery as an endogenous biological modulator in the brain (neuromodulator) by controlling synaptic plasticity, the evidence relating to its role as a physiological mediator has grown exponentially, with a wide range of effects in different systems, tissues and conditions (Predmore, Lefer and Gojon, 2012). Based on the chemical reactivity of H₂S, its mechanisms of action can be categorized into distinct groups: (i) crosstalk and scavenging ROS/RNS, (ii) binding to and redox reactions with metal centres, and (iii) oxidative post-translational modification of protein cysteines, referred as S-sulfhydration (Bindu D Paul and Snyder, 2015b). The post-translational signalling modification of proteins by H₂S is further explored in section 1.8.

1.7.1 H₂S and metal centres interaction

The interaction of H₂S (or HS⁻) with a metal centre may go through a coordination reaction, reduction of metal centre, or modify heme porphyrin covalently. A classical and well-known metal interaction with H₂S comprises mitochondrial ETC. At a low level, H₂S reduces ferric heme a₃, which promotes oxygen binding and thus serves as a substrate for mitochondrial ETC (Módis *et al.*, 2013). However, in the presence of H₂S excess, HS⁻ binds the ferric heme a₃ and Cu_B, thereby inhibiting the enzymatic activity of complex IV (Collman *et al.*, 2009). An alternative covalent reaction is between H₂S and ferric haemoglobin, which forms stable complexes (Kraus and Wittenberg, 1990).

Furthermore, H₂S oxidation can be mediated by metalloproteins, oxidising H₂S to thiosulfate (Mustafa, Gadalla and Snyder, 2009).

1.7.2 Interaction of H₂S with oxidants

Chemically, an -2 oxidation state of sulfur only allows an oxidation reaction forming sulfate, sulfite, thiosulfate, persulfides, elemental sulfur and polysulfides (Cuevasanta, Möller and Alvarez, 2017). H₂S can react with H₂O₂, with HSOH as the primary product. Peroxynitrite and H₂S reactions exhibit higher complexity involving nucleophilic substitution on peroxynitrous acid (ONOOH), giving HSOH and NO₂⁻. Subsequently, HSOH can further react with H₂S to yield HSS⁻/HSSH. Elevated content of H₂S alongside reaction with hypochlorous acid leads to elemental sulfur and polysulfides. The one-electron reduction potential of H₂S determines that only strong oxidants such as •OH can oxidise H₂S to sulfiyl radical (HS•/S•⁻). In addition, sulfiyl radicals can further react with O₂ to form SO₂⁻ that can further react with O₂ forming superoxide (Benchoam *et al.*, 2019).

Several studies have shown the ability of H₂S to scavenge ROS and RNS, like O₂⁻, in the brain and peripheral tissues (Bindu D Paul and Snyder, 2015b). However, its capacity to serve as an antioxidant is questionable due to its physiologic concentration at the sub-micromolar rate *in vivo* (Furne, Saeed and Levitt, 2008), the dependency on kinetic factors and the inability to reach adequate speed in biological contexts to support the scavenging roles. To date, evidence has concluded that scavenger of oxidants in biological systems exhibited by H₂S is more likely due to indirect effects on enzymes, transports or other targets rather than direct scavenging function (Filipovic *et al.*, 2018).

1.8 Protein S-Sulfhydration

In biological systems, chemical reactions maintain homeostasis, of which sulfur-centred chemistry is essential, and the amino acid Cys may exhibit a wide range of redox modifications. However, due to their ideally suited chemical reactivity, sensitivity and oxidation, Cys can be targeted directly in biological macromolecules, which serve as covalent modifications (Chung *et al.*, 2013). Oxidate reversible modifications of thiol groups (-SH) can be used in cellular signalling, including S-nitrosylation, S-glutathionylation, S-Sulfenylation and S-Sulfhydration (also known as persulfidation) (Figure 1.13) (Filipovic, 2015). The third mechanism mediated by H₂S that explains its

pleiotropic biological effects, S-sulfhydration, has received the attention of researchers. However, the mechanism(s) and actual physiological outcomes of biological targets affected by S-sulfhydration remain unclear.

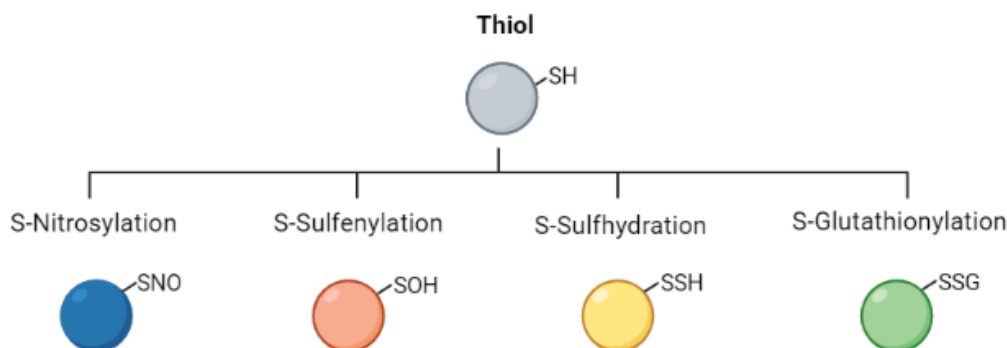


Figure 1.13 Reversible Post-translational modifications of cysteine.

1.9 Properties of Sulfhydration

This reversible covalent modification of cysteine residues with low pKa involves the conversion of free thiol group (–SH) into persulfide groups (–SSH) (Bindu D Paul and Snyder, 2015a). Thermodynamically unfavourable, H₂S cannot directly modify cysteine residues to form persulfides because both sulfur oxidation states are the same (Reaction 3).



The reaction requires prior oxidation of the thiol group to disulfide/sulfenic acid or oxidation of H₂S to polysulfides (H₂Sn) (Kimura, 2015). In addition, several enzymes involved in Cys metabolism have been reported to form persulfides in their catalytic cycle or form low molecular weight persulfides through transsulfuration reactions. For instance, the mitochondrial 3-MST enzyme forms an intermediate Cys-SSH and pyruvate through the catalysis of 3-MP. Nucleophilic sulfur of Cys-SSH will be transferred to a nucleophilic acceptor such as Trx (Abdollahi Govar *et al.*, 2020).

Several research groups highlighted polysulfide action (a bound sulfur species) as the intermediate species in H₂S-induced protein thiol modification (Yuan *et al.*, 2016) (Greiner *et al.*, 2013). In addition, polysulfides have been reported to oxidize thiols and may produce HS⁻ or persulfide by reacting with the -SH group of proteins (Benchoam *et al.*, 2019). However, the exact chemical mechanism of action of H₂S is far from clear and remains controversial (Ju *et al.*, 2017). From a chemical point of view, the persulfide group (R-SSH) carries two sulfur atoms of distinct properties. While the inner sulfur is considered sulfane sulfur with an oxidation state of 0 and becomes a target for nucleophilic attack, the outer sulfur has an oxidation state of -1, making it nucleophilic and attack electrophilic (Figure 1.14) (Filipovic, 2015).

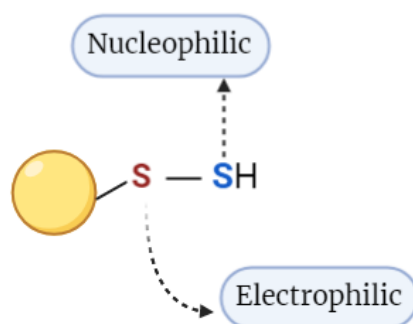


Figure 1.14 Properties of persulfide sulfur atoms in cysteine.

The inner sulfur is slightly electrophilic and thus could accept an electron pair. In contrast, the outer sulfur is nucleophilic and attacks electrophile

At physiological pH conditions, R-SSH exists predominantly in the anionic form, R-SS⁻. As a strong nucleophile, persulfides react with 1- and 2-electron oxidants (Filipovic *et al.*, 2018). The nucleophilic attack of HS⁻ anion to -SH groups can involve a series of proposed reactions, illustrated in Figure 1.15 (Iciek *et al.*, 2016). Moreover, the reversibility of persulfides sustains the idea that S-sulfhydration of thiols can prevent irreversible Cys over-oxidation (Sue, Ho and Kim, 2005). Sulfhydration is considered to be a reversible post-translational modification. It has been postulated that the Trx/TrxRD system can enzymatically reduce persulfides. The disulfide bond in Trx undergoes a 2-electron reduction and regenerates reduced Trx by TrxRD (Dóka *et al.*, 2016). Interestingly, an *in vitro* study reported that Trx has higher efficiency at reducing Cys-SSH on protein tyrosine phosphatases (PTPs) in HEK-293 cells than other reducing agents (Krishnan *et al.*, 2011).

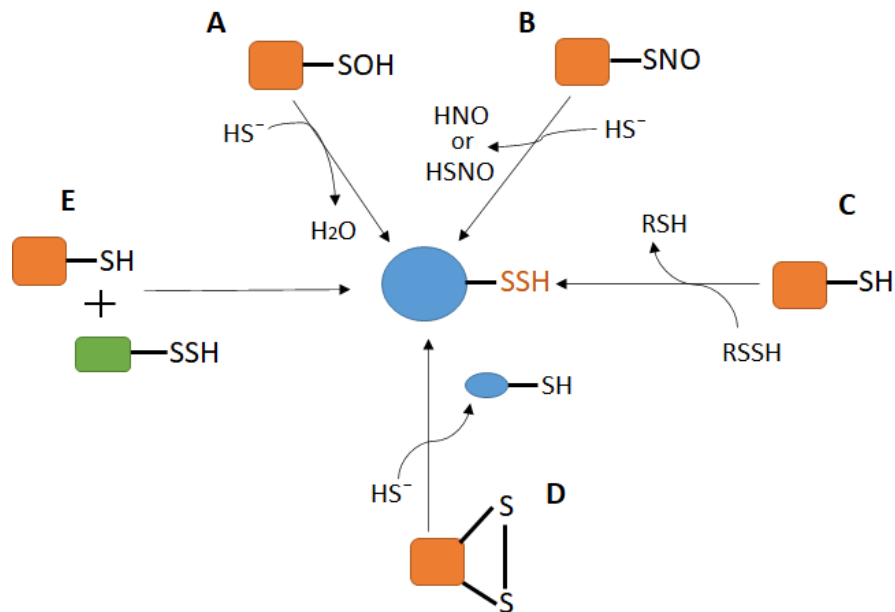


Figure 1.15 Proposed reactions for S-sulfhydrated proteins by H₂S.

At physiological pH, formation processes to form -SSH takes place. **(A)** Hydrosulfide anion (HS^-) reacts with sulfenic acids for sulfhydration thiol modification. **(B)** HS^- can interact with S-nitrosated to form sulfhydration conversion. **(C)** Persulfides can be a carrier of sulfhydration and act as the processes of displacement reactions. **(D)** Interaction with cysteine disulfides (-S-S) for sulfhydration formation. **(E)** Persulfides of small protein and protein thiol could serve to produce protein persulfide.

1.10 Involvement of H₂S in vascular diseases

S-sulfhydration could change the original function of proteins, serving as essential switches or regulators in many physiological and pathophysiological processes (Predmore, Lefer and Gojon, 2012). Comparative S-sulfhydration with other post-translational modifications, such as S-nitrosylation, has revealed some particularities of the former mechanism.

For instance, while 10-25% glyceraldehyde 3-phosphate dehydrogenase (GAPDH), β -tubulin and actin were S-sulfhydrated in rodents, S-nitrosylation of targeted proteins only is accountable for 1-2% (Mustafa *et al.*, 2009). Furthermore, S-sulfhydration usually increases the modified protein's activity in contrast to S-nitrosylation, which appears to abolish protein catalytic activity, as exemplified by GAPDH studies (Hara *et al.*, 2005).

In the vasculature, proteomic analysis has revealed that endothelial cells “S-sulfhydryl” comprise around 3446 individual cysteine residues in 1591 proteins, of which cytosolic proteins were highly S-sulfhydrated (Bibli *et al.*, 2021). Below is a brief overview of the biological effects controlled by sulfhydration of specific vascular-related proteins.

ED is ubiquitously observed in multiple vascular disorders in arteries and small vessels. It is known that H₂S contributes to vascular protection, as exemplified by the association of reduced H₂S plasma levels with many pathological conditions such as stroke (Dou, Wang and Chen, 2016), diabetes (Jain *et al.*, 2010), pulmonary hypertension (Sun *et al.*, 2014), chronic obstructive pulmonary disease (Chen *et al.*, 2005) and age-related diseases (Hou *et al.*, 2016). Over the last decade, increasing evidence has demonstrated that H₂S is essential in maintaining cardiovascular homeostasis. *In vivo* studies showed that disrupted CSE/H₂S pathway leads to enhanced atherosclerosis and ED (Wang *et al.*, 2017). Administration of H₂S donors or manipulating endogenous H₂S production can improve cardiovascular function and disease outcomes in various animal CVD models, including atherosclerosis, heart failure and myocardial infarction. The beneficial effects of H₂S are mediated through its role in anti-inflammation, anti-apoptosis, anti-oxidative stress and proangiogenic (Wang *et al.*, 2009).

Atherosclerosis is a leading risk factor for CVD, narrowing and hardening arteries due to fatty plaque formation in the artery wall. Notably, H₂S has been investigated as an attractive therapeutic option against atherosclerosis. In an ApoE^{-/-} murine atherosclerotic experimental model, lower H₂S levels and CSE expressions were reported. These *in vivo* disturbances were significantly abolished by exogenous H₂S administration (Zhang *et al.*, 2012). In addition, oxidative stress-induced mitochondrial dysfunction in vascular cells is considered to play a role in the pathogenesis of atherosclerosis. Excessive O₂⁻ production by mitochondria can trigger a pro-inflammatory response and, ultimately, atherosclerosis development (Marzetti *et al.*, 2009; Sena and Chandel, 2012).

ED plays a vital role in the pathogenesis of diabetic complications such as vascular dysfunction, nephropathy, retinopathy, neuropathy and cardiomyopathy. Plasma levels of H₂S were significantly decreased in patients with type 2 diabetes (~100 μM) compared with age-matched normal subjects (~130 μM) (Jain *et al.*, 2010). *In vivo* and *in vitro* models showed that H₂S could improve diabetes-related complications by inhibiting mitochondrial oxidative stress (Wei *et al.*, 2014; Greaney *et al.*, 2017; Ng *et al.*, 2017).

Lower plasma levels of H₂S have also been reported in hypertensive disorders. These findings are further supported by evidence showing reduced endogenous H₂S pathways in hypertensive patients (Greaney *et al.*, 2017). Many authors have explored the role of the CSE/H₂S pathway through H₂S donors to prevent and/or treat hypertension. Intraperitoneal injections of GYY4137 reversed pulmonary hypertension in rats and demonstrated that H₂S suppress oxidative stress by enhancing the activity of intracellular antioxidants such as SOD and CAT (Li *et al.*, 2019). The molecular mechanisms associated with improved mitochondrial protection upon exogenous H₂S were also demonstrated in HUVECs exposed to a high salt environment. This study showed that exogenous H₂S inhibited apoptosis, O₂⁻ production, and cyto c release restored Δψ_m (Zong *et al.*, 2015).

1.11 Research Hypothesis and Aims

As outlined in the preceding section, ED comprises a complex phenotype with oxidative stress, inflammation and apoptosis as the predominant factors (Deanfield, Halcox and Rabelink, 2007). Due to the localisation of the endothelium and pleiotropic functions of ECs, dysfunctional endothelial phenotype has been implicated in the genesis of pathologies such as atherosclerosis, metabolic disorders, ageing and preeclampsia (Bonetti, Lerman and Lerman, 2003; Young, Levine and Karumanchi, 2010; Shenouda *et al.*, 2011; Park *et al.*, 2018). Usually, ED-associated pathologies exhibit impaired mitochondrial function (Doughan, Harrison and Dikalov, 2008; Tang *et al.*, 2014), contributing to the progression of vascular damage (Shenouda *et al.*, 2011). H₂S has emerged as a beneficial biological mediator in the vasculature through the modulation of ECs functions (Yang *et al.*, 2008b). Given that reduced H₂S plasma content has been shown in vascular-related complications (Sun *et al.*, 2007) and that novel H₂S prodrugs are being evaluated in clinical trials against inflammation-related conditions (Wallace *et al.*, 2018), the present study hypothesised that H₂S might exert value as a therapeutic strategy for ED.

Research Aims:

1. To use endothelial *in vitro* model to establish and validate dysfunctional phenotype induced by TNF- α and to create an experimental design employing TNF- α and slow-releasing H₂S donor, GYY4137.
2. To determine the role of GYY4137 in reversing the TNF- α -induced ED cellular markers and its action on mitochondria function.
3. To elucidate the mechanism of S-sulfhydration *in vitro*, and the role of S-sulfhydrated proteins in ED.

2 Materials and Methods

This chapter details the cell culture procedure and molecular and biological methods involved in this research to assess endothelial function.

2.1 Materials

A complete list of consumables, including equipment, software, commercial kits and reagents with their corresponding reference numerals, are shown in Appendix a.

2.2 Cell Culture

In this thesis, two cell lines were used to address the objectives; immortalised EA.hy926 cells and primary HUVECs were used in experimental settings to test endothelial functions.

2.2.1 Cell Lines

Human **EA.hy926** cells, an umbilical vein immortalised endothelial cells line obtained from American Type Culture Collection (ATCC) (Edgell *et al.*, 1990), routinely maintained in cDMEM media for cellular maintenance (Table 2-1). This cell line has been generated by the fusion of primary human umbilical vein endothelial cells (HUVECs) with A549 (a human lung carcinoma cell line) (Lieber *et al.*, 1976).

Human primary umbilical vein endothelial cells, **HUVECs**, were obtained from PromoCell (Jaffe *et al.*, 1973) and maintained in cEGM media (Table 2-1). Primary cells like HUVECs have an average life span of 10 serial passages, which implies that no long-term *in vitro* experiments can be performed. Therefore, the behaviour of primary ECs strongly differs depending on their different donor origin.

2.2.2 Cell culture media and solutions

As in this thesis, two ECs models were used as a specific medium for growth, maintenance, passaging and treatment, which can be found in their precise content details below Table 2-1.

Table 2-1. Cell culture media

EA.hy926				
Medium	Culture Purpose	Medium Type	Medium Content	Medium Supplement
cDMEM	Cellular Growth	Dulbecco's Modified Eagle's Medium	high glucose, L- glutamine, sodium bicarbonate and without sodium pyruvate	FBS up to a final concentration of 10% (v/v) and penicillin (100 µg/ml)/ streptomycin (100 µg/ml) solution to a 1% (v/v) final concentration
cM199	Cellular Treatment and Neutralise trypsin-EDTA	Medium 199	Earle's BSS, L- glutamine, 25 mM HEPES and 2.2 g/L sodium bicarbonate	FBS up to a final concentration of 10% (v/v) and penicillin (100 µg/ml)/ streptomycin (100 µg/ml) solution to a 1% (v/v) final concentration
HUVECs				
cEGM	Cellular Growth and Cellular Treatment	Endothelial Cell Growth Medium 2	fetal calf serum, 0.02 ml/ml; epidermal growth factor, 5 ng/ml; basic fibroblast growth factor, 10 ng/ml; insulin-like growth factor, 20 ng/ml; vascular endothelial growth factor 165, 0.5 ng/ml; ascorbic acid, 1 µg/ml; heparin, 22.5 µg/ml and hydrocortisone, 0.2 µg/ml.	penicillin (100 µg/ml)/ streptomycin (100 µg/ml) solution to a 1% (v/v) final concentration.
nM199	Neutralise trypsin-EDTA	Media 199	Earle's BSS, L- glutamine, 25 mm HEPES and 2.2 g/L NaHCO ₃	FBS up to a final concentration of 20% (v/v), penicillin (100 µg/ml)/ streptomycin (100 µg/ml) solution to a 1% (v/v) final concentration

2.2.3 Cell culture maintenance

EA.hy926 cells and HUVECs were routinely cultured in 75 cm² (T75) flasks in a humidified environment at 37°C with 5% carbon dioxide (CO₂) as standard conditions. Immortalised and primary ECs were incubated until they reached 80-90% confluence, at which point they were passaged inside a laminar flow hood [Envair Lab-VCS2-4, Lancashire, UK] under sterile conditions. For experimental settings, cells were used up to passage 40 for EA.hy926; and up to passage 4 for HUVECs. The basal growth medium for each cell type was changed every 48 hours until the desired confluency was obtained.

Seeding or passaging actions were performed after detached endothelial adherent cells by adding 0.05% trypsin-EDTA (2 ml) [Sigma-Aldrich, Gillingham, UK] and incubating for 3 minutes at 37°C with 5% CO₂. Neutralisation of trypsin-EDTA was carried out with specific media for each cell type. Briefly, 10 ml of fresh pre-warm cDMEM and nM199 medium were added for EA.hy926 and HUVECs, respectively. The content was transferred into a 15 ml Falcon cell culture tube [Eppendorf #5702, Hamburg, Germany] and centrifuged at 200 x g for 6 minutes. The supernatant was discarded, and the cell pellet was resuspended into fresh warm cDMEM or cEGM medium for EA.hy926 cells and HUVECs, respectively.

2.2.4 Cell counting

Trypan blue [Thermo Fisher Scientific, Loughborough, UK] is a diazo dye that, due to its inability to cross intact cell membranes, allows selective staining of dead or dying cells, allowing distinction from live cells (Tennant, 1964). The endothelial cell suspension was diluted with trypan blue (dilution factor:2), and cells were carefully mixed before loading 10 µl of the cell suspension onto a Neubauer hemocytometer chamber and counted. The seeding of cells was carried out under aseptic conditions inside a laminar flow hood, using a wide range of cell culture plates and dishes based on the experimental settings and assay to be performed. The size of dishes and cell culture plates used, along with valuable numbers such as surface area and medium volume, are given in Table 2-2.

Table 2-2. Cell culture seeding numbers.

	Surface area (cm ²)	Seeding (cell/well)	Growth medium
Dishes			
60 mm	21.5	2.5x10 ⁵	3 to 5 ml
100 mm	56.7	3.5x10 ⁵	6 to 8 ml
Culture plates			
96-well	0.32	1.5x10 ⁴	100 to 200 µl
24-well	1.9	5x10 ⁴	500 µl to 1ml
6-well plate	9.6	2.0x10 ⁵	1 to 2 ml

2.2.5 Freezing the cells

Healthy cells were subjected to freezing in liquid nitrogen to be stored for long periods. Briefly, cells were pelleted by centrifugation (200 x g) and resuspended in 1% (v/v) dimethyl sulfoxide (DMSO) in FBS for EA.hy926 cells. HUVECs were resuspended in 1% (v/v) DMSO in nM199 medium. The resuspended pellets are placed into cryovials containing 5x10⁵ cells per vial. The vials were stored overnight in a Mr Frosty™ Freezing container with isopropanol at -80°C for 1-2 days. This simple container allows the gradual freezing of cells, preventing ice crystals' formation. Afterwards, the cryovials are transferred to the liquid vapour cylinders for long-duration storage.

2.2.6 Thawing the cells

Frozen cells were kept in cryovials in nitrogen vapour. They were thawed rapidly by being placed in a 39°C beads bath. After the cells were defrosted, they were transferred under aseptic conditions to a 15 ml universal tube containing 10 ml of prewarmed medium (cDMEM or cEGM) for EA.hy926 and HUVECs, respectively; and added dropwise with mixing. Then the cells were transferred into a T75 tissue culture flask and kept in the incubator at 37°C with 5% CO₂ to grow. Cells were routinely incubated for 48-72 h at 37°C to grow and yield the cultured confluence. Cells have split a ratio of 1/4 for either experiment, frozen down or discarded.

2.2.7 Cell Treatment settings

2.2.7.1 GYY4137 reagent

A stock solution of 50 mM of slow-releasing H₂S donor was prepared by dissolving 10 mg of GYY4137 [Sigma-Aldrich, Gillingham, UK] with dH₂O aliquoted in 0.6 ml tubes and stored at -20°C for long duration storage.

2.2.7.2 TNF- α reagent

A stock solution of 20 μ g/ml of human TNF- α [R&D Systems, Bio-Techne, Inc., Oxford, UK] was prepared by adding 1 ml of 1X phosphate-buffered saline (PBS) [Sigma-Aldrich, Gillingham, UK] with 0.1% Bovine Serum Albumin (BSA) [Fisher Scientific, Loughborough, UK]. Aliquots were stored at -20°C for long-term use.

2.2.8 Cell culture experimental settings

ECs grow into T75 flasks until desired confluency (80-90%). Then, cells were detached with trypsin-EDTA (see section 2.2.3). Based on the assay, cells were seeded into a specific culture plate at the desired density (see Table 2-2) with overnight incubation at 37°C with 5% CO₂. The next day, treatment began in specific experimental settings. In this thesis, ECs are divided into four groups unless otherwise stated:

- Control (group 1): untreated cells
- GYY4137 (group 2): treated only with GYY4137
- TNF- α (group 3): treated only with TNF- α
- TNF- α and GYY4137 (group 4): treated with TNF- α and GYY4137

Experimental settings for TNF- α -mediated ED and GYY4137 recovery's ability were optimised using the EA.hy926 cell line. After deciding on an experimental design, further experiments were conducted in HUVECs.

Concentrations and incubation time of TNF- α were selected based on previous reports using ECs (Hughes, Murphy and Ledgerwood, 2005; Tang *et al.*, 2015; S. Wang *et al.*, 2018). GYY4137 non-toxic doses were determined based on cell metabolic capacity assay (see section 2.3) and oxidant formation (see section 2.5.1). All three designs were

tested only in EA.hy926 cells, whereas the selected post-treatment was applied in HUVECs. Initial adaptation of post-treatment conditions in HUVECs was required to mimic prior results in EA.hy926 cells. Once treatments were completed, molecular and cellular assays were conducted (Figure 2.1).

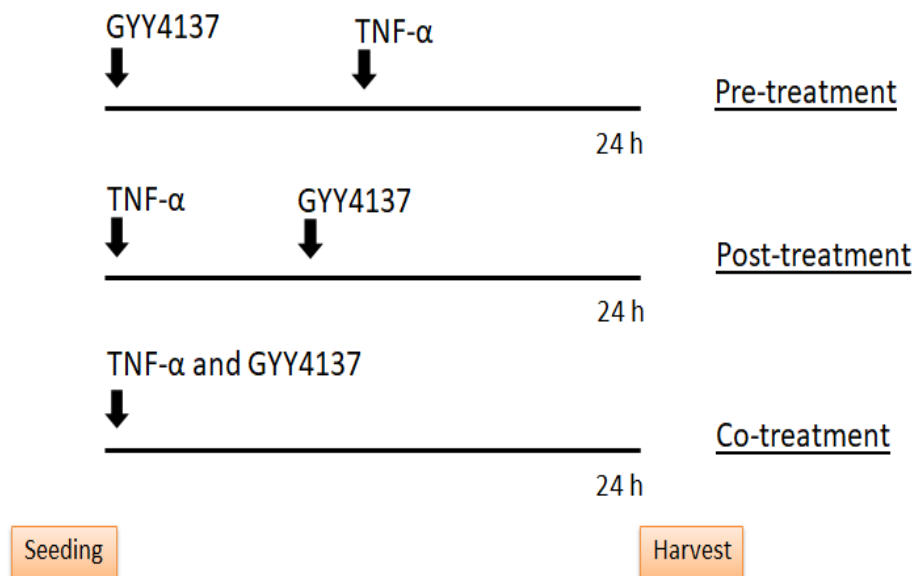


Figure 2.1. Timeline of experimental settings in ECs.

TNF- α was added to ECs at specific working concentration. Under pre-treatment setting, GYY4137 donor was added for 18 or 21 hours followed by 3 or 6 hours of TNF- α treatment. In the post-treatment setting, ECs were incubated with TNF- α for 3 or 6 hours prior GYY4137 treatment was conducted for 18 or 21 hours. Finally, both GYY4137 and TNF- α were added to the cells at the same time for 24 hours under co-treatment setting.

- 1- The pre-treatment setting was conducted by incubating ECs in a growth medium containing GYY4137 at a specific concentration for 18 or 21 hours. Then, the medium was removed, and cells were incubated in a fresh warm medium with TNF- α at particular attention for 6 or 3 hours, leading to final cell treatment up to 24 hours.
- 2- The post-treatment setting involves an initial TNF- α treatment at a specific concentration for 6 or 3 hours, followed by washing with 1X PBS. Subsequently,

ECs were incubated in a fresh warm medium with GYY4137 at a specific concentration for 18 or 21 hours, which totalled 24 hours of treatment.

- 3- The co-treatment setting was performed, incubating ECs in a fresh warm medium containing TNF- α and GYY4137 at specific concentrations for each compound for 24 hours.

2.3 Metabolic capacity assay

This fluorometric assay is based on converting blue resazurin into pink resorufin product by metabolic living cells and estimates viable cell numbers. EA.hy926 and HUVECs cells were seeded at the density of 1.5×10^4 cells/well in a 96-well tissue culture plate with their corresponding growth medium (see Table 2-1). ECs were incubated at 37°C with 5% CO₂ overnight, followed by treatment with GYY4137 in new growth pre-warm medium with 0, 50, 100, 200, 300, and 400 μ M for 24 hours. Then 20 μ l of CellTiter-Blue® reagent was added to each well. ECs were incubated at 37°C and 5% CO₂ for 3 hours according to the manufacturer's instructions.

Once incubation was completed, fluorescence values were measured at 560 nm excitation and 590 nm emission using a multi-plate reader (Spark-TECAN Trading AG, Switzerland). Samples without cells were used as a sample blank to normalise results. Samples were seeded in three replicates, and the relative cell viability (%) was calculated relative to control groups (untreated cells).

2.4 In situ cellular H₂S measurement

Free sulfide was measured in cells using a specific fluorescent probe, sulfidefluor-7-acetoxymethyl ester (SF7-AM) [Sigma-Aldrich, Gillingham, UK]. Upon exposure to H₂S, the azide functional groups are reduced to primary amines, restoring the fluorescence of the caged fluorophore and resulting in a fluorescence signal.

EA.hy926 and HUVECs cells were seeded at the density of 1.5×10^4 cells/well in a 96-well tissue culture plate with the corresponding growth medium (see Table 2-1). ECs were incubated overnight at 37°C with 5% CO₂, followed by treatment with non-toxic GYY4137 in a fresh pre-warm medium at 37°C and 5% CO₂ for 24 hours to grow.

Based on the metabolic capacity assay results, EA.hy926 cells were treated with 50 μM GYY4137, while HUVECs were treated with 100 μM GYY4137.

After the medium was discarded, cells were incubated with 2.5 μM SF7-AM in fresh growth medium for 20 minutes and rinsed gently twice with 1X PBS. To stain the nucleus DAPI [Sigma-Aldrich, Gillingham, UK] in PBS (1:1000 dilution) was added to the cells for 10 minutes in the dark. After two additional washes with PBS, the turn-on fluorescence response of SF7-AM to H_2S in ECs was visualised by a Nikon *Ti* + T-P2 fluorescence microscope (20x magnification, scale bar = 10 μm). SF7-AM fluorescence (green spectrum) was visualised at 495 nm excitation and 519 nm emission. DAPI nucleus-staining was imaged at 358 nm excitation and 461 nm emission (blue spectrum). Results of fluorescent intensity are presented as a percentage relative to the control group (untreated cells). The analysis of the fluorescence intensity was performed by ImageJ 1.80 software.

2.5 Assessment of ROS formation

2.5.1 Detection of Hydrogen peroxide production

The intracellular ROS were analysed using the fluorescence probe 2', 7'-dichlorofluorescein diacetate (CM-H2DCFDA™) [ThermoFisher Scientific, Gloucester, UK]. The assay is based on converting intracellular non-fluorescent de-esterified DCFDA to fluorescent 2', 7'-dichlorofluorescein (DCF) upon oxidation by ROS, which can be detected by fluorescence microscopy. CM-H2DCFDA was dissolved in DMSO to a final concentration of 10 mM. HUVECs were seeded at a density of 5×10^4 cells/well in a 24-well culture plate in the cEGM medium overnight at 37°C and 5% CO_2 to grow. ECs were subjected to experimental settings divided into 4 general groups (see section 2.2.8).

After treatment settings were applied, HUVECs were incubated with DAPI stain in 1X PBS (1:1000 dilution) for 10 minutes at 37°C in the dark. The PBS was removed, and cells were incubated in serum-free prewarm cEGM medium containing CM-H2DCFDA (10 μM of final concentration) for 30 minutes at 37°C in the dark. Then, cells were washed twice with PBS and resuspended in a fresh prewarm medium. The fluorescence intensity result was analysed using a Nikon *Ti* + T-P2 fluorescence microscope (20x magnification, scale bar = 10 μm) at 484 nm excitation and 529 nm emission (green

spectrum). Untreated and unstained cells were used as a negative control group [not shown]. DAPI stain for the nuclear location was determined at 358 nm excitation and 461 nm emission (blue spectrum). Results of fluorescent intensity are presented as a percentage relative to the control group (untreated cells). The analysis of the fluorescence signal in all samples was performed by ImageJ 1.80 software.

2.5.2 Detection of mitochondrial superoxide production

The MitoSox™ red probe [ThermoFisher Scientific, Gloucester, UK] is a fluorogenic dye targeted to mitochondria oxidised only by superoxide to 2-hydroxyethidium with a fluorescence response determining the relative generation of mitochondrial superoxide. MitoSox reagent was dissolved in DMSO to 5 mM as the final concentration. HUVECs cells were seeded at 5×10^4 cells/well in a 24-well culture plate in a growth cEGM medium and incubated overnight at 37°C and 5% CO₂ conditions. HUVECs were subjected to experimental settings divided into the general 4 groups (see section 2.2.8).

After treatments concluded, HUVECs were cultured with 5 µM MitoSox in fresh cEGM medium at 37°C for 30 minutes, followed by DAPI stain for 10 minutes at 37°C in the dark. Subsequently, cells were washed twice with PBS and resuspended in a fresh cEGM medium. Untreated cells without a fluorescence probe were represented as a negative control group [not shown]. The fluorescence intensity was determined at 510 nm excitation and 580 emissions (cherry spectrum) using a Nikon Ti + T-P2 fluorescence microscope (10x magnification, scale bar = 100 µm). The nucleus was stained using DAPI solution at 358 nm excitation and 461 nm emission (blue spectrum). Results of fluorescent intensity are presented as a percentage relative to the control group (untreated cells). The analysis of the fluorescence intensity in all samples was performed by ImageJ 1.80 software.

2.6 Flow Cytometry analysis

The cells were stained with a specific antibody or reagent, followed by analysis using a BD Accuri C6 Plus flow cytometer. Each sample was analysed using 10,000 cellular events, and cells were plotted according to scatter forward (FSC), and side scatters (SSC) profiles and then gated to exclude cellular debris. Due to many biological processes are co-dependent, flow cytometry allows the study of multiple variables in

parallel accomplished through the use of fluorescent probes, which differs in their wavelength (emission of fluorescent light). The BD Accuri C6 Plus flow cytometer presents four fluorophores phycoerythrin (PE), allophycocyanin (APC), fluorescein isothiocyanate (FITC) and peridinin chlorophyll protein-Cyanine5.5 (PerCP-Cy5.5).

2.6.1 Assessment of cell adhesion molecules expression

ECs were seeded at a density of 2.5×10^5 cells/well in a 6-well culture plate and incubated overnight under 37°C and 5% CO₂ conditions to grow. Cells were divided into 4 groups for experimental settings with TNF- α and GYY4137. Once treatments were completed, cells were detached with Trypsin-EDTA as previously described (see section 2.2.3). Subsequently, cells were resuspended in pre-cold 1X PBS containing 10% FBS (100 μ l). Primary antibodies (Table 2-3) were added at the required concentration and incubated for 1 hour on ice. At the end of the incubation, ECs were washed twice with PBS and pellet down by centrifugation at 200 x g for 5 minutes. The cells were washed twice with PBS and resuspended in 500 μ l PBS before analysis in the flow cytometer.

Table 2-3. Antibody used for flow cytometry.

Antibody	Conjugate	Emission/ Excitation (nm)	Concentration (μ g/ml)	Reference #
VCAM-1/CD106	PE	667/496	1.25	12106942
IgG1-CD106 K isotype	PE	667/496	1.25	12471442
ICAM-1/CD54	APC	660/650	5	17054942
IgG1-CD54 K isotype	APC	660/650	5	17471442
IgG1-CD62 K isotype	FITC	488/520	1.25	11471442
E-selectin/CD62	FITC	488/520	1.25	BMS110FI

The initial gating strategy step was plotting all events according to FSC vs SSC. Unstained and untreated cells set the photomultiplier tube amplification voltage gain and the gates. The primary acquisition gate (referred to as "cells") allows the exclusion of debris. Then, events from this gate are sorted as CD54-APC (ICAM-1), CD106-PE (VCAM-1) and CD62-FITC (E-selectin) vs Count in a histogram plot. Fluorochrome-matched isotype (IgG1) controls were used to differentiate negative from positive cells by line boundaries (Figure 2.2). Results of fluorescent intensity are presented as a percentage of each group.

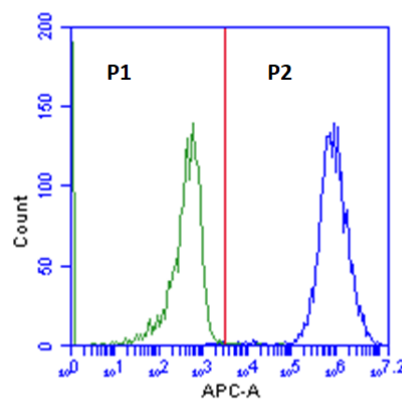


Figure 2.2 Representative flow cytometer histogram showing adhesion molecule (CD54)-positive and IgG cells.

Cells were stained with IgG1-CD54 and CD54-APC to discriminate positive from negative cells and conducted a correct gating. IgG1 was captured in the P1 channel, and the CD54 positive cells were gated in the P2 section.

2.6.2 Assessment of apoptosis using Annexin V-PI

Apoptosis was measured using Annexin V/PI Apoptosis detection Kit APC [BioLegend, UK], which employs R-phycoerythrin-labelled Annexin V in concert with Propidium iodide (PI) to evaluate the sub-population of cells undergoing apoptosis. HUVECs were seeded at a density of 2.5×10^5 cells/well in a 6-well culture plate in cEGM medium and incubated at 37°C and 5% CO_2 overnight to grow. On the following day, the post-treatment setting with $\text{TNF-}\alpha$ (1ng/ml, 3 hours) and GYY4137 (100 μM , 21 hours) was applied to the cells divided into 4 groups (see section 2.2.8). A positive control group (200 μM H_2O_2

treatment for 3 hours) was used to ensure the correct gating strategy. After treatments, the medium was discarded, and cells were detached with the Trypsin-EDTA process (see section 2.2.3). The endothelial pellet was washed twice with 1X PBS and one washed with 1X binding buffer (150 mM NaCl, 10 mM HEPES (pH 7.5), 2.5 mM CaCl₂ in distilled water) [provided by the kit]. Then, cells were resuspended in cold binding buffer at the concentration of 1.5x10⁶ cells/ml and counted by a haemocytometer. Then, 100 µl of the pellet resuspended was transferred to a flow cytometry tube per group, which was incubated with 10 µl of fluorochrome conjugate Annexin V and 5 µl of PI solution for 15 minutes at room temperature in the dark. Finally, 400 µl of Annexin binding buffer was gently added to each tube for mixing. Samples were then analysed on a BD Accuri C6 Plus flow cytometer, and data were analysed using BD Accuri C6 Plus software.

Compensation set-up was performed before each experiment to ensure the results' accuracy and quality and to discriminate the fluorescence background from the Annexin V fluorescence signal. Four tubes were set up as follows:

- Tube 1: No stain
- Tube 2: PI dye
- Tube 3: Annexin V dye
- Tube 4: Both PI and Annexin V dyes

The initial gating strategy involves plotting all events according to FSC vs SSC. Events are then sorted as Annexin V-FITC vs PerCPcy5-5 for PI stain. To generate a cell population without debris, four different gating boundaries were applied: necrotic cells (Q1), late apoptosis (Q2), live cells (Q3) and early apoptosis (Q4). Untreated and unstained cells were used to ensure accuracy. A representative analysis of the gating of the four different boundaries is displayed in Figure 2.3.

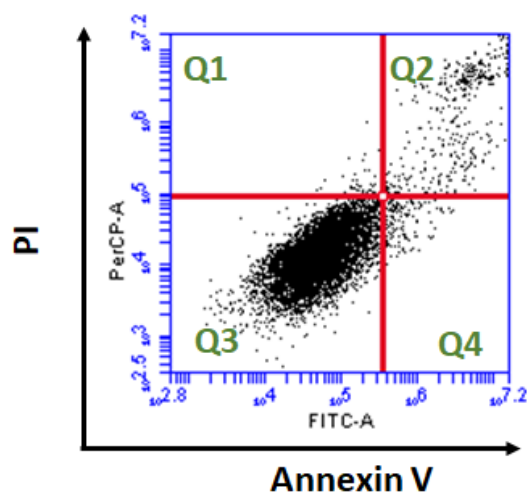


Figure 2.3 Representative diagram of annexin V staining quadrants.

Events were plotted according to FSC vs SSC to exclude debris. Then events are sorted as Annexin V for FITC vs PerCPcy5-5 for PI stain. Four different boundaries were applied to the cell population: live cells (Q3), necrotic cells (Q1), early apoptosis (Q4) and late apoptosis (death cells) (Q2).

2.7 Caspase 3/7 activity assay

The caspase 3/7 activity was conducted using the Caspase-Glo® 3/7 assay kit purchased from [Promega, GmbH, Southampton, UK]. The kit provides a luminogenic caspase 3/7 substrate [Aminoluciferin] attached to tetrapeptide, which is specific for protease cleavage by the executors' caspases, caspase 3 and caspase 7.

HUVECs were seeded in a white-walled 96-well plate at 1.5×10^4 cells/well density in cEGM medium and allowed to adhere and grow for 24 hours in an incubator at 37°C with 5% CO₂ as standard conditions. The following day, the medium was replaced, and cells (in duplicates) were incubated with TNF- α and GYY4137 in a post-treatment setting (see section 2.2.8) at 37°C with 5% CO₂. Before the execution of the experiment, H₂O₂ (1 mM) was added to normal cells in a cEGM medium for 6 hours to create a positive control signal for apoptosis. Additional controls were used to set up the assay, such as blank (reagent without cells) and negative control (untreated cells without reagent). The medium was removed, and fresh medium (100 μ l) was added per well.

A total of 100 µl of Caspase-Glo reagent was added to each well. The plate was then mixed using a plate shaker at 400 rpm for 30 seconds and left in the dark at room temperature for 1 hour. The caspase 3/7 was then measured using a luminometer plate reader [Spark®, TECAN Group Ltd., Männedorf, Switzerland]. Results were represented as luminescence relative light units (RLU) after subtracted values from the blank.

2.8 GSH: GSSG ratio assay

The GSH:GSSG ratio was conducted using the GSH:GSSG-Glo assay kit purchased from Promega, GmbH, Southampton, UK. The assay is a luminescence-based method to detect and quantify total glutathione and oxidised glutathione, which can be used to calculate the GSH:GSSG ratio in cultured cells. The light signal is directly proportional to the amount of GSH present (**Error! Reference source not found.**). HUVECs were seeded in a white opaque-walled 96-well plate at 1.5×10^4 cells/well density in cEGM medium and allowed to adhere and grow for 24 hours in an incubator at 37°C with 5% CO₂ as standard conditions. The following day, the medium was replaced, and cells (in duplicates) were incubated with TNF-α and GYY4137 in a post-treatment setting (see section 2.2.8) at 37°C with 5% CO₂. All reagents were prepared within 30 min of execution of the assay with the provided components as described in the kit documentation. For HUVECs, 50 µl Glutathione lysis reagent, 50 µl Luciferin generation reagent and 100 µl Luciferin detection reagent per reaction were used. Adjust the total volume of the reagents for the total number of responses performed, including blank (no-cells), and the standard curve was applied. Once cultured cell treatments were concluded, the medium was removed to avoid interfering with the assay, and cells were washed with prewarm 1X PBS. Once all reagents were added and incubation time completed, the luminescence was measured in a plate reader [Spark®, TECAN Group Ltd., Männedorf, Switzerland].

2.9 Immunofluorescence microscopy

Immunostaining microscopy was applied to determine immortalised cells' phenotype, the subcellular accumulation of Nrf2 and mitochondrial morphology.

2.9.1 Endothelial phenotype fluorescent microscopy

To determine the endothelial phenotype of immortalised EA.hy926 cells, the presence of two exclusive endothelial markers, Von Willebrand factor and CD31 (PECAM-1) was examined. EA.hy926 were seeded at 1.5×10^4 cells/well in a 96-well plate in cDMEM medium and incubated overnight at 37°C with 5% CO₂ to grow. The next day, the medium was discarded, and cells were washed with 1X PBS and fixed with pre-cooled methanol for 5 minutes at room temperature. Subsequently, cells were washed with cold PBS and permeabilised with 0.15% Triton X-100 in PBS for 10 minutes at room temperature. Afterwards, cells were blocked with 10% goat serum in PBS with 0.1% Tween-20 for 1 hour at room temperature. The same blocking solution was used to dilute anti-von Willebrand and anti-CD31 primary antibodies (see Table 2-4) for overnight incubation with gentle rotation at 4°C. The next day, cells were washed twice with PBS and incubated with secondary antibodies conjugated to Alexa Fluor-488 nm diluted in PBS for 2 hours at room temperature in the dark (see Table 2-5). After an additional wash, DAPI (1:1000 dilution) in PBS was added for nuclear staining (358 nm excitation and 461 nm emission, blue spectrum) with 10 minutes of incubation in the dark, followed by an additional wash step and subsequently microscopy examination. Fluorescence images were visualised by Nikon Ti + T-P2 microscope.

2.9.2 Cellular localisation of Nrf2

An immunostaining microscopy analysis was conducted to determine the distribution of Nrf2 within ECs. HUVECs were seeded at 1.5×10^4 density in 300 µl cEGM medium on 22x22 mm coverslips in a culture 10 mm dish and incubated at 37°C with 5% CO₂ to allow attachment. Then, 1 ml of cEGM medium was added to each dish, and cells were incubated overnight at 37°C with 5% CO₂. The next day, treatment of TNF-α and GYY4137 was conducted following the post-treatment setting as described in section 2.2.8. Once treatment was concluded medium was discarded, and cells were washed once with 1X PBS, followed by fixing using pre-cooled methanol for 5 minutes at room temperature. Next, methanol was discarded, and cells were washed twice with PBS and permeabilised with 0.15% Triton X-100 in PBS for 10 minutes at room temperature. Blocking with 10% goat serum in PBS with 0.15% Tween-20 for 1 hour at room temperature was conducted after cells were washed once with PBS. Cells were rinsed with primary anti-Nrf2 antibody in blocking buffer (see Table 2-4) and incubated

overnight with gentle rotation at 4°C. Then, the cells were washed three times with PBS before adding the fluorescently conjugated Alexa Fluor-488 nm secondary antibody (see Table 2-5) diluted in PBS for 2 hours with gentle rotation at room temperature in the dark and rewashed twice with PBS for 5 minutes. A DAPI mounting nuclear stain solution (350 nm excitation and 465 nm emission, blue spectrum) was added for 20 minutes before the cover glass was sealed with nail polish. Fluorescence images were visualised by Nikon Ti + T-P2 microscope.

2.9.3 Mitochondrial network fluorescence analysis

Localisation of mitochondria was determined by immunostaining followed by fluorescence microscopy. To assess the mitochondrial morphology, cells were stained with MitoTracker Red (ThermoFisher Scientific, Gloucester, UK). HUVECs were plated on 13 mm coverslips at 1.5×10^4 density in cEGM medium overnight incubation at 37°C with 5% CO₂. The next day, cells were subjected to TNF- α and GYY4137 was conducted following the post-treatment setting described in section 2.2.8. Subsequently, cells were treated with Mitotracker Red (100 nM) for 30 minutes at 37°C, followed by three times washing with 1X PBS. The cells were fixed with 4% PFA for 10 minutes at room temperature and washed with PBS.

A DAPI mounting nuclear stain solution (350 nm excitation and 465 nm emission, blue spectrum) was added for 20 minutes before the cover glass was sealed with nail polish. Cells images were acquired using a 63x objective oil APO lens using a confocal lighting microscopy TCS SP8 system [Leica Microsystems Ltd, UK] and analysed using 579 nm excitation and 599 nm emission for Mitotracker. Analysis of mitochondrial morphology was conducted using ImageJ's FIJI open-source macro tool, MiNA (Mitochondrial Network Analysis), designed by (Valente *et al.*, 2017). Settings were kept consistent across images, and a "mean" filter was selected. A total of 30 cells per group per individual experiment was consolidated and analysed. The network's branching and branch length was measured using the tool.

Table 2-4. Primary antibodies used during immunofluorescence with their specific dilutions, host and supplier details.

Primary Antibody	Host	Dilution	Manufacturer	Reference #
Von Willebrand factor	Mouse	1:50	Abcam	ab11713
CD31	Rabbit	1:50	Abcam	ab32457
Nrf2	Mouse	1:100	Santa Cruz Biotechnology	Sc-365949

Table 2-5. Secondary conjugated antibodies with their specific dilutions, host and supplier details.

Secondary Antibody	Host	Dilution	Manufacturer	Reference #
Alexa Fluor 488	Mouse	1:500	Abcam	ab11713
Alexa Fluor 488	Rabbit	1:500	Abcam	ab32457

2.9.4 Phalloidin F-actin staining

ECs cytoskeleton was assessed using Alexa Fluor 647 Phalloidin [Thermo Fisher Scientific, Loughborough, UK]. HUVECs were plated on 13 mm coverslips at 1.5×10^4 density in cEGM medium overnight incubation at 37°C with 5% CO₂. The next day, cells were incubated overnight with or without GYY4137 (100 µM). Next, the cells were fixed with 4% PFA in 1x PBS for 10 minutes at room temperature and permeabilized in 0.1% Triton X-100 for 10 minutes. Next, cells were blocked in PBS with 2% BSA for 1 hour at room temperature, followed by three washes with 1x PBS and stained with F-actin with phalloidin for 2 hours. After washing three times with 0.05% Tween-20 PBS, cells were mounted in DAPI mounting nuclear stain solution (350 nm excitation and 465 nm emission, blue spectrum) before the cover glass was sealed with nail polish. Cells images were acquired using a 63x objective oil APO lens using a confocal lighting

microscopy TCS SP8 system [Leica Microsystems Ltd, UK] and analysed using 650 nm excitation and 668 nm emission for Phalloidin.

2.10 Senescence (SA- β -gal) staining

The presence of senescence in cells was achieved using the senescence-associated SA- β -gal staining assay. Ultrapure water was used for all reagent dilutions. All reagents and chemical dilutions were prepared as described in Table 2-6. HUVECs cells were seeded at the density of 1.5×10^4 cells/well in a 96-well tissue culture plate with the corresponding growth medium (see Table 2-1). Cells were allowed to adhere and grow for 24 hours in an incubator at 37°C with 5% CO₂. The next day, cells were treated with TNF- α and GYY4137 post-treatment. After incubation, the growth medium was aspirated from cells and discarded. Subsequently, cells were washed twice with 1X PBS, and the required volume of fixation buffer (200 μ l) was added to cells with 15 min incubation at room temperature. Afterwards, fixation buffer was discarded, and cells were washed with PBS for 5 min at room temperature, followed by two additional washes with PBS/MgCl₂ for 5 min at room temperature. Then, 200 μ l of freshly prepared X-Gal solution was added to each well and incubated at 37°C in a CO₂-free incubator for 4 hours in the dark. The staining solution was removed, cells were washed twice with PBS for 5 min at room temperature, and pictures were taken. The stained blue cells were visualised using a Nikon phase contrast light microscope with a scale bar 10 μ m.

Table 2-6. Components of staining mixture for SA- β -gal staining

Reagent	Composition
	PBS/MgCl ₂
X-Gal staining solution	0.2 mM Potassium ferricyanide (III) 0.2 mM Potassium hexacyanoferrate (II) trihydrate
PBS/MgCl ₂	1mM MgCl ₂ in PBS pH: 6.0
X-Gal stock (40X)	40 mg/ml X-Gal in N, N-dimethylformamide
0.2 M Potassium ferricyanide (III)	0.66 gr in 10 ml dH ₂ O

Fixation buffer	0.5% Glutaraldehyde solution in PBS pH: 7.4
0.2 M Potassium hexacyanoferrate (II) trihydrate	0.85 gr in 10 ml dH ₂ O

2.11 ELISA assay

The pro-inflammatory effect of TNF- α and the potential protective role of GYY4137 on ECs was tested using the sandwich Enzyme-Linked Immunosorbent Assay (ELISA). Analysis of IL-6 secretion in the medium was conducted using the Human IL-6 DuoSet [R&D Systems, Minnesota, US], following the manufacturer's instructions.

Cells were cultured at 2×10^5 cells/well in a 6-well culture plate and incubated at 37°C and 5% CO₂ overnight to grow. The next day, cells were treated with specific compounds (TNF- α and GYY4137) following experimental settings (see section 2.2.8). After treatments, the culture medium was collected and transferred into 1.5 ml tubes, followed by centrifugation at 10,000 x g for 10 minutes to remove dead cells and any cell debris.

On the day of the experiment, the recombinant IL-6 standard was reconstituted in distilled water to a stock concentration following manufacturer recommendations. Then, a seven-point standard curve using a two-fold serial dilution in Reagent diluent [provided by the kit] was prepared. The plate was transferred into a microplate spectrophotometer for an optical density (OD) reading of 450 nm. Wavelength correction was carried out, setting the reading to 540 nm. The standard curve was created by generating a four-parameter logistic (4-PL) curve-fit and calculating an unknown sample concentration.

2.12 Tube formation assay

The angiogenic capacity of ECs was studied using the Tube formation assay. The assay is based on the ability of endothelial cells to form three-dimensional capillary-like tubular structures when cultured on a gel of growth factor-reduced basement membrane matrix. Matrigel matrix [Corning, UK] is a solubilised membrane rich in extracellular matrix proteins extracted from the Engelbreth-Holm-Swarm mouse sarcoma cells and is

commonly used in assessing the *in vitro* angiogenic capacity of endothelial cells (Lin *et al.*, 2020).

HUVECs were maintained in cEGM medium at 37°C and 5% CO₂ until the day before the experiment. Growth factor reduced Matrigel was thawed at 4°C overnight, and 50 µl/well was added into a cooled sterile transparent 96-well plate on ice with a cooled sterile tip and incubated at 37°C for 30 min to solid. Cells, at less than 70-80% confluence, were detached with Trypsin-EDTA (see section 2.2.3), resuspended Media199 with 1% FBS and 1% (v/v) penicillin/streptomycin and counted (see section 2.2.4). A total of 1x10⁴ cells/well in duplicate were seeded onto Matrigel. Plates were incubated at 37°C and 5% CO₂ for 1 hour.

The cells were divided into the formal 4 groups and treated with TNF-α and GYY4137 in Media199 medium following a post-treatment setting as indicated in section 2.2.8 before microscopic examination. In each well, phase-contrast images were captured at 4X magnification (scale bar = 100 µm) using a Nikon eclipse Ts2 microscope. The total tube length in each image was determined using the ImageJ software Angiogenic plugin.

2.13 Isolation of Nuclear and Cytoplasmic protein fractions

Following manufacturer instructions, cytosolic and nuclear proteins were extracted using the Nuclear Extract Kit [Active Motif, UK]. Briefly, cells were seeded in a T75 flask and incubated at 37°C with 5% CO₂ overnight. The next day, ECs were treated with TNF-α and GYY4137 compounds. After the treatment, cells were washed with ice-cold 1X PBS after removing the medium by aspiration. Trypsin-EDTA detached cells (see section 2.2.3). The cell pellet was kept on ice and resuspended in 1x hypotonic buffer [provided by the kit] gently and incubated for 15 minutes on ice to expand the cell membrane. At that time, detergent [supplied by the kit] was added to isolate cytoplasmic proteins; a homogeniser was used for 40 seconds for a complete cell lysate. The supernatant containing the cytoplasmic fraction was collected by centrifugation at 14,000 x *g* at 4°C for 1 minute. The pellet was washed with PBS and resuspended in lysis buffer [provided by the kit] supplemented with 10 mM DTT and protease inhibitor (1:100 dilution).

The protein pellet was homogenised by vortex and incubation for 30 minutes on ice. Centrifuge at 14,000 x *g* for 10 minutes allows for collecting the nuclear fraction. Cytosolic and nuclear proteins were stored at -80°C until further immunoblotting experiments.

2.14 Characterisation of Mitochondrial $\Delta\psi_m$

The lipophilic cation commercial JC-1 dye, which is specific for $\Delta\psi_m$, highly sensitive and unaffected by changes in the plasma membrane potential, was used in this thesis. The membrane-permeant fluorescent dye undergoes a reversible colour change from green fluorescence (529 nm emission) for the monomeric form to red-orange fluorescence (590 nm emission) to indicate aggregates as the $\Delta\psi_m$ increases.

HUVECs were seeded into a 24-well plate at 5×10^4 cell/well density and incubated overnight at 37°C and 5% CO₂ for cultured growth. The next day, cells were divided into the formal experimental groups and treated with TNF- α and GYY4137 following post-treatment settings, as illustrated in section 2.2.8. Cells were incubated with JC-1 to a final concentration of 5 μ M in fresh free-serum cEGM medium and set at 37°C for 20 minutes in the dark. Afterwards, cells were gently washed twice with 1X PBS and rinsed with a new cEGM medium. At this point, a Nikon Ti + T-P2 microscope captured microscopic pictures of monomers (green spectrum) and aggregates (red range). $\Delta\psi_m$ was derived from the ratio of red (aggregates) to green (monomers) fluorescence.

2.15 Characterisation of Bioenergetic profile.

2.15.1 Seahorse Mito Stress test

Cell metabolism in live ECs can be assessed by directly monitoring the oxygen consumption rate (OCR) on the Seahorse Extracellular Flux Analyzer XF24. The Seahorse XF Cell Mito Stress Test enables the measurement of critical parameters of mitochondrial function based on built-in injection ports adding pre-measured compounds, which can modulate mitochondrial electron chain components (Figure 2.4). The mentioned compounds comprise oligomycin, antimycin A, rotenone and FCCP [carbonyl cyanide-4-(trifluoromethoxyphenyl)hydrazone]. The protocol for OCR measurement assay by Seahorse XF analyser is shown below.

Stage 1: Cell culture

HUVECs were plated at 5×10^4 cells/well density into an XF 24-well microplate in cEGM medium (200 μ l) and allowed to grow at 37°C and 5% CO₂ overnight. The next day, cells were treated with TNF- α and GYY4137 following post-treatment settings as illustrated in section 2.2.8 using cEGM medium.

Stage 2: Preparation of sensor cartridge.

An XF24 sensor cartridge was hydrated overnight the day before the Mito Stress assay by submerging the sensors in an XF 24-well plate filled (800 μ l) with XF calibrant solution at 37°C without CO₂.

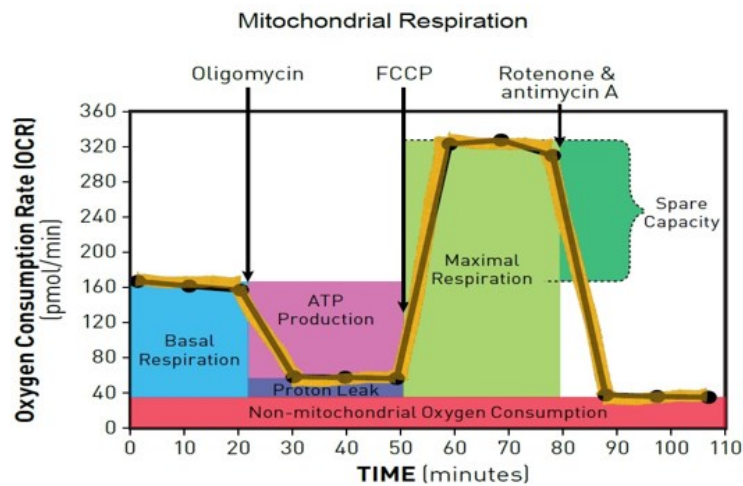


Figure 2.4 Representative graph of the Mito Stress test in the Seahorse instrument.

Illustration of the injections with complexes modulators compounds and parameters evaluated, such as basal respiration, OCR-drive ATP production, maximal respiration, spare capacity, and non-mitochondrial oxygen consumption. Figure created with Bio-render.com. Adapted from Mito Stress Kit Datasheet.

Stage 3: Seahorse Analysis

Before starting the Mito Stress assay, XF base medium was prepared using un-buffered DMEM (Agilent Scientific Instruments, US) comprising glucose (10 mM), pyruvate (1 mM) and L-glutamine (2 mM) at pH 7.35 conditions.

The treating media was removed in the cultured-cells plate, leaving 50 μl in the well. The cells were gently rinsed twice with 450 μl of prewarm XF base medium. Next, HUVECs were incubated with 475 μl XF assay medium in a non-CO₂ incubator at 37°C for 1 hour before analysis. At the same time, compounds for loading in the sensor cartridge were prepared using constant loading volume. Compounds were prepared in XF base medium, and 75 μl of each prepared compound was added into each injection port of the cartridge for each well to give the final concentrations described in Table 2-7. The sensor cartridge was then calibrated for 15 minutes on the instrument tray. After measurement of OCR basal rates, compounds were sequentially injected from the sensor cartridge ports at 14, 34 and 54 minutes for oligomycin, FCCP and rotenone/antimycin A, respectively. Rates were normalised to protein content quantified using the Bradford assay (see section 2.16). Bioenergetic parameters, including basal mitochondrial respiration, non-mitochondrial respiration, ATP production, maximal respiration, mitochondrial reserve capacity and proton leak, are automatically calculated based on the normalised protein followed rate measurement equations (see Table 2-8) using Seahorse XF Cell Mito Stress Test Report Generator.

Table 2-7. Injection Mito Stress test compounds on the XF24 Seahorse instrument

Port	Injection Compound	Actions	Stock concentration (μM)	Port concentration (μM)
A	Oligomycin	Complex V inhibitor	100	1
B	FCCP	Proton uncoupling reagent	100	0.5
C	Rotenone/Antimycin A	Complex I and III inhibitors	50	0.5

Table 2-8. Mitochondrial bioenergetic parameters for Mito Stress test.

Parameter	Indicates	Rate measurement equation
Non-mitochondrial oxygen consumption	Oxygen consumption due to cellular enzymes for accurate measure of respiration	Minimum rate measurement after Rotenone/Antimycin A injection

Basal respiration	Energetic demand on the cell under baseline conditions	(Last rate measurement before 1 st injection) – (non-mitochondrial respiration rate)
ATP production	ATP contributes to meeting the energy needs of the cell	(Last rate measurement before oligomycin injection) – (minimum rate measurement after oligomycin injection)
Maximal respiration	Maximum rate of respiration that the cell can achieve	(Maximum rate measurement after FCCP injection) – (non-mitochondrial respiration)
Mitochondrial reserve capacity	Ability to respond to energetic demand	(Maximal respiration) – (basal respiration)
Proton leak	Remaining basal respiration not coupled to ATP production	(Minimum rate measurement after oligomycin injection) – (non-mitochondrial respiration)

2.15.2 Seahorse Glycolytic Test assay

Glycolysis is one of the main energy-producing pathways in the cells. The Glycolysis test measures the extracellular acidification rate (ECAR) in basal conditions and response to modulators on the Seahorse Extracellular Flux Analyzer XF24. The Seahorse XF Glycolysis Stress Test allows the analysis of glycolytic flux parameters based on built-in injection ports adding pre-measured compounds. The Glycolysis Stress test is similar to Mito Stress assay and shares many similarities regarding cell preparation, cartridge hydration and protocol steps. Nevertheless, the modulation of the glycolytic pathway required using specific compounds and analysis of determined bioenergetic parameters, as described below. The Glycolysis Stress test comprises glucose, oligomycin and 2-deoxy-glucose (2-DG) (Figure 2.5). Measurement of ECAR in the cells was performed as described in the following protocol.

Stage 1: Cell culture

Seeding and treatment of HUVECs were conducted following the same parameters as the Mito Stress test (see section 2.15.1).

Stage 2: Preparation of sensor cartridge.

The hydration of the cartridge the day before the Glycolytic Stress assay was performed under the same conditions described in section 2.15.1.

Stage 3: Seahorse Analysis

The Glycolysis Stress assay required preparing a specific XF base medium using unbuffered DMEM with glutamine (2 mM) at pH:7.35 conditions. The cell culture treatment medium in the cell culture XF2 24-well plate was changed to a warmed glycolytic XF base medium, and place the cell culture microplate into a 37°C non-CO₂ incubator for 1 hour before the assay. Stock compounds loading into the sensor cartridge were prepared using constant loading volume (75 µl) and at specific concentrations, as detailed in Table 2-9. Then, the utility plate with the loaded sensor cartridge was placed on the instrument tray to start calibration.

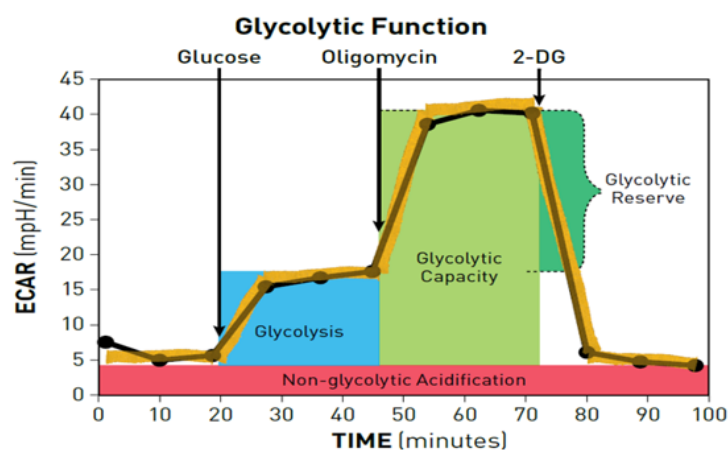


Figure 2.5 Representative graph of the Glycolysis Stress test in the Seahorse instrument.

Illustration of the injections with complexes modulators compounds and parameters evaluated, such as glycolysis, glycolytic capacity, glycolytic reserve and non-glycolytic acidification. Figure created with Bio-render.com. Adapted from Mito Stress Kit Datasheet.

Once the baseline for ECAR measurement was obtained, compounds from the sensor cartridge ports were sequentially injected. The first cells were injected with a saturating glucose concentration (at 20 minutes), the second injection comprised oligomycin (at 40 minutes), and the third injection was with 2-DG (at 60 minutes).

Like in the Mito Stress assay, normalisation to protein content was performed using the Bradford assay (see section 2.16). Glycolytic bioenergetic parameters, including glycolysis, glycolytic capacity, glycolytic reserve and non-glycolytic acidification, are automatically calculated based on the normalised protein followed rate measurement equations (Table 2-10) using Seahorse XF Cell Glycolysis Stress Test Report Generator.

Table 2-9. Injection of Glycolysis Stress test compounds on the XF24 Seahorse instrument

Port	Injection Compound	Actions	Stock concentration (mM)	Port concentration
A	Glucose	Fuels glycolysis	100	10 mM
B	Oligomycin	ATP synthase inhibitor	100	1.0 μ M
C	2-DG	Inhibits glycolysis	500	50 mM

Table 2-10. Glycolytic bioenergetic parameters for the Glycolysis Stress test.

Parameter	Indicates	Rate measurement equation
Glycolysis	Conversion of glucose to pyruvate by cell after addition of saturating amounts of glucose	(Maximum rate measurement before oligomycin injection) – (last rate measurement before glucose injection)
Glycolytic capacity	Maximum glycolysis capacity reached by a cell	(Maximum rate measurement after oligomycin injection) – (last rate measurement before glucose injection)
Glycolytic reserve	Capability of a cell to respond to an energetic demand	(Glycolytic capacity) – (glycolysis)
Non-glycolytic acidification	Alternative sources of extracellular acidification	Last rate measurement before glucose injection

2.16 Bradford assay

Total protein concentration for Seahorse bioenergetic analysis was determined in cell lysates obtained by adding RIPA lysis buffer (20 μ l) to each well of the XF 24-well microplate. A seven-point standard curve using a two-fold serial dilution in RIPA diluent was prepared in a 1.5 ml tube from 2 mg/ml BSA solution. Each tube was prefilled with 100 μ l RIPA diluent before the serial dilution.

The Bradford assay Solution A was diluted with Bradford Reagent A [Bio-Rad Laboratories, Watford, UK] and Reagent S in a 1:50 ratio. A total volume of 50 μ l of Solution A was added and mixed into each standard curve tube and each well of the XF 24-well plate. Afterwards, 400 μ l of Bradford Reagent B [Bio-Rad Laboratories, Watford, UK] was added to standards and samples. Then 200 μ l of each sample and standard dilutions were added to a clear 96-well plate in duplicates, followed by optical density measurement using a microplate reader at 595/600 nm. Standard curve values (OD) served to plot samples' protein concentration (mg/ml) using the equation of the line and to take into account the coefficient of determination [R_2] \geq 0.95 value.

2.17 Western Blot analysis

2.17.1 Protein extraction

The culture plates containing the treated groups see section 2.2.8 were removed from the incubator, the culture medium was removed, and cells were washed with pre-cold 1X PBS. At that moment, whole-cells were prepared to lysate on dry ice for 5 minutes by adding 50 μ l/well for 6-well plates or 300 μ l for a T75 culture flask of RIPA lysis buffer [25mM Tris-HCL, pH 7.6; 150 mM NaCl; 1% NP-40; 1% sodium deoxycholate and 0.1% SDS] [Thermo Scientific, Loughborough, UK] supplemented with protease inhibitor cocktails (1:100) [Sigma-Aldrich, Gillingham, UK]. Centrifugation at 14,000 x g for 30 minutes at 4°C was carried out to remove the debris. The supernatant was gently collected in a new pre-cooled 1.5 ml microtube. Determination of protein concentration was assayed by BCA protein assay, and samples of lysates were stored at - 20°C until further experiments.

2.17.2 BCA protein quantification

A protein concentration assay was performed using a Bicinchoninic acid assay (BCA) kit [Thermo Scientific, Loughborough, UK]. BSA standard curve was prepared with 2 mg/ml stock concentration with a two-fold serial dilution in RIPA buffer according to the manufacturer's instructions. The cell lysate was diluted at a 1:5 ratio, and a total volume of 10 μ l of samples and standards was added in duplicates into a 96-well clear plate. Then, a 200 μ l mixture of reagent A (sodium carbonate, sodium bicarbonate, Bicinchoninic acid and sodium tartrate in 0.1 M sodium hydroxide) and reagent B (cupric sulphate) at a 50:1 ratio was added to all wells. The plate with samples was transferred into a microplate reader [TECAN-Spark, Trading AG, Switzerland] and incubated at 37°C for 30 minutes. Purple colour had developed in the wells, and protein quantification was performed by measuring the microplate reader's optical density (OD) at 562 nm. Standard curve values (OD) served to plot samples' protein concentration (mg/ml) using the equation of the line and to take into account the coefficient of determination [R_2] \geq 0.95 value.

2.17.3 Sample preparation and gel electrophoresis

The SDS polyacrylamide gel electrophoresis (SDS-PAGE) separates proteins by molecular weight (Table 2-11). Protein samples were prepared for SDS electrophoresis by mixing them with Laemmli SDS loading buffer, reducing (6X) [Alfa Aesar-Thermo Fisher Scientific, Loughborough, UK]. Afterwards, samples were heated to 95°C for 5 minutes in a dry heating block to promote protein denaturation and then processed for gel electrophoresis. An equal amount of lysates (10-15 μ g) and molecular weight marker (Precision Plus Protein Kaleidoscope™ pre-stained, 5 μ l) [Bio-Rad Laboratories, Hemel Hempstead, UK] were loaded into SDS-PAGE (10-15%) gels. The running buffer [3 gr Tris base, 14.4 gr Glycine, and 1 gr SDS in 1 L distilled water] was added to the cassette [Bio-Rad Laboratories, Watford, UK], and the gel ran at 110 Volts at constant voltage until the samples were reached the bottom.

Table 2-11. Reagents for resolving and stacking gels

Resolving gel			Stacking gel	
Reagents	15%	10%	Reagents	4 %
Distilled water (ml)	3	5	Distilled water (ml)	4.87
1.5 M Tris base + 0.4 % (w/v) SDS pH 8.4 buffer (ml)	3	3	0.5 M Tris base + 0.4 % (w/v) SDS pH 6.8 buffer (ml)	1.87
30% (w/v) Acrylamide solution (ml)	6	4	30% (w/v) Acrylamide solution (ml)	0.75
10% (w/v) Ammonium Persulphate (APS) in distilled water (μ L)	60	100	10% (w/v) Ammonium Persulphate (APS) in distilled water (μ L)	100
TEMED (μ L)	6	10	TEMED (μ L)	10

2.17.4 Protein transfer to the membrane [Semi-dry transfer]

After SDS-PAGE electrophoresis separation, the proteins can be transferred to a solid-state membrane to allow further antibody staining and protein expression. This project used nitrocellulose membrane [Amersham™ Protran®]. The membrane is placed on top of the acrylamide gel and held in place with blotting paper in a cassette.

Once the electrophoresis was finalised, to equilibrate, the gel was submerged into transfer buffer [4.5 gr Tris base, 21.6 gr Glycine and 300 ml Methanol in 1200 ml of distilled water]. A rapid semi-dry transfer using the TransBlot® Turbo Transfer systems [Bio-Rad Laboratories, Hemel Hempstead, UK] was used to transfer the proteins from the acrylamide gel to a nitrocellulose membrane by sandwich transfer method. The transfer of proteins was carried out at 20 V for 30 minutes for each gel. The membrane was transferred into a cuvette with Tris-buffered saline (TBS) solution after the transfer with incubation for 1 minute in a rotator.

2.17.5 Blocking of membrane

After the transfer was concluded, the membranes were blocked for 2 hours with 5% (v/v) non-fat dry milk in Tris-buffered saline + 0.05% Tween 20 (TBS-T) with agitation at room temperature. Then, the membranes were washed with TBS for 5 minutes, followed by 3 additional washes with TBS-T (5 minutes each). The membrane was incubated overnight with primary antibody at 4°C with gentle shaking.

2.17.6 Primary and Secondary antibodies

Primary antibodies were diluted in TBS-T + 2% (v/v) BSA and 0.02% (v/v) sodium azide (to avoid bacteria growth) up to final volume of 10 ml. The list of antibodies used in this project is shown in Table 2-12.

Table 2-12. Primary antibody used for immunoblotting

Primary Antibody	Host	Manufacturer	Reference #	Dilution	MW
Anti-Nrf2	Mouse	Santa Cruz Biotechnology	Sc-365949	1:500	60 kDa
Anti-Keap1	Mouse	Santa Cruz Biotechnology	Sc-365626	1:500	69 kDa
Anti-Histone H3	Mouse	Santa Cruz Biotechnology	Sc-517576	1:500	15 kDa
Anti-GAPDH	Rabbit	Abcam	ab9485	1:2500	36 kDa
Anti-Trx	Rabbit	Abcam	ab16965	1:2000	12 kDa
Anti-GcLC	Rabbit	Abcam	ab53179	1:1000	73 kDa
Anti-Cyt C	Rabbit	Abcam	ab133504	1:500	kDa
Anti-NQO1	Mouse	Santa Cruz Biotechnology	Sc-32793	1:500	31 kDa
Anti-Caspase 3	Rabbit	Cell Signalling	14220	1:500	35 kDa
Anti-Cleaved caspase 3	Rabbit	Cell Signalling	9664	1:500	17-19 kDa
Anti-ACTIN	Mouse	Abcam	ab82241	1:2000	42 kDa

After incubation with a primary antibody, the membrane was washed in TBS for 5 minutes and then washed in TBS-T for 5 minutes. The membrane was incubated with fluorescence-conjugated secondary antibodies for 2 hours at room temperature with gentle shaking in the dark. All IRDye® secondary antibodies were diluted (1:10000) in Intercept blocking buffer [Li-COR Biosciences Ltd, Cambridge, UK] (Table 2-13).

Table 2-13 Secondary fluorescence-conjugated antibodies used for immunoblotting

Secondary Antibody	Fluorescent channel	Host & Reactivity	Manufacturer	Reference #
680RD	700 nm (red)	Donkey anti-mouse IgG (H+L)	LI-COR Biosciences	926-68072
		Donkey anti-rabbit IgG (H+L)		926-68073
800CW	800 nm (green)	Goat anti-mouse IgG (H+L)		926-32210
		Donkey anti-rabbit IgG (H+L)		926-32213

2.17.7 Detection of proteins

Once the fluorescence-conjugated secondary antibody incubation concluded, the membranes were washed with TBS for 5 minutes, followed by four washed of 5 minutes in TBS-T washes, gently shaking, and then detected. The band intensity was detected using the Odyssey® imaging system [Li-COR Biosciences Ltd, Cambridge, UK], following the manufacturer's guidelines. Quantification was completed using Image studio 5x version software for the target protein and loading control. The target protein expression was normalised against the loading control via the Microsoft Excel program.

2.18 Total RNA extraction and RT- qPCR analysis

2.18.1 RNA extraction and quantification

Total RNA of cells was extracted using Qiagen RNeasy Mini Kit according to the manufacturer's guidelines. Treated cells were washed with pre-cold 1X PBS followed by the combination of exposure to buffer [provided by the kit] and centrifugation steps, as

detailed manufacturer's instruction. The isolated RNA was quantified using a UV spectrophotometry NanoDrop™ 1000/1000c [Thermo Fisher Scientific, Loughborough, UK] at 260 nm (1OD= 40 µg/ml). The purity of the RNA extracted was checked by 260/280 nm and 260/230 nm ratio readings considering values ~2.0.

2.18.2 Reverse transcription

For the cDNA synthesis, random hexamers, dNTPs and total RNA were used by Biosystems thermal cycler [Sensoquest, GeneFlow]. First, 1 µg/µl of template RNA for each sample was added to a 0.6 ml microtube and maintained on ice. For each RNA sample, reverse transcriptase Scrip cDNA Master mix [Roche Diagnostic Ltd, Burgess Hill, UK] containing 4 µl of reaction buffer [provided by the kit], 2 µl of enzyme buffer [supplied by the kit] and RNase-free water were added to bring the total volume to 20 µl per sample. After brief centrifugation, the microtubes were transferred into a thermal cycler under thermal cycle settings (Table 2-14). Finally, the cDNA was diluted 1:1 in RNase-free water and used directly for real-time PCR or stored at -80°C until further experiments.

Table 2-14. Thermal cycle settings for reverse transcription from mRNA to cDNA.

Cycles	Temperature	Time
1	42°C	15 minutes
2	85°C	5 minutes
3	65°C	15 minutes
4	4°C	∞

2.18.3 Real-time PCR

Target and housekeeping genes were quantified using a real-time PCR (qPCR) Iq SYBR Green Kit [Bio-Rad Laboratories, Hempstead, UK]. The master mix was prepared by adding 3 µl of RNase-free water + 0.1 µl of each primer (reverse/forward) + 5 µl SYBR green mix and mixed gently through centrifugation. To each well, 9 µl of Master mix reaction was added to 1 µl of cDNA of samples (loaded in duplicate on a qPCR plate). The wells were sealed with strip caps and a centrifuge briefly to mix reagents.

Finally, RT-qPCR was conducted in a LightCycler 480 II platform [Roche Diagnostic Ltd, Burgess Hill, UK] set to the thermal profile detailed in Table 2-15. Automatically generating the melting curve ensures a single specific PCR product is generated with no primer dimers (Figure 2.6).

Table 2-15. Real-time qPCR thermal profile.

Stages of the reaction	Time	Temperature
Pre-incubation	10 minutes	95°C
Amplification	10 seconds	95°C
	10 seconds	58°C
	18 seconds	72°C
Number of cycles: 45		
Melting curve	5 seconds	95°C
	1 minutes	65°C
	Continuous	97°C
Cooling	10 seconds	40°C

Automatically generating the melting curve ensures a single specific PCR product is generated with no primer dimers (Figure 2.6).

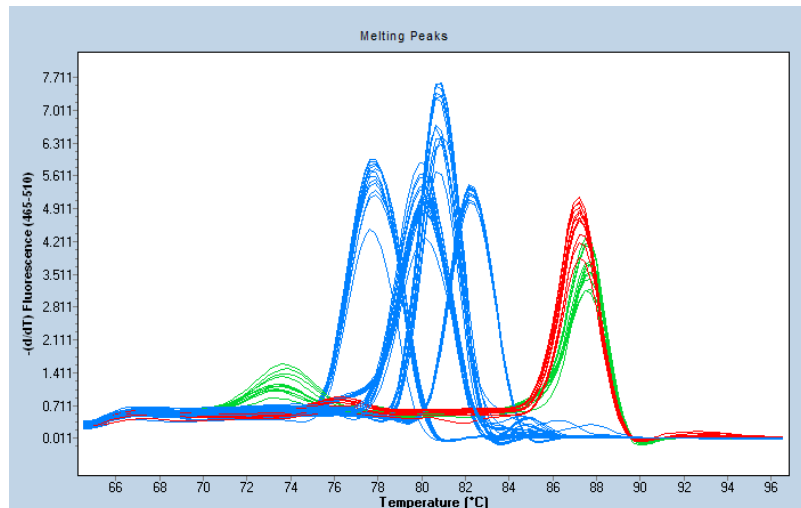


Figure 2.6. Representative Melting curves in the RT-qPCR.

A single peak indicates the generation of a pure and single specific amplification or qPCR product.

2.18.4 Quantification (Relative quantification method)

Standard calibration curve quantification was conducted using Light Cycler II software to extrapolate the Ct Using the comparative cycle threshold method [$\Delta\Delta Ct$], the target gene's Ct is normalised to the reference gene (housekeeping), which stays constant through the siRNA or any treatment of cells. In the current project, YWHAZ (tyrosine 3-monooxygenase/tryptophan 5-monooxygenase activation protein zeta) and EEF2 (eukaryotic translation elongation factor 2) genes were used as housekeeping due to their reproducibility and consistency compared with other genes (Figure 2.7).

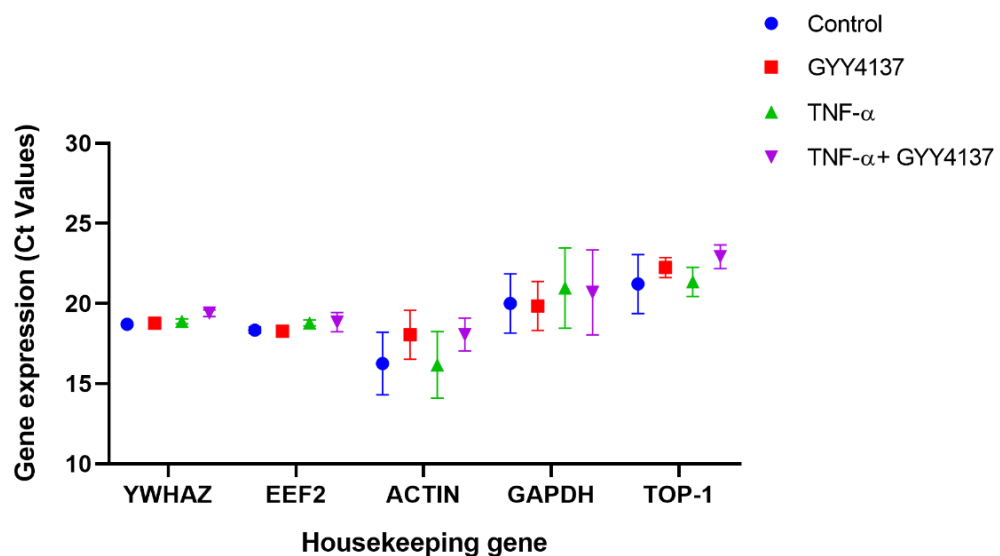


Figure 2.7 Comparative mRNA expression of different housekeeping genes. YWHAZ, EEF2, ACTIN, GAPDH and TOP-1 internal controls gene expression was examined and expressed as Ct values in endothelial cells under TNF- α and GYY4137 treatment settings. Values are represented as mean \pm SEM (n=3).

The relative fold change of the cDNA expression is calculated using the Livak method (Livak and Schmittgen, 2001). The quantitative method assumes that the target gene and the reference gene are being amplified simultaneously with amplification efficiencies between 90-110%. How to calculate the relative fold change is outlined below.

First normalisation of Ct value as ΔCt :

$$\Delta Ct = Ct (\text{target gene}) - Ct (\text{housekeeping genes})$$

Once each sample is normalised to the reference gene, the experimental samples must be normalised to the control sample.

$$\Delta\Delta Ct = \Delta Ct (\text{experimental sample}) - \Delta Ct (\text{control sample})$$

Finally, the outcome can be put in the formula from the Livak method: $2^{-\Delta\Delta Ct}$ producing the normalised expression ratio between experimental and control samples.

2.18.5 Primers

Forward and Reverse primers [Integrated DNA Technologies IDT, Iowa, US] were reconstituted to 100 μM final concentration with RNase-free water. Bio-rad [Bio-Rad Laboratories, Watford, UK] forward and reverse primers were reconstituted to 1 μM final concentration. The list of human forward and reverse primer sequences used in this thesis is shown in Table 2-16.

Table 2-16. List of forward and reverse primers sequences used in RT-qPCR experiments.

Target Gene	Forward 5' à 3'	Reverse 5' à 3'
YWHAZ	CCTGCATGAAGTCTGTAAGTCTGAG	GACCTACGGGCTCCTACAACA
EEF2	TGAACAAGATGGACCGCG	GGATCGATCATGATGTTGCC
eNOS	GCTAGCCAAAGTCACCATCG	TGGAAAACAGGAGTGAGGCT
NRF2	TGAGCCCAGTATCAGCAACA	AGTGAAATGCCGGAGTCAGA
KEAP1	CATCCACCCTAAGGTCATGGA	GACAGGTTGAAGAACTCCTCC
HO-1	GGGTGATAGAAGAGGCCAAGACT	GCAGAATCTTGCACTTTGTTGCT
TRX	GTGAAGCAGATCGAGAGCAAG	CGTGGCTGAGAAGTCAACTAC
TRXR1	ATATGGCAAGAAGGTGATGGTCC	GGGCTTGTCCTAACAAAGCTG
NQO1	CAGCTCACCGAGAGCCTAGT	GAGTGAGCCAGTACGATCAGTG
GcLC	TGTCACTGTTTTACCATTC	GGACGAGGATGAGGAGGAG
GcLM	CTCATTCCGCTGTCCAGGT	CCTTTGCAGATGTCTTTCTGAA
CAT	TCTGAAGGATCCGGACATGG	CATTCATGTGGCGATGTCCA
GPX-1	TCTCTTCGTTCTTGGCGTTC	CGGGACTACACCCAGATGAA
DRP1	AAGCTGCTGCCATAGTCTC	ACCACAGCCATGTCAGTGTC
MNF2	AACGCCAGGATTCAGAAAGCC	GGACCGTGTGCTGCTCAAAC
OPA1	TCTCATACTAGGATCGGCTGTTG	CACAATGTCAGGCACAATCCCA

UCP2	GGCTGGAGGTGGTCGGAG	CAGAAGTGAAGTGGCAAGGGAG
P21	TGAGCCGCAACTGTGATG	GTCTCGGTGACAAAGTCG
P53	CCAGGGCAGCTACGGTTTC	CTCCGTCATGTGCTGTGACTG
SOD2	TAGGGCTGAGGTTTGTCCAG	GGAGAAGTACCAGGAGGCGT

2.19 Maleimide Red assay

The maleimide assay was conducted to detect S-sulfhydrated proteins in EA.hy926 cells based on the published protocol (Bindu D Paul and Snyder, 2015b) based on the Cy5-conjugated maleimide fluorescence reagent (Alexa Fluor 680 C₂ Maleimide) (Figure 2.12). Immortalised cells were seeded at the density of 5x10⁵ in a T75 culture flask in fresh pre-warm medium cDMEM and incubated overnight at 37°C and 5% CO₂ conditions. EA.hy926 cells were treated overnight with and without GYY4137 (50 µM) in cDMEM at 37°C and 5% CO₂. Treated cells were homogenized in lysis buffer (150 mM NaCl; 50 mM Tris, pH 7.5; 1.2% Triton X-100; and 1mM EDTA). Samples were incubated with 1 µM Alexa Fluor 680 Cy5-maleimide (red maleimide)[ThermoFisher Scientific, Gloucester, UK] in lysis buffer for 2 hours at 4°C with gentle mixing. At this point, lysates were split into two tubes; therefore, one tube received lysis buffer and the other 1 mM of DTT. Samples were resuspended in SDS sample buffer without a reducing agent for gel electrophoresis separation (see section 2.17.3). The gel was scanned with the Li-Cor Odyssey system to detect red maleimide fluorescence signals. The scanned gel was transferred into a nitrocellulose membrane and subjected to western blot analysis for actin, as described in sections 2.17.6 and 2.17.7.

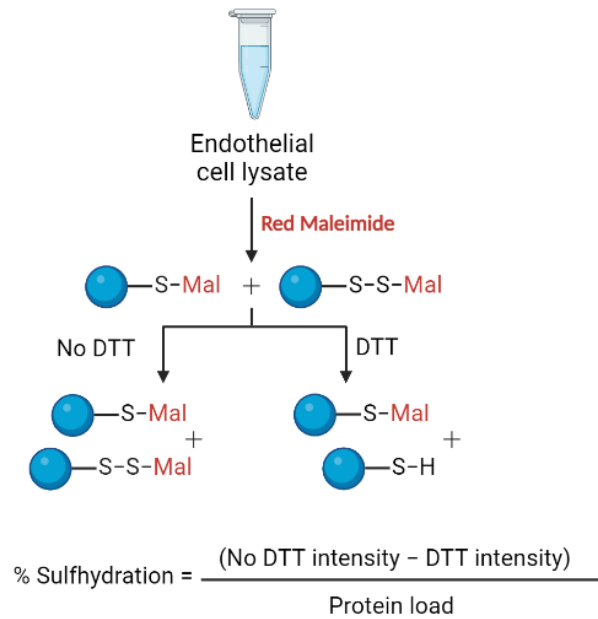


Figure 2.8 Illustration of Maleimide assay used to detect S-sulfhydration in cells. Free thiols and persulfide groups are labelled with Red maleimide. Lysate samples are separated into two groups, with only one receiving DTT. Adding the reducing agent decreases the fluorescence signal representative of S-sulfhydrated protein compared to samples without DTT.

2.20 Modified Biotin Switch assay

Based on the published protocol, the biotin-switch assay was used to detect S-sulfhydrated proteins by H₂S in endothelial cells (Mustafa *et al.*, 2009); the biochemical reaction during the assay is briefly summarised in Figure 2.9. Endothelial cells were subjected to several steps to detect sulfhydrated protein modification. The reagents and buffers composition are described in Table 2-17.

2.20.1 Experimental design conditions:

Experiment optimisation was performed using EA.hy926 cells. Immortalised cells were seeded at the density of 5x10⁵ cells in a T75 culture flask in fresh pre-warm medium cDMEM and incubated overnight at 37°C and 5% CO₂ conditions. EA.hy926 cells were

treated with and without NaHS (100 μ M) for 45 minutes and DTT (2 mM) for 30 minutes on ice before starting the experiment.

HUVECs cells were seeded at the density of 5×10^5 cells in a T75 culture flask in fresh pre-warm medium cEGM overnight. After confluency was reached, cells were divided into 4 groups and treated with TNF- α and GYY4137 compounds as described in section 2.2.8. At the endpoint of treatments, ECs were lysate by discarding the medium and washing cells with 10 ml of pre-cold 1X PBS. Pre-cold HEN buffer (400 μ l) supplemented with inhibitor cocktails (1:100), and 1% (v/v) Triton X-100 [Sigma-Aldrich, Gillingham, UK] was added to the flask containing the cells. The flask containing HUVECs was incubated for 5 minutes on dry ice. Then, the cells were scraped using a cell scraper on ice; then lysate was collected into a pre-cooled 1.5 ml microtube. Centrifugation at $14,000 \times g$ for 30 minutes at 4°C was carried out to remove the debris.

The supernatant was gently collected in a new pre-cooled 1.5 ml microtube. Protein concentration was determined by BCA assay (see section 2.17.2) and then adjusted to <0.5 mg/ml per sample. As positive control (group 5), untreated cell lysate was treated with 100 μ M NaHS [Sigma-Aldrich, Gillingham, UK] for 45 minutes prior to starting the experimental protocol.

2.20.2 Biotin Switch protocol

Protein lysates were blocked with HENS buffer (4 volumes per sample) and incubated at 50°C for 20 minutes on a thermomixer with gentle rotation and in the dark. Acetone precipitation was selected to remove the MMTS (S-4-bromobenzylmethanethiosulfanate): 4 volumes of pre-cold acetone were added into a 5 ml tube for each sample incubated at -20°C for 1 hour. The samples were centrifuged at $1500 \times g$ for 10 minutes at 4°C . The supernatant acetone was carefully removed, and the protein pellet was resuspended in 500 μ l of pre-cold acetone, followed by additional centrifugation at $1500 \times g$ for 10 minutes. Finally, protein samples were recovered by removing all the acetone.

The protein pellet was resuspended in 800 μ L HENS buffer with 1% SDS per mg of protein (starting sample) and 200 μ L of labelling Biotin-HPDP solution (4 mM final concentration). The samples were incubated at 25°C for 3 hours with gentle rotation in

the dark. Then, second acetone precipitation was performed, as explained above. During acetone precipitation, 3 mg of streptavidin beads (ml) per 0.2 mg of biotin-HPDP per sample were washed in 500 μ l of HEN buffer, followed by centrifugation at 5000 x *g* for 30 seconds. An additional volume of HEN buffer was added after discarding the supernatant, and beads were centrifuged at 5000 x *g* for 5 minutes. Finally, the beads were resuspended in 500 μ l HEN buffer.

Once the acetone precipitation was completed and the protein pellet obtained, samples were resuspended in 250 μ l of HEN buffer and 750 μ l of Neutralisation buffer. At this point, a small amount of volume (30 μ l) per sample is separated into a new 0.5 ml microtube and stored at -80°C for total load protein. While we collect input samples, Neutr-Avidin Agarose Resin beads are washed twice with HEN buffer and collected by centrifuge at 5000 x *g* for 1 minute and 5 minutes for the first and second wash, respectively. Subsequently, the remaining protein lysate mixed with HEN buffer and Neutralisation buffer was integrated with 500 μ l HEN buffer containing the Neutr-Avidin Agarose Resin beads. Protein samples with beads were incubated at 4°C overnight with gentle rotation.

The next day, the streptavidin beads were collected by centrifugation at 5000 x *g* for 30 seconds, and the supernatant was removed. The beads were washed with high salt neutralisation buffer six times, centrifuging at 5000 x *g* for 5 minutes. The supernatant was discarded, and a 1 ml syringe aspirated the dryness. Then, an elution buffer containing 1% of β -ME (50 μ l) was added to each sample and proteins with beads were incubated at 37°C for 30 minutes with agitation at 1000 rpm. After pelleting down protein samples by centrifugation at 5000 x *g* for 5 minutes, the supernatant contains sulfhydrated proteins per sample.

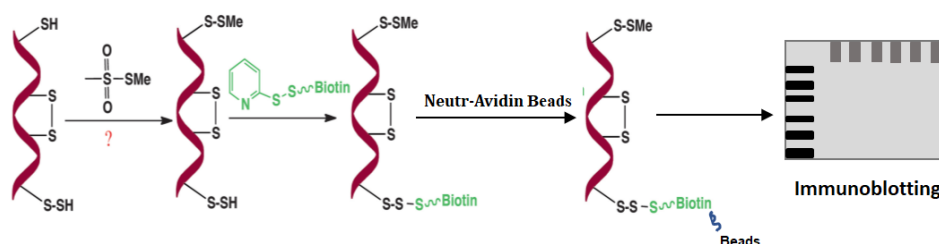


Figure 2.9 Schematic diagram of Modified Biotin switch assay.

Free thiols (-SH) in cysteine residues of protein lysate were blocked with MMTS with incubation at 50° C for 20 minutes. Modified thiol group (-SSH) were labelled with Biotin-HPDP by incubation for 3 hours at 25 °C. Neutr-Avidin Resin beads were linked to Biotin -HPDP groups in cysteine residues. After overnight incubation at 4 °C, beads were collected by centrifugation at 5000 g and modified thiol group obtained by elution buffer incubation at 37 °C. Protein-modified thiol group and input protein samples were visualised by immunoblotting with 4x SDS loading buffer without reducing compounds.

A total volume of 20 µl from each sulfhydrated sample was transferred into a new microtube. Total load and sulfhydrated samples were resuspended in 4X SDS-PAGE loading buffer without reducing agents (DTT or β-ME). Sulfhydrated and total load samples were incubated at 90°C for 5 minutes, followed by electrophoresis in a 10% SDS-PAGE gel (see section 2.17.3). Proteins were transferred into a nitrocellulose membrane, and total protein was examined before blocking the membrane using a Revert® 700 Total protein stain kit [LI-COR Biosciences, Nebraska, USA]. Target protein expression was detected using primary antibodies listed in Table 2-4 and fluorescence-conjugated secondary antibodies (Table 2-5) following the steps described in section 2.17.7. Quantification of sulfhydrated and input sample expression was conducted using ImageJ software. The expression of sulfhydrated protein was normalised against the expression of the total load sample. Results are presented relative to the control group.

Table 2-17. Reagents used for Modified Biotin Switch assay

Component	MW	pH	Final Concentration
<u>HEN Buffer</u>			
HEPES-NaOH	238.3	7.7	250 mM
EDTA	292.24	8	1 mM
Neocuproine	NA	NA	0.1 mM
Deferoxamine	656.79	NA	100 U
dH ₂ O	NA	NA	NA
Triton X-100	NA	NA	1%
<u>HENS buffer</u>			
HEN buffer	NA	NA	NA
SDS Solution	25% (w/v)		2.5%
MMTS	126.2		20 mM
<u>HENS buffer + 1 % SDS</u>			
HEN BUFFER	NA	NA	NA
SDS			1%
<u>Biotin-HPDP</u>			
Biotin-HPDP stock	539.78	NA	50 mM
Labelling biotin-HPDP	NA	NA	4 mM
<u>Neutralisation buffer</u>			
HEPES-NaOH	238.3	7.7	20 mM
NaCl	58.44	8	100 mM
EDTA	292.24	8	1 mM
Triton X-100	NA	NA	0.5%
dH ₂ O	NA		NA
<u>High Salt Neutralization buffer</u>			
HEPES-NaOH	238.3	7.7	20 mM
NaCL	58.44	8	600 mM
EDTA	292.24	8	1 mM
Triton X-100	NA	NA	0.5%

dH ₂ O	NA	NA	NA
<u>Elution Buffer</u>			
HEPES-NaOH	238.3	7.7	20 mM
NaCl	58.44	8	100 mM
EDTA	292.24	8	1 mM
β-ME		NA	1% (v/v)
dH ₂ O			

2.21 Statistical Analysis

Statistical analysis of data was carried out using GraphPad Prism® version 8 software. All normally distributed variables were compared by unpaired Student's *t*-test and non-normally variables were compared by Mann-Whitney U test. When comparing two or more groups, one-way ANOVA followed by Dunnett's, Tukey's or Sidak's *post-hoc* multiple comparisons test was applied, as specified in each experiment. Results are expressed as means ± SEM, and "*n*" represents the number of independent experiments or biological replicates. All results were statistically significant at *p*-values of **p*<0.05, ***p*<0.01 and ****p*<0.001.

3 Assessment of endothelial in vitro model using TNF- α and GYY4137 compounds

3.1 Introduction

Reclassifying the endothelium from a simple cell barrier to a dynamic endocrine organ generated a lot of attention and contributed to the expansion of vascular system research (Durand and Gutterman, 2013; Rajendran *et al.*, 2013). The endothelium phenotype can vary between organs, neighbouring cells within the same organ, and the subtype of blood vessels. Such variations include morphology, gene profile expression, extracellular matrix and cell surface properties (Aird, 2003). For example, the vWf is expressed within the endothelium of veins, whereas the endothelium present in the microvasculature of the heart lacks this marker (J. Liu *et al.*, 2011).

ECs culture has been a robust tool for studying the endothelium under physiological and pathophysiological conditions (Bachetti and Morbidelli, 2000). Nowadays, appreciation of endothelium function emerged primarily from studying primary ECs such as HUVECs. As an *in vitro* model, HUVECs provide a more understandable idea of the actual physiological *in vitro* environment and the possibility for multifunctional prodrug tests. Indeed, ED can be studied using HUVECs pro-inflammatory agents such as TNF- α (Jiang *et al.*, 2016). Furthermore, previous authors have investigated the underlying mechanisms of endothelium-mediator molecules, including H₂S, in pathological cardiovascular scenarios using HUVECs as *in vitro* model (Park *et al.*, 2006; Lin *et al.*, 2020). However, a limited life span (within 10 passages) and the possibility of batch-to-batch variation in HUVECs have increased the demand for immortalised cells (Jaffe *et al.*, 1973). One of the most frequently used and best-characterised immortalised cell lines is EA.hy926, a hybrid of epithelial adenocarcinoma cell line A549 and HUVECs (Xie, Feng, *et al.*, 2016). EA.hy926 cells exhibit several advantages such as unlimited life span, consistency across passages and presenting basic phenotypic features of ECs such as the presence of Weibel-palade bodies (Bouïs *et al.*, 2001). However, their biological nature has been altered slightly due to cellular fusion, and thus EA.hy926 are a less representative *in vitro* model of true endothelial function.

The pleiotropic cytokine TNF- α can regulate several signalling pathways in the endothelium by binding to its receptors (Aggarwal, Gupta and Kim, 2012). TNF- α is a cytokine that activates the endothelium and leads to the upregulation of surface proteins such as ICAM-1, VCAM-1 and E-selectin, which aid in the inflammatory process by binding to leukocyte receptors.

The migration of leukocytes into the subendothelium can occur as a defence mechanism, which further recruits leukocytes by releasing cytokines and chemokines (Muller, 2003; Yang, Zhao and Tian, 2016). In fact, TNF- α participates as a modulator against infection, as revealed in transgenic mice models with *Listeria monocytogenes* (Torres *et al.*, 2005).

However, malfunctioning ECs or continuous insult stimuli can lead to unregulated leukocyte recruitment and impair endothelial functions, degenerating into ED and later tissue damage (Manning *et al.*, 2021). In line with these observations, TNF- α contributes to irreversible I/R injury, post-myocardial infarction and heart failure in association with ED in a dose- and time-dependent manner in ECs (Kleinbongard, Heusch and Schulz, 2010). Furthermore, ECs damage upon TNF- α exposure has been previously reported *in vitro* by increased ROS levels, impaired antioxidant defence, pro-apoptotic environment and release of pro-inflammatory cytokines (e.g., IL-6 and IL-1 β) (Liao *et al.*, 2010; C. Xu *et al.*, 2015; Galkin *et al.*, 2016; Batko *et al.*, 2019).

The endogenous H₂S content comprises nanomolar to micromolar levels in most vascular beds (Filipovic *et al.*, 2018; Beltowski, 2019). Interestingly, H₂S can regulate the vascular tone, redox state, inflammatory response and cell death (Predmore, Lefer and Gojon, 2012). For instance, vasodilation of SMVCs through ATP-sensitive K⁺ channels has been previously described by H₂S (Zhao, 2001). Yang and colleagues later confirmed this physiological effect using a CSE knockout mouse model, in which blood vessel relaxation decreased, and blood pressure was elevated (Yang *et al.*, 2008b). However, precautions are needed when working with H₂S since high concentration results in cell death and tissue damage by inhibiting the mitochondrial ETC complex (Szabo, 2018). The manipulation of H₂S content and its endogenous actions without cellular toxicity have been achieved using prodrugs (Yuan, Zheng and Wang, 2020). One well-established donor is GYY4137, a water-soluble derivative of Lawesson's reagents that release H₂S upon hydrolysis slowly over a sustained period (Li *et al.*, 2008). These features have supported the application of GYY4137 as a suitable H₂S donor in biological systems. For instance, GYY4137 protects against atherosclerosis, diabetes and mitochondrial dysfunction without cytotoxic effects by reducing oxidative damage and apoptosis in mice (Liu *et al.*, 2013; Qiu *et al.*, 2018) and ECs (Xie, Feng, *et al.*, 2016).

Currently, most *in vitro* studies have described H₂S modulation as a pre-treatment, where exogenous H₂S is given before the systemic/cellular insult (Wen *et al.*, 2013; Xie, Feng, *et al.*, 2016; Potenza *et al.*, 2017; Hao *et al.*, 2019) or as co-treatment (Shen *et al.*, 2013; Zhu *et al.*, 2021); thereby focusing on a prevention strategy. For instance, GYY4137 pre-treatment for 4 hours exhibits anti-apoptotic and oxidative damage effects in H₂O₂-mediated EA.hy926 cells (Xie, Feng, *et al.*, 2016). Even though these experimental approaches have advantages when investigating the manifestation of a condition, post-treatment may offer the ability to investigate underlying mechanisms to revoke a disease condition and test the suitability of a drug (Wallace *et al.*, 2020).

3.2 Aims

This chapter aimed to optimise TNF- α as endothelial stressor stimuli and GYY4137 as a suitable H₂S donor for applying the optimum experimental design to investigate H₂S function in TNF- α -induced ED.

This chapter focuses on methodology development, including the optimisation of agents with a focus on titration of the optimum dose for each compound and characterisation of the experimental design for the primary cell model. These key subjects demonstrated the workflow applied to achieve a cell culture model best suited for investigating the H₂S role in altered endothelium.

3.3 Materials and Methods

3.3.1 Endothelial cell culture

EA.hy926 cell line was used for all characterisation and optimisation experiments to identify the TNF- α dose and duration most suitable to induce ED and to select an experimental setting approach for TNF- α and GYY4137 treatments. EA.hy926 cells were maintained under standard cell culture conditions as described in section 2.2.3, unless otherwise stated.

HUVECs were used for data transferability from immortalised to the primary cell model. Comparable impact of TNF- α from EA.hy926 cells to HUVECs was assessed. Non-toxic GYY4137 was determined in HUVECs, the ongoing concentration for further

experiments. HUVECs were maintained following standard cell culture settings as explained in section 2.2.3, unless otherwise stated.

3.3.2 Fluorescence microscopy

Immunofluorescence staining of vWf and CD31 (platelet/endothelial cell adhesion molecule-1) was performed using Alexa Fluor 488 fluorescence conjugated antibodies to determine endothelial phenotype as described in section 2.9.1.

SF7-AM fluorescence staining was used to assess intracellular H₂S content, see section 2.4.

MitoSox fluorescence probe was used to analyse O₂⁻ described in section 2.5.2.

3.3.3 ELISA

The release of IL-6 was analysed using supernatant by ELISA assay. For details of the entire procedure, see section 2.11.

3.3.4 RT-qPCR

Quantitative real-time PCR was performed by extracting the total RNA. Fold change relative expression was calculated using the $\Delta\Delta C_t$ method when comparing gene expression under different treatments using YWAZ and EEF2 as housekeeping genes. For full details, see section 2.18.

3.3.5 Flow cytometry

The expression of the cell adhesion molecule, ICAM-1, was evaluated by flow cytometer analysis using the BD Accuri C6 Plus system. For full details on cell population gating and fluorescent antibodies, please refer to section 2.6.1.

3.3.6 Statistical Analysis

All values presented are as mean \pm SEM. Unless otherwise stated, all usually distributed variables between two groups were compared by unpaired Student *t*-test. When

comparing two groups or more one-way ANOVA followed by Turkey's and Dunnett's *post-hoc* multiple comparison tests were applied. For statistical tests, p values less than 0.05 ($p < 0.05$) were considered significant.

3.4 Results

3.4.1 Characterisation of EA.hy926 cells as *in vitro* endothelial model.

The EA.hy926 cell line is one of the most common cell lines used for vascular research. (Edgell *et al.*, 1990; Unger *et al.*, 2002). To support previous observations and confirm that the EA.hy926 cell line is suitable *in vitro* EC model, endothelial phenotypic markers such as vWf and CD31 were examined. Immunofluorescence analysis showed positive staining for vWf (**Figure 3.1 A**) and CD31 (**Figure 3.1 B**) by ECs.

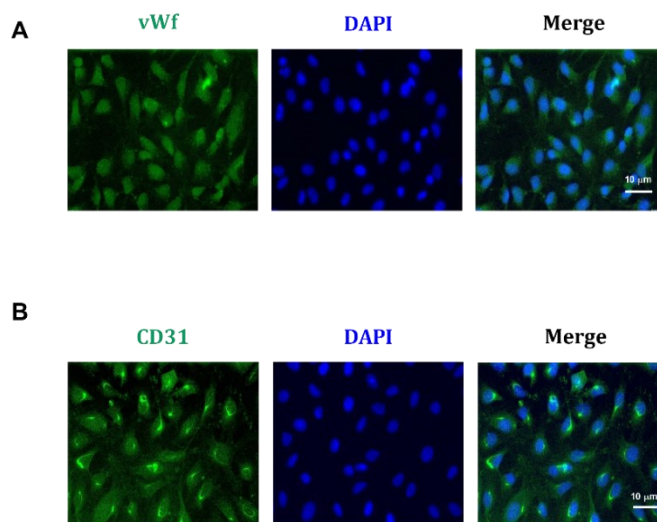


Figure 3.1 Expression of endothelial markers by EA.hy926 cells. Immunofluorescence staining images of **(A)** Von Willebrand factor (vWf) and **(B)** CD31 (green spectrum) in EA.hy926 cell. Nuclei stained with DAPI (blue spectrum). EA.hy926 cell line shows the typical cobblestone morphology. Pictures were taken using a Nikon Ti-S fluorescence microscope (20x magnification; scale bar is 10 μm).

Furthermore, EA.hy926 cells displayed typical morphological characteristics of ECs, including polygonal cobblestone, elongated, and aligned features. These results demonstrate that the EA.hy926 cell line expressed EC markers, making it a suitable cell

culture model for studying vascular functions (Bachetti and Morbidelli, 2000; Riederer *et al.*, 2010).

3.4.2 Titration of the optimum GYY4137 dose and assessing intracellular H₂S content in EA.hy926 cells.

Several H₂S donors are commercially available (e.g., sulfide salts) but can release non-realistic high H₂S concentrations. GYY4137 was the chosen donor as it has exhibited a gradual and sustained release of H₂S rate *in vivo* and *in vitro* (Li *et al.*, 2008). H₂S can exhibit cell toxicity at high concentrations by inhibiting mitochondrial cyto c oxidase activity; therefore, examination of toxicity was required (Liu *et al.*, 2013; Aroca *et al.*, 2020). Titrating the optimum dose of GYY4137 to increase intracellular H₂S content without toxicity was undertaken using a well-established CellTiter-Blue metabolic activity assay. In Figure 3.2 A, five doses of GYY4137 were tested [0 µM (control), 50 µM, 100 µM, 200 µM, 300 µM] to fit with doses of exogenous H₂S donor widely used in previous studies with ECs (Xie, Feng, *et al.*, 2016). After cells were treated with increasing doses of GYY4137 for 24 hours, samples were incubated with CellTiter-Blue allowing them to progress through colourimetric changes to assess the metabolic capacity of viable cells. As shown in Figure 3.2 A, exposure of EA.hy926 cells to 50 µM did not cause a decline in the metabolic ability of viable cells compared to untreated cells. Although 100 µM GYY4137 concentration causes a significant reduction in metabolic capacity compared to untreated cells, treatment with 200 µM, 300 µM and 400 µM showed a more profound reduction in the number of viable cells (**p<0.0001).

Secondly, it was essential to distinguish whether treatment with GYY4137 was associated with changes in the intracellular H₂S content. For this purpose, intracellular H₂S levels were explored using the fluorescent probe SF7-AM (a cell-trappable fluorescent probe for H₂S signalling), previously used in HUVECs (Yuan *et al.*, 2016) (Figure 3.2 B). After EA.hy926 cells were cultured in the absence (0 µM) or presence of GYY4137 (50 µM), samples were stained with SF7-AM and analysed by fluorescence microscopy. As shown in Figure 3.2 B, after EA.hy926 cells were incubated with GYY5147 (50 µM) for 24 hours, H₂S content increased compared to the control group, as evidenced by increased fluorescence emission of SF7-AM. These observations suggest that the threshold of intracellular H₂S content is stimulated by non-toxic treatment with GYY4137 (50 µM) in ECs.

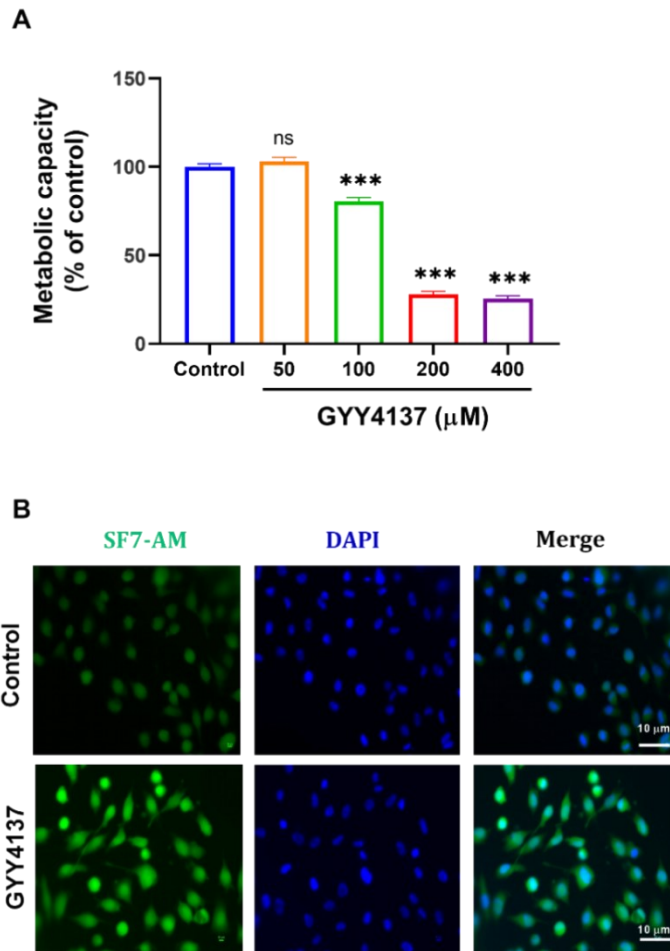


Figure 3.2 Titration of non-toxic GYY4137 dose and analysis of intracellular H₂S content in EA.hy926 cells.

(A) CellTiter-Blue™ assay on EA.hy926 cells was conducted to determine the metabolic capacity of GYY4137 dose-dependent treatment [50 µM, 100 µM, 200 µM, 300 µM and 400 µM] in comparison to the control group [0 µM] for 24 hours. **(B)** Intracellular H₂S content was evaluated by SF7-AM (2.5 µM) staining probe (green spectrum) in untreated and treated EA.hy926 cells. Nucleus was stained with DAPI (blue spectrum). Pictures were taken using a Nikon Ti-S Inverted fluorescence microscope (20x magnification; scale bar is 10 µm). Data are represented as mean ± SEM (n=3) and analysed by one-way ANOVA, followed by a Dunnett's multiple comparison test. ***p < 0.0001 vs. control group.

3.4.4 Characterisation of TNF- α as an agent to alter endothelial functions in EA.hy926 cells.

To investigate the impact of H₂S on impaired endothelium, a stress stimulus was used to generate and activate endothelial phenotype. In this thesis, TNF- α was the chosen stressor agent as it has been reported to alter endothelial functions in a pleiotropic manner (Csiszar *et al.*, 2008). In Figure 3.3, increasing concentrations of TNF- α [0 ng/ml (control), 1 ng/ml, 5 ng/ml and 10 ng/ml] were tested to fit with those doses, and an incubation time (6 hours) previously used on the literature in EA.hy926 cells (S. Wang *et al.*, 2018). The ability of TNF- α to modulate endothelial phenotype was identified using vital biological markers of endothelium function such as eNOS mRNA levels and pro-inflammatory cytokine (IL-6).

EA.hy926 cells were subjected to culture with the indicated doses of TNF- α , the supernatant was collected for IL-6 secretion analysis, and total RNA was extracted from samples for RT-qPCR analysis (Figure 3.3). All tested doses of TNF- α significantly decreased eNOS mRNA levels compared to untreated cells (**p<0.01) (**p<0.0001) (Figure 3.3 A). Furthermore, EA.hy926 cells exposed to TNF- α displayed a significant increase in the secretion of L-6 relative to control cells in a dose-dependent manner (**p<0.01) (**p<0.0001) (Figure 3.3 B). The lowest and highest levels of eNOS mRNA levels and IL-6 secretion were observed in the presence of 10 ng/ml. These results suggest that TNF- α might induce endothelial activation at the transcriptional level and inflammatory response in EA.hy926 cells.

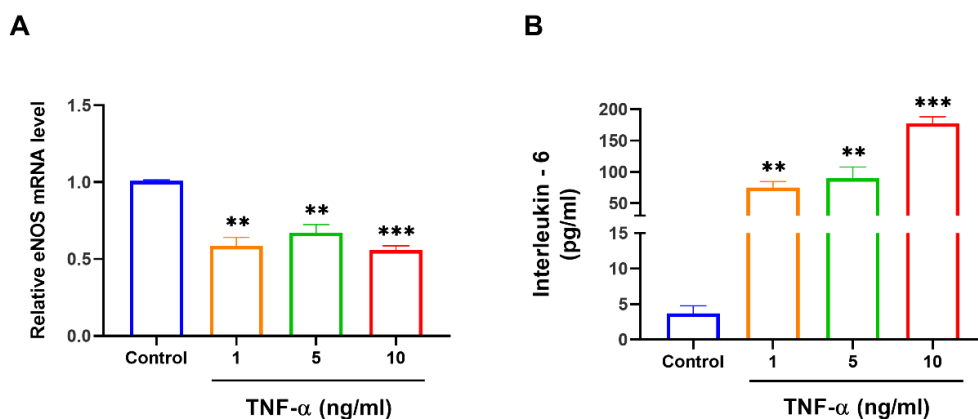


Figure 3.3 Assessing TNF- α effect on endothelial activation in EA.hy926 cells.

Cells were treated with TNF- α indicated concentrations for 6 hours before analysis. **(A)** Total RNA was isolated and analysed for eNOS mRNA levels using RT-qPCR. **(B)** Supernatants were collected, and IL-6 content (pg/ml) was assessed by ELISA assay. Results were shown as mean \pm SEM (n=3). Significance was determined by one-way ANOVA followed by Dunnett's post-test comparing treatments to the 0 ng/ml TNF- α treated cell (control), **p<0.01 and ***p<0.001 vs. control.

3.4.5 Establishing an *in vitro* experimental model using TNF- α and GYY4137 compounds in EA.hy926 cells.

All tested doses of TNF- α produced enhanced endothelial activation and inflammatory response following 6 hours of incubation. In addition, GYY4137 (50 μ M) enhanced intracellular H₂S content without toxicity. The next step was monitoring different experimental settings using both compounds. This approach would allow the assessment of the optimal *in vitro* conditions to investigate H₂S effects on TNF- α -induced ED. To fit with those H₂S experimental intervals used in previous studies, three cell culture models (pre, co and post-treatment) were tested (Xie, Feng, *et al.*, 2016; Potenza *et al.*, 2017; Zhu *et al.*, 2021). EA.hy926 cells were cultured with increasing TNF- α concentrations [1, 5 and 10 ng/ml] and with GYY4137 (50 μ M) for the specified time. ELISA assay was chosen to examine the different cell culture designs (Figure 3.4).

As shown in Figure 3.4 A, the pre-treatment setting relies on overnight (18 hours) GYY4137 incubation before the addition of TNF- α for 6 hours. On the other hand, the co-treatment set-up comprises incubation with both agents (TNF- α and GYY4137) for 24 hours at indicated concentrations. Upon the post-treatment approach, cells are incubated with TNF- α for 6 hours, followed by overnight (18 hours) GYY4137 treatment. In Figure 3.4 B, analysis of IL-6 secretion following the pre-treatment setting revealed that all three TNF- α concentrations significantly increased IL-6 levels compared to control cells (* $p < 0.05$), with 10 ng/ml as the dose with the most significant rise (** $p < 0.0001$). Notably, pre-treatment with GYY4137 did not modify the TNF- α -induced effect, as exemplified by IL-6 content. However, due to the poor efficiency of the pre-treatment experimental setting to prevent the pro-inflammatory effect of TNF- α and the time restraints of this thesis, the pre-treatment model was discarded, and an alternative practical interval was tested.

Subsequently, the co-treatment interval was approached by culturing EA.hy926 cells with TNF- α and GYY4137 simultaneously for 24 hours. Figure 3.4 C shows that IL-6 content increases in line with the escalation of TNF- α doses, with 5 ng/ml (* $p < 0.05$) and 10 ng/ml (** $p < 0.01$) expressing a significant response compared to the control group. In the presence of TNF- α at 10 ng/ml concentration, the highest increase of IL-6 secretion compared to untreated cells was observed. GYY4137 stimulation did not reduce IL-6 levels in TNF- α -treated EA.hy926 cells. Furthermore, Figure 3.4 C shows that the GYY4137 treatment slightly reduced IL-6 content at 5 ng/ml TNF- α compared to the TNF- α treatment alone, but the change did not reach significance. These observations suggest that the H₂S co-treatment model also failed to reduce the pro-inflammatory response in TNF- α -induced ECs. As a result, this treatment setting was abandoned.

Finally, a post-treatment culture setting was investigated with cells undergoing TNF- α incubation before GYY4137 treatment. Similar to the previous experimental settings, EA.hy926 cells exposed to TNF- α exhibited a significant increase in IL-6 content in a dose-dependent (* $p < 0.05$), with 10 ng/ml dose leading to the highest rise (** $p < 0.01$) (Figure 3.4 D). Interestingly, the secretion of IL-6 (pg/ml) in the post-treatment setting is around 6-fold lower than in pre-treatment and co-treatment experimental models. Similar to pre-and co-treatment intervals, EA.hy926 cells treated with GYY4137 alone did not increase the secretion of IL-6 compared to control cells.

Upon TNF- α (1 ng/ml and 5 ng/ml) stimulation, no significant reduction in IL-6 levels was observed after GYY4137 treatment. Notably, TNF- α at 10 ng/ml followed by GYY4137 post-treatment is the only interval that displayed a trend to decrease IL-6 secretion, although values did not reach statistical significance. These observations suggest that post-treatment might be a suitable culture model to investigate H₂S underlying signalling mechanisms in dysfunctional endothelium. Considering the current results and the project's time limitations, the post-treatment design was selected for future experimental designs.

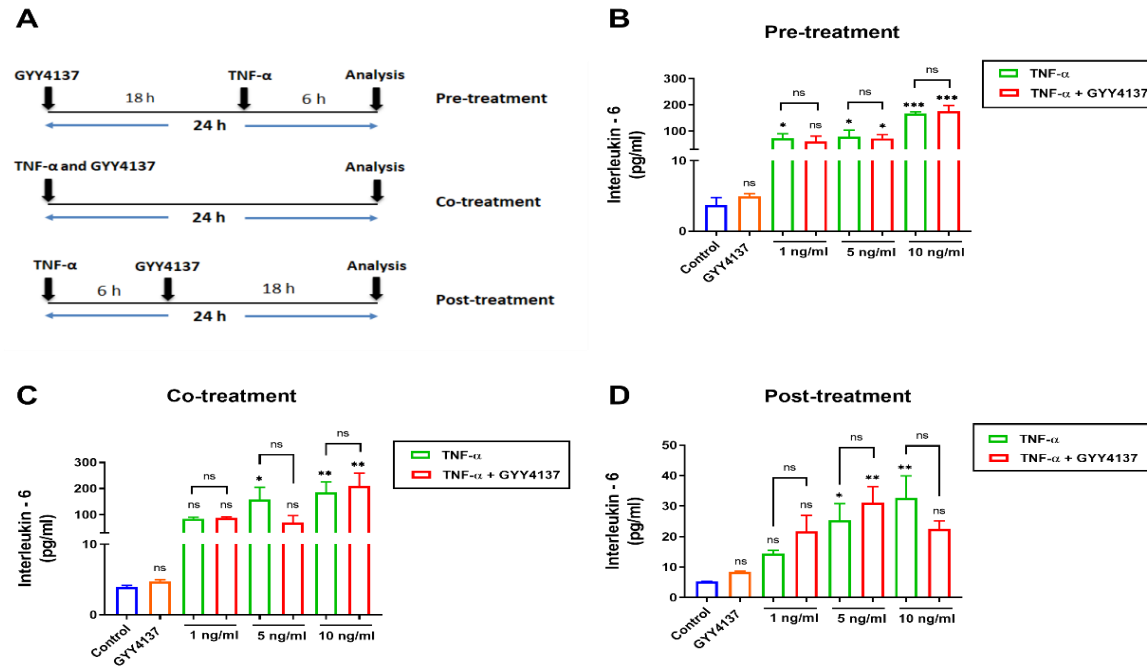


Figure 3.4 Comparison between three experimental settings on the IL-6 secretion in EA.hy926 cells.

(A) Scheme of the applied practical setting using TNF- α (1, 5 and 10 ng/ml) and GYY4137 (50 μ M) compounds. Cells were cultured with indicated approach, and ELISA assay analysed IL-6 cytokine content (pg/ml). Graph bar for IL-6 content upon (B) pre-treatment, (C) co-treatment and (D) post-treatment experimental settings using TNF- α and GYY4137 treatments at indicated concentrations. Results are shown as means \pm SEM (n=3). Significance was defined by one-way ANOVA followed by Tukey's *post-hoc* comparing treatments, whereby *p<0.05, **p<0.01 and ***p<0.001 vs. control.

3.4.6 Assessment of the optimum and non-toxic dose of GYY4137 for HUVECs.

While immortalised, EA.hy926 cells are a suitable cell line for optimisation due to their long life span, reliability through the culture passages, and easy to handle; their hybrid nature provides a less representative model (Bouïis *et al.*, 2001; Jiang *et al.*, 2016). Once the optimum experimental design for the current thesis was selected (post-treatment), a more human-representative model was chosen. To fit with the cell culture model widely used in previous studies with TNF- α and GYY4137, HUVECs were selected (Jiang *et al.*, 2016; Lin *et al.*, 2020). However, HUVECs and EA.hy926 cells have different origins and some phenotypic features; therefore, readjustment was required (Lidington *et al.*, 1999).

To select a non-toxic GYY4137 concentration, increasing doses of GYY4137 were tested. Titrating of four doses of GYY4137 was investigated [0 μ M (control), 50 μ M, 100 μ M, 200 μ M, 400 μ M] to fit with doses tested in previous studies using HUVECs (Zhu *et al.*, 2021). Due to GYY4137 doses did not change the metabolic activity of HUVECs (S.3.1), an alternative method to identify the optimum GYY4137 concentration for HUVECs was assessed. Analysis of oxidant formation, in particular, $O_2^{\cdot-}$ was used as H_2S exhibited toxicity by targeting mitochondria ETC (Feng *et al.*, 2020). Once treatment with a specific GYY4137 dose for 24 hours was concluded, cells were stained with MitoSox, and the fluorescence intensity signal was analysed (Figure 3.5). As shown in Figure 3.5 A, exposure of HUVECs to 50 μ M and 100 μ M did not cause a significant increase in $O_2^{\cdot-}$ level, as indicated by the MitoSox fluorescence signal, with both doses showing similar $O_2^{\cdot-}$ levels. On the other hand, exogenous stimulation with 200 μ M and 400 μ M GYY4137 results in a significant rise in intracellular $O_2^{\cdot-}$ fluorescence signal to control group (** $p < 0.01$).

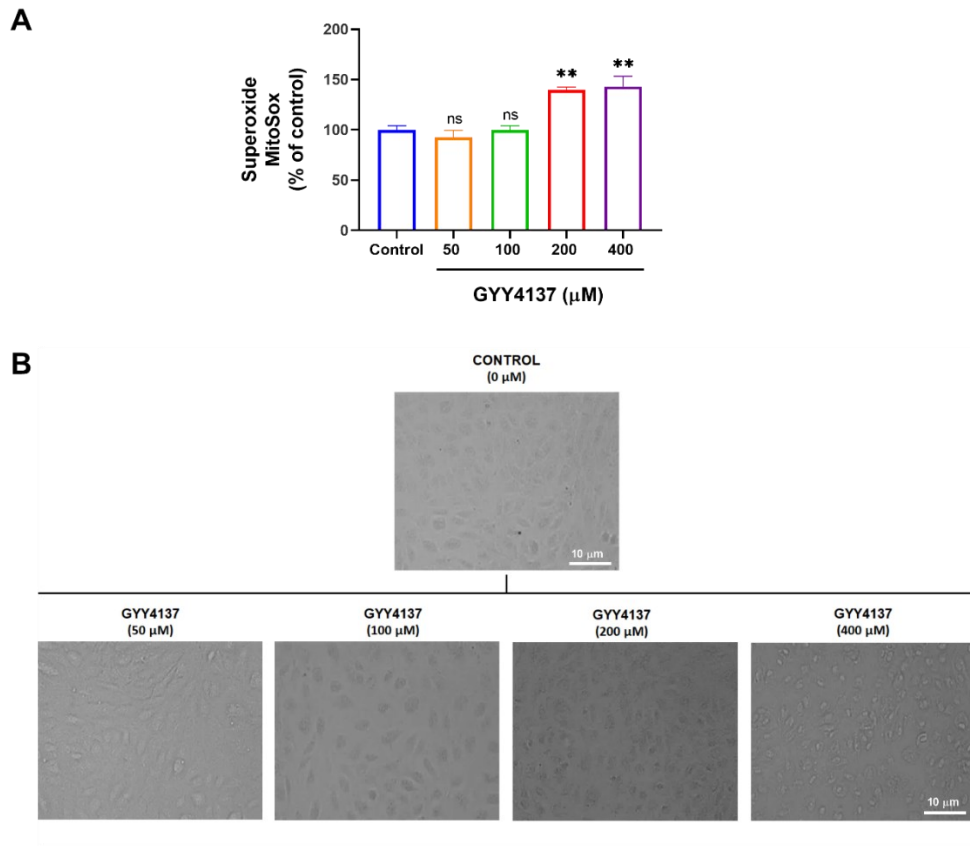


Figure 3.5 Characterisation of optimal non-toxic GYY4137 dose in HUVECs.

Cells were treated with increasing GYY4137 concentration [50 μM, 100 μM, 200 μM and 400 μM] in comparison to the control group [0 μM] for 24 hours, followed by incubation with O₂⁻ fluorogenic probe-MitoSox (5 μM) for 30 minutes. **(A)** Graph bar showing O₂⁻ levels in the presence of GYY4137 increasing doses. **(B)** To examine morphological changes, the endothelial phenotype was viewed under a Nikon Eclipse T s 2 inverted routine microscopes (20x magnification, scale bar is 10 μm). Data are represented as mean ± SEM (n=3) and analysed by one-way ANOVA, followed by a Dunnett's multiple comparison test. **p< 0.01 vs. control group.

Since toxicity is a biological phenomenon that can induce morphological changes, HUVECs morphology was examined by phase-contrast microscopy to confirm further results obtained by MitoSox analysis. Figure 3.5 B illustrates that the typical cobblestone structure of ECs is modified in the presence of GYY4137 at 200 μM and 400 μM doses compared to control cells. This evidence suggests that GYY4137 may exhibit toxicity starting at 200 μM in HUVECs. Therefore, to observe the maximum effect without toxicity in H₂S-cultured HUVECs and in line with previous HUVECs studies, GYY4137 at 100 μM was chosen as a suitable dose (Henderson *et al.*, 2010; Hao *et al.*, 2019).

To further confirm that GYY4137 is a suitable exogenous H₂S donor at 100 μM in HUVECs, an examination of the intracellular H₂S content was required. Likewise, in section 3.4.2, changes in H₂S content linked to GYY4137 stimulation were assessed by the fluorescent probe SF7-AM (Figure 3.6). As shown in Figure 3.6 A, after 24 hours of incubation with GYY4137 (100 μM), HUVECs displayed higher fluorescence intensity than untreated cells, suggesting an increased intracellular H₂S content.

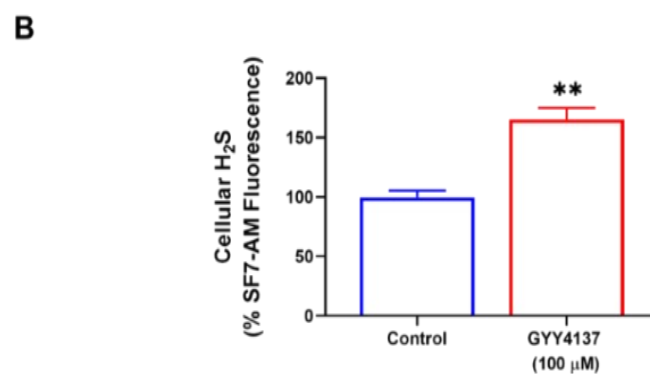
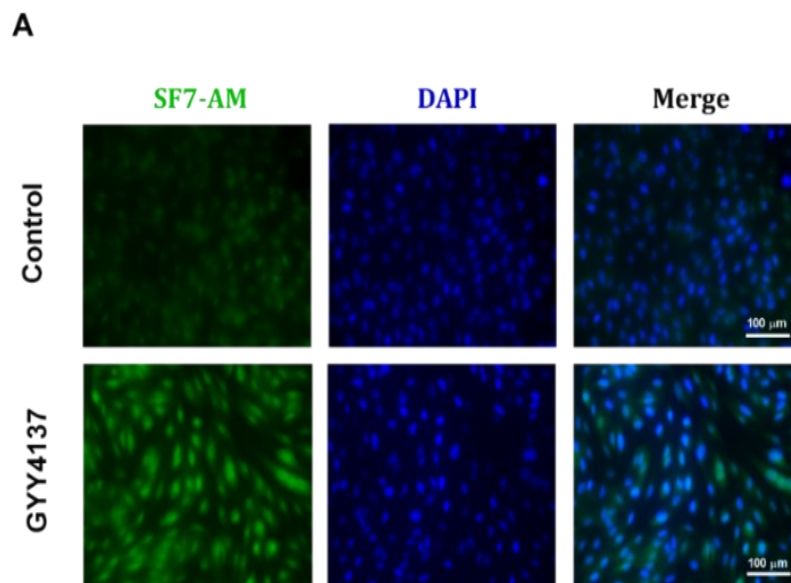


Figure 3.6 Intracellular H₂S content in the presence of GYY4137 in HUVECs.

Cells were treated with GYY4137 at 100 μ M for 24 hours before staining with SF7-AM (2.5 μ M) probe, followed by microscopy analysis. **(A)** Fluorescent images show SF7-AM-associated signals (green spectrum) in untreated and GYY4137-treated HUVECs. Nucleus stained with DAPI (blue spectrum). Photos were taken with a Nikon Ti-S Inverted fluorescence microscope (20x magnification; scale bar is 10 μ m). **(B)** Quantification of fluorescence intensity of untreated and GYY4137-treated HUVECs. Data are represented as mean \pm SEM (N=3) and analysed by an unpaired Student *t*-test. ***p*<0.01 vs. control group.

The quantification of the SF7-AM-associated fluorescence signal evidence that GYY4137 can enhance intracellular H₂S content significantly in HUVECs (***p*<0.01) (Figure 3.6 B). These observations indicate that the threshold of intracellular H₂S content is stimulated by non-toxic treatment with GYY4137 (100 μ M) in HUVECs. These results suggest that 100 μ M is suitable for elevating intracellular H₂S levels without toxicity in HUVECs. Therefore, GYY4137 at 100 μ M is this thesis's selected dose for subsequent experiments.

3.4.7 Establishing TNF- α as an agent to induce endothelial activation in HUVECs.

After acquiring the optimum GYY4137 concentration, adjustment of TNF- α in HUVECs was assessed. As primary cells, HUVECs are more sensitive than immortalised EA.hy926 cells; thus, the impact of TNF- α in primary cells at low doses could be comparable to high TNF- α doses in EA.hy926 cells. Creating an impaired endothelial environment without absolute cell death allows the examination of underlying signalling mechanisms during endothelial activation and dysfunction. Thus, titrating the optimum TNF- α dose was undertaken using three increasing concentrations [1 ng/ml, 5 ng/ml and 10 ng/ml] to fit with doses tested in the above EA.hy926 cells experiments. Moreover, the sensitivity of HUVECs to extracellular insult stimuli also required a rearrangement in the incubation time. Previous studies demonstrated that TNF- α impacts apoptotic signalling pathways within 2 to 6 hours of treatment (Tafani *et al.*, 2000; Hughes, Murphy and Ledgerwood, 2005). In line with an earlier study using HUVECs, TNF- α treatment was set up for 3 hours (Grambow *et al.*, 2020).

TNF- α is linked to ED via oxidative stress, which depends, in part, on the excessive and sustained formation of oxidant species that might lead to an oxidising redox state (Scioli *et al.*, 2020). However, due to the present thesis's aim to investigate the redox state of ECs, it could be helpful to have a preliminary view of TNF- α effects on the redox state. To pursue this, O₂⁻ formation was analysed using the MitoSox probe in untreated and TNF- α -treated HUVECs. Cells subjected to TNF- α treatment displayed a significant increase in O₂⁻ levels compared to untreated cells in a dose-dependent manner, as exemplified by the MitoSox-associated fluorescence intensity (*p<0.05) (**p<0.0001) (Figure 3.7 A). Considering the scope of the current project and based on TNF- α -mediated O₂⁻ levels in HUVECs, 1 ng/ml of TNF- α was chosen as a suitable dose.

Endothelial activation and dysfunction are linked with leukocyte trafficking and a pro-inflammatory state, which depends on the cell surface expression of adhesion molecules such as ICAM-1 (Clark *et al.*, 2007; Steyers *et al.*, 2014). To analyse that TNF- α at 1 ng/ml may mediate endothelial activation in HUVECs and to fit with the previous TNF- α impact for 3 hours, ICAM-1 expression was evaluated by flow cytometer (Grambow *et al.*, 2020). In this case, increased expression of ICAM-1 after TNF- α treatment would be expected. Primary cells were treated in the presence and absence of TNF- α for 3 hours, followed by adding fresh medium for up to 24 hours. At this point, samples were collected and incubated with ICAM-1 antibody, followed by BD Accuri C6 Plus flow cytometer analysis. IgG-ICAM-1 samples were run to 10,000 events to gate the region of the cell population in a histogram plot. The histogram plot revealed a higher ICAM-1-associated fluorescence with TNF- α (Figure 3.7 B). As shown in Figure 3.7 C, TNF- α incubation significantly increased the cell surface expression levels of ICAM-1, indicative of endothelial activation (**p<0.0001). These observations suggest that in HUVECs, TNF- α treatment at 1 ng/ml concentration can shift endothelial phenotype toward an activated state with an oxidising redox environment. Therefore, TNF- α at 1 ng/ml is the selected dose for further experiments in HUVECs.

Together, the results in this chapter show that GYY4137 is a suitable H₂S donor in ECs by increasing its endogenous content. In addition, TNF- α treatment results in endothelial activation in immortalised and primary cells. Finally, a post-treatment experimental design offers an advantage model to investigate H₂S effects on TNF- α -induced ED, which is examined in the following chapters.

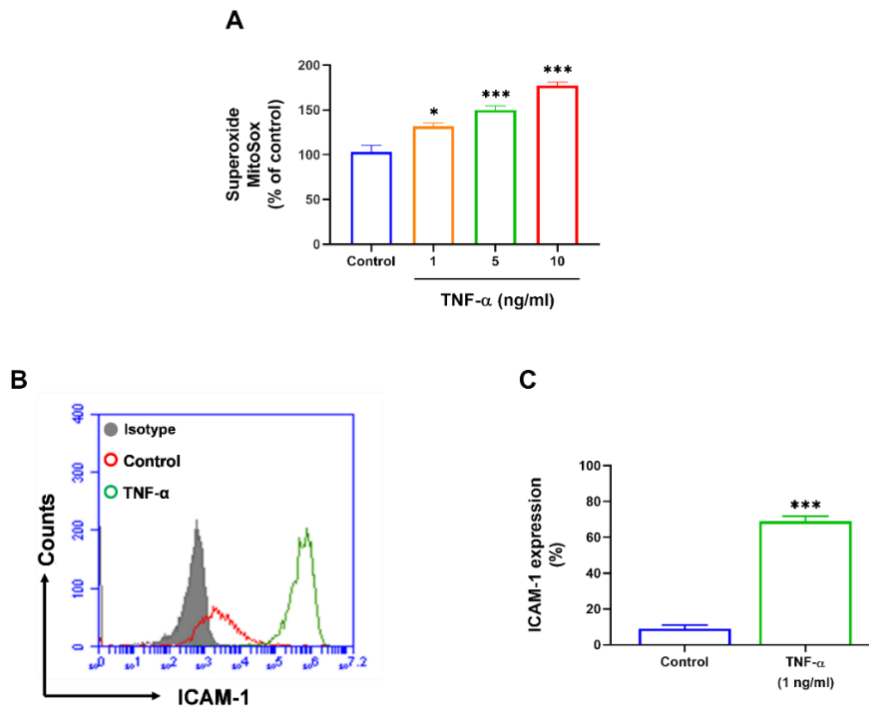


Figure 3.7 Effect of TNF- α increasing doses on endothelial activation in HUVECs.

(A) Cells were treated with increasing TNF- α [1 ng/ml, 5 ng/ml and 10 ng/ml] doses in comparison to the control group [untreated] for 3 hours. MitoSox (5 μ M) probe was used to analyse $O_2^{\cdot-}$ levels. Data presented as mean \pm SEM (n=3) and analysed by one-way ANOVA followed by Dunnett's multiple comparison test. *p<0.05 and ***p<0.001 vs. control group. **(B)** HUVECs were cultured with or without indicated TNF- α dose followed by ICAM-1 antibody staining. The histogram plot represents the flow cytometry analysis of ICAM-1-activated HUVECs. **(C)** Bar graph quantification of ICAM-1 mean fluorescence signal in HUVECs with and without TNF- α treatment. Data presented as mean \pm SEM (n=3) and analysed by unpair Student *t*-test. *p<0.05, **p<0.01 and ***p<0.0001 vs. control group.

3.5 Discussion

The research presented in this chapter aimed to determine the optimum TNF- α dose to activate ECs and establish a non-toxic GYY4137 concentration, which modulates intracellular H₂S content. In addition, to identify a suitable cell culture experimental setting using TNF- α and H₂S prodrug in endothelial cells, any H₂S-mediated changes in TNF- α -stimulated endothelial cells can be explored.

The endothelium exhibits numerous biological functions through complex signalling pathways (Durand and Gutterman, 2013). Perturbations in the endothelium represent a hallmark in several vascular conditions (Incalza *et al.*, 2018). In the present study, the initial step required was establishing a full-bodied endothelial model to test the hypothesis that H₂S can mediate beneficial roles in ED. The culture of ECs has been indispensable in identifying signalling mechanisms and detecting complicated pathophysiological processes occurring within the vessel wall (Riederer *et al.*, 2010). To date, isolation and culture methods for primary ECs have been successfully established (Riederer *et al.*, 2010). This evidence embraces *in vitro* culture of primary cells as a fit model to study endothelial function. The *in vitro* cell model selected for the current project was HUVECs due to its primary nature and representation of the *in vivo* state providing a comprehensible idea of the physiological environment (Bachetti and Morbidelli, 2000). In addition, the monolayer of HUVECs has provided a critical model for significant breakthroughs in molecular medicine (Park *et al.*, 2006). Previous work has shown how to study ED concerning pro-inflammatory agents such as TNF- α using HUVECs as *in vitro* model (Jiang *et al.*, 2016). In addition, the study of gasotransmitters such as H₂S has been extensively investigated using HUVECs as a cell culture system (Park *et al.*, 2006; Lin *et al.*, 2020).

However, due to HUVECs' limited life span and time limitations of the present work, optimisation of experimental design and methods for the current research work was first applied in immortalised cells (Lidington *et al.*, 1999; Bouïs *et al.*, 2001). Immortalised ECs have been used to identify the endothelium's biochemical and functional features, providing insight into cell interactions, which can be later verified in primary cells and *in vivo* models (Wang *et al.*, 2021). The EA.hy926 cell line is one of the most frequently used and best-described immortalised macrovascular lines (Bouïs *et al.*, 2001).

Therefore, to assess the suitability of agents and experimental conditions for analysis of H₂S roles in subsequent chapters, EA.hy926 cells were used as starting point as they represent a cell line close to HUVECs. Rieder and colleagues compared several phenotypic endothelial markers such as CD31, CD105 (endoglin), factor-VIII-related antigen, ICAM-1 and vWf in both EA.hy926 and HUVECs, showing the similarity between both culture models (Riederer *et al.*, 2010). These observations align with current results in which endothelial markers such as vWf and CD31 were expressed by EA.hy926 cells, indicating that the EA.hy926 system is suitable for developing an optimum cell culture design (Wagner, Olmsted and Marder, 1982; Gale and Yancopoulos, 1999).

Manipulating intracellular H₂S content has allowed the study of its underlying mechanisms and, subsequently, its effect on vascular conditions. Some research groups select alteration of H₂S-generating enzymes in transgenic mice such as CBS (George *et al.*, 2019), CSE (Cheung *et al.*, 2014) or 3-MST (Ahmad, Druzhyna and Szabo, 2019). Others rely on potent inhibitors of H₂S enzymatic such as β-cyanoalanine or propargylglycine for CSE activity (Asimakopoulou *et al.*, 2013). Furthermore, some groups opted for prodrugs to deliver a particular dose in the biological system of choice (Yuan, Zheng and Wang, 2020). Within the H₂S-prodrugs category, sulfide salts donors such as NaHS have been widely used in previous vascular studies (Sen *et al.*, 2009; Han *et al.*, 2011; R. Guan *et al.*, 2019). For instance, NaHS improved diabetic-mediated ED by regulating vasorelaxation and NO bioavailability (Ng *et al.*, 2017). However, NaHS releases H₂S fast within biological systems, which could lead to non-realistic endogenous concentration and toxicity (Y. Zheng *et al.*, 2015). For instance, aortic concentrations of free H₂S levels comprise ~1.5 μM. In contrast, NaHS has been reported to release H₂S up to 400 μM within the first 2 hours, followed by a drastic drop off nearly to undetected values in epithelial cells (Levitt, Abdel-Rehim and Furne, 2011; Wei Lee *et al.*, 2011). An amperometric comparison revealed that while NaHS was released with a peaking time of ~ 8 seconds, GYY4137 stimulation peaks at 10 minutes in phosphate buffer pH 7.4. The authors also showed a sustained H₂S release rate in phosphate buffer (pH 7.4) for over 60 minutes with an increase in the rate at lower Ph, as determined spectrophotometrically (Li *et al.*, 2008). A later study reported that GYY4137 maintained H₂S levels in cell culture above baseline for over seven days (Wei Lee *et al.*, 2011).

To create the most accurate *in vitro* model within the capability of the laboratory, the GYY4137 compound was selected as an H₂S-releasing donor in this thesis based on its ability to maintain a sustained H₂S release over time within a physiological intracellular concentration range (Li *et al.*, 2008; Wei Lee *et al.*, 2011). In concordance with these results, immunofluorescence microscopy and metabolic enzymatic analysis showed that GYY4137 at a specific dose increased endogenous H₂S content for 24 hours while maintaining endothelial homeostasis.

To pursue this project's aims, ECs must be activated and progress to ED, characterised by a shift toward abnormal function. While some ED-inducing stimuli (e.g. high glucose) tend to induce stress in cells in a manner that is dependent on the phase of the cell cycle (N. Liu *et al.*, 2017); pro-inflammatory cytokine TNF- α activates the endothelium in a pleiotropic way by binding to its membrane receptors, TNFR1 and TNFR2 (Aggarwal, Gupta and Kim, 2012). TNF- α -mediated activation of the endothelium can progress toward ED under sustaining stimuli and an inefficient ability to cope with stress (S. Wang *et al.*, 2018). ED upon TNF- α exposure has been previously reported *in vitro*, characterised by impaired redox state, secretion of pro-inflammatory cytokines and upregulation of cell adhesion molecules (Liao *et al.*, 2010; Galkin *et al.*, 2016; Batko *et al.*, 2019). Upon activation by stimuli, including TNF- α , NF- κ B translocates into the nucleus, followed by downstream regulation of pro-inflammatory genes such as IL-8 and IL-6 (Steyers *et al.*, 2014; Chang *et al.*, 2016). A complex interaction between inflammation and oxidative stress is responsible for the initiation and progression of ED (Savoia *et al.*, 2017). Oxidative stress in ECs emerges partly due to the excessive formation of ROS alongside the inability of antioxidant defence mechanisms to cope with an excessive oxidising redox state (Chang *et al.*, 2016; Deshmukh *et al.*, 2017). TNF- α was previously shown to mediate vascular dysfunction through increased ROS formation in renal disease patients (Batko *et al.*, 2019).

These findings align with the present results as TNF- α increased IL-6 secretion, O₂⁻ levels and ICAM-1 in ECs. Furthermore, NO bioavailability is a critical factor in the activation of ECs and progression toward dysfunction due to its role as a vasodilator and its ability to form toxic oxidants such as peroxynitrite (Sue, Ho and Kim, 2005). In concordance with previous findings, TNF- α efficiently reduced eNOS mRNA levels in a dose-dependent manner in ECs, as demonstrated by RT-qPCR analysis (Liu *et al.*, 2018).

These observations confirmed that TNF- α is a suitable stressor agent for endothelial activation and pro-inflammatory state and impairs endothelial function. Transferable settings of TNF- α optimum dose in HUVECs revealed that TNF- α treatment with 1 ng/ml leads for 3 hours to endothelial activation and impaired functions, mimicking previous TNF- α -treated primary ECs observations (Yang, Zhao and Tian, 2016; Grambow *et al.*, 2020). Therefore, 1 ng/ml was the chosen TNF- α dose for subsequent studies in HUVECs in the following chapters.

Since its discovery, H₂S has exhibited beneficial roles in the endothelium, including vascular tone, redox state, inflammation and cell death (Predmore, Lefer and Gojon, 2012). However, most ECs studies investigating H₂S rely on pre-treatment or co-treatment approaches (Shen *et al.*, 2013; Xie, Feng, *et al.*, 2016). These culture settings apply H₂S donors before or side-by-side with the systemic/cellular insult, thereby preventing rather than revoking cell damage. For instance, pre-treatment with an H₂S-releasing donor in HUVECs exposed to H₂O₂ preserved the redox state and mitochondrial function by decreasing excessive ROS formation and cyto c release into the cytosol (Wen *et al.*, 2013). Co-treatment with GYY4137 protected hypertensive-rats isolated ECs by increasing eNOS expression and vascular growth (Zhu *et al.*, 2021).

A post-treatment approach offers the benefit of evaluating the suitability of a drug as a treatment for a disease condition. Moreover, post-treatment is a less-represented model in the literature, allowing the production of data that contributes insight into H₂S mechanisms as a therapeutic agent (Wallace *et al.*, 2020). With a list of possible identified experimental H₂S settings, three culture models with TNF- α were performed to test the quantification of IL-6 release in supernatants. ELISA analysis allows for examining different measurements in an accountable, fast and accurate way. Titration of optimum practical design in EA.hy926 cells using IL-6 content revealed that pre-treatment and co-treatment were unsuitable culture approaches using TNF- α and GYY4137 compounds to investigate the H₂S beneficial role in impairing endothelium. These findings differ from previous studies where co-treatment with NaHS and TNF- α for 24 hours reduced IL-6 expression in cardiomyocytes reported by Lee and co-workers. However, a direct comparison with Lee and colleagues' report is impossible as different compound and cell models were used in the current project (Lee *et al.*, 2019).

On the other hand, GYY4137 post-treatment in TNF- α -treated cells showed a reduced IL-6 secretion suggesting that post-treatment is a suitable experimental setting for investigating the H₂S role in dysfunctional cells. This approach aligns with recent results investigating ECs integrity, inflammation and ROS formation using HUVECs with GYY4137 post-treatment settings (Spassov *et al.*, 2022). Taken together, the post-treatment setting was selected for subsequent experiments in the following chapters as the optimum experimental cell culture model for H₂S effects on TNF- α -treated ECs.

In summary, the present study demonstrates that TNF- α could modulate endothelial function, induce endothelial activation, and upregulate the expression of endothelial dysfunction markers. The addition of slow-releasing H₂S donor GYY4137 results in the increase of endogenous H₂S content without cytotoxicity. After titration of the optimum experimental setting for cell culture with both agents and readjustment of TNF- α and GYY4137 doses for HUVECs, cultured with TNF- α at 1 ng/ml for 3 hours followed by post-treatment with GYY137 (100 μ M) was the selected approach for the further experiments in the following chapters.

4 Investigation of the effect of H₂S on TNF- α - induced ED

4.1 Introduction

The previous chapter demonstrated that TNF- α is a suitable stressor to induce endothelial activation by enhancing a pro-inflammatory and oxidising redox state environment. Moreover, H₂S slow-releasing donor GYY4137 increased H₂S intracellular content without toxicity *in vitro*. In addition, a post-treatment experimental setting with both agents was chosen to investigate whether H₂S can revoke TNF- α -induced ED.

Cardiovascular and metabolic conditions are the leading cause of morbidity and mortality globally. Oxidative stress and ED have been identified as the main alterations involved in the pathogenesis of macrovascular diseases. Endothelium impairment is a complex pathophysiological event that includes increased ECs activation and the onset of ED. Several studies have shown that oxidative stress plays a pivotal role in mediating the production and secretion of cytokines, thus linking ROS with inflammation and ED (Andersson-Sjöland, Karlsson and Rydell-Törmänen, 2016). Indeed, elevated ROS levels have been involved in the onset of several diseases, including neurodegenerative disorders, cancer, renal diseases, and metabolic diseases (Scialò, Fernández-Ayala and Sanz, 2017; Hameister *et al.*, 2020).

In a healthy cell, the intracellular environment is maintained under reducing conditions, but the redox state could switch to a more oxidising state under stress stimuli. Oxidative stress can emerge due to the excessive formation of oxidants overwhelming the cellular antioxidant defence within a biological system, leading to a shift in the redox state of the biological compartments towards one that is more oxidising (Meo *et al.*, 2016). The dysfunctional activity of many proteins characterises this shift in the redox status. Impaired expression of homeostatic vascular molecules (e.g., NO), physical cell alterations (e.g., membrane lipids) and impaired bioenergetic profile (e.g., oxidative phosphorylation chain) have been observed in endothelial-oxidative stress (Nordberg and Arnér, 2001). Notably, the terms "free radicals" and "ROS" are also not synonymous, as many ROS (e.g., H₂O₂ and peroxynitrite) are not free radicals. However, excessive ROS production is associated with a redox state switch towards oxidising state and progress towards oxidative stress in individuals with cardiovascular risk factors in the arterial wall.

Over time oxidative stress can cause direct and irreversible oxidative damage to macromolecules alongside disruption of key redox-dependent signalling processes in the vascular wall. Perhaps the best-characterised mechanisms by which oxidative stress can promote vascular disease is via disruption of the vasoprotective NO signalling by either directly reacting with NO and forming peroxynitrite (a powerful oxidant); or by reducing the bioavailability of tetrahydrobiopterin leading to uncoupled eNOS enzyme, which causes NO lower bioavailability (Thomas, Witting and Drummond, 2008).

In addition, ROS may directly promote vascular inflammation. Indeed, ROS actions can lead to the oxidation of crucial signalling proteins (e.g., kinases and phosphatases) and activate the pro-inflammatory redox-dependent transcription factor NF- κ B. The activation of NF- κ B results in the overexpression of cell adhesion molecules and the migration of leukocytes and macromolecules towards the subendothelium (Lugrin *et al.*, 2014). Furthermore, it was suggested that ROS could initiate the assembly of multiprotein signalling complexes known as inflammasomes, thereby leading to the processing and secretion of the pro-inflammatory cytokines. Regarding the pro-inflammatory scenario, it has been demonstrated that the antioxidant compound N-acetyl cysteine (NAC) can attenuate TNF- α -induced apoptosis, implicating a ROS in the response (Shakibaei *et al.*, 2005; Binniecka *et al.*, 2011; Jiang *et al.*, 2016).

H₂S is a mediator of several vascular endothelial functions, including regulating antioxidant enzymes and scavenging ROS/RNS species (Calvert *et al.*, 2009). It is accepted that H₂S mediates cytoprotective and antioxidant effects against excessive ROS production, which leads to oxidative stress and ED. These beneficial roles include cellular processes such as decreased ROS levels, amelioration of impaired ROS-sources activity, increased antioxidant enzymes and upregulation of antioxidant systems (Yang *et al.*, 2008a; Mustafa *et al.*, 2009; Xie, Liu and Bian, 2016; Wu *et al.*, 2017). Thus, through the downregulation of ROS levels and upregulation of antioxidant defence, H₂S regulates the redox state towards a reducing environment. This cytoprotective role ultimately decreased ED and tissue injury in several vascular conditions (Yu *et al.*, 2014). Furthermore, it has been reported that H₂S affects cells' inflammatory state and apoptotic signalling (Zanardo *et al.*, 2006). For example, fast-release H₂S donors reduced oxidative stress and inflammatory environment in TNF- α -treated ECs by reducing cell adhesion molecule expression, enhancing antioxidant HO-1 protein expression and diminishing NF- κ B activation (Pan *et al.*, 2011).

4.2 Aims

Following the previous chapter, the experimental post-treatment design with TNF- α and GYY4137 was applied to the analysis of ED in HUVECs. This chapter aimed to investigate whether GYY4137 post-treatment could reduce TNF- α -induced ED to uncover potential signalling targets in ECs regulated by H₂S. For this purpose, several objectives were conducted:

- To investigate oxidative stress damage by TNF- α treatment in HUVECs.
- To study the role of H₂S post-treatment with slow-releasing donor GYY4137 in oxidative stress in TNF- α -treated HUVECs.
- To investigate the effect of TNF- α -induced inflammatory and apoptotic signalling pathway in HUVECs, and the role of GYY4137 post-treatment.

4.3 Materials and Methods

4.3.1 Endothelial cell culture.

HUVECs were routinely maintained in T75 flasks with the complete supplemented medium at 37°C and 5% CO₂ (see section 2.2.2). Endothelial seeding and experimental settings were explicitly conducted for each assay following general maintenance, as indicated in section 2.2.3. Cells were treated following the post-treatment experimental design with TNF- α (1 ng/ml) for 3 hours, followed by post-treatment with GYY4137 at a non-toxic concentration (100 μ M) for 21 hours, giving an overall 24 hours experimental treatment. Next, HUVECs were analysed specifically for the desired assay. In general, cells were divided into four groups unless otherwise stated: control (untreated cells), GYY4137 (alone), TNF- α (alone), and TNF- α + GYY4137 (post-treatment model).

4.3.2 Fluorescence microscopy

CM-H₂DCFDA™ staining probe was used to investigate H₂O₂ formation as described in section 2.5.1.

4.3.3 RT-qPCR

Quantitative real-time PCR was performed by extracting the total RNA. Fold change relative expression was calculated using the $\Delta\Delta C_t$ method. When comparing gene expression, the fold change relative mRNA levels of GcLC, GcLM, Trx1, TrxRD1, HO-1 and eNOS were calculated using YWAZ and EEF2 as housekeeping genes. Full details, see section 2.18.

4.3.4 Flow cytometry

The mean fluorescence intensity signal of ICAM-1, E-selectin and VCAM-1 were evaluated by flow cytometer analysis using the BD Accuri C6 Plus system. For full details on cell population gating and fluorescent antibodies, please refer to section 2.6.1.

Annexin V/PI assay was used to determine the apoptotic rate using a BD Accuri C6 Plus flow cytometer. For full details on the experiment, please refer to section 2.6.2.

4.3.5 Western blot

Immunoblotting analysis of Trx protein expression was determined by SDS-PAGE as described in section 2.17.

4.3.6 ELISA

Plate-based assay for IL-6 secretion was determined as described in section 2.11.

4.3.7 GSH: GSSG ratio assay

The GSH: GSSG-Glo assay kit was conducted to assess the GSH: GSSG ratio following the manufacturer's instructions [Promega, GmbH, Southampton, UK]. For full details of the experiment, please refer to section 2.8.

4.3.8 Statistical analysis

All values presented are as mean \pm SEM. Unless otherwise stated, all usually distributed variables between two groups were compared by unpaired Student *t*-test. When comparing two groups or more one-way ANOVA followed by Sidak's *post-hoc* comparisons was applied. For statistical tests, *p* values less than 0.05 ($p < 0.05$) were considered significant.

4.4 Results

4.4.1 Intracellular H₂O₂ content in TNF- α -treated HUVECs with GYY4137 post-treatment.

The starting point to investigate whether TNF- α could induce oxidative stress was to analyse oxidants formation. H₂O₂, as a non-radical ROS, is produced by many different cell types and is considered the most abundant and stable ROS in the vasculature. Thus, the effect of TNF- α treatment on HUVECs was evaluated by determining H₂O₂ production using CM-H2DCFDA fluorescence staining (green spectrum) combined with fluorescent microscopy analysis to determine the H₂O₂ fluorescence intensity signal in ECs. Representative images show that when HUVECs were stimulated with TNF- α , CM-H2DCFDA-associated fluorescence intensity was increased compared to the control group. GYY4137 post-treatment ameliorated the CM-H2DCFDA-associated fluorescence intensity in TNF- α -treated cells (Figure 4.1 A). Quantitative analysis of the fluorescent intensity signal revealed that TNF- α treatment significantly increased H₂O₂ generation in the presence (*p<0.05) or absence of GYY3147 (**p<0.0001) compared to untreated cells (control). This effect was partially reversed by post-treatment of HUVECs with GYY4137 in TNF- α -induced cells (##p<0.01) (Figure 4.1 B).

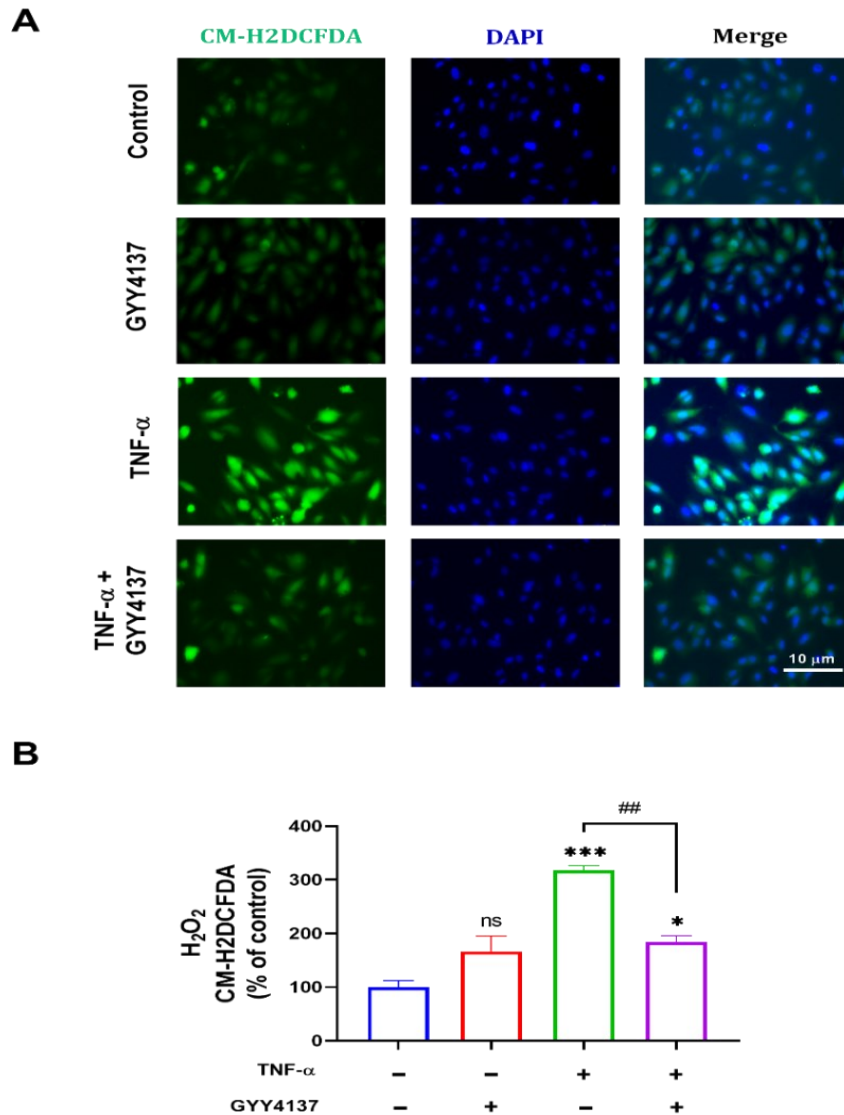


Figure 4.1 Effect of TNF- α and GYY4137 on H₂O₂ levels in HUVECs.

HUVECS were seeded in a 24-well plate and treated with TNF- α (1 ng/ml, 3h) followed by GYY4137 post-treatment (100 μ M, 21h) in cEGM medium. Next, cells were exposed to CM-H2DCFDA (10 μ M) for 30 minutes in the dark followed by PBS wash and microscopy examination. **(A)** Representative fluorescence images of HUVECs stained for H₂O₂ (green spectrum). The nucleus is counter-stained with DAPI (blue spectrum). Pictures were taken using a Nikon Ti-S Inverted fluorescence microscope (20x magnification, scale bar 10 μ m). **(B)** Analysis and quantification of fluorescence intensity was conducted by ImageJ software. Results were shown as mean \pm SEM (n=3). Significance was determined by ANOVA test followed by Sidak's *post-hoc* test comparing treatments, whereby ns, (*) and (***) represents non-significant, p<0.05 and p<0.0001 respectively vs. control group. (##p<0.01) comparison between TNF- α alone and TNF- α with GYY4137 post-treatment.

4.4.2 Antioxidant effect of GYY4137 post-treatment in TNF- α -treated HUVECs.

Several antioxidant enzymes and antioxidant signalling systems maintain the cellular redox state balance (Shaito *et al.*, 2022). To assess the effect of TNF- α on the levels of antioxidant transcriptional level in ECs and to test whether GYY4137 post-treatment could reverse TNF- α -actions, mRNA from treated and untreated groups was assessed using RT-qPCR. Data show that TNF- α did not change the HO-1 and eNOS mRNA levels to untreated cells, although differences did not reach statistical significance (Figure 4.2). Notably, in the presence of GYY4137, post-treatment HO-1 and eNOS mRNA levels were significantly elevated in HUVECs cultured with TNF- α (#p<0.05) (Figure 4.2 A-B).

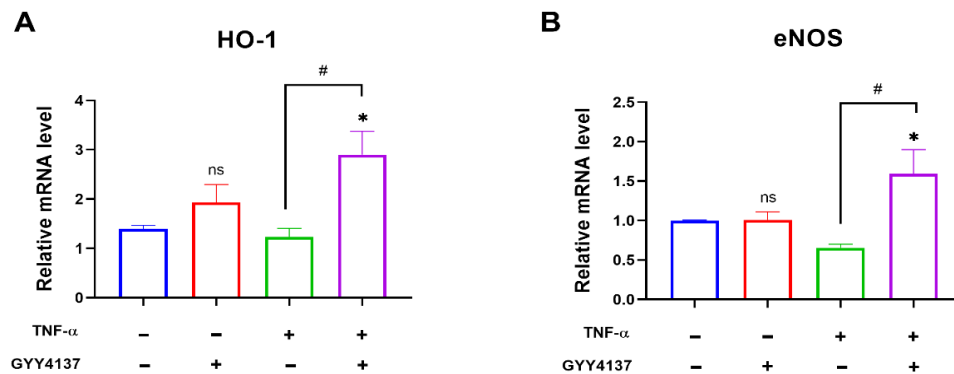


Figure 4.2 Effects of TNF- α and GYY4137 post-treatment on antioxidant genes.

HUVECs were subjected to TNF- α and GYY4137 post-treatment. Total RNA was extracted using a Qiagen RNA extraction kit. The extracted RNA was reverse-transcribed to cDNA followed by the analysis of mRNA levels by RT-qPCR. Bar graphs of relative HO-1 (A) and eNOS (B) mRNA expressions were analysed by RT-qPCR. YWHAZ and EE2 were used as housekeeper genes. Results were shown as mean \pm SEM (n=3-5). Significance was determined by the ANOVA test followed by Sidak's *post-hoc* test, whereby ns. and (*) represent non-significant and p<0.05, respectively vs. control. (#p<0.01) represents a comparison to TNF- α alone.

4.4.3 Thioredoxin and GSH systems in TNF- α and GYY4137 post-treated HUVECs.

Cells are well-endowed with antioxidant mechanisms, including GSH and Trx systems, to combat oxidative stress. The thioredoxin system is comprised of Trx, NADPH and Trx reductase. GSH synthesis, via expression of rate-limiting enzyme glutamate-cysteine ligase (GcL), GSH peroxidase and balance between reduced and oxidised GSH comprised the GSH antioxidant system the most important in mammals (Ahsan *et al.*, 2009; Forman, Zhang and Rinna, 2009).

Firstly, RT-qPCR and protein analysis was performed to investigate whether the Trx system reduces oxidant levels in TNF- α -treated cells. Treatment with TNF- α and GYY4137 post-treatment showed a significant increase in Trx1 mRNA levels compared to TNF- α alone ($\#p<0.05$) (Figure 4.3 A). Furthermore, RT-qPCR analysis revealed no significant differences between untreated and treated HUVECs for TrxRD1, as showed Figure 4.3 B. Immunoblotting analysis did not show Trx protein expression changes in HUVECs subjected to treatments (Figure 4.3 C-D).

Following the analysis of the Trx system, the GSH antioxidant pathway components were examined to assess whether the observed decrease in ROS formation was also mediated by GSH signalling. HUVECs were treated with TNF- α before GYY4137 post-treatment for a final 24 hours. The mRNA levels for GcLC show that TNF- α treatment significantly increases GcLC mRNA, not GcLM (Figure 4.4 A-B), compared to control cells. GYY4137 post-treatment in TNF- α -treated HUVECs significant increase GcLC mRNA levels in comparison to untreated cells ($*p<0.05$) (Figure 4.4 A), but this trend was not observed in the analysis of GcLM (Figure 4.4 B). The GSH:GSSG ratio in treated and untreated HUVECs was assessed by quantifying luminescence. As shown in Figure 4.4 C, the GSH/GSSG ratio trend increased in TNF- α -treated HUVECs, but the data was not statistically significant compared to the control group.

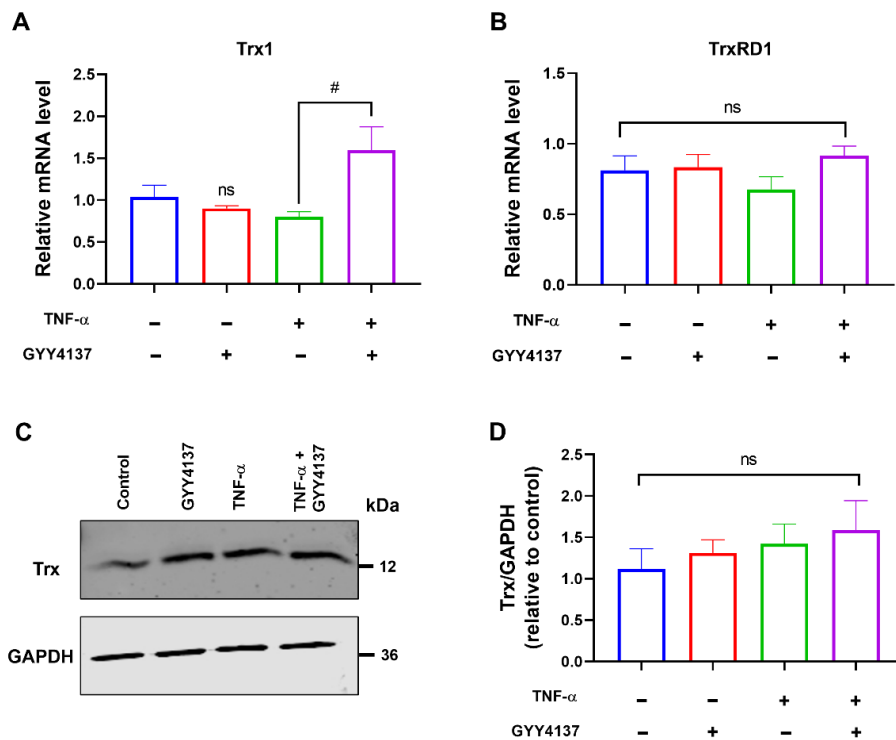


Figure 4.3 Effects of TNF- α and GYY4137 post-treatment on Trx antioxidant system in HUVECs.

HUVECs were treated with TNF- α and GYY4137 post-treatment followed by collection of total RNA and protein samples. Total RNA was reverse transcribed to cDNA and RT-qPCR analysis for target genes. **(A)** Relative Trx1 and **(B)** TrxRD1 mRNA levels were analysed by RT-qPCR with YWHAZ and EEF2 as housekeeper genes. **(C)** Protein concentration was determined by BCA assay. The nitrocellulose membranes were stained with antibodies against Trx and GAPDH (loading control) and detected by LICOR imaging system. Densitometry analysis of blots was performed using ImageJ software. **(D)** Bar graph showing Trx protein quantification relative to control. Results were shown as mean \pm SEM; (n=3-5). Significance was determined by ANOVA test followed by Sidak's *post-hoc* test comparing treatments to control (untreated cells), whereby ns. represents non-significant vs. control. (#p<0.05) represents comparison to TNF- α alone.

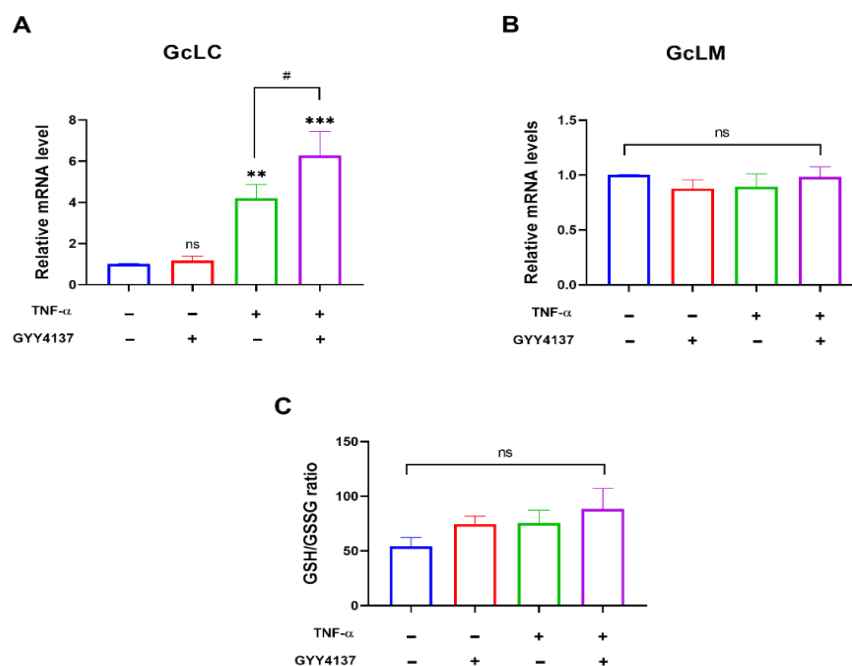


Figure 4.4 Glutathione role on the redox signalling state in treated HUVECs.

After treatments, extracted RNA was reverse transcribed to cDNA. Bar graphs of relative **(A)** GcLC and **(B)** GcLM mRNA levels were analysed by RT-qPCR with YWHAZ and EEF2 as housekeeper genes. **(C)** The GSH/GSSG ratio was detected using Promega GSH/GSSG-Glo kit with luminescence detection. Results were shown as mean \pm SEM (n=3-6). Significance was determined by ANOVA test followed by Sidak's *post-hoc* test comparing treatments to control (untreated cells), whereby ns., (*) and (**) represents non-significant, $p < 0.05$ and $p < 0.01$, respectively vs. control group.

4.4.4 Assessing modulatory effects of TNF- α and GYY4137 on cell adhesion molecules surface expression.

To test the activation of ICAM-1, VCAM-1 and E-selectin by TNF- α and whether GYY4137 post-treatment could ameliorate these molecules' surface expression was evaluated by flow cytometer. Live cells without debris were gated in the forward scatter (FSC), and side scatters (SSC) plot by running samples in the flow cytometer for 10,000 events (Figure 4.5 A). Then, the IgG1 (isotype control) for ICAM-1 was run to determine the threshold of the ICAM-1 fluorescence intensity signal (Figure 4.5 B). Subsequently, treated and untreated cells with TNF- α and GYY4137 were analysed (Figure 4.5 C-F). After incubation with TNF- α , the fluorescence intensity in histogram plots revealed higher

ICAM-1-associated fluorescence with peaks significantly shifted compared to the control group. Further detailed analysis of the flow cytometry results from independent replicates indicates that ICAM-1 mean fluorescence intensity (MFI) following TNF- α treatment was significantly increased compared to untreated cells ($***p<0.0001$). Post-treatment with GYY4137 significantly decreased ICAM-1-associated MFI expression in TNF- α -treated ECs (Figure 4.5 G) ($##p<0.01$). However, the expression of ICAM-1 remains significantly increased in TNF- α -treated HUVECs after GYY4137 treatment compared to the control group ($***p<0.0001$).

Next, E-selectin expression, which enables the initial attachment for leukocyte rolling, was also analysed by flow cytometry. Consistent with ICAM-1 examination, live cells were precisely gated, and IgG1 was used as a fluorescence signal control (Figure 4.6 A-B). HUVECs subjected to a post-treatment setting with TNF- α and GYY4137 were run in the flow cytometer and analysed in histogram plots (Figure 4.6 C-F). As shown in Figure 4.6 G, flow cytometry results from independent replicates reveal that E-selectin MFI following TNF- α treatment was significantly increased compared to untreated cells ($*p<0.05$). GYY4137 post-treatment trend to reduce E-selectin-associated fluorescence in TNF- α -cultured cells, but differences were not significant. Notably, the E-selectin-associated MFI levels were five times lower than ICAM-1-associated MFI intensity.

Finally, VCAM-1, another critical adhesion molecule in leukocyte attachment, was also examined by a flow cytometer. After living cells were gated and IgG1 as control analysed, treated and untreated cells were subject to VCAM-1 fluorescence intensity analysis as evidenced by histogram plots (Figure 4.7 A-F). Histogram plots revealed that GYY4137 treatment alone did not alter VCAM-1 fluorescence intensity compared to untreated cells. TNF- α treatment resulted in a higher VCAM-1-associated fluorescence with peaks shifted positively than in the control group. Analysis of VCAM-1 MFI results confirmed the significant differences in TNF- α compared to untreated cells ($***p<0.0001$). Post-treatment with GYY4137 significantly reduced VCAM-1 MFI levels in TNF- α -treated HUVECs ($#p<0.05$). Notably, the expression of VCAM-1-associated fluorescence intensity remains significantly increased in TNF- α -treated HUVECs after GYY4137 treatment compared to the control group ($*p<0.05$) (Figure 4.7 G).

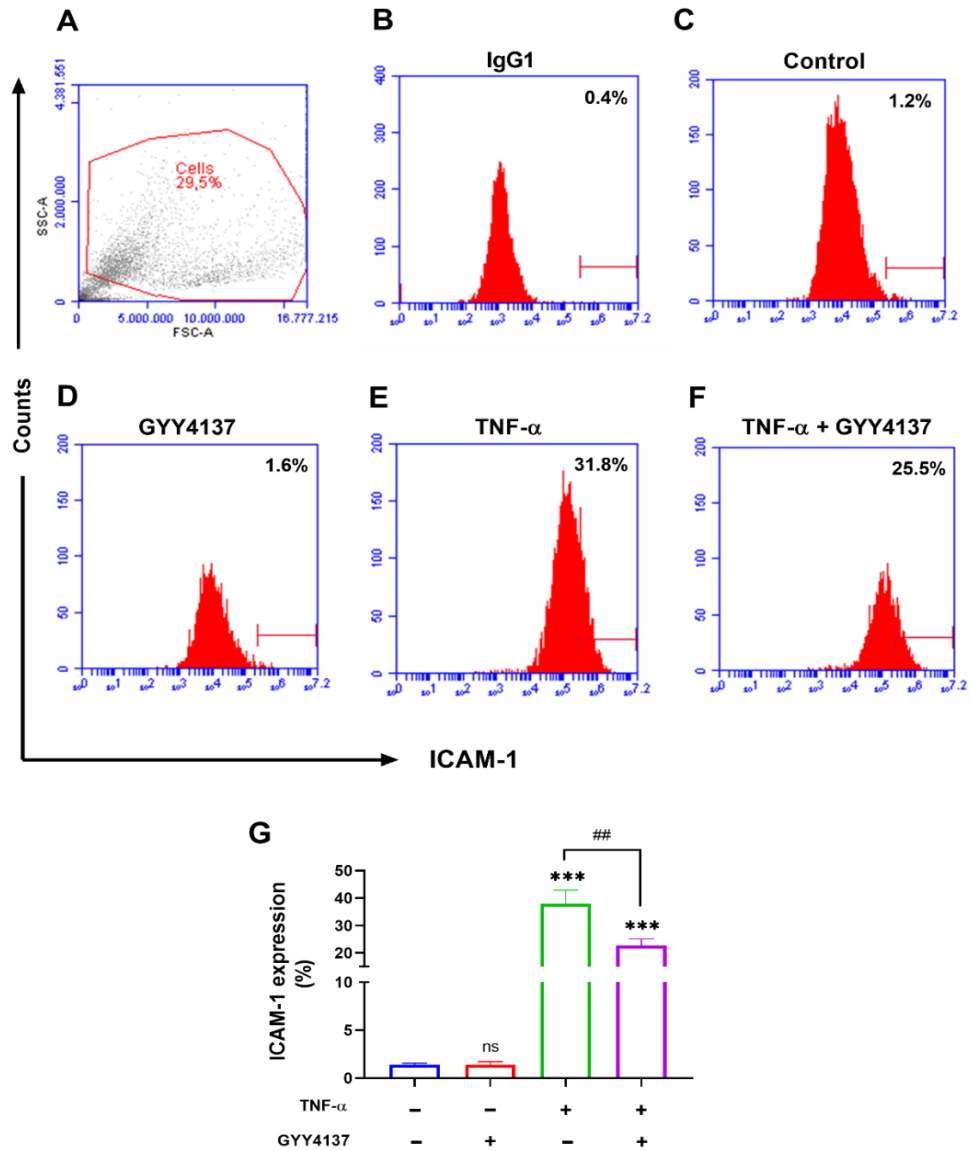


Figure 4.5 Flow cytometric primary plots analysis and quantification of ICAM-1 MFI (%) in ECs following TNF- α and GYY4137 treatment.

HUVECs were incubated with anti-ICAM-1 antibody for 1 hour. Samples were analysed using a BD Accuri C6 flow cytometer showing ICAM-1 expression (CD54) at APC-A spectrum. **(A)** Representative live cells based on the forward scatter/side scatter (FSC/SSC) plot and **(B)** stained histogram plot IgG1 were used to set the gate for positive population of cells. **(C-F)** Representative histograms of control and treated groups, a marker was set on the left edge of control cells to set the ICAM-1 APC-geo MFI of cells (%) and used for comparison. **(G)** MFI (%) of ICAM-1 expression in HUVECs was plotted in bar graphs. Results were shown as mean \pm SEM, (n=5). Significance was determined by ANOVA test followed by Sidak's post-test comparing treatments to control (untreated cells), whereby (***) and ns. represents $p < 0.001$ and non-significant, respectively vs. control. (## $p < 0.01$) represents comparison to TNF- α alone.

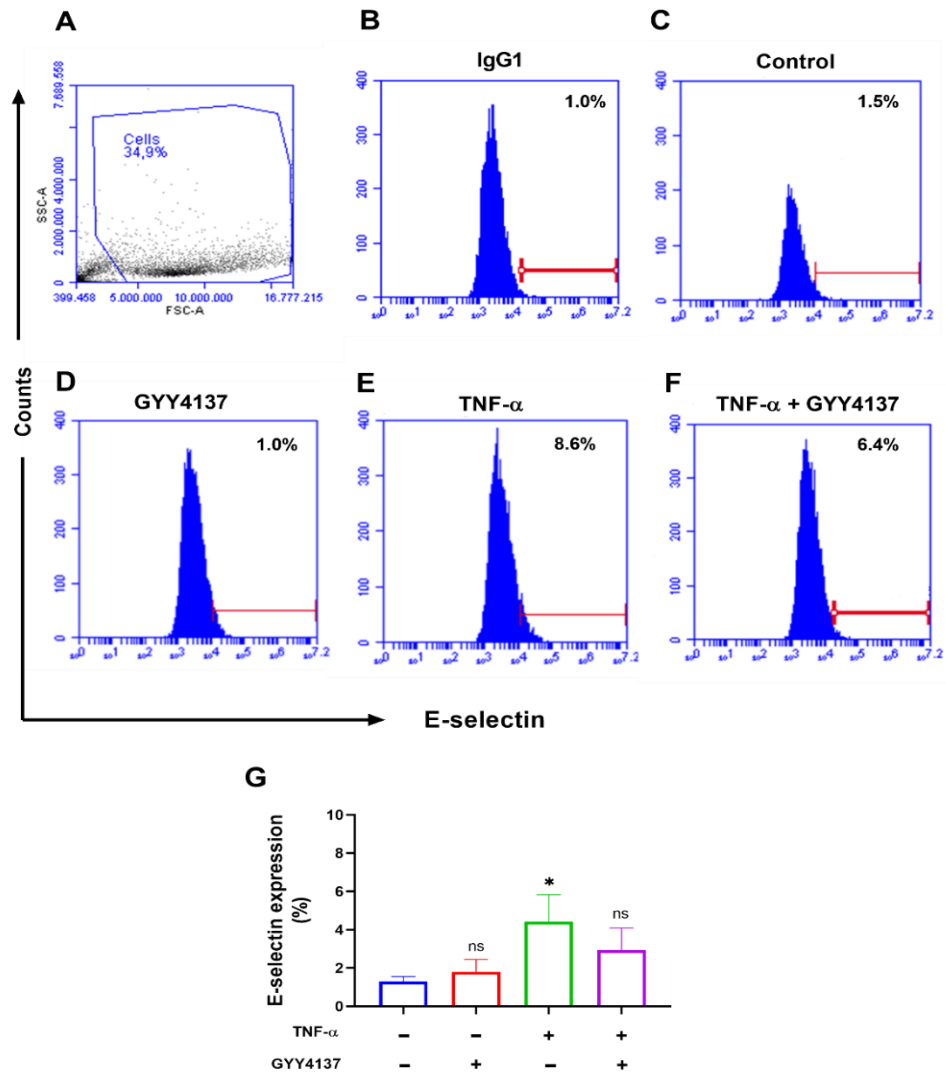


Figure 4.6 Flow cytometric primary plots analysis and quantification of E-selectin MFI (%) in ECs following TNF- α and GYY4137 treatment.

HUVECs were incubated with anti-E-selectin antibody for 1 hour in the dark. Samples were analysed using a BD Accuri C6 flow cytometer showing E-selectin expression (CD62) at FITC-A spectrum. **(A)** Representative live cells based on the forward scatter/side scatter (FSC/SSC) plot and **(B)** stained histogram plot IgG1 were used to set the gate for positive population of cells. **(C-F)** Representative histograms of control and treated groups, a marker was set on the left edge of control cells to set the E-selectin FITC-geo MFI of cells (%) and used for comparison. **(G)** MFI (%) of E-selectin expression in HUVECs was plotted in bar graphs. Results were shown as mean \pm SEM (n=3). Significance was determined by ANOVA test followed by Sidak's *post-hoc* test vs. control (untreated cells), whereby ns. and (*) represents non-significant and p<0.05, respectively vs. control.

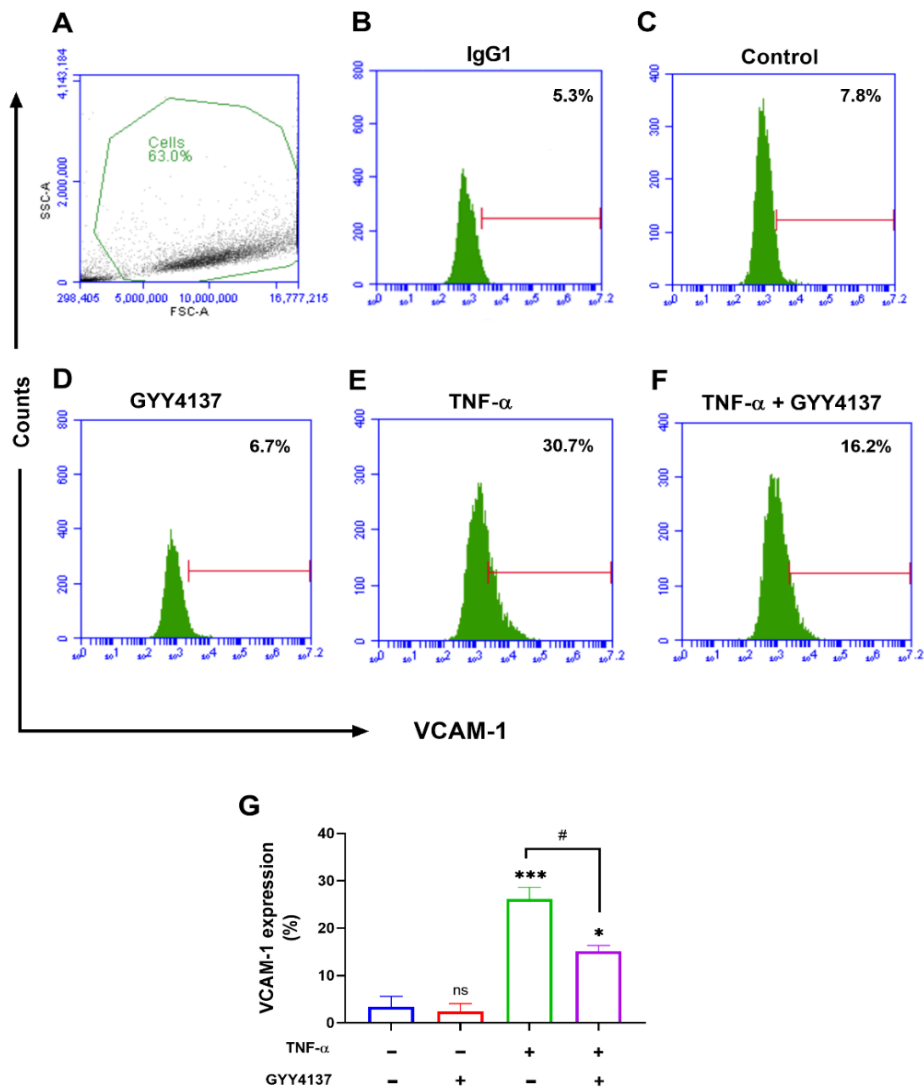


Figure 4.7 Flow cytometric primary plots analysis and quantification of VCAM-1 MFI (%) in ECs following TNF- α and GYY4137 treatment.

Samples were analysed using a BD Accuri C6 flow cytometer showing VCAM-1 expression (CD106) at PE-A spectrum from the different stimulant stained: [IgG1] are untreated cells with anti-CD106-conjugate isotype antibody. **(A)** Representative live cells based on the forward scatter/side scatter (FSC/SSC) plot. **(B)** Stained histogram plot IgG1 were used to set the gate for positive population of cells. **(C-F)** Representative histograms of control and treated groups, a marker was set on the left edge of control cells to set the VCAM-1 PE-geo MFI of cells (%) and used for comparison. **(G)** MFI (%) of VCAM-1 expression in HUVECs was plotted in bar graphs. Results were shown as mean \pm SEM (n=3). Significance was determined by ANOVA test followed by Sidak's *post-hoc* test comparing treatments to control (untreated cells), whereby ns. (***) and (*) represents non-significant, $p < 0.0001$ and $p < 0.05$, respectively vs. control. (# $p < 0.05$) represents comparison to TNF- α alone.

4.4.5 Monitoring inflammation and apoptosis in HUVECs subjected to TNF- α and GYY4137 post-treatment.

The continuous activation of cell adhesion molecules is related to changes in the vessel network referred to as angiogenesis under TNF- α (S.4.1), specifically a significant reduction in the number of branches (* p <0.05), which is ultimately linked with inflammation and dysfunctional endothelium. Research suggests angiogenesis, ROS formation and activated adhesion molecules are associated with an inflammatory response, which may lead to apoptotic signalling in ECs (Du *et al.*, 2014; Zhao *et al.*, 2017). This evidence and the above results in this chapter suggest that TNF- α could instigate inflammation and cell death. To investigate the inflammatory state of HUVECs, the secretion of pro-inflammatory cytokines was examined by ELISA assay. The results presented in Figure 4.8 A show that increased IL-6 secretion in the presence of TNF- α treatment was significantly increased compared to control cells (** p <0.0001). Post-treatment with GYY4137 can significantly revoke IL-6 content compared to the control group (** p <0.01) and compared to TNF- α -treated ECs (# p <0.05).

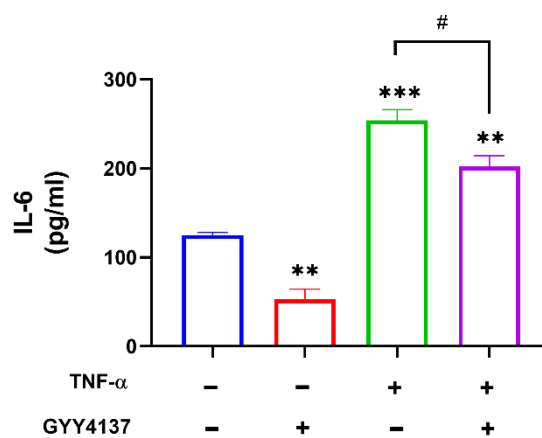


Figure 4.8 Secretion of pro-inflammatory cytokines in response to TNF- α and GYY4137 stimulation in ECs.

HUVECs were treated with TNF- α and GYY4137 post-treatment setting as described in section 4.31. Once treatments were concluded, the supernatant was collected, and the presence of cytokine IL-6 was. Results were shown as mean \pm SEM (n=3-4). Significance was determined by the ANOVA test followed by Sidak's *post-hoc* test comparing treatments to control (untreated cells), whereby ns. (*), (**), and (***) represent non-significant, p <0.05, p <0.01 and p <0.0001, respectively vs. control. (# p <0.05) represents a comparison to TNF- α alone.

To confirm that the pro-inflammatory stimulation mediated by TNF- α could lead to cell death, the apoptotic rate of ECs was analysed using an Annexin V and PI staining kit by flow cytometer. The BD Accuri C6 Plus flow cytometer uses a 488nm blue laser to excite Annexin V-FITC or PI if bound to cells resulting in green and red wavelength emitted light that the cytometer measures and records. Scatter plots (FSC-A/SSC-A) (Figure 4.9 A) were used to gate the cell population and exclude debris. Then events within the gate were separated into four areas by gating boundaries: live cells (Annexin V⁻/PI⁻), early apoptotic cells (Annexin V⁺/PI⁻), late apoptotic cells (Annexin V⁻/PI⁺) and death cells (Annexin V⁺/PI⁺). As shown in Figure 4.9 B, positive control confirms the sensibility of the assay. Representative drop plots of early and late apoptosis quadrants displayed similar cell distribution in control and GYY4137-treated cells. It is clear that following TNF- α stimulation, stained-cell distribution is higher in the late apoptotic quadrant. On the other hand, after GYY4137 post-treatment, cells are lost from the late apoptotic zone of the TNF- α -treated HUVECs stained plots (Figure 4.9 C-F).

Quantification of cell-positive Annexin V/PI staining (early and late apoptosis) in HUVECs under treatments revealed a significant increase in the apoptotic rate in the presence of TNF- α compared to the control group (*p<0.05). Post-treatment with GYY4137 shows a statistically significant decrease in the apoptotic rate in TNF- α -stimulated cells (#p<0.05) (Figure 4.9 G). Research studies have demonstrated that TNF- α treatment has detrimental consequences on ECs by causing apoptosis and premature cellular senescence (Yamagata, Suzuki and Tagami, 2016; Khan *et al.*, 2017). While SA- β -Gal staining exhibited a slight trend in SA- β -Gal-stained cells in the presence of TNF- α (S.4.2), transcriptional expression of cell cycle regulatory markers associated with senescence such as p21 and p53 did not show any significant changes in the presence of TNF- α or GYY4137 treatment.

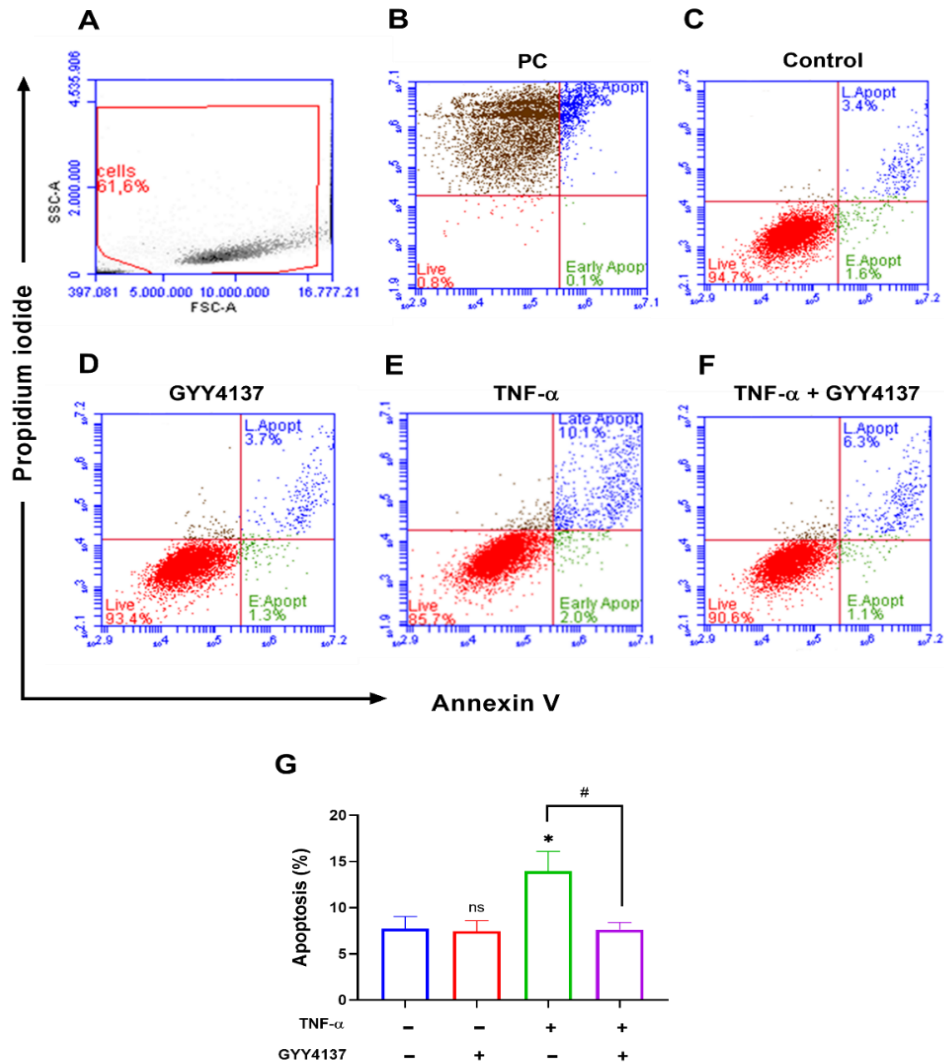


Figure 4.9 Flow cytometric primary plots analysis and quantification of apoptosis rate on ECs following TNF- α and GYY4137 treatment.

The initial gating involves plotting all events based on FSC/SSC to exclude debris (gate: cells). Then events within the gate were sorted as Annexin V-FITC spectrum vs PI-PerCP-Cy5.5 in a scatter plots with four gating boundaries applied: live cells (red highlight), early apoptosis (green highlight) and late apoptosis (blue highlight). **(B)** Cells cultured with ethanol as positive control. **(C-F)** Representative scatter plots for Annexin Vs PI and the four gating boundaries applied for each group. **(G)** Apoptosis rate (%) in HUVECs was plotted in bar graphs. Results were shown as mean \pm SEM (n=7). Significance was determined by ANOVA test followed by Sidak's *post-hoc* test comparing treatments to control (untreated cells), whereby ns. and (*) represents non-significant and $p < 0.05$ vs. control. (# $p < 0.05$) represents comparison to TNF- α alone.

4.5 Discussion

The research presented in this chapter aimed to determine the effects of TNF- α on endothelial activation and dysfunction and investigate the effects of exogenous H₂S as a beneficial mediator. ECs are routinely cultured with exogenous H₂S under pre-treatment or co-treatment models. Still, in the post-treatment experimental approach, cells were cultured with a non-toxic concentration of GYY4137 under a post-treatment model. The results presented in this chapter showed that TNF- α induced endothelial activation, oxidative stress, inflammation, and apoptosis. These findings agree with several studies where TNF- α has been described as a pro-inflammatory and pro-apoptotic molecule (Du *et al.*, 2014; Zhao *et al.*, 2017). The results confirmed that exogenous H₂S could generate an antioxidant response and decrease the inflammatory environment and apoptotic rate in dysfunctional ECs.

The role of oxidants in inducing inflammation has been vigorously investigated in all experimental models. Among the commonly used inflammatory mediators in the vasculature, the cytokine TNF- α is a common pro-inflammatory molecule. TNF- α superfamily can impair ROS-dependent cellular functions (Gaur and Aggarwal, 2003). Early studies have demonstrated that 1 ng/ml of TNF- α is within the TNF- α levels detected in patients with vascular conditions such as myocardial ischemia-reperfusion (Başaran *et al.*, 1993). Furthermore, *in vitro* analysis using human aortic ECs demonstrated that short-term incubation (20 minutes) with TNF- α (1 ng/ml) can increase ROS formation (Yang, Zhao and Tian, 2016).

This chapter shows that treating HUVECs with TNF- α (1 ng/ml, 3 hours) increases intracellular ROS, specifically H₂O₂, determined by CM-H2DCFDA staining. Moreover, GYY4137 was able to decrease this elevation in post-treated HUVECs. The reduction in H₂O₂ production observed upon GYY4137 was comparable to the previous pre-treatment study in high glucose-induced EA.hy926 cells (Xie, Feng, *et al.*, 2016). Due to most *in vivo* and *in vitro* vascular studies have described H₂S roles in a pre-treatment setting or co-treatment design (L. L. Liu *et al.*, 2014; Feng *et al.*, 2016; Hu *et al.*, 2017; N. Liu *et al.*, 2017; Behera, Kelly and Tyagi, 2021), the present study has expanded on the small amount of evidence on the effect of H₂S against ED in post-treatment settings (L. L. Liu *et al.*, 2014).

However, besides the used fluorogenic probe CM-H₂DCFDA has been used in TNF- α -treated HUVECs (de Oliveira *et al.*, 2018); oxidation upon exposure to light may give a false increase in fluorescence leading to misleading results (Kalyanaraman *et al.*, 2012; Brandes, Rezende and Schröder, 2018). Further analysis combining the effect of CM-H₂DCFDA with flow cytometry or HPLC could offer a sensitive and selective reading of H₂O₂ content; in combination with robust controls such as silencing-H₂O₂ enzymes (Lippert, Van De Bittner and Chang, 2011; Tsuboi, Maeda and Hayashi, 2018).

Furthermore, ROS exhibits a multi-functional role in ECs, including proliferation, migration and angiogenesis (Freed and Gutterman, 2013). According to published angiogenic analysis, TNF- α negatively affects endothelial vessel formation (Zhu *et al.*, 2007; Shi *et al.*, 2018). Stimulation of vessel formation observed in exogenous H₂S confirms previous data (Papapetropoulos *et al.*, 2009).

ROS-scavenger capacity in the vasculature is associated with an antioxidant response. GSH and Trx are central antioxidant systems alongside several antioxidant enzymes. HO-1 and eNOS have been previously demonstrated to exhibit antioxidant roles (Choi *et al.*, 2018). In agreement with previous evidence, exogenous H₂S upregulates antioxidant gene expression in HUVECs treated with TNF- α (Nicholson *et al.*, 2013; Leskova *et al.*, 2017). However, to conclude that H₂S can upregulate antioxidant response completely, an assessment of the levels of the corresponding proteins and antioxidant enzyme activity would be required. This limitation is essential for future experiments as the presence of changes at the transcriptional level (mRNA levels) does not imply that proteins behave in the same proportion.

The Trx-GSH antioxidant systems are commonly linked to regulating cellular oxidation/reduction and protecting cells from oxidative stress (Munro *et al.*, 2016). Interestingly, Trx and GSH systems significantly maintain sulfide signalling by fine-tuning sulfide signalling pathways (Dóka *et al.*, 2016). It has been demonstrated that Trx1 is essential for the exogenous H₂S cardioprotective role in murine (Nicholson *et al.*, 2013). In this study, exogenous H₂S enhanced the Trx and GSH machinery by increasing Trx1, and GcLC mRNA levels in TNF- α stimulated cells. Although GSH/GSSG ratio shows no significant difference in the GYY4137-treated cells, previously exogenous H₂S improved GSH/GSSG ratio and increased Trx1 expression in the injured liver (Jha *et al.*, 2008).

When oxidised, GSSG is either recycled to GSH by the enzyme GR or exported out of the cell to maintain the intracellular redox, which may explain the GSH/GSSG ratio observed in H₂S post-treatment (Forman, Zhang and Rinna, 2009). From our data, it can be suggested that H₂S donors could ameliorate TNF- α -induced ROS production by enhancing antioxidant defence through the intervention of Trx-GSH systems, which might create a positive feedback loop maintaining sulfide signalling. However, without additional experiments (e.g. activity of antioxidant enzymes), a direct link between H₂S's beneficial role and Trx-GSH antioxidant systems cannot be assumed.

Evidence has emerged that oxidative stress plays a crucial role in the development of inflammation (Kundu *et al.*, 2012). ECs activate upon stimulation with pro-inflammatory cytokines such as TNF- α , LPS or IL-1 β . During activation, the expression of adhesion molecules for leukocytes binding on the luminal surface dramatically increases, and the endothelium becomes procoagulant. Selectins mediate the weak adhesion of leukocytes, while firm adhesion involves VCAM-1 and ICAM-1 action (Videm and Albrigtsen, 2008; Lugin *et al.*, 2014). Exposure to TNF- α (50 ng/ml) increased leukocyte transmigration via E-selectin expression and ROS formation associated with phosphorylation of p66^{Shc}, an inducer of oxidative stress (Laviola *et al.*, 2013). In line with previous observations, exposure of HUVECs with TNF- α showed a significant increase in ICAM-1, VCAM-1, and E-selectin mean fluorescence intensity levels, as demonstrated by flow cytometry analysis (Laviola *et al.*, 2013; Yang, Zhao and Tian, 2016; Gapizov *et al.*, 2018). To note, the low levels of E-selectin compared to ICAM-1 and VCAM-1 could be explained due to ECs not expressing E-selectin constitutively. Therefore, it is plausible that E-selectin expression decreased after weak adhesion mediated by E-selectin and strong adhesion by ICAM-1 and VCAM-1 (Silva, Videira and Sackstein, 2018).

In addition, in the present study there was a visible decrease in ICAM-1 and VCAM-1 MFI levels in ECs with exogenous H₂S treatment; this effect reached significance. Pre-treatment with a fast-release H₂S donor has been shown to reduce ICAM-1 and VCAM-1 protein expression and E-selectin mRNA levels in TNF- α -treated HUVECs (Pan *et al.*, 2011). Although direct comparison cannot be assessed due to the variety in the experimental approach between the current work and Pan's study, the present data suggest that slow-releasing H₂S donors can reduce cell adhesion molecules in TNF- α -treated cells.

Activated ECs led to endothelial inflammation by releasing pro-inflammatory cytokines and chemokines such as IL-6, IL-8 and IP-10 (Gapizov *et al.*, 2018). Previous evidence shows that TNF- α induces inflammation associated with elevated ROS formation and activation of NF- κ B. Interaction between IL-6 and TNF- α contributes to ED in the type 2 diabetes murine model (Lee *et al.*, 2017). Previously, exogenous GYY4137 exhibited anti-atherosclerotic activity in mice through ROS inhibition and decreased ICAM-1 and IL-6 mRNA levels (Liu *et al.*, 2013). Here, H₂S post-treatment decreased IL-6 secretion in ECs exposed to TNF- α , suggesting that H₂S has beneficial effects against endothelial inflammation.

When inflammation exceeds defensive cell capacity, the caspase signalling cascade is activated, causing cell death (Steyers *et al.*, 2014). Previous evidence showed that TNF- α (> 10 ng/ml) induces apoptosis in vascular cells and *in vivo* models (Xu *et al.*, 2011; Jiang *et al.*, 2016). Conversely, TNF- α has shown cellular apoptosis and senescence stimulation in ECs (Yamagata, Suzuki and Tagami, 2016; Khan *et al.*, 2017). Although present data showed no detectable change in the expression of pro-senescence genes, SA- β -Gal staining seems to display an effect of TNF- α in ECs. Due to HUVECs culture exhibiting narrow cell culture passages limiting senescence study and considering the scope of the present study, no further investigation regarding senescence was conducted.

A HUVECs report showed that the apoptotic rate under TNF- α (1 ng/ml) treatment for 24 hours was not significantly increased (Tang *et al.*, 2015). In contrast to this observation, the present work shows that TNF- α at 1 ng/ml can dramatically enhance apoptosis rate, as evidenced by flow cytometry analysis. Discrepancies with this study could rely on the unspecified details of whether the apoptotic rate was concluded from early and late apoptosis combined data reported by the authors. In addition, the differences in the incubation time with 24 hours of treatment could lead to an adaptation to TNF- α by ECs. Moreover, exogenous H₂S revoke apoptosis in stress-ECs by flow cytometry analysis, which aligns with the previous anti-apoptotic effect of H₂S in ECs (Xie, Feng, *et al.*, 2016). Besides its substantial advantages, Annexin V/PI assay false positive results may appear due to binding to negatively charged aldehyde adducts or unbound labelled protein contributing to background signal (Demchenko, 2013).

In the current study, using several controls and correct sample manipulation supports the strength of the obtained data. However, results are limited to the specific duration and concentration of TNF- α treatment. Thus, further investigation of TNF- α effects in a dose-dependent manner by a kinetic analysis might clarify the progression from early to late apoptosis in ECs.

Overall, this study supports previously published work on TNF- α -induced endothelial activation, which progress to ED and H₂S exhibits a protective effect against TNF- α -induced ED. One limitation of this study was that the selected TNF- α concentration might not lead to a chronic inflammatory response; therefore, some features of prolonged inflammation were not detectable or significantly different compared to basal levels. Furthermore, this study used HUVECs as *in vitro* model, which restricted the culture passages, causing a limitation of prolonged pro-inflammatory and pro-apoptotic effects. In future work, it would be interesting to determine whether senescence in TNF- α is highly associated with cytokine concentration or by a biphasic effect of concentration and culture passaging.

5 Assessment of the effect of H₂S and TNF- α in mitochondria

5.1 Introduction

Mitochondria are crucial organelles to maintain cell viability via energy-linked processes and metabolic activities. Paradoxically, this simple notion contradicts the established concept that mitochondria play a unique role in cell death (Crompton, 1999). Events related to mitochondrial dysfunction include the profound imbalance between ATP synthesis, the impairment of ionic homeostasis and ROS formation, and accelerating or even determining the evolution of cell injury toward apoptosis or necrosis (Madamanchi and Runge, 2007; Dikalov and Ungvari, 2013). The main link between mitochondria and vascular damage is oxidative stress, as evidenced by several vascular-related conditions such as atherosclerosis and hypertension (Lisa *et al.*, 2009; Dikalov and Ungvari, 2013). Mitochondria are not only the source of ROS in vascular cells but also represent targets of cellular ROS. Oxidative modifications of mitochondrial proteins, lipids and DNA result in losing their functions (Zorov, Juhaszova and Sollott, 2014). When $O_2^{\cdot-}$ and NO are produced, they rapidly react, yielding the highly oxidising peroxynitrite anion, which is also toxic to mammalian mitochondria (Radi, Cassina and Hodara, 2002). In HUVECs, TNF- α induces ROS formation mainly at the ubisemiquinone site, as exemplified by the use of mitochondrial ETC inhibitors desipramine and dimethylaminopurine (Corda *et al.*, 2001). In addition, several factors tightly regulate mitochondrial ROS generation, including antioxidant systems that maintain the redox state in equilibrium. For example, SOD dismutase $O_2^{\cdot-}$ to H_2O_2 is diffusible across the mitochondrial membrane (Andersson-Sjöland, Karlsson and Rydell-Törmänen, 2016).

Cellular metabolism compromises the utilisation of carbohydrates, fats and proteins to synthesise energy (Nolfi-Donagan, Braganza and Shiva, 2020). In 1957, Peter Siekevitz referred to the mitochondrion as the “powerhouse” of the cell. Since then, it has become clear that mitochondria are highly dynamic organelles that contribute to cellular homeostasis by producing ATP (Siekevitz, 1957). Furthermore, mitochondria are highly dynamic organelles that contribute to cellular homeostasis by maintaining ATP levels and generating basal ROS levels for cell signalling (Zhang and Gutterman, 2007; Nolfi-Donagan, Braganza and Shiva, 2020). For instance, $O_2^{\cdot-}$ produced by mitochondria mediates shear stress- H_2O_2 production in human coronary arteries (Liu *et al.*, 2003). Notably, the importance of mitochondria function varies by cell type. Cardiomyocytes rely on mitochondria to supply >95% of the energy required.

In contrast, ECs rely more heavily on glycolysis than mitochondria for ATP formation (Oldendorf, Cornford and Brown, 1977; Barth *et al.*, 1992). As one of the primary sources of ROS formation, early studies estimated that 1-2% of electrons entering the ETC contributed to $O_2^{\cdot-}$ production, which has been re-evaluated to a lower value *in vivo* with fluctuations depending on ETC function (Turrens, 2003; Quinlan *et al.*, 2012). Complex III has been reported as the primary source of ROS production in HUVECs in the presence of TNF- α (Mukherjee, Mukhopadhyay and Hoidal, 2005).

Physiologically, OXPHOS is not entirely coupled, and low levels of proton leak dissipate the proton electrochemical gradient potential or electrochemical protonmotive force (Δp) (Jastroch *et al.*, 2010). The total force driving protons into the mitochondria combines the $\Delta\psi_m$ and the mitochondrial pH gradient (ΔpH) (Cadenas, 2018). While Δp provides the bioenergetic driving force and regulates ATP generation, the $\Delta\psi_m$ component provides the charge gradient required for mitochondrial Ca^{2+} sequestration and regulates ROS production (Cai, Yang and Jones, 1998). During cellular stress, $\Delta\psi_m$ may be altered by dysregulation of intracellular ionic charges, subsequently changing Δp and thus ATP production. The expression of specific uncoupling proteins (UCPs) within the inner mitochondrial membrane facilitates the leak of inducible protons from the intermembrane space back to the matrix without the involvement of the ATP synthase (Fink *et al.*, 2005). Research shows that TNF- α mediates mitochondrial uncoupling and enhances ROS-dependent migration via NF- κB in liver cells (Kastl *et al.*, 2014).

Selective elimination of damaged mitochondria by autophagy occurs in specific settings, while large-scale autophagy of mitochondria has been described during apoptosis, where the opening of the MPTP was found (Wang *et al.*, 2012). Cell death can involve a cascade of molecular events through the extrinsic pathway via transmembrane receptor death receptors affecting the activation of caspase 8 and downstream caspases cascade (Chandrasekar *et al.*, 2004; Obeng, 2021). On the other hand, mitochondria-initiated events comprise the activation of Bcl-2 family proteins triggering MPTP opening and release of pro-apoptotic mediators from mitochondria into the cytosol, which leads to the activation of initiator and executor caspases (Chandrasekar *et al.*, 2004; Peña-Blanco and García-Sáez, 2018). Notably, although TNF- α is known to mediate the extrinsic apoptotic pathway by the death receptor binding, evidence reported an impact on the intrinsic way (Chandrasekar *et al.*, 2004).

Furthermore, it has been shown that the TNF- α -induced apoptotic effect is associated with changes in $\Delta\psi_m$, upregulation of cyto c plasma levels and activation of caspase 3 and 7 in ECs (Xu *et al.*, 2011).

Observations suggest an individualistic and linear model of the mitochondrial life cycle: a mitochondrion gradually deteriorates to $\Delta\psi_m$ dissipation, at which energy is targeted for recycling by autophagy (Twig, Hyde and Shirihai, 2008). Mitochondria undergo constant cycles of fission and fusion to maintain quality control and metabolic requirements (Westermann, 2010). Mitochondrial dynamics are tightly regulated by nuclear-encoded GTPases (fission and fusion proteins) (Tilokani *et al.*, 2018). Fission is driven by the DRP1 protein, whereas fusion is mediated by MFN1/2 and OPA1 anchor proteins that promote fusion of the mitochondrial outer and inner membrane, respectively (Losó n *et al.*, 2013; Tilokani *et al.*, 2018).

Under pathological conditions, pro-fission proteins and signalling pathways are increased, and autophagy is impaired, leading to a loss of mitochondrial networks, mitochondrial fragmentation, and increased mitochondrial ROS (Watanabe *et al.*, 2014). Previous studies showed that vitamin D3 could decrease TNF- α -induced lung inflammation by reducing mitochondrial fission and fragmentation (Y. C. Chen *et al.*, 2021). On the other hand, the disruption of pro-fusion proteins results in mitochondrial dysfunction (Kushnareva *et al.*, 2012).

To date, limited studies have investigated the role of H₂S on endothelial function by preserving mitochondrial function through different prodrugs. Wen *et al.* demonstrated that NaHS reduced H₂O₂-induced apoptosis by improving $\Delta\psi_m$, ATP synthesis and antioxidant defence in HUVECs (Wen *et al.*, 2013). In addition, exogenous NaHS treatment restored mitochondrial function in cardiomyocytes exposed to TNF- α (Lee *et al.*, 2019). Moreover, decreased intracellular H₂S content by CBS knockdown HUVECs is associated with an impaired mitochondrial bioenergetic profile and a change of mitochondrial morphology toward fragmentation (Rao *et al.*, 2020).

The *in vitro* data discussed in the previous chapter revealed that TNF- α stimulates the apoptosis rate in HUVECs. The role of mitochondrial in altered endothelium and previous observations hint that TNF- α may also affect mitochondria in dysfunctional HUVECs. However, although H₂S beneficial effects have been observed in TNF- α -induced

cardiomyocytes by improving mitochondria function (Lee *et al.*, 2019), effects with a post-treatment design in an inflammatory-mediated endothelial environment are unexplored.

5.2 Aims

Following on from the previous chapter, this study aimed to identify the effect of TNF- α on mitochondria function and mitochondrial morphology. In addition, to determine whether H₂S donors could be able to alleviate TNF- α -induced mitochondrial dysfunction in HUVECs. For this purpose, several objectives were conducted:

- To investigate bioenergetic profile and parameters at baseline and after exposure to TNF- α and GYY4137.
- To assess mitochondria dysfunction in response to TNF- α with and without GYY4137 post-treatment.
- To investigate changes in mitochondrial morphology in the presence of TNF- α followed by GYY4137 post-treatment.
- To assess TNF- α effect on mitochondrial-mediated apoptotic signalling pathway and effects of GYY4137 post-treatment.

5.3 Materials and Methods

5.3.1 Endothelial cell culture.

HUVECs were routinely maintained in T75 flasks with the complete supplemented medium at 37°C and 5% CO₂ (see section 2.2.2). Endothelial seeding and experimental settings were explicitly conducted for each assay following general maintenance, as indicated in section 2.2.3. Cells were treated following the post-treatment experimental design with TNF- α (1 ng/ml) for 3 hours, followed by post-treatment with GYY4137 at a non-toxic concentration (100 μ M) for 21 hours, giving an overall 24 hours experimental treatment. Next, HUVECs were analysed specifically for the desired assay. In general, cells were divided into four groups unless otherwise stated: control (untreated cells), GYY4137 (alone), TNF- α (alone), TNF- α + GYY4137 (post-treatment model).

5.3.2 Fluorescence microscopy

MitoSox fluorescence probe was used to analyse $O_2^{\cdot-}$ described in section 2.5.2.

MitoTracker staining probe was analysed by confocal fluorescence microscopy to determine the mitochondrial network using the specific ImageJ macro (MiNa). For full details, see section 2.9.3.

JC-1 staining probe was used to investigate $\Delta\psi_m$ as described in section 2.14.

5.3.3 RT-QPCR

Quantitative real-time PCR was performed by extracting the total RNA. Fold change relative expression was calculated using the $\Delta\Delta C_t$ method. When comparing gene expression, the fold change relative expression of Mnf1, OPA1, DRP1, UCP2, CAT, SOD2 and GPx1 were calculated using YWAZ and EEF2 as housekeeping genes. Full details, see section 2.18.

5.3.4 Extracellular Flux analyser (Seahorse technology)

The Mito Stress test was assessed using the Seahorse XF24 instrument to examine mitochondrial respiration rate and bioenergetic parameters. For full details, see section 2.15.1.

The Glycolytic Stress test examined the extracellular acidification rate using the Seahorse XF24 instrument described in section 2.15.2.

5.3.5 Western blot

Immunoblotting analysis of cyto c, caspase 3 and cleaved caspase 3 protein expression was determined by SDS-PAGE as described in section 2.17

5.4 Statistical analysis

All values presented are as mean \pm SEM. Unless otherwise stated, all usually distributed variables between two groups were compared by unpaired Student *t*-test. When

comparing three groups or more one-way ANOVA followed by Sidak's *post-hoc* comparisons was applied. For statistical tests, p values less than 0.05 ($p < 0.05$) were considered significant.

5.5 Results

5.5.1 Evaluation of the mitochondrial-mediated redox state in TNF- α and GYY4137 post-treated cells.

Since mitochondria are one of the primary sources of ROS and an easy target for robust oxidants species, mitochondrial-derived ROS formation was assessed (Zorov, Juhaszova and Sollott, 2014). Mitochondrial ROS are produced due to the leakage of electrons by ETC, mainly at complexes I and III, of which $O_2^{\cdot-}$ anion radical is the most abundant and with the most oxidative capacity (Zorov, Juhaszova and Sollott, 2014). Therefore, the levels of $O_2^{\cdot-}$ in HUVECs treated with TNF- α and GYY4137 post-treatment were assessed using the MitoSox Red probe combined with fluorescent microscopy analysis. Data show that cells in the presence of TNF- α display a higher proportion of MitoSox-positive cells (Figure 5.1 A), and the quantification of MitoSox-associated fluorescence showed a significant increase compared to untreated cells ($***p<0.0001$) (Figure 5.1 B). As shown in Figure 5.1 A-B, HUVECs subjected to GYY4137 did not show higher fluorescence intensity with no statistical differences versus the control group. Notably, the differences in MitoSox-associated fluorescence were facilitated in the presence of GYY4137 post-treatment, with a significant decrease of $O_2^{\cdot-}$ in TNF- α -treated cells ($####p<0.0001$).

Within mitochondria, H_2O_2 is degraded by several peroxiredoxins, including SOD, CAT and GPX1 (Zielonka and Kalyanaraman, 2010). The rate of mitochondrial redox state depends, in part, on the $O_2^{\cdot-}$ production and rate of degradation (Figure 5.2 A). Therefore, the expression pattern of genes involved in mitochondrial function and stress responses was assessed by RT-qPCR. Figure 5.2 B shows that HUVECs with TNF- α -treatment significantly upregulate SOD2 mRNA levels ($*p<0.05$). A significant rise in the enhanced SOD2 mRNA levels in TNF- α -induced HUVECs was observed after GYY4137 post-treatment ($*p<0.05$) compared to control cells. In addition, the enzyme CAT, which can be found in cytosol, mitochondria and peroxisomes, was also analysed by RT-qPCR. In the presence of TNF- α , cells tended to increase CAT mRNA levels, but values did not reach statically significance. Notably, in the presence of GYY4137 post-treatment, HUVECs displayed a significant upregulation of CAT mRNA levels after TNF- α treatment compared to the control group ($*p<0.05$) (Figure 5.2 C). Although Figure 5.2 D revealed a trend of increase in TNF- α -treated HUVECs with or without GYY4137 post-treatment

regarding GPx1 mRNA levels, the differences between the groups were insignificant. This data suggests that GYY4137 could enhance $O_2^{\cdot-}$ -scavenging sinks in the TNF- α -altered redox state.

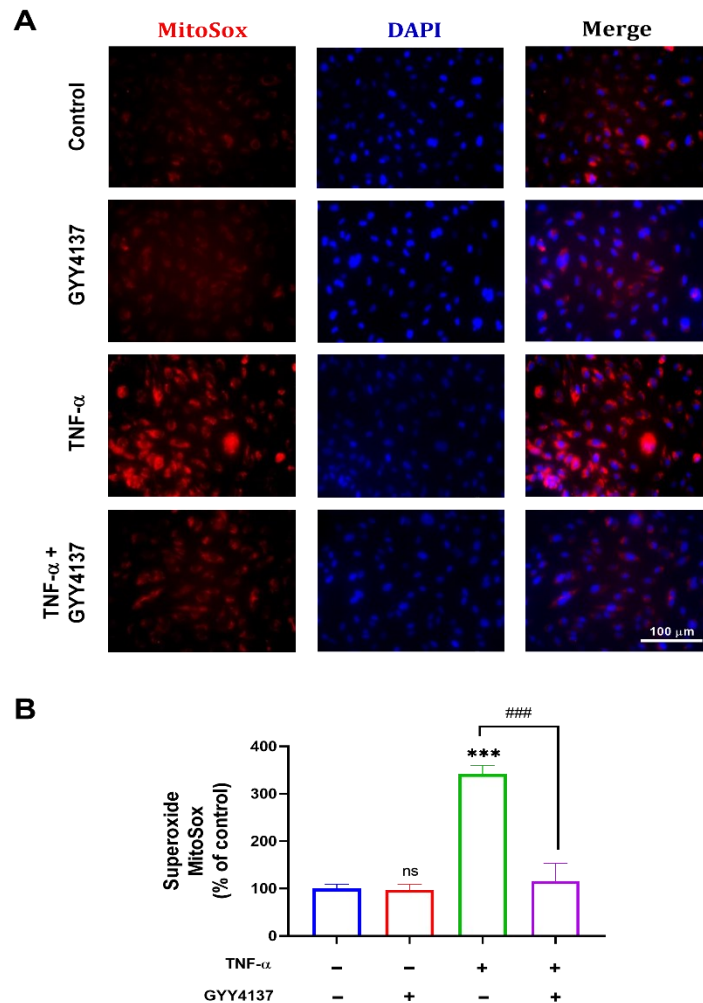


Figure 5.1. Effect of TNF- α and GYY4137 post-treatment on $O_2^{\cdot-}$ levels.

HUVECs were incubated with MitoSox (5 μ M) for 30 minutes in the dark before microscopy evaluation. **(A)** Representative fluorescence images of HUVECs stained for $O_2^{\cdot-}$ (red spectrum). DAPI was used to visualise nuclei (blue spectrum). Pictures were taken using a Nikon Ti-S Inverted fluorescence microscope (10x magnification, scale bar: 100 μ m). **(B)** Analysis and quantification of fluorescence intensity were conducted by ImageJ software. Results were shown as the mean \pm SEM (n=3). Significance was determined by a one-way ANOVA test followed by Sidak's post-test comparing treatments, whereby ns. and (***) represent non-significant and $p < 0.001$, respectively vs. the control group. (### $p < 0.0001$) represents a comparison between TNF- α alone and TNF- α with GYY4137 post-treatment.

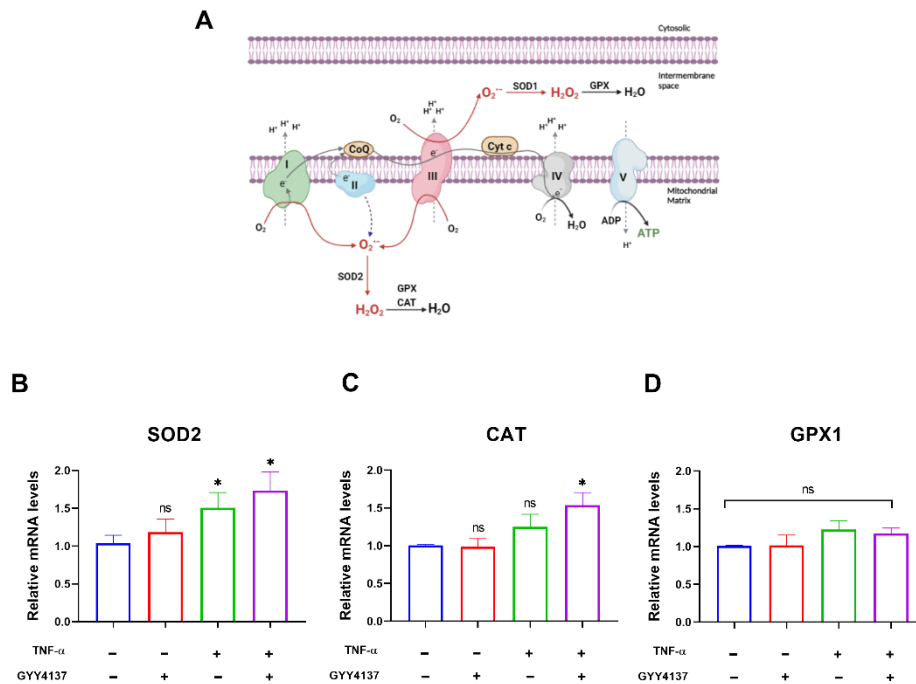


Figure 5.2. RT-qPCR mRNA levels in TNF- α and GYY4137 stimulated HUVECs.

(A) Major sites for mitochondrial $O_2^{\bullet-}$ generation and detoxification. Upon respiration, $O_2^{\bullet-}$ is inevitably generated at respiratory complexes I and III; CAT: catalase; SOD1/2: superoxide dismutase 1 and 2; GPX: glutathione peroxidases. The relative mRNA levels of (B) SOD2, (C) CAT and (D) GPx1 were analysed by RT-qPCR. YWHAZ and EEF2 were used as housekeeper genes. Results were shown as the mean \pm SEM (n=3-5). A one-way ANOVA test was carried out to determine the statistical significance of changes in mRNA, followed by Sidak's post hoc test. To normalise for multiple comparisons comparing treatments to control (untreated cells), whereby ns. and (*) represent non-significant and p<0.05, respectively vs. control. Created with Bio-render.com.

5.5.2 Analysis of mitochondrial bioenergetics in HUVECs.

Studies have been carried out on the efflux of $O_2^{\bullet-}$ and H_2O_2 from isolated mitochondria to enable generalisations about the cellular sites that favour $O_2^{\bullet-}$ production being complexes I and III within mitochondrial ETC, the major sites (Murphy, 2009). Therefore, clarifying how vascular endothelial damage is associated with energy supply is essential. Given the above results, a more functional and in-depth study of the metabolism of cells using Seahorse extracellular flux analysis XF24 Analyzer was assessed.

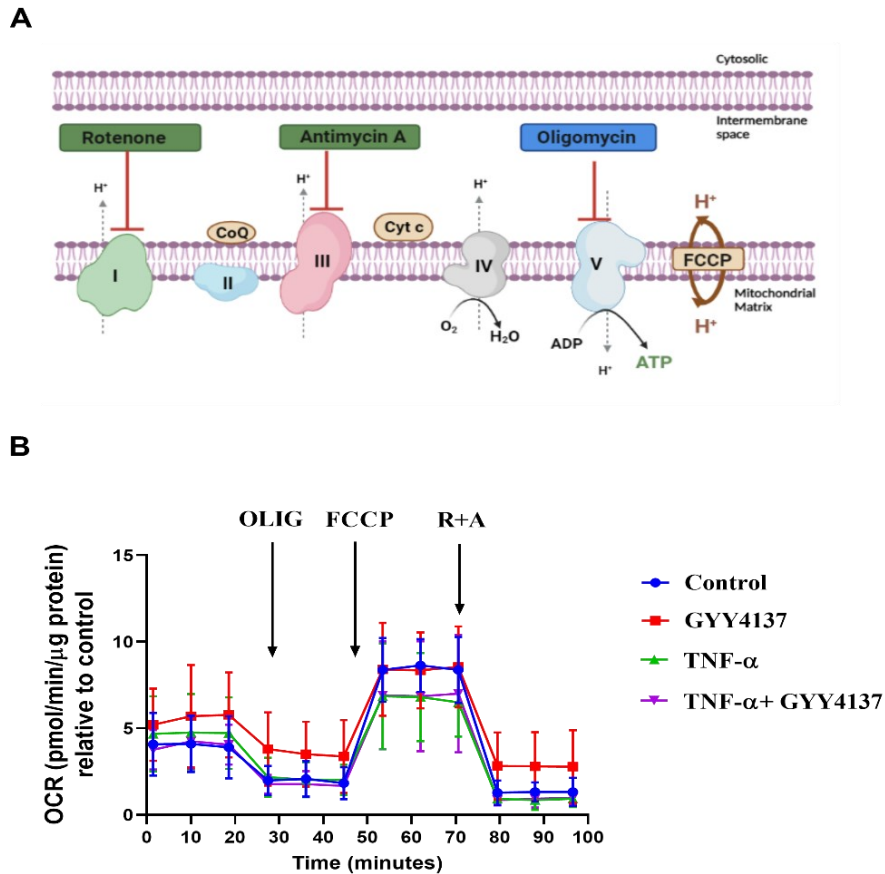


Figure 5.3. Mitochondrial OCR profile upon TNF- α and GYY4137 post-treatment. (A) Representative illustration of Agilent Seahorse XF Mito Stress Test with modulators of the ETC. (B) HUVECs were plated at 0.5×10^6 /well in XF 24-well plate and treated with TNF- α and GYY4137 post-treatment before the day of the Mito Stress test. Cell mitochondrial respiration profiles were plotted as OCR readout for 12-time-points after sequential injection of OLIG (oligomycin), FCCP and R+A (rotenone and antimycin A) using a Seahorse XF24 Analyser. The differential respiration profiles from untreated and treated groups were plotted. Results were shown as the mean \pm SEM, (n=5). Created with Bio-render.com.

To investigate whether TNF- α affected mitochondrial metabolism, quantification of the bioenergetic profile using a Seahorse XF Cell Mito Stress Test was assessed. During the Mito Stress test, the readout oxygen consumption rate (OCR, indicative of OXPHOS rates) is evaluated in the presence of specific mitochondrial complexes mediators, including rotenone and antimycin A mix (0.5 μ M), FCCP (0.5 μ M) and oligomycin (1 μ M) (Figure 5.3 A).

When ECs are challenged with GYY4137, the continuous OCR in response to the Mito Stress test tends to enhance after oligomycin and the rotenone/antimycin A mix. The OCR of TNF- α -treated HUVECs after FCCP injection dropped, which differs from those cells treated with GYY4137 (Figure 5.3 B).

To gain a detailed perspective of how the oxidative profile of HUVECs subjected to TNF- α and GYY4137 post-treatment change, examination of mitochondrial respiration parameters was calculated and analysed using Seahorse XF Cell Mito Stress Test Report Generator. At baseline, HUVECs had significantly higher basal respiration compared to untreated cells (** $p < 0.01$) (Figure 5.4 A). In the presence of TNF- α and GYY4137 treatment, a significant decrease compared with TNF- α -treated HUVECs was observed (* $p < 0.05$). The ATP-linked OCR analysis revealed that HUVECs had a significantly elevated ATP-dependent OCR rate in the presence of TNF- α compared to the control (* $p < 0.05$). Although the ATP production tends to be reduced in GYY4137 post-treatment in TNF- α -cultured HUVECs, it did not reach significance (Figure 5.4 B).

Proton leak (protons entering the mitochondrial matrix without producing ATP) assessment revealed a significant increase in TNF- α -HUVECs in comparison to untreated cells (** $p < 0.0001$). GYY4137 post-treatment significantly reduced high proton leak levels in HUVECs subjected to TNF- α (#### $p < 0.0001$) (Figure 5.4 C). Maximal respiration rate analysis shows that in the presence of TNF- α , this OCR-related parameter tends to decrease, although the value did not reach significance. Similar, GYY4137 post-treatment tended to increase the maximal respiration rate in TNF- α -treated HUVECs but did not reach significance (Figure 5.4 D).

This data indicates differences in mitochondrial function in treated-HUVECs relative to untreated cells. The data highlighted the relevance of elevated proton leak, which suggests a dissipation of protonmotive force. Cells can switch between energy-producing routes, thereby adapting to environmental changes. Thus, it is relevant to examine glycolysis as the alternative major energy-producing route in the cell.

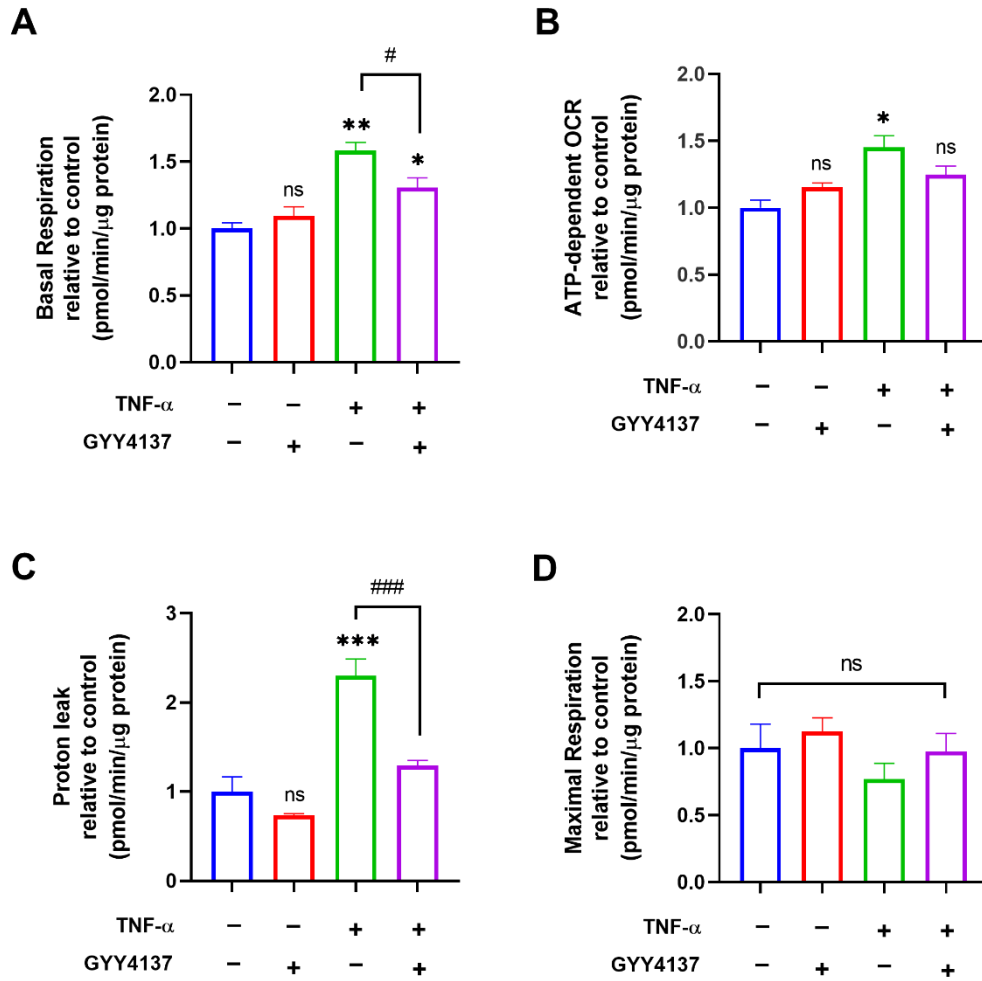


Figure 5.4. Comparison of mitochondrial respiration parameters of untreated and treated HUVECs.

Mitochondrial parameters calculated from OCR obtained from mitochondrial respiration profiles are presented as bar graphs of basal respiration (A) ATP-linked OCR production (B), proton leak (C) and maximal respiration (D). Wave software (Agilent) was used for data analyses. The data were presented as mean \pm SEM (n=5). Significance was determined by a one-way ANOVA test followed by Sidak's post-test comparing treatments to control, whereby ns., (*), (**) and (***) represent non-significant, $p < 0.05$, $p < 0.01$ and $p < 0.001$, respectively vs. control. (# $p < 0.05$) and (### $p < 0.001$) represents comparison to TNF- α alone.

5.5.3 Analysis of glycolysis in HUVECs

Metabolisms of glucose to pyruvate result in two primary possibilities: the metabolism of pyruvate to lactate or the oxidative decarboxylation of pyruvate to acetyl CoA for entry into the TCA cycle (Figure 5.5 A). Due to ECs obtaining >80% of energy production from the glycolytic activity and the Seahorse XF Glycolysis Stress Test on a Seahorse XF24 Analyzer offers a time-resolved view of changes in glycolysis rate, HUVECs were subjected to Glycolysis Stress Test. The readout extracellular acidification rates (ECAR) detect small changes in acidification of the medium due to lactic acid synthesis, the end-product of glycolysis. The overall ECAR profile of HUVECs showed an increased rate after glucose and oligomycin injections in the presence of TNF- α and GYY4137 compounds. In addition, cells treated with TNF- α alone and GYY4137 post-treatment in TNF- α -treated cells share a similar ECAR profile throughout the analysis (Figure 5.5 B).

The glycolytic parameters, including glycolysis, glycolytic capacity and glycolytic reserve, were calculated and analysed using Seahorse XF Cell Glycolysis Test Report Generator. Treatment of HUVECs with TNF- α alone leads to a significant increase in glycolysis and glycolytic capacity ($***p<0.0001$) as well as glycolysis reserve ($*p<0.05$) in comparison to control group (Figure 5.6 A-C). In the presence of TNF- α and GYY4137 post-treatment, glycolysis and glycolytic capacity levels were significantly increased ($***p<0.0001$) compared to untreated cells. This data indicates differences in glycolysis function in the presence of TNF- α , specifically an enhanced ECAR profile suggesting an increase to sustain energetic demands upon cellular stress via the mediation of the glycolytic pathway, which is the primary energy source in ECs.

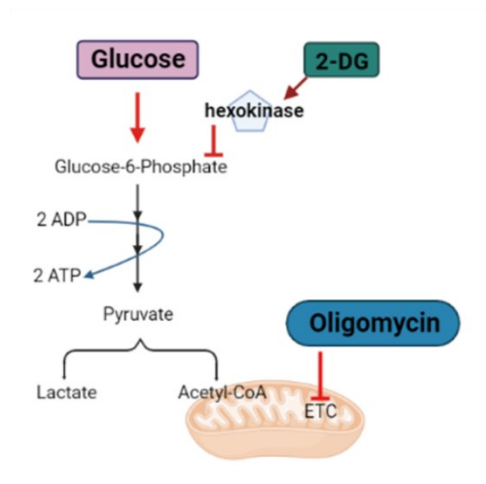
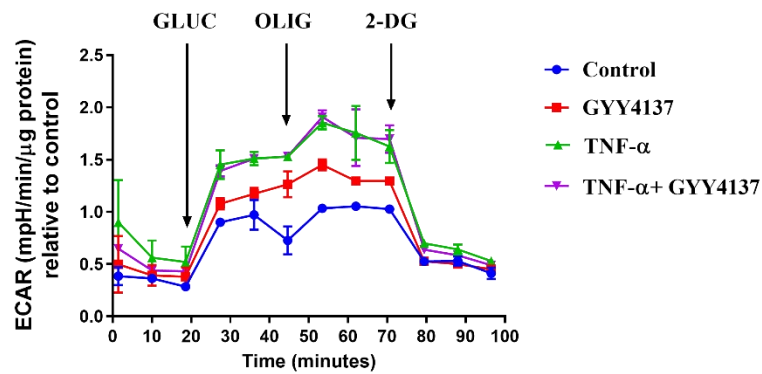
A**B**

Figure 5.5. ECAR rate in TNF- α and GYY4137-cultured HUVECs.

(A) Representation of Agilent Seahorse XF Glycolysis Stress Test and the sites of action of the modulators of the glycolytic pathway. (B) HUVECs were plated at 0.5×10^6 /well in XF 24-well plate and treated with TNF- α and GYY4137 post-treatment prior to the day of the Glycolysis Stress test. Representative glycolytic profiles of HUVECs were plotted as traces of extracellular acidification rates (ECAR) for 12-time-points after sequential injections of GLUC (glucose), OLIG (oligomycin) and 2-DG (2-deoxy-glucose) using a Seahorse XF24 Analyser. The differential glycolytic profiles from untreated and treated groups were plotted. Results were shown as the mean \pm SEM, (n=4). Created with Bio-render.com.

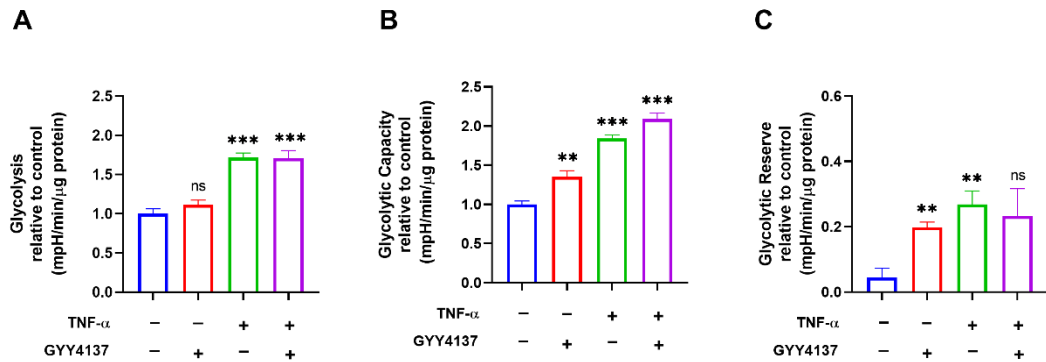


Figure 5.6. Comparison of glycolytic parameters in untreated and treated-HUVECs. Parameters of the glycolytic pathway: glycolysis (A) glycolytic capacity (B) and glycolytic reserve (C) calculated from ECAR profiles are displayed as bar graphs. Wave software (Agilent) was used for data analyses. The data were presented as mean \pm SEM (n=5). Significance was determined by one-way ANOVA test followed by Sidak's post-test comparing treatments to control; whereby ns, (*), (**) and (***) represents non-significant, $p < 0.05$, $p < 0.01$ and $p < 0.001$, respectively vs. control.

5.5.4 Uncoupling proteins in TNF- α and GYY4137-treated HUVECs.

The above results showed a robust increase in proton leak rate in the presence of TNF- α compared to untreated HUVECs. In the mitochondrion, the total proton leak is determined by the basal leak and proton leak processes. While the former is an unregulated leak, the latter is catalysed by specific mitochondrial inner membrane proteins named UCPs. UCPs are solute carrier proteins that regulate proton flux across the inner mitochondrial membrane to re-enter the matrix. UCPs appear to regulate mitochondrial membrane potential as inducible proton leaks result in membrane depolarisation (Jastroch *et al.*, 2010; Cadenas, 2018) (Figure 5.7 A). The elevated proton leak data observed could result from the UCPs function. Based on the role of UCP2 in the vasculature and to fit with the UCPs isotype analysed in previous endothelial studies, RT-qPCR analysis for UCP2 mRNA level was conducted (Lee *et al.*, 2005; He *et al.*, 2014; Pierelli *et al.*, 2017). The RT-qPCR assay showed that TNF- α treatment significantly increased UCP2 mRNA compared to untreated HUVECs (* $p < 0.05$). In addition, GYY4137 post-treatment significantly reduced the elevated UCP2 mRNA levels in TNF- α -treated HUVECs, restoring them to basal levels (## $p < 0.01$) (Figure 5.7 B).

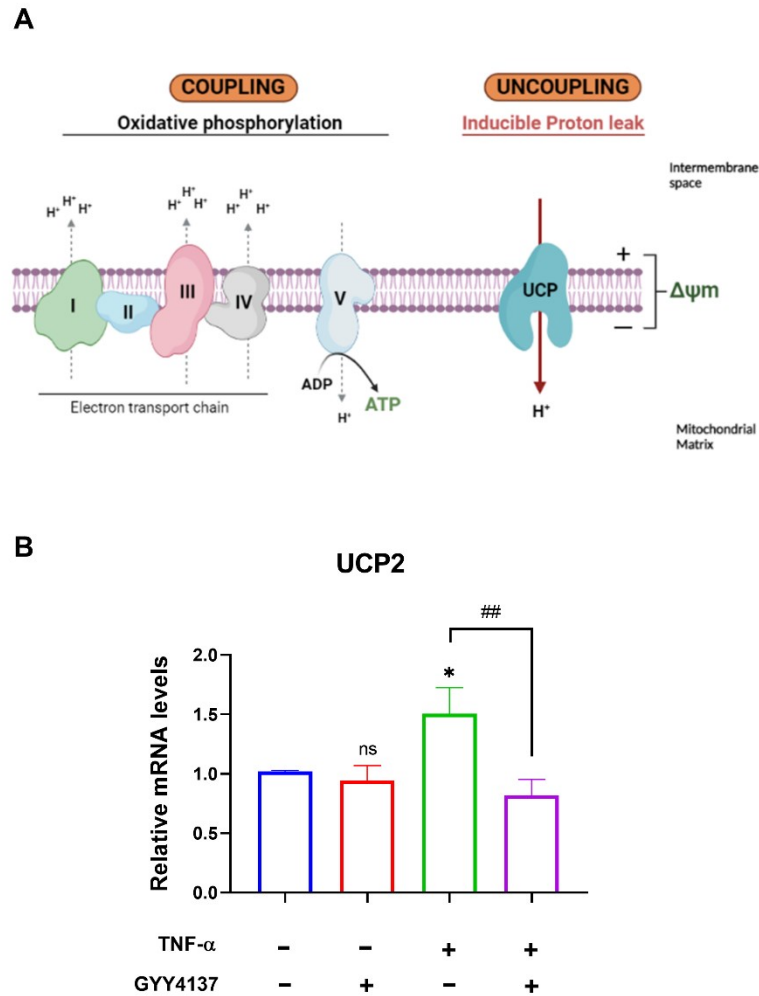


Figure 5.7. TNF- α and GYY4137 post-treatment effect on UCP2 mRNA levels in HUVECs.

(A) Schematic representation of coupling, uncoupling proton leak components within mitochondria include the oxidative phosphorylation complexes, UCPs and $\Delta\psi_m$. (B) UCP2 mRNA levels was analysed by RT-qPCR and calculated using the $\Delta\Delta C_t$ value method. YWHAZ and EEF2 were used as housekeeper genes. Results were shown as mean \pm SEM, (n=9). To determine statistical significance of changes in mRNA a one-way ANOVA test was carried out followed by Sidak's post hoc test to normalise for multiple comparisons comparing treatments to control, whereby ns. and (*) represents non-significant and $p < 0.05$ respectively vs. control. (## $p < 0.01$) represents comparison to TNF- α alone. Created with Bio-render.com.

5.5.5 Analysis of $\Delta\psi_m$ in HUVECs.

The $\Delta\psi_m$ is a fundamental parameter that has been used as an indicator of the function of mitochondria and regulates mitochondrial ATP synthesis and protonmotive force (Madamanchi and Runge, 2007). TNF- α -induced endothelial injury may result in mitochondrial membrane depolarisation and pro-apoptotic factors release (Zhou *et al.*, 2017, 2019). A straightforward approach to assessing $\Delta\psi_m$ of cells is to load their mitochondria with JC-1, a selectively accumulated probe in mitochondria. As a cationic dye, JC-1 accumulates in the energised mitochondria, where healthy cells with high $\Delta\psi_m$ form complexes known as J-aggregates that emit red fluorescence. In contrast, in unhealthy cells with low $\Delta\psi_m$, JC-1 remains in a J-monomeric form that emits green fluorescence. The higher the red-to-green fluorescence ratio, the higher the polarization of the $\Delta\psi_m$ (Sivandzade, Bhalerao and Cucullo, 2019). JC-1-associated fluorescence intensity analysis revealed that TNF- α causes an increase in monomers' fluorescence intensity (green spectrum). This switch causes an imbalance in aggregates/monomers rate compared to control HUVECs suggesting that the TNF- α treatment impaired the $\Delta\psi_m$ (Figure 5.8 A). In addition, HUVECs upon GYY4137 post-treatment displayed a low monomers fluorescence signal compared to the TNF- α treatment alone. Quantification of the JC-1 red/green fluorescence ratio showed that TNF- α significantly decreased $\Delta\psi_m$ compared to untreated HUVECs (* $p < 0.05$). GYY4137 significantly abolished this effect by increasing the JC-1 red/green fluorescence ratio in HUVECs-treated with TNF- α (## $p < 0.01$) (Figure 5.8 B). These results suggest that ECs, upon TNF- α treatment, lose $\Delta\psi_m$, suggesting a dissipation of $\Delta\psi_m$ and supporting that TNF- α -mediate ED is associated with an impaired mitochondrial function, which GYY4137 can restore.

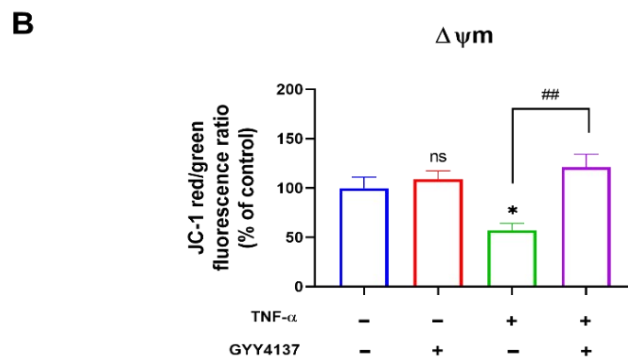
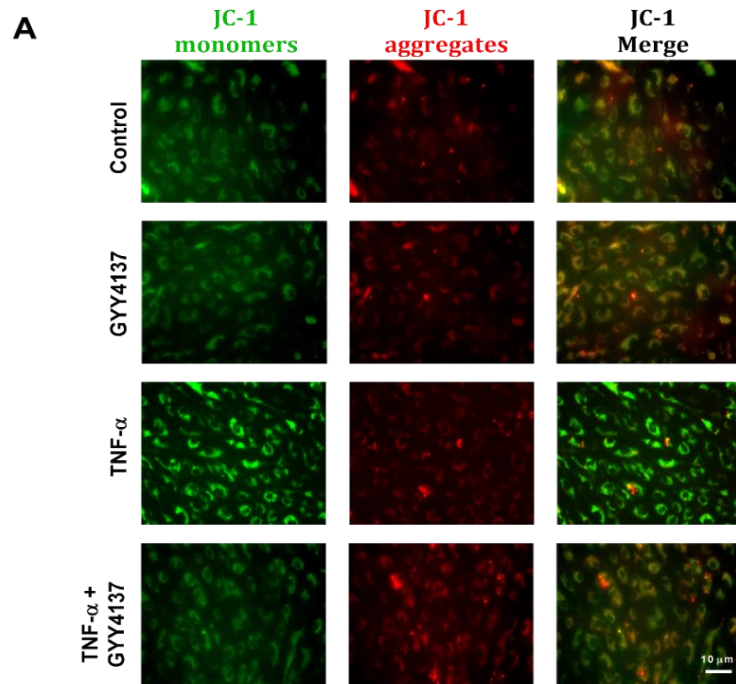


Figure 5.8. Effects of TNF- α and GYY4137 on $\Delta\psi_m$ in HUVECs.

(A) Cells were incubated with 5 μ M JC-1 dye for 20 minutes in the dark followed by wash with PBS. $\Delta\psi_m$ was determined by measuring fluorescence intensity for red fluorescence (energized mitochondria) and for green fluorescence (depolarized mitochondria) using a Nikon Ti-S Inverted fluorescence microscope. (B) Bar graphs of ratio red/green fluorescence from JC-1 assay was calculated. The data were presented as the mean \pm SEM, (n=3). Significance was determined by one-way ANOVA test followed by Sidak's post-test comparing treatments vs control group, whereby ns. and (*) represents non-significant and $p < 0.05$, respectively vs. control. (## $p < 0.01$) represents comparison to TNF- α alone.

5.5.6 Mitochondrial morphology and dynamic machinery in HUVECs.

Mitochondria are highly dynamic organelles that constantly undergo fusion and fission cycles. This process is central to mitochondrial function and depends on a cell's metabolic state and the $\Delta\psi_m$ (Twig *et al.*, 2008). Given that in the above data, TNF- α leads to $\Delta\psi_m$ loss; it is probable that TNF- α also affects the fusion/fission machinery and thus, mitochondrial dynamics. For this purpose and to visualised mitochondrial morphology alterations, mitochondria were labelled by MitoTracker Red fluorescence probe combined with mitochondrial network analysis using the Mitochondrial Network Analysis (MiNA), which fits with the previous study using HUVECs as *in vitro* model (Rao *et al.*, 2020). As expected, confocal fluorescence analysis shows that most mitochondria observed in the presence of TNF- α shifted from tubular and long structure to globular and spherical morphology (Figure 5.9 A). Mitochondria mean branch length is the average length (in microns) of all branches in one network. Mitochondrial network size is defined as the average number of branches per network (in microns). Semi-quantitative analysis of mitochondrial network parameters showed that TNF- α significantly decreased the mean branch length (Figure 5.9 B) and the mean network size (Figure 5.9 C) compared to the control group (**P<0.0001). Furthermore, GYY4137 post-treatment significantly ameliorated mean branch length (##p<0.01) and mean network size decreased (###p<0.0001) in TNF- α -treated HUVECs. These data suggested that TNF- α -mediates altered mitochondrial morphology.

Subsequently, mitochondrial fission and fusion machinery were analysed to confirm further the impaired mitochondrial dynamic in ECs cultured with TNF- α . While fission and fusion dynamics are balanced under physiological conditions, vascular conditions or oxidative stress damage provoke a shift towards fission, resulting in excessive and un-regulated mitochondrial fragmentation (Shenouda *et al.*, 2011). To assess the impact on the fission machinery, DRP1 mRNA levels were investigated by RT-qPCR. As indicated in Figure 5.10 A, DRP1 mRNA levels significantly increased in the TNF- α -treated ECs compared to the control group (**p<0.01). Furthermore, post-treatment with GYY4137 significantly revoked the changes in DRP1 mRNA levels by TNF- α treatment (#p<0.05).

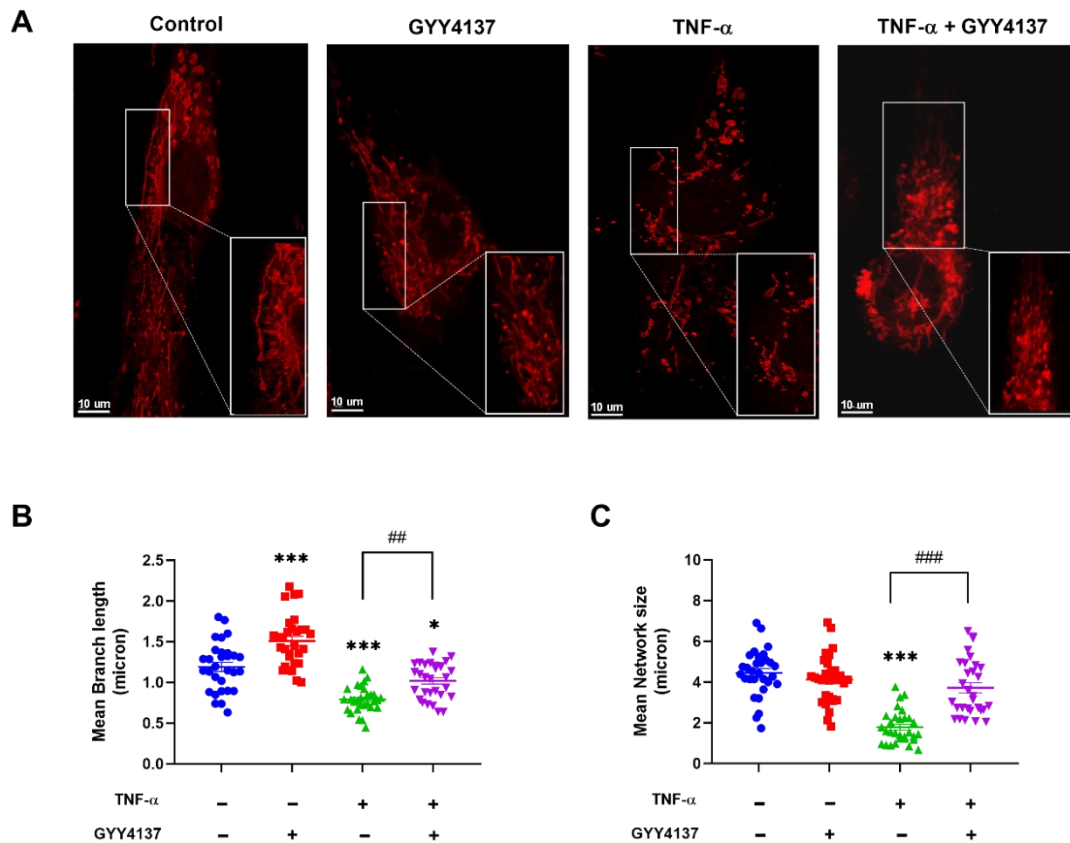


Figure 5.9. Mitochondrial network parameters in HUVECs.

Cells were treated with TNF- α and GYY4137 in a post-treatment setting. **(A)** Cells were stained with MitoTracker Red (100 nM) and imaged by confocal microscopy (red spectrum). Scale bar: 10 μ m. **(B)** Mean branch length and **(C)** mean network size were semi-quantitatively assessed using the Mitochondrial Network Analysis (MiNA) toolset (ImageJ). Thirty cells per group per independent experiment were analysed. Statistical analysis was conducted using a one-way ANOVA test followed by Sidak's comparison test. Data are shown as means \pm SEM; (n=3)(***p<0.001) vs. control while (##p<0.001) represents a comparison to TNF- α -treated group alone.

Subsequently, to determine whether TNF- α impacts the fusion machinery, levels of pro-fusion factors MFN1, which facilitate fusion on the mitochondrial outer membrane, were investigated by RT-qPCR. Analysis of mRNA levels showed that TNF- α tends to reduce MFN1 mRNA levels compared to control, but values did not reach significance. Notably, post-treatment with GYY4137 significantly elevates MFN1 mRNA levels in TNF- α -treated HUVECs (##p<0.01) (Figure 5.10 B).

Finally, OPA1, essential for mitochondrial inner membrane fusion and mitophagy, was also investigated by RT-qPCR. Interestingly, it is observed that TNF- α significantly increased OPA1 mRNA (* p <0.05). Although GYY4137 post-treatment results in a trend to reduce OPA1 mRNA levels, the levels did not reach significance compared to TNF- α -treated HUVECs (Figure 5.10 C). This particular increase could be related to OPA1 regulation of the mitophagy rather than the fusion role. Overall, the results showed that TNF- α alters mitochondrial morphology via modulation of fission/fusion genetic profile and might further mediate mitophagy signalling.

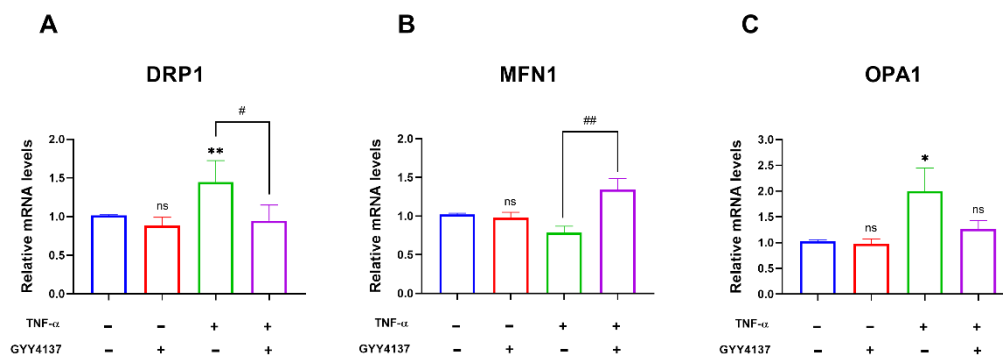


Figure 5.10 Disruption of the mitochondrial fission/fusion balance machinery in HUVECs.

Total RNA was extracted using a Qiagen RNA extraction kit. The extracted RNA was reverse transcribed to cDNA and calculated using the $\Delta\Delta C_t$ value method. **(A)** Analysis of pro-fission gene showing mRNA levels of DRP1. **(B,C)** RT-qPCR test of pro-fusion mRNA expression of MFN1 and OPA1. YWHAZ and EEF2 were used as housekeeper genes. Results were shown as mean \pm SEM (n=6-9). One-way ANOVA test was carried out followed by Sidak's post hoc test to normalise for multiple comparisons comparing treatments vs. to control (untreated cells), whereby ns., (*) and (**) represent non-significant, p <0.05 and p <0.01; respectively compared to control. (# p <0.05) and (## p <0.01) represents a comparison to the TNF- α group alone.

5.5.7 Regulation of TNF- α and GYY4137 on apoptotic-related proteins in HUVECs.

The apoptotic caspase cascade signal has been associated with the release and redistribution of cyto c from the mitochondria to the cytosol related to the loss of $\Delta\psi_m$ and opening of the MPTP (Cai, Yang and Jones, 1998). During activation, caspase 3 undergoes maturation from its unprocessed performance to its active cleaved form, which proteolytically cleaves a range of substrates, leading to cell death (Shalini *et al.*, 2014). Notably, TNF- α has been reported to mediate mitochondrial-dependent apoptotic pathways (Deng *et al.*, 2017).

Having shown that TNF- α treatment increases the apoptotic rate and dissipation of $\Delta\psi_m$, the possibility that TNF- α influences apoptosis by mediating intrinsic pathway was investigated. To this end, proteins extracted from HUVECs upon TNF- α and GYY4137 experimental design were separated by electrophoresis and incubated with anti-cyto c, anti-caspase 3 and anti-cleaved caspase 3 antibodies with actin as a loading control (Figure 5.11 A). Quantification of immunoblotting by ImageJ revealed that TNF- α significantly increased cyto c protein expression in the cytosol of treated-HUVECs compared to control cells (* $p < 0.05$). Post-treatment with GYY4137 was able to significantly reduce cyto c protein accumulation in the cytosol (# $p < 0.05$) (Figure 5.11 B). Notably, there was no significant change in the expression of caspase 3 protein in the presence or absence of GYY4137 and TNF- α (Figure 5.11 C). Furthermore, the increased protein expression of cleaved caspase 3 was significantly reduced by GYY4137 post-treatment in TNF- α -treated cells (# $p < 0.05$) (Figure 5.11 D).

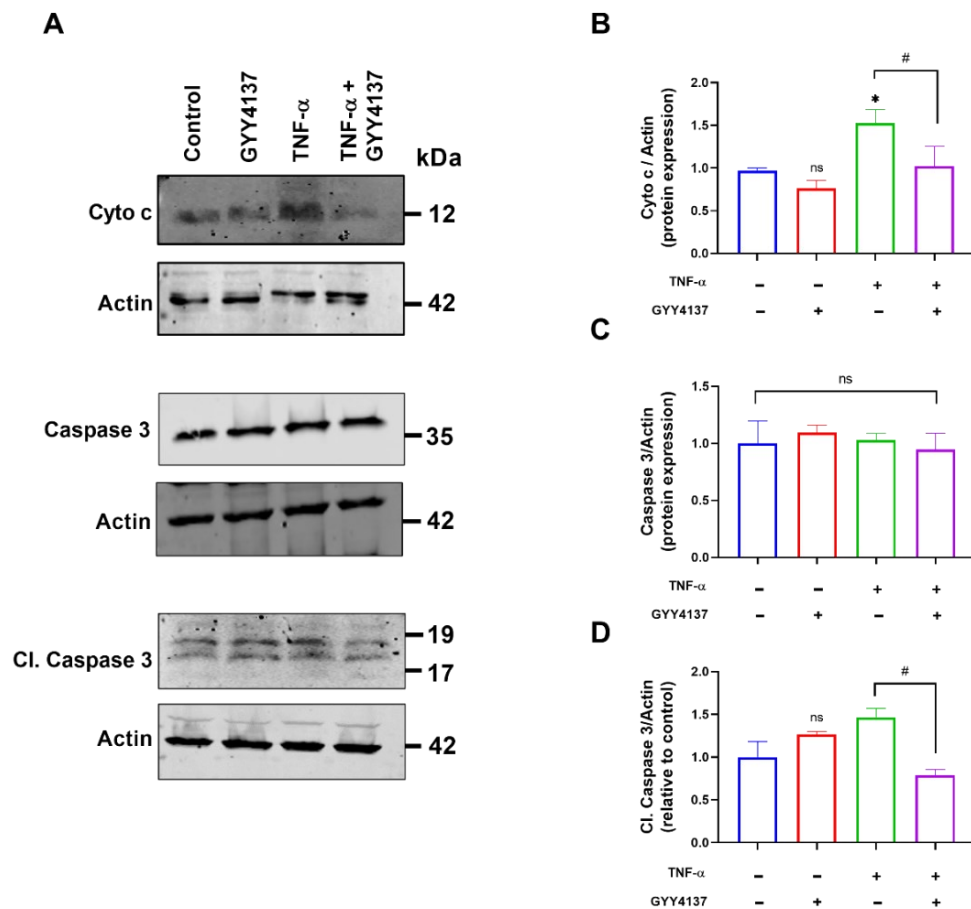


Figure 5.11 TNF- α and GYY4137 modulated apoptotic-associated proteins in HUVECs. Once TNF- α and GYY4137 treatments were conducted, protein concentration was determined by BCA assay. The nitrocellulose membranes were incubated with antibodies against cyto c, caspase 3, cleaved caspase 3 and actin (loading control) and detected by the LICOR imaging system. **(A)** Densitometry analysis of blots was performed by ImageJ software. **(B)** Bar graph showing cyto c, **(C)** caspase 3 and **(D)** cleaved caspase 3 quantification relative to control. Results were shown as mean \pm SEM; (n=3-5). Significance was determined by a one-way ANOVA test followed by Sidak's post-hoc test comparing treatments to control (untreated cells), whereby ns. and (*) represent non-significant and ($p < 0.05$) vs. control. (# $p < 0.05$) represents a comparison to TNF- α alone.

5.6 Discussion

This chapter investigated whether TNF- α -induced ED is associated with impaired mitochondrial function. When dissecting the possible causes for excessive ROS formation and apoptosis observed in TNF- α -treated HUVECs, it was possible to rule out that the defective cells have impaired uncoupling proton leak in the mitochondria displayed dissipation of $\Delta\psi_m$, which subsequently allowed cyto c release into the cytosol. In addition, cells exposed to TNF- α exhibit mitochondrial fragmentation alongside defective fission/fusion machinery. In addition, H₂S slow-releasing donor, GYY4137, repressed mitochondrial dysfunction reported upon TNF- α treatment.

It is now clear that organisms have developed a method of utilising ROS in critical processes at cellular levels (e.g. AMP-activated kinase), systems-level (e.g. thyroid peroxidase function) (Moreno *et al.*, 2002) or immune system (e.g. lacking NOX2 in granulomatous disease) (Mauch *et al.*, 2007). On the other hand, excessive ROS formation with inefficient antioxidant defence can cause damage to cellular constituents, including DNA, proteins and lipids, contributing to vascular-related diseases (Nakamura *et al.*, 2012; Zhang, 2018; Gavazzi and Faury, 2021).

Major sources of ROS include cellular respiration and metabolic processes. The generation of mitochondrial ROS results from oxidative phosphorylation as a by-product (Zorov, Juhaszova and Sollott, 2014). ROS are observed as a cascade of transitions from one species to another, typically with an initial reaction forming O₂⁻. In addition, mitochondria are the source of ROS in vascular cells and represent targets for ROS attack, such as peroxynitrite (Zorov, Juhaszova and Sollott, 2014). Many diseases, including cardiovascular, acute kidney injury and diabetes, have been reported that oxidative stress can result in mitochondrial dysfunction (Sivitz and Yorek, 2010; Nakamura *et al.*, 2012; Yuan *et al.*, 2019). Therefore, it is essential to understand the effect of mitochondrial ROS signalling on TNF- α -mediated ED. In line with previous studies, TNF- α increases mitochondrial O₂⁻ levels, as evidenced MitoSox microscopy analysis (Zhao *et al.*, 2017). Furthermore, high-glucose models demonstrated the ability to decrease mitochondrial ROS and endothelial impairment by NaHS pre-treatment (Guan *et al.*, 2012) and co-treatment with DATS in HUVECs (L. L. Liu *et al.*, 2014). Additionally, the mitochondrial-targeted H₂S donor, AP39, exhibits comparable findings in microvascular ECs challenged with high-glucose culture (Geró *et al.*, 2016).

Spassov and co-authors have shown by microscopy analysis that post-treatment of GYY4137 in stretched HUVECs decreases $O_2^{\cdot-}$ radical levels (Spassov *et al.*, 2022). These observations align with the current $O_2^{\cdot-}$ fluorescence intensity signal under a post-treatment with GYY4137 in TNF- α -treated HUVECs. In contrast to Spassov's study, an inflammatory stimulus rather than physical stress was conducted here. Besides *in vitro* and *in vivo* evidence, precautions must be considered as fluorescent probes for mitochondrial-localised ROS, such as MitoSOX, are not fully quantitative methods (Zielonka and Kalyanaraman, 2010). Nevertheless, this probe might be a suitable indicator of overall changes in the intracellular redox state. Through HPLC-combined MitoSox analysis, robust results could be obtained (Zielonka and Kalyanaraman, 2010).

To note, alternative mitochondrial elements such as p66shc and monoamine oxidase (MAOs) proteins can contribute to mitochondrial ROS levels. For instance, MAOs mediated increased ROS production, contributing to adverse remodelling in the heart with maladaptive hypertrophy (Kaludercic *et al.*, 2010). Within the mitochondria, p66^{shc} catalysed electron transfer from cyto c to O_2 , and its role as a mitochondrial ROS-generating source has been demonstrated by its deletion in rodents (Lisa *et al.*, 2009). Contributing to mitochondrial ROS generation might be a combination of different mitochondrial sources.

The balance between production and degradation is essential for the survival of organisms. Exposure to an extreme oxidising environment has led organisms to develop defence mechanisms, including antioxidant defences (e.g., SOD, CAT and GPX enzymes). Non-enzymatic antioxidants are represented by ascorbic acids such as vitamin C, E, flavonoids and GSH. (Valko *et al.*, 2007). Inhibition of ROS-metabolising systems has implications for cancer treatment since malignant cells depend highly on SOD for protection (Huang *et al.*, 2000). Interestingly, in the present study, HUVECs treated with TNF- α expressed an increased SOD2 and CAT gene-transcriptional levels. These findings differ from previous studies reporting decreased antioxidant molecules in HUVECs exposed to TNF- α . However, the authors tested antioxidant activity, while in the present study, mRNA levels were assessed (Sun *et al.*, 2012; Zhou *et al.*, 2017).

Here, in the presence of GYY4137, the target genes displayed higher mRNA levels, suggesting that exogenous H₂S donor might enhance the already alert antioxidant defence. However, RT-qPCR analysis only offer partial information and further analysis, including protein expression and enzyme activity it is required to have a full picture regarding antioxidant defence.

Enhanced ROS production is associated with impaired OXPHOS capacity in the endothelium. OXPHOS and glycolysis are the two major energy-producing pathways in the cells, switching between them based on the surrounding environment (Kaczara *et al.*, 2016). Recent reports described that although ECs are mainly glycolytic, proliferating, and lymphatic ECs can use OXPHOS for fatty acid oxidation to sustain DNA synthesis and epigenetic regulation of gene expression (Schoors *et al.*, 2015; Wong *et al.*, 2016). In the present work, the energetic demand of the cell under baseline conditions was significantly increased in the presence of TNF- α alone and with GYY4137 post-treatment. The opposite effect was observed in cardiomyocytes in the presence of 10 ng/ml TNF- α for 24 h, restored after NaHS exogenous treatment (Lee *et al.*, 2019). Notably, a recent study found that co-stimulation with interferon-gamma (IFN- γ) and TNF- α (5 ng/ml) increases basal respiration and ATP-linked OCR production in cardiomyocyte cells. In addition, the authors showed induction in proton leak, indicating an alteration of the mitochondrial integrity (Nunes *et al.*, 2021). Here, an increase in drive ATP formation could be linked to TNF- α -induced stress resulting in an initial energetic demand, enhanced proton leak (Hill *et al.*, 2012), or increased glycolysis (Vaughan *et al.*, 2013).

Notably, proton leak was significantly elevated in the presence of TNF- α and reduced after GYY4137 cultured-HUVECs. The significant increase in TNF- α treatment aligns with previous observations in cardiomyocytes and adipocyte cells (Hahn *et al.*, 2014; Nunes *et al.*, 2021). Exogenous H₂S treatment results in a robust proton leak decrease in TNF- α -challenge ECs, which is in line with AP39 effects in CSE-compromised ECs (Sanchez-Aranguren, Rezai, *et al.*, 2020). The maximum rate of respiration the cell can achieve was insignificant in any group; HUVECs cultured with TNF- α seem to have a low level. This finding aligns with a previous study where TNF- α (10 ng/ml) cause a reduction in maximal respiration and spare respiratory capacity *in vitro* (Lee *et al.*, 2019). These observations hint that, under specific scenarios, cells may respond to TNF- α with an elevation of specific bioenergetic parameters to maintain cellular energy demand.

Conversely, that adverse effect might be distinctive for mitochondrial' parameters associated with ETC flux.

Although the Mito Stress test offered considerable information about the mitochondrial bioenergetics profile, mitochondria content in ECs is low compared with other cell types (Du *et al.*, 2021). Overall glycolytic parameters were also increased by TNF- α treatment in HUVECs. Glycolysis and glycolytic capacity remained elevated after GYY4137 post-treatment in ECs CSE-knockdown ECs showed a significant increase in ECAR glycolytic parameters, supporting that under cellular stress, ECs could upregulate the glycolytic pathway to sustain energetic demands (Sanchez-Aranguren, Ahmad, *et al.*, 2020). It has been reported that an increase in the activities of several glycolytic enzymes may precede the metabolic changes in cardiac hypertrophy and that TNF- α (100 ng/ml, 24h) alters mitochondrial biogenesis machinery leading to elevate glucose oxidation (Palomer *et al.*, 2009).

Since in this study, HUVECs were analysed just after 24h with TNF- α treatment for 3 hours; it is feasible that changes in the glycolysis rate may occur after the initial increase in glucose oxidation. Alternatively, maintenance of $\Delta\psi_m$ might also explain the glucose metabolism described in this study as ECs maintain $\Delta\psi_m$ using ATP produced in glycolysis and impaired mitochondrial respiration; or high glycolytic activity can induce a switch of the ATP synthase to work in reverse mode (Yao *et al.*, 2011; Kaczara *et al.*, 2016). Nevertheless, quantitative and pathway analysis of sulfhydrated peptides by LC-MS/MS revealed that H₂S promotes aerobic glycolysis during stress in β cells in association with S-sulfhydrated proteins such as pyruvate carboxylase, suggesting an adaptive mechanism for the survival of β cells to chronic endoplasmic reticulum stress controlling hyperglycaemia in diabetes (Gao *et al.*, 2015). These results imply that TNF- α can alter ECs' homeostasis environment by relying on glucose oxidation to sustain energetic demand as the primary energy source. In addition, H₂S can partially enhance glycolysis via post-translational modification of proteins.

Inducible proton leak is catalysed by specific mitochondrial inner membrane potential proteins, UCPs. It is recognised as a sign of mitochondrial damage (Brand *et al.*, 2004) by mitochondrial ROS (Starkov and Fiskum, 2003). This statement agrees with the excessive UCP2 mRNA levels observed in TNF- α treated-HUVECs. However, the data were analysed for informative purposes due to discrepancies regarding UCPs' role in

vascular cells (He *et al.*, 2016). Several authors have reported the beneficial role of UCP2 in high-glucose-induced apoptosis in HUVECs (He *et al.*, 2016) and the impairment of cell function in UCP2 knockout mice (Hass and Barnstable, 2019).

On the other hand, the evidence described increased mitochondrial UCPs expression in the hyperthyroid rat heart associated with increased uncoupling and myocardial deficiency (Boehm *et al.*, 2001). Low doses of uncouplers on TNF- α -mediated inflammatory activation of ECs revealed that long-term (4 days) mild uncoupling did not alter mitochondria mtDNA, improving mitochondrial quality control of fragmented organelle and enhanced antioxidant defence and $\Delta\psi_m$ (Romaschenko *et al.*, 2015). Further investigation is required to determine whether UCPs increased by TNF- α would implicate a protective mechanism in ECs. Based on the data, it is possible to suggest that TNF- α alters the proton efflux in HUVECs as the UCP2 mRNA level is affected, and proton leak indicates an effect on the protonmotive force. However, the analysis of UCP2 was conducted only using mRNA levels; therefore, further research on the translational level is required.

Notably, UCP2 has crosstalk with ROS as evidence that uncoupling proteins enhances ROS production and dissipates Δp (Brookes, 2005). In addition, ROS also seems to cause an increase in inducible proton leak, which is regulated by $\Delta\psi_m$ (Boveris and Chance, 1973; Starkov and Fiskum, 2003). Indeed, peroxynitrite was reported to stimulate state four respiration accompanied by a decrease in $\Delta\psi_m$ and an increase suggesting an increase in the proton leak in rat brain mitochondria (Brookes *et al.*, 1998). Reduction in $\Delta\psi_m$ is described as a phenomenon in mitochondrial uncoupling (Kadenbach, 2003). For instance, an examination of stress rat brain mitochondria reported a proton leak increase and a decrease in $\Delta\psi_m$ (Brookes *et al.*, 1998). The florescent-imaging assay revealed that TNF- α -treated HUVECs lost $\Delta\psi_m$, suggesting a dissipation of the Δp . Damage to mitochondria by pathological stress results in $\Delta\psi_m$ collapses, leading to the activation of cell death pathways and the development of CVD and metabolic diseases (Sivitz and Yorek, 2010; Tahrir *et al.*, 2019). Cellular stress manifesting in reduced $\Delta\psi_m$ is ameliorated by post-treatment with GYY4137.

The protective role of H₂S by attenuation of $\Delta\psi_m$ can be found in several experimental models, including ED (Wen *et al.*, 2013), the ischemia-reperfusion model (Wetzell and Wenke, 2019) and high-glucose treated cells (N. Liu *et al.*, 2017). Mitochondrial-targeted

H₂S donors also normalise $\Delta\psi_m$ as a protective mechanism against hyperglycemic injury in microvascular ECs (Gerő *et al.*, 2016).

This suggests that TNF- α mediate impaired mitochondria function at proton leak and uncoupling levels, which is translocated to the $\Delta\psi_m$ and results in its dissipation. Exogenous H₂S can restore these different cellular markers to basal levels in ECs. Although the JC-1 probe is widely used to examine $\Delta\psi_m$, semiquantitative information can only be acquired from this probe. This limitation is based on the sensitivity of the JC-1 aggregate form that can change upon H₂O₂ (Chinopoulos, Tretter and Adam-Vizi, 1999), which requires precautions during the interpretation of results. JC-1 is a “yes/no” assessment for this thesis to determine mitochondria’s polarised and unpolarised states (Perry *et al.*, 2011).

$\Delta\psi_m$ is a crucial determinant of mitochondrial structure, and its dissipation has been shown to cause mitochondrial fragmentation by modifying mitochondrial dynamic machinery toward fission (Collins *et al.*, 2002). As double membrane-bound organelles, mitochondria are characterised by tubular shape, which vary according to the cell type and cellular state (Bereiter-Hahn, 1990; Rafelski and Marshall, 2008). To maintain cells throughout life, mitochondria undergo continuous fission and fusion cycles that balance their morphology, number, distribution and function (Twig, Hyde and Shirihai, 2008). A shift toward fusion favours interconnected mitochondria, whereas a displacement of the mitochondria balance toward fission forms mitochondrial fragments (Collins *et al.*, 2002). The present study assessed and quantified fluorescence analysis of the mitochondrial network in untreated and treated HUVECs by ImageJ plugin software. The work presented here showed that HUVECs exposed to TNF- α exhibit mitochondrial fragmentation as evidenced by the vesicular rather than tubular shape, significantly reducing the mitochondrial branch length and the network size. In addition, GYY4137 restore homeostatic cells’ mitochondrial structure in TNF- α -treated ECs. Mitochondrial dynamic genes were analysed to assess whether or not TNF- α -induced mitochondrial fragmentation was induced through fission and fusion machinery.

Exposure of HUVECs to TNF- α manifests an imbalance in the fission/fusion cycle at the transcriptional level, as evidenced by the reduction in the pro-fusion mRNA MFN1 expression and increased pro-fission DRP1 mRNA levels. The effect of TNF- α is consistent with early studies, which showed that *in vitro* models exposed to TNF- α (10

ng/ml) decreased $\Delta\psi_m$ and increased mitochondrial DRP1 phosphorylation and protein expression in alveolar epithelial cells (Y. C. Chen *et al.*, 2021). The protective role of exogenous H₂S through the orchestration of mitochondrial dynamics has been reported in apoptotic (Hao *et al.*, 2019) and high-glucose ECs (N. Liu *et al.*, 2017). Consistent with these reports, GYY4137 revoke fragmentation by reducing pro-fission and increasing pro-fusion genes.

Interestingly, TNF- α treatment causes a significant increase in the mRNA levels of OPA1. OPA1 is a dynamic-like GTPase that regulates mitophagy through fusion-dependent and independent mechanisms and has been previously reported to offer protection against myocardial infarction and cardiomyocyte reperfusion by promoting mitophagy (Cao *et al.*, 2019; L. Guan *et al.*, 2019; Xin and Lu, 2020). Intriguingly, the pro-fusion protein OPA1 has been involved in the TNF- α -NF- κ B-OPA1 regulatory pathway, where the activation of NF- κ B ultimately increases the production of OPA1 protein (Nan *et al.*, 2017; Erchova, Sun and Votruba, 2021). Although further studies are required to determine the impact of TNF- α in mitophagy, as only gene-transcriptional expression was examined, the present work proposes a mechanistic model in which TNF- α may exhibit a dual effect by causing mitochondrial fragmentation as well as increased mitophagy in ECs.

The activation of the pro-death pathway is accompanied by the collapse of the reticular form of mitochondria into fragments, which are dysfunctional mitochondria selectively targeted for mitophagy-promoting cell survival or when the oxidative stress is high apoptotic pathway is onset (Bordi, Nazio and Campello, 2017; Martinez-Carreres, Nasrallah and Fajas, 2017). Excess ROS formation switches the redox state, leading to mitochondria damage by opening the PTP, which fails to maintain $\Delta\psi_m$ and cannot import mitochondrial proteins synthesised into the cytosol. Suppose a large portion of the mitochondrial population opens their pores. In that case, this can disrupt the outer mitochondrial membrane, release cyto c and set up apoptosis-inducing proteins (Cai, Yang and Jones, 1998). In this regard, TNF- α has been reported to activate caspases, including initiator and executor caspases, via extrinsic and intrinsic pathways (Pang *et al.*, 2007; Álvarez *et al.*, 2011).

TNF- α leads to cytosolic cyto c release and activation of executors caspase 3 and 6 in ECs (Daniel *et al.*, 2004) and progenitor ECs (Xu *et al.*, 2011). The current study supports previous observations regarding TNF- α -mediated cyto c redistribution into the cytosol as evidence of immunoblotting in HUVECs.

Notably, it has been reported that mitochondrial permeability transition pore is required for TNF- α -mediated cyto c release and cell death in hepatocytes (Bradham *et al.*, 1998) which was also confirmed in fibroblasts (Tafari *et al.*, 2000), suggesting that the observed cyto c re-localisation might be accompanied by the opening of MPTP. TNF- α -induced cyto c translocation from mitochondria to cytosol was reversed by co-incubation with vitamin C, a known antioxidant agent, blocking apoptotic signalling in HUVECs (Rössig *et al.*, 2001).

In the current study, mitochondrial cyto c was released to the cytosol in TNF- α treated HUVECs, alleviated by H₂S post-treatment. Although the H₂S effect on cyto c accumulation has been previously assessed in HUVECs treated with H₂O₂ (Wen *et al.*, 2013) and high-glucose (N. Liu *et al.*, 2017), the authors focused on a pre-treatment approach with a fast-release donor. To our knowledge, the present work is a pioneer study regarding H₂S revoking role in TNF- α -induced cyto c release by post-treated HUVECs.

Previous studies showed increased caspase 3 protein with TNF- α (20 ng/ml) treatment for 2 hours in HUVECs (Fratantonio *et al.*, 2018). In contrast to this data, the present study did not show any change in caspase 3 protein expression in the presence of TNF- α . However, this discrepancy might be attributed to the low dose of TNF- α used here. On the other hand, TNF- α tends to increase cleaved caspase 3 protein expression, in contrast to a previous study showing elevation of cleaved caspase 3 by TNF- α has been previously described in ECs (Xu *et al.*, 2011). Furthermore, NaHS pre-treatment abolished cleaved caspase 3 expressions in the presence of high-glucose HUVECs (Lin *et al.*, 2018) and rat aortic ECs (N. Liu *et al.*, 2017). In line with these reports, post-treatment with GYY4137 reduced cleaved caspase 3 expressions. During activation, the maturation of caspase 3 occurs to its active cleaved form, which exerts its pro-apoptotic role (Shalini *et al.*, 2014). Thus, the change in cleaved caspase 3 rather than its pro-caspase 3 in the presence of TNF- α could be attributed to the maturation process and analytic examination of the sample, whereby at the time of immunoblotting analysis, pro-

caspase 3 has already been cleaved. A time-dependent analysis of the TNF- α effect on executor caspases could offer an attractive insight into the cytokine signalling processes.

In summary, the work presented in this chapter suggests that upon TNF- α treatment, mitochondrial function and dynamics are dysfunctional. Furthermore, exogenous H₂S is beneficial for altered-ECs at the mitochondrial level, indicating that the anti-apoptotic role observed in the previous chapter can be associated directly with mitochondria function. However, future work is needed to gain more information about specific signalling pathways such as mitophagy.

6 Preliminary assessment and quantification of protein S-sulfhydration in HUVECs

6.1 Introduction

Previous chapters demonstrated that TNF- α could induce a dysfunctional phenotype in ECs. Furthermore, H₂S donor GYY4137 was able to alleviate TNF- α -induced ED. These observations investigated the signalling mechanism by which H₂S mediates its beneficial effects in TNF- α -induced ED with GYY4137 post-treatment.

Post-translational modification (PTMs) refers to the covalent modification of proteins, proteolytic cleavage of regulatory subunits, or degradation of entire proteins following protein biosynthesis, increasing the complexity from the genome to the proteome level. PTMs occur at distinct amino acid side chains and influence proteins' activity, localisation and/or interactions with other molecules (Chen *et al.*, 2022). PTMs categories include phosphorylation, methylation, acetylation and ubiquitylation (Altaany *et al.*, 2014; Krajewski, 2019; Deng and Marmorstein, 2021). For example, phosphorylation is the most well-studied PTMs as it is critical in regulating many cellular processes by adding phosphate groups via kinases (Ardito *et al.*, 2017b).

H₂S has been proposed to regulate biological functions via reversible PTMs, called protein S-sulfhydration (Bindu D Paul and Snyder, 2015b). Protein S-sulfhydration is characterised by converting a protein's thiol group (R-SH) to persulfides (R-SSH) and can occur by nucleophilic attack of an HS⁻ anion on the sulfur atoms of disulfides, -SNOs or -SOHS, as well as by the transsulfuration reaction (Iciek *et al.*, 2016). S-sulfhydration can change the original function of a protein, serving as a relevant switch or regulator in many physiological and pathophysiological processes (Sanchez *et al.*, 2022).

Since its description as an abundant post-translational modification in biological samples, as exemplified by 10-25% of GADPH, actin and β -tubulin being sulfhydrated under physiological conditions, various cellular signalling and biological pathways have been reported (Mustafa *et al.*, 2009). For instance, the S-sulfhydration of eNOS increases its activity by promoting eNOS phosphorylation and ultimately expanding NO bioavailability (Altaany *et al.*, 2014). Ion channels such as ATP-sensitive potassium (K_{ATP}) and Ca²⁺ transient receptor potential (TRP) have also been reported to be S-sulfhydrated, allowing cells to respond to extracellular changes (Jiang *et al.*, 2010; Y. Liu *et al.*, 2014).

Interestingly, Li and Yang (2015) showed that S-sulfhydration of interferon regulatory factor-1 (IRF-1) improves its binding to DNA methyltransferase 3a, making it unable to methylate mitochondrial transcription factor A (TFAM) promoter, enhancing mitochondrial biogenesis (Li and Yang, 2015). Furthermore, certain sirtuins such as SIRT3 undergo S-sulfhydration, which enhances their catalytic activity, ultimately leading to the reduction of mitochondria dysfunction, improvement of mitochondrial ETC activity and ATP production in the vasculature (R. Guan *et al.*, 2019; Sun *et al.*, 2019).

One of the significant and well-established defence antioxidant mechanisms, the Keap1-Nrf2 system, is S-sulfhydrated by H₂S (Calvert *et al.*, 2009). Under basal conditions, Nrf2 is expressed at low levels, mainly by Keap1-mediated proteasomal degradation (Itoh *et al.*, 1999). Keap1, a redox-regulated adaptor, binds to Nrf2 through its C-terminal Kelch domain, which binds with the DLG and ETGE motifs in the (Nrf2-ECH homology 2 (Neh2) domain of Nrf2 (Kobayashi and Yamamoto, 2006). In addition, the N-terminal bric-a-brac (BTB) domain in Keap1 binds with the ubiquitin ligase complex Cul3-Rbx1, facilitating the ubiquitination of Nrf2 in the cytoplasm and degradation by 26S proteasome (Furukawa and Xiong, 2005). The constitutive degradation of Nrf2 ensures that only required genes for maintaining homeostasis are expressed (Kaspar, Niture and Jaiswal, 2009).

While over 27 Cys residues in Keap1 may be a molecular target of thiol-reactive chemical inducers, there are four Cys residues (Cys²⁵⁷, Cys²⁷³, Cys²⁸⁸ and Cys²⁹⁷) that are the preferred sites of labelling (Dinkova-Kostova *et al.*, 2002). Two Cys residues located in the linker domain of Keap1, Cys²⁷³ and Cys²⁸⁸ are critically required for Keap1-mediated repression of Nrf2-dependent transcription under basal conditions. On the other hand, from the three Cys expressed in the Keap1 BTB domain (Cys⁷⁷, Cys¹⁵¹ and Cys¹⁷¹), Cys¹⁵¹ is uniquely required for inhibition of Keap1-dependent degradation of Nrf2 with a disruption between Nrf2 and Cul3-Rbx1; and activation of Nrf2-dependent transcription by oxidative stress. Therefore, Nrf2 avoids proteasomal degradation, stabilises and translocates into the nucleus. Furthermore, PTMs on Keap1 are uniquely dependent upon the integrity of Cys¹⁵¹. Thus, Cys¹⁵¹ has become the most well-characterised in the literature as it provides a bridge between the ability of inducers to block Keap1-mediated repression of Nrf2 and to induce post-translational modification of proteins of Keap1 (Zhang and Hannink, 2003; Kaspar, Niture and Jaiswal, 2009).

In the nucleus, Nrf2 can form a heterodimer with sMaf or Jun proteins, which are recognised and bind to the antioxidant response element (ARE) region (Katsuoka and Yamamoto, 2016). The activation of ARE results in the expression of specific genes that protect the cell from permanent damage. The encoded proteins include phase II xenobiotics- antioxidants, DNA repair enzymes, anti-inflammatory proteins and cell metabolism (Figure 6.1) (Kaspar, Niture and Jaiswal, 2009). Research data showed that S-sulfhydration of Keap1 induces dissociation of Nrf2 from the Keap1/ubiquitin complex and promotes Nrf2 nuclear translocation, which can cause a wide range of downstream genes with antioxidant roles to be activated (Yamamoto *et al.*, 2008; Meng *et al.*, 2017). The importance of H₂S-mediated S-sulfhydration of the Keap1-Nrf2 system has been observed as beneficial in several cardiovascular conditions *in vitro* and *in vivo* (Meng *et al.*, 2018).

H₂S has been reported to exhibit cardioprotective effects under ischemic stress by S-sulfhydration Keap1 and promoting nuclear translocation of Nrf2 (Yang *et al.*, 2013b). Regulation of the Nrf2-downstream signalling by H₂S showed protection against cellular senescence (Yang *et al.*, 2013a) and suppressing atherosclerotic phenotype in HUVECs (Xie, Gu, *et al.*, 2016). In addition, Nrf2 has been positively associated with mitochondrial biogenesis and ROS production (Ryoo and Kwak, 2018). However, DATS administration showed protection against myocardial ischemia/reperfusion injury in mice by regulating mitochondrial respiration and NO bioavailability but without Nrf2-dependent signalling (Predmore *et al.*, 2012). As such, the H₂S-mediated effect on Nrf2-downstream signalling may vary on different H₂S-releasing compounds and cell types.

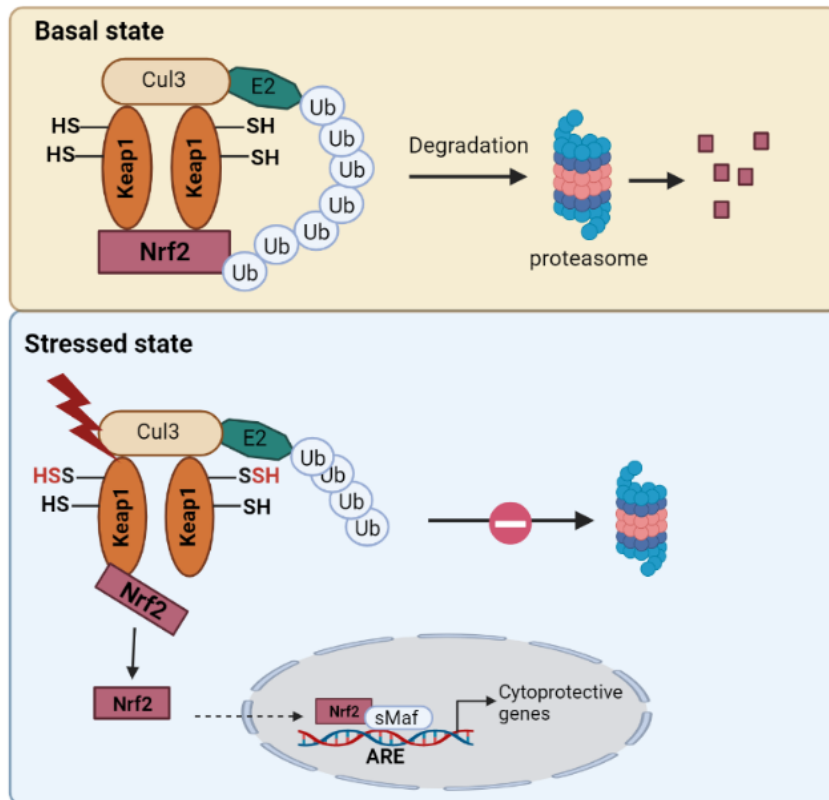


Figure 6.1 Schematic overview of the redox sensor Keap1-Nrf2 system.

Under basal conditions, Nrf2 is continuously sequestered by Keap1 and degraded by 26S proteasome. **Under the stressed state**, the Keap1-Nrf2 complex is disrupted, leading to activation and further nuclear translocation of Nrf2. In addition, activated Nrf2 accumulates in the nucleus, interacting with other transcription factors and ARE regions on target genes. Target genes encode proteins involved in antioxidants, detoxification, metabolism, and inflammation processes. Adapted from (Bindu D Paul and Snyder, 2015a).

During inflammation and apoptotic signalling, caspase 3 is the most crucial executor in extrinsic and intrinsic apoptotic pathways (Chandrasekar *et al.*, 2004). S-sulfhydration also plays a role in apoptosis signalling as there is evidence of S-sulfhydration of caspase 3 at Cys¹⁶³, which caused downregulation of caspase 3 activity, and ultimately offered protection against neuronal ischemia-reperfusion injury (Marutani *et al.*, 2015). As a pro-apoptotic enzyme, caspase 3 activity has been associated with vascular dysfunction and cell death (Chen *et al.*, 2011). In addition, recent work has suggested an effect of fast-release H₂S donors in caspase cascade signalling.

The authors showed rapid inhibition of caspase 3 activity via S-sulfhydration of its catalytic site by biochemical analysis in carcinoma HeLa cells (Braunstein *et al.*, 2020). Remarkably, a proteomic study recently revealed thousands of sulfhydrated proteins in the vascular cells and different S-sulfhydration intensities in a cell type-dependent manner. (Bibli *et al.*, 2021). This evidence suggests that H₂S signalling via S-sulfhydration could be through a pleiotropic signalling network, in which distinct S-sulfhydrated proteins may be simultaneously regulated based on the stressed stimuli, biological sample and cell demands.

6.2 Aims

Following previous chapters, molecular and biological experiments have shown that intracellular H₂S content is stimulated by the GYY4137 donor and revokes ED, partly by decreasing oxidative stress and apoptosis. This chapter aimed to investigate whether S-sulfhydration is an underlying signalling mechanism mediated by GYY4137 to exert its beneficial effects in TNF- α -induced ED.

- To establish a suitable S-sulfhydration detection method.
- To assess S-sulfhydration of oxidative stress sensor, Keap1, in HUVECs.
- To investigate Nrf2 regulation and its downstream signalling in HUVECs.
- To assess S-sulfhydration of the pro-apoptotic enzyme, caspase 3, in HUVECs.

6.3 Material and Methods

6.3.1 Endothelial cell culture

HUVECs were routinely maintained in T75 flasks with the complete supplemented medium at 37°C and 5% CO₂ (see section 2.2.2). Endothelial seeding and experimental settings were explicitly conducted for each assay following general maintenance, as indicated in section 2.2.3. Cells were treated following the post-treatment experimental design with TNF- α (1 ng/ml) for 3 hours, followed by post-treatment with GYY4137 at a non-toxic concentration (100 μ M) for 21 hours, giving an overall 24 hours experimental treatment. Next, HUVECs were analysed specifically for the desired assay. In general, cells were divided into four groups unless otherwise stated: control (untreated cells), GYY4137 (alone), TNF- α (alone), TNF- α + GYY4137 (post-treatment model).

6.3.2 Maleimide Red assay

The maleimide-based assay was conducted to detect protein S-sulfhydration. For full details, see section 2.19.

6.3.3 Modified Biotin switch assay

Protein S-sulfhydration was assessed by applying the Modified Biotin switch assay as described in section 2.20.

6.3.4 Fluorescence microscopy

Fluorescence analysis of Nrf2 localisation was assessed as described in section 2.9.2.

6.3.5 Western blot

Immunoblotting analysis of NQO1 and GcLC was assessed as described in section 2.17. Nuclear extraction was conducted as described in section 2.13 and immunoblotting analysis of Nrf2 was conducted following section 2.17.

6.3.6 Caspase 3/7 activity assay

The Caspase-Glo 3/7 assay kit was conducted to assess caspase 3/7 activity following the manufacturer's instructions [Promega, GmbH, Southampton, UK]. For full details of the experiment, please refer to section 2.7.

6.3.7 Statistical analysis

All values presented are as mean \pm SEM. Unless otherwise stated, all usually distributed variables between two groups were compared by unpaired Student *t*-test. When comparing three groups or more one-way ANOVA followed by Sidak's *post-hoc* comparisons was applied. For statistical tests, *p* values less than 0.05 ($p < 0.05$) were considered significant.

6.4 Results

6.4.1 Preliminary analysis of S-sulfhydrated proteins using Maleimide assay.

Multiple methods are described in the literature to detect S-sulfhydrated proteins (Filipovic *et al.*, 2018). One main barrier to detecting S-sulfhydrated groups is the instability and similar reactivity to other sulfur species (Filipovic, 2015). To find a suitable method to detect S-sulfhydration, this chapter compared two methods (1) maleimide assay and (2) modified biotin switch assay.

Snyder's group proposed a modified NEM (N-ethylmaleimide) method for the persulfide labelling of purified proteins. Cy5 red maleimide was used to block free thiols and persulfides (Sen *et al.*, 2012). The product of this reaction can be reduced by DTT, resulting in a decrease of the in-gel fluorescent signal; as a readout for persulfide group levels (Sen *et al.*, 2012). EA.hy926 cells were used to conduct a preliminary analysis with or without non-toxic GYY4137 concentration (Figure 6.2 A).

Unexpectedly, in-gel total protein images with cultured GYY4137 did not show loss of fluorescence signal following DTT treatment, and no apparent bands were changed after DTT incubation, as indicative of S-sulfhydration. As shown in Figure 6.2 B, specific proteins (indicated by white arrows) displayed higher fluorescence signals than the overall blot.

Immunoblotting of actin was conducted based on the molecular weight and previously reported S-sulfhydrated proteins at similar conditions (Mustafa *et al.*, 2009) (Figure 6.2 C). S-sulfhydrated actin has been previously linked to the rearrangement of the actin cytoskeleton by polymerisation (Mustafa *et al.*, 2009). In the current work, only a preliminary examination of cytoskeletal architecture was visualised by confocal microscopy using F-actin staining with phalloidin displaying a reorganisation of the filamentous actin (S.6.1). However, based on this observation, it is impossible to conclude that H₂S donors directly affect the cytoskeletal actin network via S-sulfhydration-mediated polymerisation. Future examinations could offer a fascinating insight into the filamentous actin network and cells' cytoskeleton.

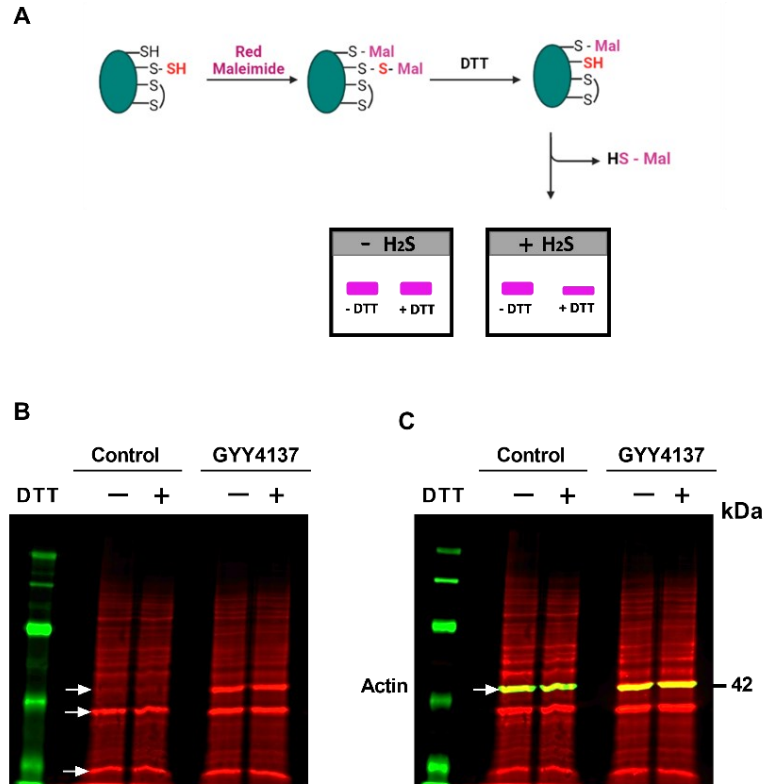


Figure 6.2 Preliminary analysis of S-sulfhydration using the Maleimide assay in EA.hy926 cells.

(A) Schematic overview of red maleimide method. In this detection assay both persulfide and free thiol would be blocked by the thiol fluorescently labelled Cy5 conjugated maleimide (5 μ M). The adduct of persulfide and Cy5 red maleimide is a disulfide that will be then cleaved by the DTT leading to a decrease of the fluorescence signal in the samples containing persulfides. (B) Red fluorescence intensity in untreated and GYY4137 group with or without DTT in endothelial cells. Arrows indicate protein bands with intense fluorescence signal. (C) Immunoblotting using anti-actin antibody was conducted by SDS-PAGE western blot. (n=1)

6.4.2 Preliminary Detection of S-sulfhydrated proteins using Modified Biotin Switch assay.

The modified biotin switch assay, a modification of the S-nitrosylation assay, was the first method proposed in the literature for labelling and detecting protein S-sulfhydration. After free thiols were blocked with MMTS, the undisturbed thiol modifications (-SSH) were labelled with biotin-HPDP conjugated and captured by streptavidin beads (Figure 6.3 A).

To confirm whether this assay could detect S-sulphydrated proteins, preliminary analysis using EA.hy926 cells as *in vitro* model and a fast-release H₂S donor, NaHS was conducted. As shown in Figure 6.3 B, the immunoblotting expression of S-sulphydrated actin was higher upon NaHS treatment than in untreated cells. In addition, densitometry blots showed that S-sulphydrated actin expression was strongly reduced in the presence of DTT. This preliminary data suggests that in the presence of an H₂S-releasing donor, the modified biotin switch assay may detect the formation of persulfide groups due to Cys residue modification in ECs-proteins. Consequently, in this chapter modified biotin switch assay was selected as a suitable method to provide a semiquantitative estimate of protein S-sulphydration levels in ECs samples.

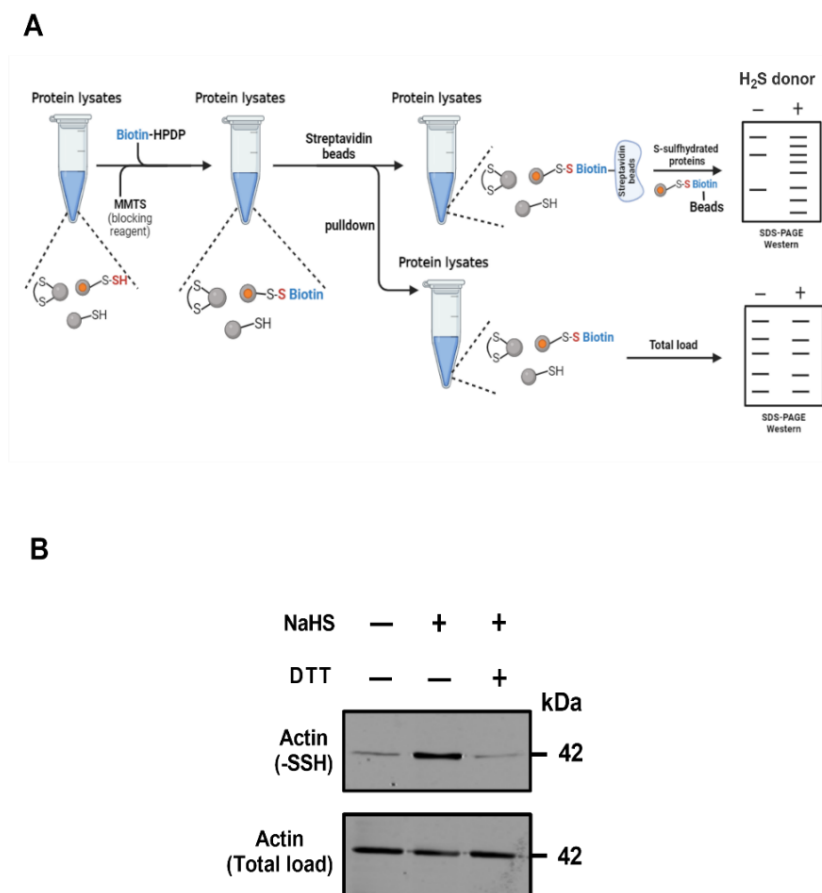


Figure 6.3 Preliminary analysis of the Modified Biotin Switch assay in EA.hy926 cells.

(A) Protein lysates subjected to exogenous H₂S comprise free thiols (-SH) and the persulfides (-SSH) groups. Cell lysates are incubated with MMTS to block free thiols and allow labelled persulfides with Biotin-HPDP conjugated. Then persulfides are captured by streptavidin beads. S-sulfhydrated proteins and total load proteins are subjected to SDS-PAGE western blotting. Created with Bio-render.com (B) EA.hy926 cell lysates were treated with 100 µM NaHS for 45 min and subjected to the modified biotin switch assay to detect S-sulfhydration. DTT treatment (2 mM) was used as a reducing agent to reverse Cys residue modification. Samples were subjected to electrophoresis, and blots were incubated with an anti-actin antibody in S-sulfhydrated and total load samples. (n=1).

6.4.3 Assessment of S-sulfhydrated Keap1 in TNF- α and GYY4137-treated HUVECs.

The complex Keap1-Nrf2 is one of the most effective antioxidant mechanisms within the cell, characterised by Nrf2-downstream activation of cytoprotective and anti-inflammatory genes (Meng *et al.*, 2017). The Keap1-Nrf2 complex was investigated by H₂S-induced sulfhydration using a modified biotin switch assay. Firstly, total load and S-sulfhydrated protein samples were approached using the Revert™ Total protein staining kit, allowing us to observe the overall biotinylated load protein in ECs. As shown in Figure 6.4 A, the total load protein bands were equal in all groups of HUVECs. Additionally, a higher positive signal was observed in the presence of GYY4137 in the total S-sulfhydrated blot, as illustrated by total protein staining in HUVECs (Figure 6.4 B). Furthermore, the TNF- α treatment lane demonstrated a low total S-sulfhydrated protein-related signal.

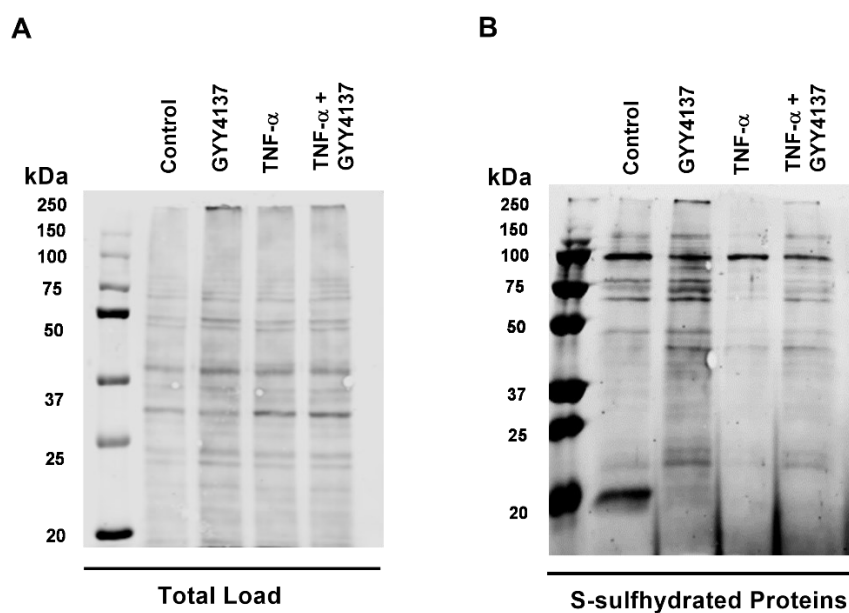


Figure 6.4 Total protein staining of S-sulfhydrated and total load proteins in the presence of TNF- α and GYY4137 post-treatment setting via Biotin Switch Assay.

HUVECs were treated with TNF- α (1 ng/ml, 3h) before post-treatment with GYY4137 (100 μ M, 21 h) for up to 24 hours. Protein lysate samples were subjected to the Modified Biotin Switch assay. **(A)** Representative densitometry blot of overall total biotinylated proteins and **(B)** S-sulfhydrated proteins in HUVECs stained with Revert Total protein stain kit and analysed with Odyssey LICOR system. (n=3).

Secondly, a specific examination of S-sulfhydrated Keap1 expression was conducted by immunoblotting analysis with an anti-Keap1 antibody. Although an elevation in Keap1 signal in the densitometry blot relative to the control group is observed, in the absence of a statistically significant increase, it is impossible to conclude that Keap1 undergoes S-sulfhydration in HUVECs in the present study (Figure 6.5 A). Treatment with TNF- α and GYY4137 trends to increase Keap1 S-sulfhydration relative to untreated Keap1 protein expression, although these results were not statistically significant (Figure 6.5 B). Although the data show a trend on Keap1 S-sulfhydration in HUVECs by GYY4137, additional independent experiments are required to determine if a statistically significant increase can be reached.

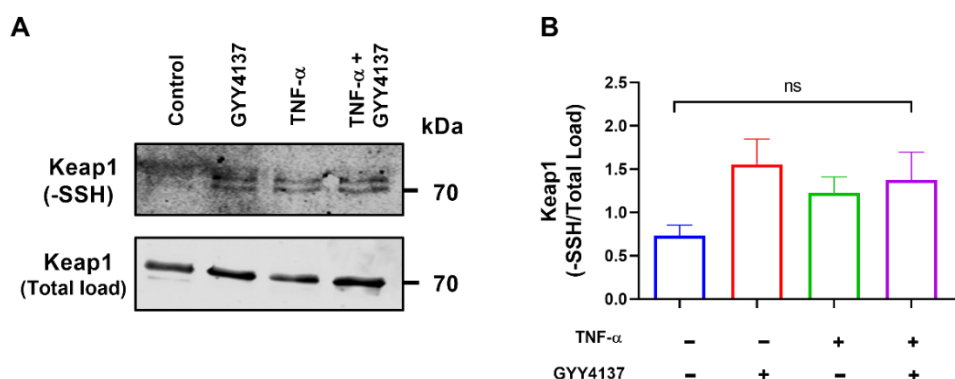


Figure 6.5 Analysis of Keap1 S-sulhydratration in HUVECs.

HUVECs were treated with TNF- α (1 ng/ml, 3h) before post-treatment with GYY4137 (100 μ M, 21 h) for up to 24 hours. **(A)** Protein lysate samples were subjected to Modified Biotin Switch assay followed by immunoblotting with anti-Keap1 antibody. **(B)** Bar graph representing Keap1 S-sulhydrated relative to Keap1 total load. The data were presented as the mean \pm SEM (n=3). Significance was determined by a one-way ANOVA test followed by Sidak's post-test comparing treatments to control, whereby ns; represents non-significant.

6.4.4 Relation between GYY4137 and Nrf2 nuclear translocation.

With these data in hand, it was envisioned that H₂S might enable the regulation of Nrf2-downstream signalling in ECs. Nuclear accumulation of Nrf2 in HUVECs with TNF- α and GYY4137 was examined to assess this possibility post-treatment. Immunofluorescence evaluation might offer a practical alternative approach for subcellular fractions, by which its simplicity avoids tedious subcellular separation, presenting a view of the molecule's location. Therefore, a preliminary examination of Nrf2 localisation in HUVECs using immunofluorescent staining was conducted.

Interestingly, preliminary examination of immunofluorescent localisation staining of Nrf2 with TNF- α within cells showed a possible re-localisation of Nrf2 surrounding the nucleus, as exemplified by the higher fluorescence signal. In the presence of GYY4137 and TNF- α , the fluorescence signal surrounding the nucleus remains low. It is accompanied by higher fluorescence intensity within the nucleus than the untreated control and TNF- α treated group staining (Figure 6.6).

However, this preliminary analysis only allows the assumption that there is a possible effect on Nrf2-nuclear accumulation. Further microscopy analysis, including the proportion of cells with Nrf2 levels in the nucleus, ratio cytoplasmic vs nuclear fluorescence and additional independent experiments, would be conducted in future experiments.

Nevertheless, fluorescence microscopy was considered informative rather than quantitative. To underscore the hypothesis that H₂S-releasing donor enables Nrf2 nuclear translocation in TNF- α -cultured HUVECs, Nrf2 subcellular expression was further recapitulated by western blotting analysis of nuclear fraction. Subcellular isolation was performed as described previously, and protein lysates were incubated with an anti-Nrf2 antibody with Histone H3 as a loading control within the nucleus (Figure 6.7 A). Although no statistically significant increase was observed upon GYY4137 treatment, a trend to elevate was observed. HUVECs subjected to TNF- α treatment tend to promote Nrf2 nuclear expression compared to untreated cells. Post-treatment of GYY4137 after TNF- α stimulation showed a higher increase in the Nrf2 nucleus accumulation, noted by increased protein signal compared to TNF- α alone, but levels did not reach statistical significance (Figure 6.7 B).

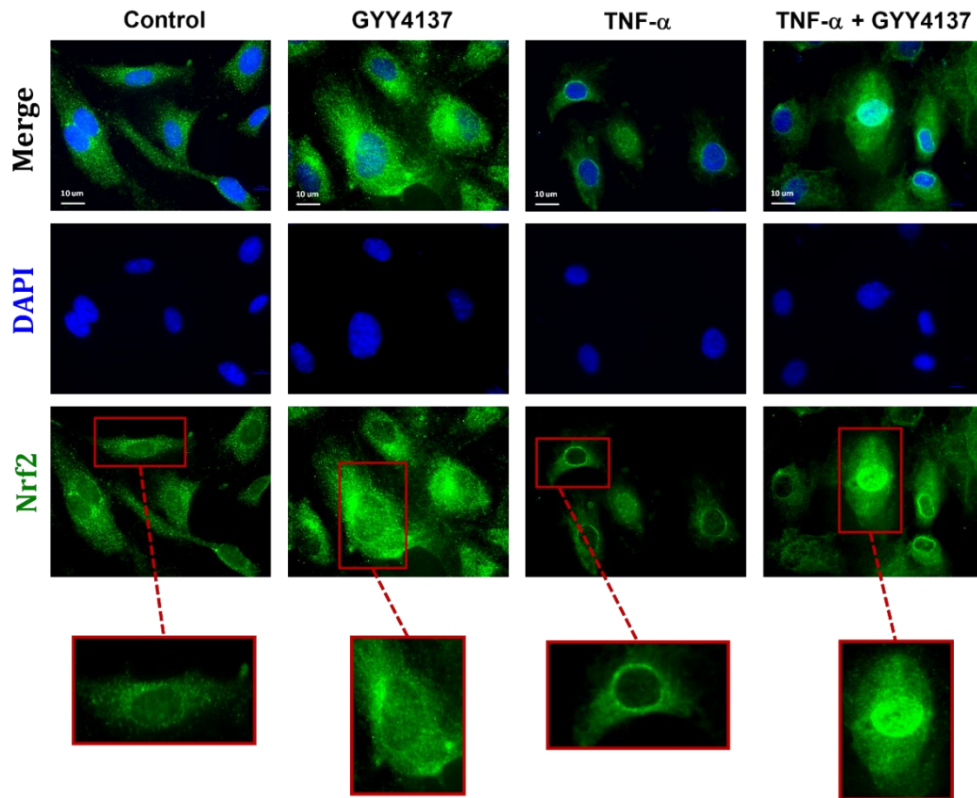


Figure 6.6 Preliminary analysis of Nrf2 localisation in HUVECs treated with TNF- α and GYY4137 post-treatment.

Cells were treated upon TNF- α (1 ng/ml, 3h) and GYY4137 (100 μ M, 21 h) post-treatment settings. Then, immunofluorescence was applied with anti-Nrf2 antibody incubation overnight, followed by secondary Alexa Fluor 488. Immunofluorescent staining images of Nrf2 localisation (green spectrum). The nuclei were stained with DAPI (blue spectrum). Pictures were taken using a Nikon Ti-S Inverted fluorescence microscope (20x magnification, scale bar 10 μ m) (n=1).

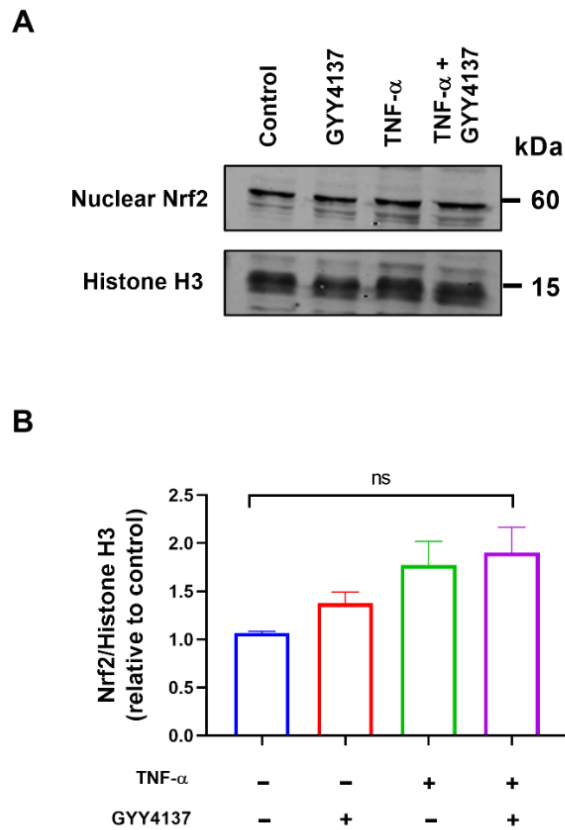


Figure 6.7 Analysis of Nrf2 protein accumulation in the nucleus in HUVECs.

Cells were treated upon TNF- α (1 ng/ml, 3h) and GYY4137 (100 μ M, 21 h) post-treatment settings. Nuclear fractions were obtained by using Nuclear extraction kit. **(A)** Nuclear extracts were immunoblotted for Nrf2 and Histone H3 (nuclear loading control). **(B)** Immunoblotting analysis of Nrf2 using Histone H3 as loading control by ImageJ software. Results presented as mean \pm SEM (n=3), whereby ns. represents non-significant vs control group.

6.4.5 Impact of GYY4137 on the mRNA levels of Nrf2 targets.

After nuclear translocation, Nrf2 forms heterodimers with sMAF, recognising ARE in the regulatory regions of over 250 genes. These ARE genes encode a network of cooperating enzymes involved in metabolism, purine metabolism, inflammation, proteostasis and redox balance (He, Antonucci and Karin, 2020).

Chapter 4 showed that GYY4137 treatment enhanced mRNA levels of specific antioxidant Nrf2-mediated genes (HO-1, GcLC, Trx1). Western blotting was used to analyse protein expression of NQO1 and GcLC protein expression. Diversity in the regulation of Nrf2-induced protein levels is observed. As shown in Figure 6.8 A-B, NQO1 protein expression significantly increases in the presence of GYY4137 with or without TNF- α treatment (* p <0.05). Although TNF- α stimulation alone tends to increase NQO1 expression, a statistically significant difference was not reached. In Figure 6.8 C-D, GcLC protein expression showed a non-significant reduction in the presence of TNF- α treatment compared to the control group. Notably, in the presence of GYY4137, post-treatment GcLC protein levels were significantly increased compared to TNF- α -treated cells (* p <0.05). These results suggest that Nrf2-dependent enzyme regulation can vary within cells.

Together, these results indicate that the H₂S-releasing donor may affect Nrf2 protein localisation expression in ECs and that Nrf2-downstream response is observed in specific proteins, which might drive antioxidant activity.

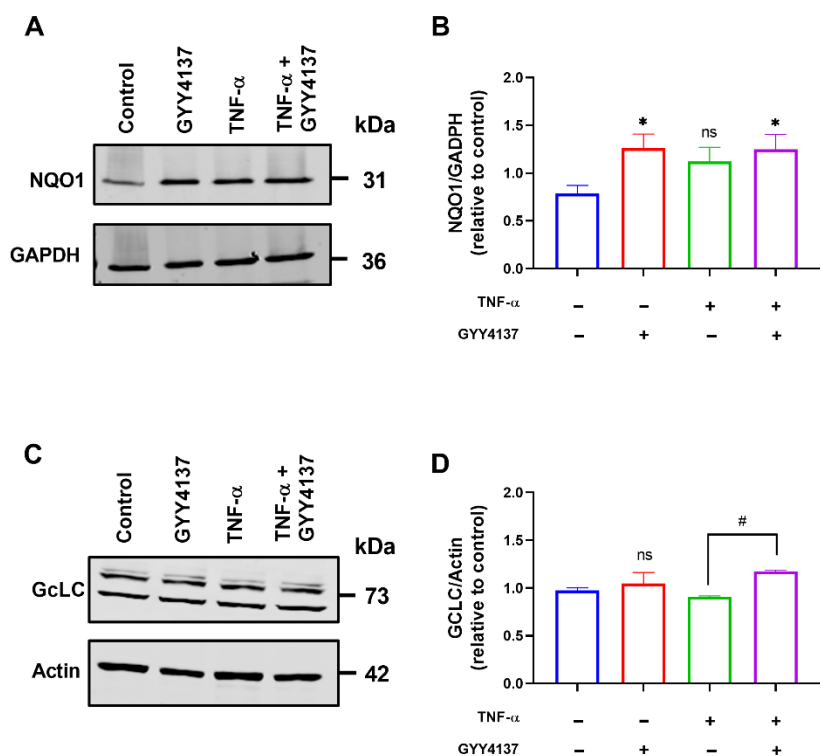


Figure 6.8 Analysis of GYY4137 and TNF- α effect in Nrf2-downstream target proteins.

The extracted protein was separated by electrophoresis, and membranes were incubated with anti-GcLC and anti-NQO1. GAPDH and actin were used as loading controls. Densitometry analysis was performed using ImageJ software to compare target protein expression to GAPDH or actin. **(A-B)** Densitometry blots and analysis of the NQO1 protein expression. **(C-D)** Protein immunoblots incubated with anti-GcLC antibody. Results are the mean \pm SEM (n=3-5). Significance was determined by a one-way ANOVA test followed by Sidak's post-test, whereby ns and (*) represent non-significant and $p < 0.05$, respectively, vs. control.

6.4.6 Analysis of S-sulhydrated Caspase 3 in TNF- α and GYY4137-treated HUVECs.

Chapter 4 shows that TNF- α leads to endothelial apoptosis and post-treatment with GYY4137 declined this effect, partly by reducing cleaved caspase 3 and cytosolic cyto c protein expression. Caspases are primarily known for their role in regulating cell death. In mammals, executor apoptotic mediators include caspase 3, 6 and 7, whereby caspase 3 is the most crucial facilitator (Shalini *et al.*, 2014).

Previously, it has been shown that the active site in caspase 3 (Cys¹⁶³) is the predominant site of S-sulfhydration (Figure 6.9 A) (Marutani *et al.*, 2015). However, exploration of the potential of S-sulfhydrated caspase 3 is limited. Indeed, effects of persulfide formation in caspase 3 have only been assessed in SH-5YSY, HeLa and H9c2 cell lines upon fast H₂S-releasing donors (Na₂S, NaHS and Na₂S₄) with short incubation time (30 min, one hour or two hours) (Marutani *et al.*, 2015; Braunstein *et al.*, 2020; Ye *et al.*, 2022).

The modified biotin switch assay was conducted to explore whether the anti-apoptotic effects of GYY4137 post-treatment were associated with the S-sulfhydration of caspase 3. Protein samples were incubated with an anti-caspase 3 antibody and analysed by western blotting. Immunoblotting membranes showed that the S-sulfhydrated caspase 3 expression signal was more significant after incubation with GYY4137 than untreated and TNF- α -treated HUVECs (Figure 6.9 B). Quantitative analysis of immunoblots using ImageJ exhibits a markedly significant increase in S-sulfhydrated caspase 3 upon GYY4137 treatment alone compared to the control group (**p<0.01). HUVECs cultured with TNF- α alone showed no change in S-sulfhydration of caspase 3. GYY4137 post-treatment in TNF- α -treated cells displayed a significant increase in S-sulfhydrated caspase 3 compared to TNF- α -treated cells alone (##p<0.01) (Figure 6.9 C).

Following the results of S-sulfhydrated caspase 3 in treated HUVECs, it was hypothesised that in response to S-sulfhydration of caspase 3, the apoptotic executor might become inactivated (Alvarado-Kristensson *et al.*, 2004). Thus, the relative luminescence unit for caspase 3/7 activity was quantified using a commercially available Caspase-Glo 3/7 activity kit. As shown in Figure 6.10, the RLU values revealed a significant increase in the caspase 3/7 activity after TNF- α treatment in HUVECs compared to untreated cells (***p<0.0001). As hypothesised, GYY4137 post-treatment significantly reduced caspase 3/7 activity in TNF- α -stimulated HUVECs compared with untreated cells (**p<0.01). Similarly, GYY4137 post-treatment significantly declined TNF- α -stimulated caspase 3/7 activity compared to TNF- α -treated cells (####p<0.0001). Together, these cellular data suggest that ECs cultured with an exogenous H₂S donor trigger the S-sulfhydration of caspase 3, causing its inactivation.

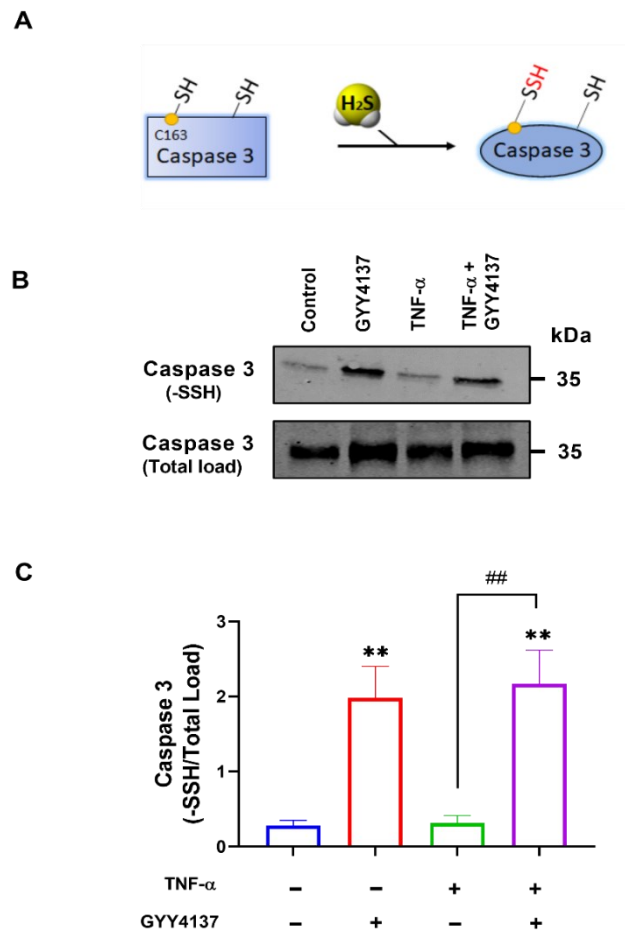


Figure 6.9 Analysis of S-sulfhydration of caspase 3 in HUVECs.

(A) Persulfide (-SSH) formation in the active catalytic site of caspase 3 (Cys¹⁶³) has been previously reported (Ye *et al.*, 2022). (B) Protein lysates were subjected to a Modified Biotin switch assay to detect S-sulfhydrated caspase 3 and total load caspase 3. (C) Densitometry analysis was performed on the blots using ImageJ software to compare S-sulfhydrated caspase 3 relative to total caspase 3 loaded. Bar graphs of S-sulfhydrated caspase 3 quantification relative to total load. Results are the mean \pm SEM (n=3). Significance was determined by one-way ANOVA followed by Sidak's comparison post-test, whereby (**) and (##) represent $p < 0.01$ for to control group and TNF- α alone, respectively.

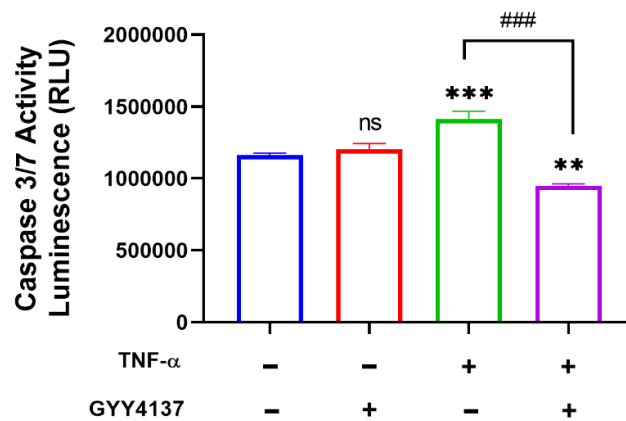


Figure 6.10 Activity of caspase 3/7 upon TNF- α and GYY4137 treatments in HUVECs. HUVECs were treated with TNF- α and GYY4137 post-treatment design in 96-well plate. Caspase 3/7 activity was measured using Caspase-Glo 3/7 assay system (Promega). Readings were taking 1 h after in the Tecan plate reader system. Caspase 3/7 activity are expressed as relative luminescence units (RLU). Data in the graphs represent \pm SEM (n=4). Significance was determined by one-way ANOVA followed by Sidak's comparison post-test; whereby ns., (**) and (***) represents non-significant, p<0.01 and p<0.0001, respectively vs. to control. (###) represents p<0.0001 compared to TNF- α alone.

6.5 Discussion

It has been suggested that one-third of proteins could be S-sulfhydrated, indicating a high prevalence of these PTMs. In the vasculature, the S-sulfhydrome was revealed to comprise over three thousand Cys residues in over a thousand proteins in ECs, which exhibit different intensities clusters and S-sulfhydration motifs (Bibli *et al.*, 2021). The data presented in this chapter suggest that H₂S slow-releasing donor could regulate Nrf2 downstream antioxidant response and that this effect might be partly associated with Keap1 S-sulfhydration. Moreover, S-sulfhydration of caspase 3 leads to its inactivation, eliciting a decline in cleaved caspase 3 expressions and thus having anti-apoptotic effects.

However, the detection and analysis of Cys S-sulfhydration comprise several challenges. The disadvantages regarding S-sulfhydration labelling methods rely on relative instability, enhanced nucleophilicity of persulfides and difficulty in discriminating from other sulfur-containing groups (Filipovic *et al.*, 2018). Several methods have been developed based on the ability of the persulfide group to react faster with thiol-blocking electrophiles due to their greater nucleophilicity of the outer sulfur (Cuevasanta *et al.*, 2015). One of these methods comprises fluorescent thiol-blocking reagent Cy5-conjugated maleimide for S-sulfhydrated Cys residue labelling. The loss of in-gel red fluorescence signal of Cys S-sulfhydrated is detected by adding the reducing agent, DTT (Vandiver *et al.*, 2013). The Maleimide assay was trialled first in this study to estimate S-sulfhydration levels. The simplicity of this method and the commercial availability of the reagents were two of the advantages considered. For example, the Maleimide assay has previously been used to analyse S-sulfhydration of Parking in HEK293 cells (Vandiver *et al.*, 2013), p65 subunit of NF- κ B in TNF- α -treated macrophages (Sen *et al.*, 2012) and transcription factor specificity protein 1 in HUVECs (Saha *et al.*, 2016).

Surprisingly, we were unable to show the detection of S-sulfhydration levels in the presence of GYY4137 using the Maleimide assay based on the detected fluorescence signal. In the current study, an *in vitro* model was used instead of animal tissue and purified proteins, which may account for the observed differences in the expected loss signal by DTT compared to previous reports (Vandiver *et al.*, 2013; C. Wang *et al.*, 2018).

The discrepancies with previous maleimide-based studies might also be explained by the ability of maleimides to react with amines (compounds containing nitrogen atoms with an lone pair), which can lead to excessive fluorescence intensity background (Filipovic *et al.*, 2018). This extensive labelling aligns with the observed data in the present work, suggesting that the persulfide groups might be hidden. Furthermore, the maleimide assay does not distinguish between S-sulfhydration and other Cys PTMs such as S-glutathionylation (Bindu D. Paul and Snyder, 2015); which has been reported as a critical “redox-switch” mechanism in EC homeostasis and could also explain the excessive fluorescence background signal (Lermant and Murdoch, 2019). A practical approach to overcome the limitations associated with the maleimide assay could be using iodoacetyl-PEG₂-Biotin followed by LC-MS/MS analysis (Gao *et al.*, 2015).

The present study used the modified biotin switch assay to analyse S-sulfhydrated proteins to overcome the reactivity and instability challenges regarding persulfide group detection. This method uses MMTS as a blocking agent, in which persulfides remain unreacted and are pulled down by streptavidin-biotin beads (Mustafa *et al.*, 2009). The suitability of this assay was preliminarily analysed using EA.hy926 cell protein lysates incubated with NaHS, as reported (Mustafa *et al.*, 2011). In line with previous reports, the results from the immunoblots showed Cys residues in actin are susceptible to S-sulfhydration in the presence of H₂S donor in ECs, as exemplified by higher protein actin expression in the presence of NaHS and ablation upon reducing agent (Saha *et al.*, 2016; Grambow *et al.*, 2020). Although only one independent experiment was conducted, densitometry blot suggests that the above method is suitable for detecting persulfide formation in ECs. Indeed, published reports have characterised the beneficial role of S-sulfhydration by this method against atherosclerosis (Cheung and Lau, 2018), apoptotic cardiomyocytes (Ye *et al.*, 2022) and neurodegeneration (Vandiver *et al.*, 2013). This observation is corroborated by incubation of GYY4137 or synthesised sodium salt derivative of GYY4137 (NaGYY), which has previously been shown to induce S-sulfhydration in adrenocortical and HEK923 cells, also detected by the modified biotin switch assay (C. Wang *et al.*, 2018; Giovinazzo *et al.*, 2021). In this regard, it is apparent from the immunoblotting with actin observed here that the modified biotin switch assay is likely to detect S-sulfhydrated proteins.

Continuous methodological progress, such as proteomic mapping and profiling of proteomic persulfides, has expanded the earliest inventory of S-sulfhydrated proteins in complex proteomes and their biological effects (Fu *et al.*, 2020; Bibli *et al.*, 2021). A well-known cellular target includes the Keap1-Nrf2 system. As a master regulator of the intracellular antioxidant response, Nrf2 signalling is involved in attenuating inflammation, apoptosis, oxidative stress and initiating mitochondrial function in ECs upon death receptor ligands such as TNF- α and LPS (Chang *et al.*, 2016; Cen *et al.*, 2021). Keap1 acts as a negative regulator of Nrf2, regulating its steady state by continuous proteasomal degradation. Keap1 presents reactive Cys residues, which can be targeted for S-sulfhydration (Xie, Liu and Bian, 2016). H₂S enriches persulfide formation in Keap1, leading to Nrf2 nuclear translocation and thus offers protection against diabetes-accelerated atherosclerotic mice (Xie, Gu, *et al.*, 2016) and oxidative stress and mitochondrial dysfunction in rats (Liu *et al.*, 2020).

Here, Keap1 S-sulfhydration in HUVECs is inconsistent with previously published data in which a significant increase in S-sulfhydration levels of Keap1 was observed in high-glucose EA.hy926 cells (Xie, Gu, *et al.*, 2016). Discrepancies may be linked to GYY4137 co-treatment for short-time incubation (2 hours) using a tag-switch method rather than the modified biotin switch assay used in this study. Nevertheless, immunoblotting analysis suggests a trend of Keap1 S-sulfhydrated level followed by GYY4137 treatment. These data indicate that the GYY4137 cytoprotective and anti-inflammatory role observed in chapters 4 and 5 could be associated with Keap1 S-sulfhydration.

To note, MMTS could generate artificial intermolecular and intramolecular protein disulfide bonds, influencing the results (Karala and Ruddock, 2007). In addition, the chemical foundation of the Modified Biotin switch assay, which relies on the selective reactivity of MMTS only with thiols, has been questioned as it has been suggested that MMTS can react with persulfides (Pan and Carroll, 2013). These observations required precautions to conduct and interpret S-sulfhydrated data from the modified biotin switch assay. Nevertheless, decreased S-sulfhydrated labelling in CBS (Y. Liu *et al.*, 2014) and CSE (Mustafa *et al.*, 2011; Yang *et al.*, 2013b) knockout cell lines and tissues continue to show the capabilities of the method. Furthermore, the mutagenesis approach has validated the formation of persulfide groups in Cys residue by treatment with exogenous H₂S donors in HUVECs (Zhao *et al.*, 2014).

One possible chemical explanation for S-sulfhydrated labelling using this method could rely on a faster reaction of persulfide groups with MMTS than free thiols. The reaction yields a trisulfide product that could be attached by residual free thiol, leaving a free thiol located in the origin localisation of persulfide, which can subsequently interact with biotin-HPDP (Figure 6.11) (Pan and Carroll, 2013; Filipovic *et al.*, 2018).



Figure 6.11 Proposed labelling mechanism of persulfide groups during Modified Biotin switch assay.

Labelling may be achieved via thiol exchange with the formation of trisulfide, which could react with trace-free thiols and subsequently allow labelling with Biotin-HPDP.

Hence, an assessment of proteomic S-sulfhydrated proteins using a highly selective method, such as a dimedone-based assay (Zivanovic *et al.*, 2019) and a sensitive detection tool (LC-MS/MS) in dysfunctional HUVECs should be considered for future work. This approach will provide a robust analysis of S-sulfhydrated signalling mechanisms involved in the physiological roles of ECs, such as metabolism, barrier function and morphologic dynamics.

Previous reports demonstrate that HUVECs, upon TNF- α treatment, reduce Nrf2 nuclear accumulation (Fratantonio *et al.*, 2018; He *et al.*, 2021). In this study, preliminary fluorescence microscopy examination showed that Nrf2 localisation trends to surround the nucleus in TNF- α -treated HUVECs, suggesting a possibility for a nearby nuclear localisation of Nrf2 before translocation. Nuclear fraction isolation and immunoblotting further revealed a trend that TNF- α treatment alone augments Nrf2 nuclear accumulation rather than decreasing HUVECs, but without any conclusive outcome. In contrast to prior reports using high doses of TNF- α in vascular cells [20 ng/ml, 40 ng/ml, 50 ng/ml] (De Palma *et al.*, 2006; Xia *et al.*, 2006; W. Xu *et al.*, 2015), the current study utilised low doses of TNF- α . Considering these observations, it appears that TNF- α may both promote and interrupt Nrf2 nuclear accumulation within ECs in a dose-dependent manner.

Nevertheless, H₂S slow-releasing drugs have previously demonstrated the importance of Nrf2 nuclear translocation in protecting the vasculature from damage (Qiu *et al.*, 2018; Zhang *et al.*, 2020). It is, therefore, possible that HUVECs cultured with GYY4137 exhibit PTMs of Keap1 Cys residues to promote Nrf2 nuclear translocation resulting in the upregulation of downstream signalling antioxidant genes such as NQO1 and GcLC (Kaspar, Niture and Jaiswal, 2009; Raghunath *et al.*, 2018). Here, the analysis of Nrf2-nuclear translocation was not conclusive and Nrf2-mediated proteins expression was significantly increased in TNF- α -treated HUVECs by exogenous H₂S. These findings align with previous studies where fast-releasing H₂S donors increased these target proteins in stress-hepatic cells (J. Zheng *et al.*, 2015) and high-glucose monocytes (Jain, Huning and Micinski, 2014). Thus, these observations suggest that H₂S slow-releasing donor may contribute to an antioxidant response. This signalling mechanism might be partly linked to the S-sulfhydration mechanism of Keap1 and modification of Nrf1-downstream signalling in ECs subjected to the low dose of TNF- α . However, further analysis and independent experiments are required to obtain a robust conclusion.

Published proteomic analysis and t-distributed stochastic embedding visualisation revealed similarities and differences in the subcellular localisation of S-sulfhydration motifs and the intensity of the alteration with up to 12 distinct clusters in native ECs and H₂S-treated ECs (Bibli *et al.*, 2021). These observations suggest an S-sulfhydration network by which H₂S intervenes in several intracellular pathways by S-sulfhydration. Previous reports demonstrated that the anti-apoptotic effect in ECs and vascular rodent models mediated by H₂S was caspases-signalling related (Elrod *et al.*, 2007; Rao *et al.*, 2020), including caspase 3 in HUVECs (Lin *et al.*, 2018). Notably, S-sulfhydration of caspase 3 at the catalytic site (Cys¹⁶³) and, subsequently, anti-apoptotic effects have been previously reported in neuro-like SH-SY5Y cells. Authors noted that persulfide formation in Cys residues alters caspase 3 function, leading to its inactivation (Marutani *et al.*, 2015). Studies have shown increased caspase 3 activation in the presence of TNF- α (5 ng/ml) treatment in EA.hy926 cells (Galkin *et al.*, 2016).

A recent report revealed that cardiomyocytes treated with fast-release H₂S donors without cellular stress exhibit decreased caspase 3 activity and cell death via S-sulfhydrated caspase 3 (Ye *et al.*, 2022). In line with these findings, S-sulfhydrated caspase 3 levels and reduction of caspase 3/7 activity were observed in the presence of an H₂S donor. During activation, the maturation of caspase 3 occurs to its active cleaved

form, which exerts its pro-apoptotic role; therefore, disruption in the activity of caspase 3 could affect its maturation to cleaved caspase 3 and ultimately reduce the apoptotic signal (Shalini *et al.*, 2014). Due to time limitations, the examination of S-sulfhydration of cleaved caspase 3 was not examined in the current study. However, Braunstein's report showed that cleaved caspase 3 was slightly S-sulfhydrated under basal conditions in HeLa cells, and increased S-sulfhydrated levels were observed under stress stimulation (Braunstein *et al.*, 2020). These observations suggest that S-sulfhydration of the caspase cascade might co-occur at distinct pathway levels.

Overall, it can be concluded that the beneficial effects of GYY4137 post-treatment in TNF- α -treated ECs are not a simple process and comprises simultaneous regulatory pathways to revoke impaired redox state, pro-inflammatory and pro-apoptotic response. Understanding protein S-sulfhydration induced by H₂S emerges as a vital cellular process in ameliorating dysfunctional phenotype in ECs.

7 General Conclusions & Limitations

This research aimed to understand the role of H₂S in ED. It is known that H₂S can mediate beneficial effects in the vasculature through anti-inflammatory and redox-modulating regulatory mechanisms. While testing H₂S as a potential therapeutic agent in pre-clinical settings, it is essential to establish appropriate experimental conditions. Many of these reported *in vitro* studies focus on experimental settings based on pre-and co-treatment of H₂S. Therefore, they lose information on whether the administration of exogenous H₂S can revoke rather than prevent vascular damage. In addition, this study successfully applied slow-releasing H₂S donors in inflammatory stimuli-induced ED in a post-treatment setting to identify signalling pathways with therapeutic potential. Furthermore, S-sulfhydration upon post-treatment with slow H₂S releasing donor in ECs can expand the available limited reports.

7.1 Summary of findings

7.1.1 Characterisation of ED and H₂S experimental setting.

The culture of ECs has been essential for detecting complicated pathophysiological processes within the vessel wall (Riederer *et al.*, 2010). To pursue the aims of this project, primary cells HUVECs and immortalised cell line-EA.hy926 cells were utilised as their advantages outweigh their disadvantages in meeting those aims. Based on their standardised conditions and reproducible results, immortalised cells offer benefits in testing conditions (see Chapter 3) (Bouïs *et al.*, 2001). On the other hand, HUVECs become a more representative *in vitro* model to study beneficial signalling routes mediated by H₂S throughout the thesis (Chi *et al.*, 2003). Notably, the study of H₂S has been executed using both cell models (Park *et al.*, 2006; Xie, Feng, *et al.*, 2016), offering accountability for the current study.

This study used TNF- α as a stimulant to initiate ED. The pleiotropic cytokine TNF- α regulates several pathways by binding to its membrane receptors, TNFR1 and TNFR2 (Aggarwal, Gupta and Kim, 2012). TNF- α activates the endothelium, which leads to ED upon sustaining stimuli and an inefficient ability to cope with stress (S. Wang *et al.*, 2018). Development of ED upon TNF- α exposure has been previously reported *in vitro*, characterised by impaired redox state, pro-apoptotic environment and sub-localisation effects such as the ER and mitochondria (Liao *et al.*, 2010; C. Xu *et al.*, 2015; Galkin *et al.*, 2016; Batko *et al.*, 2019).

A low dose of TNF- α suitably initiates ED by disturbing the redox state and enhancing pro-inflammatory and pro-apoptotic responses, which mimics what is seen in the literature using primary ECs (Yang, Zhao and Tian, 2016). In contrast to the current project, some studies have used high doses of TNF- α (5-40 ng/ml), which might exhibit discrepancies with the present findings (McDonnell *et al.*, 2003; Fratantonio *et al.*, 2018; S. Wang *et al.*, 2018; Y. C. Chen *et al.*, 2021). For example, in this study, protein expression of caspase 3 was not significantly increased upon TNF- α compared to the control group (see Chapter 5); but Fratantonio and colleagues (2018) showed a significant elevation of caspase 3 expressions in HUVECs when using 20 ng/ml TNF- α for 2 hours (Fratantonio *et al.*, 2018). The discrepancies could be justified by different doses associated with TNF- α stimulation; explain why more sensitive processes such as redox status and mitochondria performance are strongly affected by a low dose of TNF- α . In contrast, angiogenesis and senescence require a high and sustained dose of TNF- α treatment. Hence, careful attention is needed when using TNF- α as an inducer for ED.

Since its discovery, H₂S has exhibited beneficial roles in the endothelium, including vascular tone, maintenance of redox state, and anti-inflammatory and anti-apoptotic response (Predmore, Lefer and Gojon, 2012). However, precautions using H₂S are required as high concentrations can result in cell damage via inhibition of the mitochondrial ETC (Szabo, 2018). Research groups adopt modulation of H₂S by targeting the transsulfuration pathway in transgenic rodents (Cheung *et al.*, 2014) or by pharmacological inhibitory intervention (Asimakopoulou *et al.*, 2013). On the other hand, other groups opt for prodrugs to deliver a particular concentration of exogenous H₂S. One of the most widely used H₂S donors, NaHS, exhibits a fast release within a short time, leading to non-realistic endogenous concentrations (Y. Zheng *et al.*, 2015; Yuan, Zheng and Wang, 2020). This study uses a slow-releasing H₂S donor, GYY4137, in both cell models to increase intracellular H₂S content without disturbing basal endothelial functions, which aligns with previous ECs findings (Xie, Feng, *et al.*, 2016; Rao *et al.*, 2020). Additionally, organelle-targeted donors (Sanchez-Aranguren, Ahmad, *et al.*, 2020) and combined prodrugs (Latorre *et al.*, 2018); may be worthy of study, given higher sensitivity in subcellular pools such as mitochondria.

Most *in vitro* studies have described H₂S modulation as a pre-treatment, where exogenous H₂S is given before the systemic/cellular insult (Henderson *et al.*, 2010; Wen *et al.*, 2013; Xie, Feng, *et al.*, 2016; Potenza *et al.*, 2017; Hao *et al.*, 2019). In addition, co-treatment is also a widely used approach (Wu *et al.*, 2012; Shen *et al.*, 2013; Zhu *et al.*, 2021), thereby preventing rather than rescuing cell damage. For example, pre-treatment of GYY4137 for a short duration (4 hours) protects against apoptosis, impaired mitochondria function and oxidative stress in EA.hy926 exposed to H₂O₂ (Xie, Feng, *et al.*, 2016). Even though pre- and co-treatment allow for investigation of the prevention or occurrence of disease, post-treatment offers the benefit of evaluating the suitability of a drug as a treatment for a disease condition (Wallace *et al.*, 2018). Based on preliminary experimental results using EA.hy926 cells via IL-6 levels, the post-treatment design for H₂S was selected against ED as the most beneficial model. This practical approach aligns with recent developments investigating ECs integrity, inflammation and ROS formation using HUVECs with GYY4137 (Spassov *et al.*, 2022). Hence, the current study expanded on the limited evidence regarding the H₂S role in ED in a post-treatment setting.

7.1.2 The role of H₂S in TNF- α -mediate impaired redox state.

Oxidative stress is generally characterised by excess oxidant levels over the antioxidant response in biological systems, leading to a shift towards oxidising redox status and promoting vascular damage (Khatri *et al.*, 2004). The current study observed that a low dose of TNF- α alters the redox state by increasing ROS formation, specifically H₂O₂ and O₂⁻. Moreover, post-treatment with exogenous H₂S was able to switch the redox state towards a more reducing environment. The reduction in H₂O₂ production observed upon GYY4137 was comparable to the previous pre-treatment study in HG-induced EA.hy926 cells (Xie, Feng, *et al.*, 2016); while revoking effect of O₂⁻ levels has been reported by GYY4137 post-treatment against stretched-stress HUVECs (Spassov *et al.*, 2022).

Due to immense variety, high reactivity, extremely short half-life and sensitivity of DCF to O₂ and pH levels, measuring intracellular ROS levels remains difficult (Halliwell, 2014). The American Heart Association stated that care should be taken with MitoSox as a detection dye as it may be affected by $\Delta\mu$ m and misleading outcomes (Griendling *et al.*, 2016).

Thus, precautions are required during CM-H₂DCFDA and MitoSox-associated levels, as misleading results may appear (Zielonka and Kalyanaraman, 2010; Kalyanaraman *et al.*, 2012; Brandes, Rezende and Schröder, 2018). Combining the conjugated effect of fluorogenic probes with flow cytometry or HPLC with robust controls such as silencing RNA of oxidants generating enzymes could offer a sensitive reading of oxidants content (Lippert, Van De Bittner and Chang, 2011; Tsuboi, Maeda and Hayashi, 2018).

In addition to detecting ROS levels, antioxidant molecules were quantified by RT-qPCR, immunoblotting or luminescence-reading to assess changes in the antioxidant defence in ED. Quantitative PCR analysis demonstrated upregulation of HO-1, SOD2 and CAT in the presence of GYY4137 in TNF- α -treated HUVECs, which agrees with the prior reports on HUVECs (Choi *et al.*, 2018; Zhu *et al.*, 2021). In addition, H₂S enhanced secondary antioxidant routes such as Nrf2-downstream mediating NQO1 and GcLC proteins in the presence of TNF- α , in agreement with a study in vascular cells (Aghagolzadeh *et al.*, 2017) and high-glucose monocytes (Jain, Huning and Micinski, 2014).

Furthermore, exogenous H₂S showed a trend to boost major cellular antioxidant systems such as GSH and Trx pathways by targeting Trx and the first rate-limiting enzyme of GSH synthesis. Although the data presented in this project did not reach a conclusive outcome, the importance of both molecules in the thiol-dependent redox systems, whereby disulfide in oxidised Trx/GSH is converted to thiols through redox cycling has been reported (Ren *et al.*, 2017). The Trx and GSH systems reduce oxidative thiol modifications, thus preventing irreversible oxidation modification of proteins in TNF- α -treated ECs (Hanschmann *et al.*, 2013). Notably, the Trx system has exhibited a crucial role in the reverse reaction of excessive S-sulphydration of GAPDH, which could lead to neuronal conditions (Mir, Sen and Sen, 2014). Hence, in the current study, stimulation of the Trx system by GYY4137 could also be associated with preventing damage by excessive S-sulphydration.

7.1.3 The role of H₂S in TNF- α -mediated inflammation and apoptosis.

When considering the impact of ED on the cardiovascular system, the development of inflammation and apoptosis emerge as common underlying factors (Favero *et al.*, 2014). During inflammation, enhanced vascular permeability and cell adhesion molecules alongside the release of pro-inflammatory cytokines occur (Ley *et al.*, 2007). TNF- α is one of many pro-inflammatory cytokines associated with worsened clinical outcomes after stroke (Ormstad *et al.*, 2011) and elevated plasma levels in systolic heart failure patients (Xia Li *et al.*, 2020). Here, TNF- α -treated ECs displayed increased cell adhesion molecules linked to the trafficking of macromolecules, including ICAM-1, VCAM-1 and E-selectin, as evidenced in earlier studies (Clark *et al.*, 2007; Zhao *et al.*, 2017; Gapizov *et al.*, 2018). In concordance with the earlier reported effects of TNF- α -treated ECs, a pro-inflammatory environment in the current work was confirmed by ELISA analysis (Chi *et al.*, 2001; Gapizov *et al.*, 2018). Exposure of TNF- α -treated HUVECs to H₂S post-treatment remarkably revokes pro-inflammatory response (see Chapter 4). These findings support H₂S anti-inflammatory role in protecting against ED described in angiotensin II-treated HUVECs (Hu *et al.*, 2017) and rodent models (Liu *et al.*, 2013; Yang *et al.*, 2018). As an example, a study conducted by Pan *et al.* (2011) demonstrated the decrease of ICAM-1, E-selectin, VCAM-1 expression and inhibition of the canonical NF- κ B apoptotic pathway in ECs exposed to TNF- α (10 ng/ml, 6 h) by NaHS pre-treatment (Pan *et al.*, 2011). To our knowledge, the current work is the first to highlight these inflammatory findings regarding TNF- α -cultured HUVECs, followed by post-treatment with a slow-release H₂S donor. Further *in vivo* approaches to mimic these findings might be of interest to demonstrate the potential of H₂S revoking anti-inflammatory events.

Progression from inflammation towards apoptosis can be associated with extrinsic or intrinsic caspase cascade signalling. Both intrinsic and extrinsic mechanisms have been reported to be mediated by TNF- α (Deng *et al.*, 2017). For instance, HUVECs treated with TNF- α (10 ng/ml) showed a significant rise in apoptotic rate after 24 hours of treatment through caspase 7 activation (Tang *et al.*, 2015). On the other hand, TNF- α comprises cyto c release from mitochondria to cytosol with caspase 3 activation in fibroblasts (Tafari *et al.*, 2000). Due to the complexity of cell death, several events occur,

including the release of several mitochondrial factors, activation of a cascade of cytoplasmic caspase enzymes and changes in mitochondrial $\Delta\psi_m$, condensation of chromatin and fragmentation of DNA (Obeng, 2021). In this study, several experimental approaches were conducted to study cellular apoptosis concerning these versatile events, including apoptotic rate via Annexin V/PI assay, mitochondrial $\Delta\psi_m$, cyto c release and caspase cascade pathway (see Chapter 4 and Chapter 5).

Mitochondria that have undergone MPTP opening are sufficient to release cyto c, activate pro-caspase 3, cleave caspase 3 and initiate the autocatalytic apoptotic cycle (Penna, Perrelli and Pagliaro, 2013). Moreover, oxidants such as H_2O_2 can evoke MPTP opening (Zorov, Juhaszova and Sollott, 2014). Remarkably, the pore opening is required for TNF- α mediated apoptosis and further cyto c release, and the latter is required for caspase 3 activation (Tafari *et al.*, 2000). This linked-cascade signalling suggests that the cytosolic cyto c release by TNF- α is directly associated with altered mitochondria. Here, the accumulation of cyto c in the cytosol and activation of mature caspase 3 confirmed the alteration of the mitochondria-mediated intrinsic pathway by TNF- α in ECs.

Cytosolic cyto c accumulation has been previously reported in human monocytic cells (U937) treated with 5 ng/ml TNF- α after 2 hours (Hughes, Murphy and Ledgerwood, 2005). Same protein accumulation upon high doses of TNF- α (10-50 ng/ml) has been reported in peripheral blood mononuclear cells (Xu *et al.*, 2011), neuroblastoma SK-N-MC cells (Álvarez *et al.*, 2011) and PC12 cells (Zhang *et al.*, 2007). Regarding ECs, elevated cyto c release upon TNF- α treatment in porcine aortic ECs alongside increased caspase 8, 2, 3 and 6 activities and loss of $\Delta\psi_m$ was reported (Daniel *et al.*, 2004). TNF- α -induced cyto c translocation from mitochondria to cytosol was reversed by co-incubation with vitamin C, a known antioxidant agent, blocking apoptotic signalling in HUVECs (Rössig *et al.*, 2001). In the current study, the release of cytosolic cyto c in TNF- α treated HUVECs was alleviated by the actions of exogenous H_2S post-treatment. Although the H_2S effect on cytosolic cyto c accumulation has been previously assessed in HUVECs treated with H_2O_2 , the authors focused on a pre-treatment approach with a fast-release donor (Wen *et al.*, 2013). To our knowledge, the present work is a pioneer study regarding H_2S revoking role in TNF- α -induced cyto c release in HUVECs by post-treatment design.

7.1.4 The role of H₂S and TNF- α on mitochondria.

TNF- α altered mitochondrial redox state, as evidenced MitoSox microscopy analysis of O₂⁻ levels. Spassov and co-authors have shown by microscopy analysis that GYY4137 post-treatment in stretched HUVECs decreases O₂⁻ radical levels (Spassov *et al.*, 2022). These observations align with current O₂⁻ results post-treatment with GYY4137 in TNF- α -treated HUVECs. In contrast to Spassov's study, an inflammatory stimulus rather than physical stress was conducted here. To note, NOX enzymes are also a vital vascular source of O₂⁻ within the cell (Douglas *et al.*, 2012), and NOX2 can target mitochondrial ROS, creating a continuous positive feedback loop (Nazarewicz *et al.*, 2013). To discriminate the contribution of NOX enzymes to the cellular oxidants content from a single mutation in the p22^{phox} subunit of NOX, a key component in the activation of NOXs can be used, as these strategies were shown to succeed in macrophages (Bulua *et al.*, 2011).

Excessive ROS production is associated with impaired mitochondrial OXPHOS capacity in the endothelium (Scialò, Fernández-Ayala and Sanz, 2017). ECs rely on glycolysis for energy supply due to low mitochondrial content compared with other vascular beds (Oldendorf, Cornford and Brown, 1977). Nevertheless, mitochondrial OXPHOS can support fatty acid oxidation for DNA synthesis, suggesting a pleiotropic role apart from ATP formation (Schoors *et al.*, 2015; Wong *et al.*, 2016). The overall view of the metabolic environment within ECs was assessed by Seahorse technology. The glycolytic parameters revealed that GYY4137 and TNF- α elevated overall glycolytic flux in HUVECs. The effect of TNF- α agrees with previous findings in epithelial cells (Vaughan *et al.*, 2013) and fibroblasts (Koedderitzsch *et al.*, 2021), suggesting a metabolic shift towards a more glycolytic phenotype. These observations could be explained by an initial rise in glycolytic activity as a compensatory mechanism to sustain energetic cellular demands (Palomer *et al.*, 2009). A possible feedback loop between both active systems might occur as hyperglycemic aortic ECs modulate mitochondrial electron flux (Du *et al.*, 2000). Further analysis of the implications of GYY4137 and TNF- α in the glycolytic metabolism of ECs could be assessed by analysing the glutamine and fatty acid dependency through inhibitors such as BPTES for glutaminase or etomoxir targeting fatty acid pathway (Nunes *et al.*, 2021).

In addition, a metabolic switch from OXPHOS to glycolysis, known as the Warburg effect, occurs in tumorigenesis. Investigating this feature in TNF- α -mediate ECs, as TNF- α tends to induce lactate export, which is observed in the classical aerobic glycolytic Warburg effect (Vaughan *et al.*, 2013). Interestingly, recent studies have suggested that H₂S protects against dysfunctional cognition by promoting the Warburg effect (Chen *et al.*, 2020; Yang *et al.*, 2020). However, these observations have not been addressed in vascular cells. Therefore, examination of the role of H₂S regarding the Warburg effect via modulation of the transsulfuration enzymatic pathway or by using H₂S prodrugs could expand the limited knowledge regarding H₂S-mediated action in vascular metabolism.

The total force driving protons into the mitochondria partially depends on $\Delta\psi_m$. During cellular stress, the $\Delta\psi_m$ is altered, affecting the integrity of the mitochondrial membrane and its components (Cadenas, 2018). Reduction in $\Delta\psi_m$ is described as a phenomenon in mitochondrial uncoupling (Kadenbach, 2003) and is associated with elevated proton leak (Crompton, 1999). In addition, the loss of $\Delta\psi_m$ can account for cyto c release, followed by a series of caspase activations (McDonnell *et al.*, 2003). Fluorescent microscopy revealed that TNF- α leads to $\Delta\psi_m$ loss in HUVECs, suggesting depolarisation of $\Delta\psi_m$ (see Chapter 5). The data agree with previous studies, whereby significant reduction of $\Delta\psi_m$ in the presence of TNF- α was confirmed by microscopy and flow cytometry analysis in murine hepatocytes (Kastl *et al.*, 2014), epithelial cells (Y. C. Chen *et al.*, 2021) and Hela cells (Kim *et al.*, 2010). The evidence indicates an effect of fast-release H₂S donor on depolarised $\Delta\psi_m$ in HUVECs subjected to H₂O₂, as illustrated by the increase in $\Delta\psi_m$ (Wen *et al.*, 2013). This observation aligns with the current study findings in TNF- α -treated HUVECs with GYY4137 post-treatment. Overall, these observations indicate that dissipation of $\Delta\psi_m$ by TNF- α can be revoked by exogenous H₂S in ECs.

When considering an explanation for the loss of $\Delta\psi_m$, proton leak mediated by uncoupling protein, the opening of the MPTP and changes in mitochondrial Ca²⁺ emerges as possible options. Whereas in the current project, alteration of proton leak and UCP2 was observed in TNF- α -treated ECs, the use of inhibitors of UCP2 such as genipin, could be an avenue to confirm the direct role of UCPs in the dissipation of $\Delta\psi_m$ in ECs (Zhang *et al.*, 2006).

Although cyto c release to the cytosol indicates opening actions of the MPTP, culturing cells with inhibitors of the opening MPTP, such as cyclosporin A can provide a route to test the direct involvement of MPTP in the depolarisation of $\Delta\psi_m$ (Broekemeier and Pfeiffer, 1989). The flux of Ca^{2+} into the mitochondria or efflux from the inter-membrane space to the matrix has dissipated the $\Delta\psi_m$ (Abramov and Duchen, 2008). Although Ca^{2+} analysis was beyond the scope of the present study, future examination of Ca^{2+} flux in ECs exposed to TNF- α could be approached by using the Ru360 compound to block mitochondrial Ca^{2+} uniporter, as exemplified by the rescue of $\Delta\psi_m$ loss in neurons (Abramov and Duchen, 2008).

As a dynamic organelle, mitochondria build a dense network with a characteristic tubular shape by specific active mechanisms, including fusion, fission, transport and mitophagy (Twig, Hyde and Shirihai, 2008). $\Delta\psi_m$ is a crucial determinant of mitochondrial structure, and its dissipation has been shown to cause mitochondrial fragmentation by modifying mitochondrial dynamic machinery toward fission (Collins *et al.*, 2002; Twig *et al.*, 2008). Mitochondrial dysfunction in diabetes-mediated ED was characterised by altered dynamic machinery with mitochondria fragmentation as a key mechanism (Shenouda *et al.*, 2011). It has been reported that ROS triggers a mitochondrial shift towards fission in apoptotic and mitophagy stress responses (Bordi, Nazio and Campello, 2017; Martinez-Carreres, Nasrallah and Fajas, 2017). Diabetes mellitus-mediated ED (Shenouda *et al.*, 2011) and oxidised cardiomyocytes (Rao *et al.*, 2020) are associated with mitochondrial fragmentation. In line with the preceding evidence, in the present study, exposure of HUVECs to TNF- α resulted in mitochondrial fragmentation manifesting as an imbalance in the fusion/fission cycle by fluorescence microscopy analysis of mitochondria morphology analysis and RT-qPCR assay.

The role of H_2S in mitochondria dynamics has been previously reported in rat high-glucose-mediated ED with NaHS co-treatment by regulating DRP1 and MFN1 protein expression (N. Liu *et al.*, 2017). Comparable to DATS pre-treatment in high-glucose HUVECs, GYY4137 modulation of mitochondrial morphology was orchestrated by regulating dynamic genes (Hao *et al.*, 2019). Furthermore, due to the limited scope of the present thesis, the effect of TNF- α on mitophagy in this model was not analysed. However, based on the OPA1 data and its implications in mitophagy, analysis of the OPA1 via knockdown or overexpression would be a central focus for follow-on studies (Xin and Lu, 2020).

Taken together, the data up to this point indicated that TNF- α -induced ED via four major aspects: (i) oxidative stress, (ii) inflammation, (iii) apoptosis and (iv) mitochondrial dysfunction. Based on the presumption that H₂S exhibits its cytoprotective roles, in part, by S-sulfhydration signalling, it could be conceivable to assume that the beneficial effects observed in this thesis are linked to protein S-sulfhydration.

7.1.5 S-sulfhydration as an H₂S underlying signalling mechanism.

Keap1-Nrf2 system: The stress response transcription factor Nrf2 is essential in the cell's defence against oxidative and electrophilic stress (Kobayashi and Yamamoto, 2006). Importantly, overexpressed Nrf2 can lead to an oncogenic response, highlighting the importance of maintaining Nrf2 in a proper balance within the cell (He, Antonucci and Karin, 2020). Historically, Keap1 mediates the degradation of Nrf2 via 26S proteasome protein, regulating its activity (Kaspar, Niture and Jaiswal, 2009). Under stressed conditions, disruption of the Keap1-Nrf2 complex facilitates increased Nrf2 nuclear import. Besides stress conditions, Keap1 can be unbound from Nrf2 by PTMs of Cys residue mediated by H₂S. S-sulfhydration of Keap1 followed by Nrf2 nuclear accumulation impacts cellular homeostasis and exhibits cytoprotection (Yamamoto *et al.*, 2008; Meng *et al.*, 2017). Here, H₂S donors might affect Keap1 S-sulfhydration in HUVECs, as evidenced by modified biotin switch assay. A prior research group showed upregulation of S-sulfhydrated Keap1 in the presence of GYY4137 in EA.hy926 cells, which aligns with the current work, and was enhanced upon induced stress (Xie, Gu, *et al.*, 2016).

Following Keap1 S-sulfhydration, translocation of Nrf2 into the nucleus is expected with subsequent upregulation of Nrf2-downstream genes (Hayes and Dinkova-Kostova, 2014). Although no conclusive outcome regarding Keap1 S-sulfhydration was obtained in the current study, analysis of Nrf2-downstream response was examined. Fast-release H₂S donors previously showed increased protein expression of downstream target-Nrf2 genes (NQO1, GcLC and HO-1) in stress-hepatic cells (J. Zheng *et al.*, 2015) and in high-glucose monocytes (Jain, Huning and Micinski, 2014). In line with these observations, immunoblotting analysis displayed a possible modification on NQO1 and GcLC downstream proteins. However, correlation with Nrf2-nuclear translocation was not determined as only preliminary and non-significant data was observed in the current project.

Additionally, alternative PTMs need to be considered regarding the accountability of H₂S-mediated Keap1 S-sulfhydration and Nrf2 accumulation due to a percentage of Nrf2 nuclear translocation attributed to phosphorylation of Nrf2 itself or regulators of Nrf2 (Bloom and Jaiswal, 2003). For instance, phosphorylated Akt mediates Nrf2 atomic translocation in cardiomyocyte cells stimulated by GYY4137 (Qiu *et al.*, 2018). One avenue to test the contribution of other PTMs in the Nrf2 activation would be using a single mutation of Keap1 at Cys¹⁵¹, the predominant Cys residue targeted during S-sulfhydration, as these strategies were shown before in EA.hy926 cells (Xie, Gu, *et al.*, 2016). In addition, regulatory mechanisms exist to avoid cytotoxicity by H₂S through mitochondrial metabolism with robust regulation of enzymatic activity (e.g., SQR, XO or ETHE1) or by sulfane-sulfur storage. This intracellular regulation could decrease H₂S level as the adaptive mechanism, which could also justify the non-significant data for Keap1 S-sulfhydration (Picton *et al.*, 2002; Caliendo *et al.*, 2010a).

Caspases: *In vitro* models revealed that exogenous H₂S could ameliorate caspase 3 protein expression in hypoxic HUVECs upon co-treatment (Shen *et al.*, 2013) and cleaved caspase 3 by the pre-treatment approach (Lin *et al.*, 2018). In neuron-like SH-SY5Y cells, S-sulfhydration of caspase 3 at its catalytic site leads to its inactivation (Marutani *et al.*, 2015). Similarly, the Modified Biotin switch assay confirmed GYY4137 S-sulfhydrated caspase 3 in HUVECs, suggesting that exogenous H₂S can alter caspase cascade signalling. Examination of caspase 3/7 activity and cleaved caspase 3 expression further supports this hypothesis, as reduced activity and protein levels were observed in the presence of GYY4137 in TNF- α -induced HUVECs. In line with the current study, a recent cardiomyocyte study showed that H₂S decreased caspase 3 activity and cleaved caspase 3 expressions by S-sulfhydration of caspase 3 at its catalytic site (Ye *et al.*, 2022). In addition, a report by Braunstein's group showed that cleaved caspase 3 can also be S-sulfhydrated in stressed-Hela cells (Braunstein *et al.*, 2020). In addition, the assessment of whether GYY4137 regulates S-sulfhydrated cleaved caspase 3 was beyond the scope of this thesis due to time limitations. Nevertheless, other H₂S donors, such as Na₂S₄, showed that cleaved caspase 3, caspase 9 and pro-caspase 9 were S-sulfhydrated in the presence of staurosporine in Hela cells (Braunstein *et al.*, 2020). Overall, the present study is, to our knowledge, the first work to demonstrate S-sulfhydration of caspase 3 by a slow-releasing H₂S donor post-treatment in ECs.

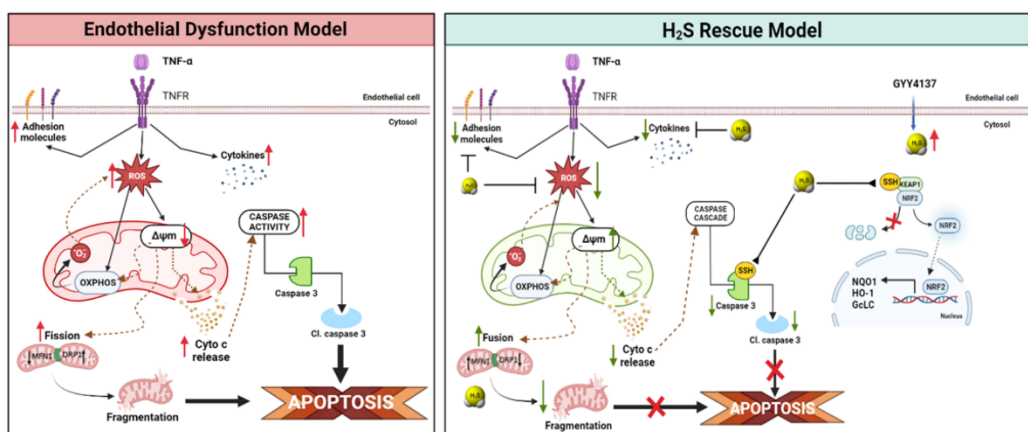


Figure 7.1 Hypothetical model proposed for cell ED triggered by TNF- α and rescue model mediated by H₂S.

ED model: oxidative stress, inflammation, and apoptosis can be triggered by TNF- α stimulation in ECs, in part, via regulation of the intrinsic apoptotic pathway. Rescue model: in the presence of H₂S, excessive ROS formation, pro-inflammatory cytokines and mitochondrial dysfunction are alleviated, in part, through S-sulfhydration of Keap1 and Caspase 3; that ultimately reduces cell death.

Taken together, these *in vitro* studies revealed that H₂S alleviated ED via S-sulfhydration of Keap1 and further Nrf2-nuclear translocation with downstream upregulation of target antioxidant genes. In parallel, inactivation of caspase 3 activity and disruption of the cascade signalling route involves S-sulfhydration of caspase 3 (Figure 7.1). Further investigations are required to confirm the present findings *in vivo* models and to establish whether S-sulfhydration target proteins may be a suitable therapeutic approach in vascular conditions.

7.2 Future work

7.2.1 Optimising experimental approach

This study only selected one-time points (24 hours) to study the beneficial effect of GYY4137. Since GYY4137 is a slow-releasing donor, it is essential to investigate its therapeutic ability beyond 24 hours. This approach could be informative in understanding the efficacy of GYY4137 and which cell targets are regulated by H₂S over a more extended time. Ours and most of the published literature reports *in vitro* settings using 2 Dimensional (2D) monolayer cultures of ECs. However, this culture microenvironment cannot reflect the endothelium's physiological characteristics inside vascularised tissue. The 3D microenvironment offers structural support and a source of biochemical and biophysical signals that regulate cell functions such as matrix stiffness, shear stress and interactions with other cell types. This improved cell culture approach has been reported in TNF- α -treated HUVECs, in which primary cells in 3D cultures are more sensitive to TNF- α at low concentrations than those in 2D cultures, therefore, exacerbating TNF- α -induced HUVECs oxidative stress (Wang *et al.*, 2020). In addition, specific *in vivo* rodent models targeting specific vascular conditions such as diabetes, ageing or hypertension could help to understand the effect of H₂S at the tissue level and its implications in the overall biological system and avoid failure in clinical trials (Steinhubl, 2008).

7.2.2 Protein S-sulphydration in vascular cells.

The proteomic analysis and genetic sequencing assessment could lead to understanding vascular networks and accurately quantifying post-translational modifications in this study's model. Notably, the new method based on dimedone-based probes offers a robust and adaptative approach for screening, proteomic analysis and confocal microscopy. Recently this method has been used to show the endothelial S-sulphydrome with more than a thousand vascular proteins challenged with shear stress and H₂S donor, SG1002 (Bibli *et al.*, 2021). However, proteomic analysis of vascular S-sulphydrome upon inflammatory stimuli has yet to be assessed. This experimental approach would better understand S-sulphydration events and functional features in endothelial stress and dysfunction. Among several proteins that have been reported, only a few of them have been investigated for mechanistic implications (Fu *et al.*, 2020).

In this regard, actin is essential for cells' vascular permeability and integrity, and it has been reported to be S-sulfhydrated. However, the implications of S-sulfhydrated actin in the structure and cytoskeleton of ECs have not been investigated (Mustafa *et al.*, 2009). Therefore, understanding the impact of S-sulfhydrated actin on vascular function could help to explore the H₂S role in cell integrity-related conditions.

7.2.3 Increasing the number of replicates

Many differences observed in ED that were quantified for antioxidant enzymes were not statistically significant, which may have resulted from the small number of replicates processed during the study. While some studies address the problems with enzymatic activity rather than expression (Zhang *et al.*, 2016), the power of the experiment is inherent. It would require many more replicates to ascertain protein modifications at transcriptional, translational and functionality levels (Pollard, Pollard and Pollard, 2019).

7.3 Final conclusions

In summary, the work described in this thesis revealed that H₂S is a potent biological mediator that regulates endothelial function under physiological and pathophysiological scenarios. The work presented here demonstrates that post-treatment of H₂S under inflammatory conditions could revoke ED. This approach enables the depiction of changes in subcellular organelles such as mitochondrion, where the impact goes beyond energy supply, compromises organelle morphology, and affects the apoptotic cascade. As mentioned before, the modified Cys residues on target proteins by H₂S could protect by scavenging oxidants and disrupting cell death signals. From the data obtained in this study and the research undertaken in other groups, ED mediated by pro-inflammatory stimuli is a downstream result of a combination of factors resulting from the rise of oxidant production and intrinsic apoptotic signalling pathway. The H₂S's pivotal role in protecting against impaired endothelium involves the S-sulfhydration of crucial proteins, with novel targets highlighted. In cardiomyocytes, S-sulfhydration of caspase 3 and inactivation of its activity was seen (Ye *et al.*, 2022), supporting the data in this thesis. While methodology, experimental power and biological sample can still be further optimised to expand the functional activity of the S-sulfhydrated proteins, the current post-treatment approach with slow-release H₂S donor can be adapted to investigate S-sulfhydrated candidates for inflammatory diseases.

8 References

Abdollahi Govar, A. *et al.* (2020) '3-Mercaptopyruvate sulfurtransferase supports endothelial cell angiogenesis and bioenergetics', *British Journal of Pharmacology*, 177(4), pp. 866–883.

Abe, K. and Kimura, H. (1996) 'The possible role of hydrogen sulfide as an endogenous neuromodulator.', *The Journal of neuroscience : the official journal of the Society for Neuroscience*, 16(3), pp. 1066–71.

Abo, M. and Weerapana, E. (2019) 'Chemical Probes for Redox Signaling and Oxidative Stress', <https://home.liebertpub.com/ars>, 30(10), pp. 1369–1386.

Abou-Hamdan, A. *et al.* (2015) 'Oxidation of H₂S in mammalian cells and mitochondria', in *Methods in Enzymology*. Academic Press Inc., pp. 201–228.

Abramov, A. Y. and Duchen, M. R. (2008) 'Mechanisms underlying the loss of mitochondrial membrane potential in glutamate excitotoxicity', *Biochimica et biophysica acta*, 1777(7–8), pp. 953–964.

Aggarwal, B. B., Gupta, S. C. and Kim, J. H. (2012) 'Historical perspectives on tumor necrosis factor and its superfamily: 25 years later, a golden journey', *Blood*, 119(3), pp. 651–665.

Aghagolzadeh, P. *et al.* (2017) 'Hydrogen sulfide attenuates calcification of vascular smooth muscle cells via KEAP1/NRF2/NQO1 activation', *Atherosclerosis*, 265, pp. 78–86.

Ahmad, A., Druzhyna, N. and Szabo, C. (2019) 'Effect of 3-mercaptopyruvate Sulfurtransferase Deficiency on the Development of Multiorgan Failure, Inflammation, and Wound Healing in Mice Subjected to Burn Injury', *Journal of Burn Care & Research*, 40(2), pp. 148–156.

Ahsan, M. K. *et al.* (2009) 'Redox Regulation of Cell Survival by the Thioredoxin Superfamily: An Implication of Redox Gene Therapy in the Heart', *Antioxidants & Redox Signaling*, 11(11), p. 2741.

Aird, W. C. (2003) 'Endothelial cell heterogeneity', in *Critical Care Medicine*. Lippincott Williams and Wilkins.

Aird, W. C. (2007) 'Phenotypic heterogeneity of the endothelium: I. Structure, function, and mechanisms', *Circulation Research*, 100(2), pp. 158–173.

Al-Jameil, N. *et al.* (2014) 'A brief overview of preeclampsia.', *Journal of clinical medicine research*, 6(1), pp. 1–7.

Al-Magableh, M. R. *et al.* (2014) 'Hydrogen sulfide protects endothelial nitric oxide function under conditions of acute oxidative stress in vitro.', *Naunyn-Schmiedeberg's Archives of Pharmacology*, 387(1), pp. 67–74.

Altaany, Z. *et al.* (2014) 'The coordination of S-sulfhydration, S-nitrosylation, and phosphorylation of endothelial nitric oxide synthase by hydrogen sulfide.', *Science*

signaling, 7(342), p. ra87.

Altenhöfer, S. *et al.* (2010) 'One enzyme, two functions: PON2 prevents mitochondrial superoxide formation and apoptosis independent from its lactonase activity', *The Journal of biological chemistry*, 285(32), pp. 24398–24403.

Alvarado-Kristensson, M. *et al.* (2004) 'p38-MAPK signals survival by phosphorylation of caspase-8 and caspase-3 in human neutrophils', *The Journal of experimental medicine*, 199(4), pp. 449–458.

Álvarez, S. Á. *et al.* (2011) 'TNF- α Contributes to Caspase-3 Independent Apoptosis in Neuroblastoma Cells: Role of NFAT', *PLoS ONE*, 6(1).

Andersson-Sjöland, A., Karlsson, J. C. and Rydell-Törmänen, K. (2016) 'ROS-induced endothelial stress contributes to pulmonary fibrosis through pericytes and Wnt signaling', *Laboratory Investigation*, 96(2), pp. 206–217.

Ardito, F. *et al.* (2017a) 'The crucial role of protein phosphorylation in cell signaling and its use as targeted therapy (Review)', *International Journal of Molecular Medicine*, 40(2), p. 271.

Ardito, F. *et al.* (2017b) 'The crucial role of protein phosphorylation in cell signaling and its use as targeted therapy (Review)', *International Journal of Molecular Medicine*, 40(2), p. 271.

Aroca, A. *et al.* (2020) 'Hydrogen sulfide: From a toxic molecule to a key molecule of cell life', *Antioxidants*. MDPI AG, pp. 1–24.

Asimakopoulou, A. *et al.* (2013) 'Selectivity of commonly used pharmacological inhibitors for cystathionine β synthase (CBS) and cystathionine γ lyase (CSE).', *British journal of pharmacology*, 169(4), pp. 922–32.

Bachetti, T. and Morbidelli, L. (2000) 'Endothelial cells in culture: A model for studying vascular functions', *Pharmacological Research*, 42(1), pp. 9–19.

Bakalarz, D. *et al.* (2021) 'Novel hydrogen sulfide (H₂S)-releasing bw-hs-101 and its non-h₂s releasing derivative in modulation of microscopic and molecular parameters of gastric mucosal barrier', *International Journal of Molecular Sciences*, 22(10), p. 5211.

Balligand, J. L. *et al.* (1995) 'Nitric oxide-dependent parasympathetic signaling is due to activation of constitutive endothelial (type III) nitric oxide synthase in cardiac myocytes', *The Journal of biological chemistry*, 270(24), pp. 14582–14586.

Barth, E. *et al.* (1992) 'Ultrastructural quantitation of mitochondria and myofilaments in cardiac muscle from 10 different animal species including man', *Journal of Molecular and Cellular Cardiology*, 24(7), pp. 669–681.

Başaran, Y. *et al.* (1993) 'Serum tumor necrosis factor levels in acute myocardial infarction and unstable angina pectoris', *Angiology*, 44(4), pp. 332–337.

- Batko, K. *et al.* (2019) 'Endothelial injury is closely related to osteopontin and TNF receptor-mediated inflammation in end-stage renal disease', *Cytokine*, 121, p. 154729.
- Beauchamp, R. O. *et al.* (1984) 'A Critical Review of the Literature on Hydrogen Sulfide Toxicity', *CRC Critical Reviews in Toxicology*, 13(1), pp. 25–97.
- Bedard, K. and Krause, K. H. (2007) 'The NOX family of ROS-generating NADPH oxidases: Physiology and pathophysiology', *Physiological Reviews*, 87(1), pp. 245–313.
- Behera, J., Kelly, K. E. and Tyagi, N. (2021) 'Hydrogen sulfide prevents ethanol-induced ZO-1 CpG promoter hypermethylation-dependent vascular permeability via miR-218/DNMT3a axis', *Journal of Cellular Physiology*, 236(10), pp. 6852–6867.
- Beltowski, J. (2019) 'Synthesis, metabolism, and signaling mechanisms of hydrogen sulfide: An overview', in *Methods in Molecular Biology*. Humana Press Inc., pp. 1–8.
- Beltowski, J. and Jamroz-Wiśniewska, A. (2014) 'Hydrogen sulfide and endothelium-dependent vasorelaxation', *Molecules*. MDPI AG, pp. 21183–21199.
- Benchoam, D. *et al.* (2019) 'Hydrogen sulfide and persulfides oxidation by biologically relevant oxidizing species', *Antioxidants*. MDPI AG.
- Benhar, M. (2020) 'Oxidants, Antioxidants and Thiol Redox Switches in the Control of Regulated Cell Death Pathways', *Antioxidants 2020, Vol. 9, Page 309*, 9(4), p. 309.
- Bereiter-Hahn, J. (1990) 'Behavior of Mitochondria in the Living Cell', *International Review of Cytology*, 122(C), pp. 1–63.
- Berry, C. E. and Hare, J. M. (2004) 'Xanthine oxidoreductase and cardiovascular disease: molecular mechanisms and pathophysiological implications', *The Journal of physiology*, 555(Pt 3), pp. 589–606.
- Bevilacqua, M. P. *et al.* (1987) 'Identification of an inducible endothelial-leukocyte adhesion molecule', *Proceedings of the National Academy of Sciences of the United States of America*, 84(24), pp. 9238–9242.
- Bibli, S. I. *et al.* (2021) 'Mapping the Endothelial Cell S-Sulfhydryl Highlights the Crucial Role of Integrin Sulfhydrylation in Vascular Function', *Circulation*, 143(9), pp. 935–948.
- Biniecka, M. *et al.* (2011) 'Successful tumour necrosis factor (TNF) blocking therapy suppresses oxidative stress and hypoxia-induced mitochondrial mutagenesis in inflammatory arthritis', *Arthritis Research and Therapy*, 13(4), p. R121.
- Bloom, D. A. and Jaiswal, A. K. (2003) 'Phosphorylation of Nrf2 at Ser 40 by Protein Kinase C in Response to Antioxidants Leads to the Release of Nrf2 from I κ Nf2, but Is Not Required for Nrf2 Stabilization/Accumulation in the Nucleus and Transcriptional Activation of Antioxidant Response Element', *The Journal of biological chemistry*, 278(45), pp. 44675–44682.

- Boehm, E. A. *et al.* (2001) 'Increased uncoupling proteins and decreased efficiency in palmitate-perfused hyperthyroid rat heart', *American journal of physiology. Heart and circulatory physiology*, 280(3).
- Bonetti, P. O., Lerman, L. O. and Lerman, A. (2003) 'Endothelial dysfunction: a marker of atherosclerotic risk.', *Arteriosclerosis, thrombosis, and vascular biology*, 23(2), pp. 168–75.
- Bordi, M., Nazio, F. and Campello, S. (2017) 'The Close interconnection between mitochondrial dynamics and mitophagy in cancer', *Frontiers in Oncology*, 7, p. 81.
- Bouïs, D. *et al.* (2001) 'Endothelium in vitro: A review of human vascular endothelial cell lines for blood vessel-related research', *Angiogenesis*. *Angiogenesis*, pp. 91–102.
- Boveris, A. and Chance, B. (1973) 'The mitochondrial generation of hydrogen peroxide. General properties and effect of hyperbaric oxygen', *The Biochemical journal*, 134(3), pp. 707–716.
- Bradham, C. A. *et al.* (1998) 'The mitochondrial permeability transition is required for tumor necrosis factor alpha-mediated apoptosis and cytochrome c release', *Molecular and cellular biology*, 18(11), pp. 6353–6364.
- Brand, M. D. *et al.* (2004) 'Mitochondrial superoxide: production, biological effects, and activation of uncoupling proteins', *Free radical biology & medicine*, 37(6), pp. 755–767.
- Brandes, R. P., Rezende, F. and Schröder, K. (2018) 'Redox regulation beyond ROS why ROS should not be measured as often', *Circulation Research*, 123(3), pp. 326–328.
- Braunstein, I. *et al.* (2020) 'Opposing effects of polysulfides and thioredoxin on apoptosis through caspase persulfidation', *Journal of Biological Chemistry*, 295(11), pp. 3590–3600.
- Brenneman, K. A. *et al.* (2000) 'Olfactory neuron loss in adult male CD rats following subchronic inhalation exposure to hydrogen sulfide', *Toxicologic pathology*, 28(2), pp. 326–333.
- Broekemeier, K. M. and Pfeiffer, D. R. (1989) 'Cyclosporin A-sensitive and insensitive mechanisms produce the permeability transition in mitochondria', *Biochemical and Biophysical Research Communications*, 163(1), pp. 561–566.
- Brookes, P. S. *et al.* (1998) 'Peroxynitrite and brain mitochondria: evidence for increased proton leak', *Journal of neurochemistry*, 70(5), pp. 2195–2202.
- Brookes, P. S. (2005) 'Mitochondrial H(+) leak and ROS generation: an odd couple', *Free radical biology & medicine*, 38(1), pp. 12–23.
- Bulua, A. C. *et al.* (2011) 'Mitochondrial reactive oxygen species promote production of proinflammatory cytokines and are elevated in TNFR1-associated periodic syndrome (TRAPS)', *Journal of Experimental Medicine*, 208(3), pp. 519–533.

- Butawan, M., Benjamin, R. L. and Bloomer, R. J. (2017) 'Methylsulfonylmethane: Applications and Safety of a Novel Dietary Supplement', *Nutrients*, 9(3).
- Cadenas, S. (2018) 'Mitochondrial uncoupling, ROS generation and cardioprotection', *Biochimica et Biophysica Acta (BBA) - Bioenergetics*, 1859(9), pp. 940–950.
- Cai, J., Yang, J. and Jones, D. P. (1998) 'Mitochondrial control of apoptosis: the role of cytochrome c', *Biochimica et Biophysica Acta (BBA) - Bioenergetics*, 1366(1–2), pp. 139–149.
- Caliendo, G. *et al.* (2010a) 'Synthesis and Biological Effects of Hydrogen Sulfide (H₂S): Development of H₂S-Releasing Drugs as Pharmaceuticals', *Journal of Medicinal Chemistry*, 53(17), pp. 6275–6286.
- Caliendo, G. *et al.* (2010b) 'Synthesis and biological effects of hydrogen sulfide (H₂S): development of H₂S-releasing drugs as pharmaceuticals', *Journal of medicinal chemistry*, 53(17), pp. 6275–6286.
- Calvert, J. W. *et al.* (2009) 'Hydrogen sulfide mediates cardioprotection through Nrf2 signaling.', *Circulation research*, 105(4), pp. 365–74.
- Camici, G. G. *et al.* (2007) 'Genetic deletion of p66Shc adaptor protein prevents hyperglycemia-induced endothelial dysfunction and oxidative stress', *Proceedings of the National Academy of Sciences of the United States of America*, 104(12), pp. 5217–5222.
- Cao, T. *et al.* (2019) 'Increased calpain-1 in mitochondria induces dilated heart failure in mice: role of mitochondrial superoxide anion', *Basic research in cardiology*, 114(3).
- Carmeliet, P. and Jain, R. K. (2011) 'Molecular mechanisms and clinical applications of angiogenesis', *Nature*, 473(7347), p. 298.
- Caro, A. A. *et al.* (2012) 'Effect of garlic-derived organosulfur compounds on mitochondrial function and integrity in isolated mouse liver mitochondria', *Toxicology Letters*, 214(2), pp. 166–174.
- Cen, M. *et al.* (2021) 'MitoQ protects against hyperpermeability of endothelium barrier in acute lung injury via a Nrf2-dependent mechanism', *Redox biology*, 41.
- Chandrasekar, B. *et al.* (2004) 'Activation of intrinsic and extrinsic proapoptotic signaling pathways in interleukin-18-mediated human cardiac endothelial cell death.', *The Journal of biological chemistry*, 279(19), pp. 20221–20233.
- Chang, H. C. *et al.* (2016) 'Hericium erinaceus Inhibits TNF- α -Induced Angiogenesis and ROS Generation through Suppression of MMP-9/NF- κ B Signaling and Activation of Nrf2-Mediated Antioxidant Genes in Human EA.hy926 Endothelial Cells', *Oxidative medicine and Cellular longevity*, p. 8257238.
- Chaudhry, R., Miao, J. H. and Rehman, A. (2021) 'Physiology, Cardiovascular', *StatPearls*.

- Chen, C. A. *et al.* (2010) 'S-glutathionylation uncouples eNOS and regulates its cellular and vascular function', *Nature*, 468(7327), p. 1115.
- Chen, H.-J. *et al.* (2022) 'Hydrogen sulfide-induced post-translational modification as a potential drug target', *Genes & Diseases*.
- Chen, J.-X. *et al.* (2021) 'Effects and mechanism of arachidonic acid against TNF- α induced apoptosis of endothelial cells.', *Clinical hemorheology and microcirculation*, 77(3), pp. 259–265.
- Chen, S. M. *et al.* (2020) 'Hydrogen sulfide attenuates postoperative cognitive dysfunction through promoting the pathway of Warburg effect-synaptic plasticity in hippocampus', *Toxicology and Applied Pharmacology*, 409, p. 115286.
- Chen, Y.-H. *et al.* (2005) 'Endogenous hydrogen sulfide in patients with COPD.', *Chest*, 128(5), pp. 3205–3211.
- Chen, Y.-H. *et al.* (2009) 'Endogenous hydrogen sulfide reduces airway inflammation and remodeling in a rat model of asthma', *Cytokine*, 45(2), pp. 117–123.
- Chen, Y. C. *et al.* (2021) 'Vitamin D3 decreases TNF- α -induced inflammation in lung epithelial cells through a reduction in mitochondrial fission and mitophagy', *Cell Biology and Toxicology*, 1, p. 1.
- Chen, Z.-F. *et al.* (2011) 'Hydrogen sulfide regulates vascular endoplasmic reticulum stress in apolipoprotein E knockout mice.', *Chinese medical journal*, 124(21), pp. 3460–3467.
- Cherney, M. M. *et al.* (2010) 'Crystal Structure of Sulfide:Quinone Oxidoreductase from *Acidithiobacillus ferrooxidans*: Insights into Sulfidotrophic Respiration and Detoxification', *Journal of Molecular Biology*, 398(2), pp. 292–305.
- Cheung, S. H. *et al.* (2014) 'Anti-atherogenic effect of Hydrogen sulfide by over-expression of cystathionine gamma-lyase (CSE) gene', *PLoS ONE*, 9(11), p. 113038.
- Cheung, S. H. and Lau, J. Y. W. (2018) 'Hydrogen sulfide mediates athero-protection against oxidative stress via S-sulphydration', *PLOS ONE*. Edited by U. Sen, 13(3), p. e0194176.
- Chi, J.-T. *et al.* (2003) 'Endothelial cell diversity revealed by global expression profiling.', *Proceedings of the National Academy of Sciences of the United States of America*, 100(19), pp. 10623–10628.
- Chi, L. *et al.* (2001) 'Interleukin-6 production by endothelial cells via stimulation of protease-activated receptors is amplified by endotoxin and tumor necrosis factor- α ', *Journal of interferon & cytokine research: the official journal of the International Society for Interferon and Cytokine Research*, 21(4), pp. 231–240.
- Chia, P. Y., Teo, A. and Yeo, T. W. (2020) 'Overview of the Assessment of Endothelial Function in Humans', *Frontiers in Medicine*, 7, p. 614.

- Choi, E. S. *et al.* (2018) 'Ligustilide attenuates vascular inflammation and activates Nrf2/HO-1 induction and, NO synthesis in HUVECs', *Phytomedicine*, 38, pp. 12–23.
- Chung, H. S. *et al.* (2013) 'Cysteine oxidative posttranslational modifications: Emerging regulation in the cardiovascular system', *Circulation Research*, pp. 382–392.
- Circu, M. L. and Aw, T. Y. (2008) 'Glutathione and apoptosis', *Free radical research*, 42(8), pp. 689–706.
- Clark, P. R. *et al.* (2007) 'Increased ICAM-1 Expression Causes Endothelial Cell Leakiness, Cytoskeletal Reorganization and Junctional Alterations', *Journal of Investigative Dermatology*, 127(4), pp. 762–774.
- Coletta, C. *et al.* (2015) 'Regulation of vascular tone, angiogenesis and cellular bioenergetics by the 3-mercaptopyruvate sulfurtransferase/H₂S pathway: Functional impairment by hyperglycemia and restoration by dl- α -lipoic acid', *Molecular Medicine*, 21(1), pp. 1–14.
- Collins, T. J. *et al.* (2002) 'Mitochondria are morphologically and functionally heterogeneous within cells', *The EMBO Journal*, 21(7), pp. 1616–1627.
- Collman, J. P. *et al.* (2009) 'Using a functional enzyme model to understand the chemistry behind hydrogen sulfide induced hibernation.', *Proceedings of the National Academy of Sciences of the United States of America*, 106(52), pp. 22090–5.
- Conway, E. M., Collen, D. and Carmeliet, P. (2001) 'Molecular mechanisms of blood vessel growth', *Cardiovascular research*, 49(3), pp. 507–521.
- Cordeiro, S. *et al.* (2001) 'Rapid reactive oxygen species production by mitochondria in endothelial cells exposed to tumor necrosis factor- α is mediated by ceramide', *American Journal of Respiratory Cell and Molecular Biology*, 24(6), pp. 762–768.
- Corretti, M. C. *et al.* (2002) 'Guidelines for the ultrasound assessment of endothelial-dependent flow-mediated vasodilation of the brachial artery: a report of the International Brachial Artery Reactivity Task Force', *Journal of the American College of Cardiology*, 39(2), pp. 257–265.
- Crompton, M. (1999) 'The mitochondrial permeability transition pore and its role in cell death.', *The Biochemical journal*, 341 (Pt 2(Pt 2)), pp. 233–249.
- Cross, M. J. and Claesson-Welsh, L. (2001) 'FGF and VEGF function in angiogenesis: signalling pathways, biological responses and therapeutic inhibition', *Trends in pharmacological sciences*, 22(4), pp. 201–207.
- Csiszar, A. *et al.* (2008) 'Inflammation and endothelial dysfunction during aging: role of NF- κ B', *Journal of Applied Physiology*, 105(4), p. 1333.
- Csiszar, A. *et al.* (2019) 'Overexpression of catalase targeted to mitochondria improves neurovascular coupling responses in aged mice', *GeroScience*, 41(5), p. 609.

- Cuevasanta, E. *et al.* (2012) 'Solubility and permeation of hydrogen sulfide in lipid membranes', *PloS one*, 7(4).
- Cuevasanta, E. *et al.* (2015) 'Reaction of Hydrogen Sulfide with Disulfide and Sulfenic Acid to Form the Strongly Nucleophilic Persulfide', *The Journal of biological chemistry*, 290(45), pp. 26866–26880.
- Cuevasanta, E., Möller, M. N. and Alvarez, B. (2017) 'Biological chemistry of hydrogen sulfide and persulfides', *Archives of Biochemistry and Biophysics*, 617, pp. 9–25.
- Daniel, S. *et al.* (2004) 'A20 protects endothelial cells from TNF-, Fas-, and NK-mediated cell death by inhibiting caspase 8 activation', *Blood*, 104(8), pp. 2376–2384.
- Deanfield, J. E., Halcox, J. P. and Rabelink, T. J. (2007) 'Endothelial Function and Dysfunction', *Circulation*, 115(10), pp. 1285–1295.
- Debbabi, H. *et al.* (2010) 'Noninvasive assessment of endothelial function in the skin microcirculation', *American journal of hypertension*, 23(5), pp. 541–546.
- Demchenko, A. P. (2013) 'Beyond annexin V: fluorescence response of cellular membranes to apoptosis', *Cytotechnology*, 65(2), p. 157.
- Deng, S. and Marmorstein, R. (2021) 'Protein N-Terminal Acetylation: Structural Basis, Mechanism, Versatility, and Regulation', *Trends in Biochemical Sciences*, 46(1), pp. 15–27.
- Deng, X. *et al.* (2017) 'TNF- α Mediates the Intrinsic and Extrinsic Pathway in Propofol-Induced Neuronal Apoptosis Via PI3K/Akt Signaling Pathway in Rat Prefrontal Cortical Neurons', *Neurotoxicity Research*, 32(3), pp. 409–419.
- Deshmukh, P. *et al.* (2017) 'The Keap1–Nrf2 pathway: promising therapeutic target to counteract ROS-mediated damage in cancers and neurodegenerative diseases', *Biophysical Reviews*, 9(1), p. 41.
- Dikalov, S. I. and Ungvari, Z. (2013) 'Role of mitochondrial oxidative stress in hypertension', *American Journal of Physiology - Heart and Circulatory Physiology*. American Physiological Society, p. H1417.
- Dikalova, A. *et al.* (2016) 'Tetrahydrobiopterin oral therapy recouples eNOS and ameliorates chronic hypoxia-induced pulmonary hypertension in newborn pigs', *American journal of physiology. Lung cellular and molecular physiology*, 311(4), pp. L743–L753.
- Dinkova-Kostova, A. T. *et al.* (2002) 'Direct evidence that sulfhydryl groups of Keap1 are the sensors regulating induction of phase 2 enzymes that protect against carcinogens and oxidants.', *Proceedings of the National Academy of Sciences of the United States of America*, 99(18), pp. 11908–13.
- Doeller, J. E. *et al.* (2005) 'Polarographic measurement of hydrogen sulfide production and consumption by mammalian tissues', *Analytical biochemistry*, 341(1), pp. 40–51.

Dóka, É. *et al.* (2016) 'A novel persulfide detection method reveals protein persulfide- and polysulfide-reducing functions of thioredoxin and glutathione systems', *Science Advances*, 2(1), p. e1500968.

Donnarumma, E., Trivedi, R. K. and Lefer, D. J. (2017) 'Protective actions of H₂S in acute myocardial infarction and heart failure', *Comprehensive Physiology*, 7(2), pp. 583–602.

Dou, Y., Wang, Z. and Chen, G. (2016) 'The role of hydrogen sulfide in stroke', *Medical Gas Research*. BioMed Central Ltd., pp. 79–84.

Doughan, A. K., Harrison, D. G. and Dikalov, S. I. (2008) 'Molecular mechanisms of angiotensin II-mediated mitochondrial dysfunction: Linking mitochondrial oxidative damage and vascular endothelial dysfunction', *Circulation Research*, 102(4), pp. 488–496.

Du, G. *et al.* (2014) 'Simvastatin attenuates TNF- α -induced apoptosis in endothelial progenitor cells via the upregulation of SIRT1.', *International journal of molecular medicine*, 34(1), pp. 177–182.

Du, W. *et al.* (2021) 'Endothelial Cell Glucose Metabolism and Angiogenesis', *Biomedicines*, 9(2), pp. 1–17.

Durand, M. J. and Gutterman, D. D. (2013) 'Diversity in Mechanisms of Endothelium-Dependent Vasodilation in Health and Disease', *Microcirculation (New York, N.Y. : 1994)*, 20(3), p. 239.

Edgell, C.-J. S. *et al.* (1990) 'Endothelium specific Weibel-Palade bodies in a continuous human cell line, EA.hy926', *In Vitro Cellular & Developmental Biology*, 26(12), pp. 1167–1172.

Elmore, S. (2007) 'Apoptosis: a review of programmed cell death.', *Toxicologic pathology*, 35(4), pp. 495–516.

Elrod, J. W. *et al.* (2007) 'Hydrogen sulfide attenuates myocardial ischemia-reperfusion injury by preservation of mitochondrial function', *Proceedings of the National Academy of Sciences of the United States of America*, 104(39), pp. 15560–15565.

Enokido, Y. *et al.* (2005) 'Cystathionine β -synthase, a key enzyme for homocysteine metabolism, is preferentially expressed in the radial glia/astrocyte lineage of developing mouse CNS', *The FASEB Journal*, 19(13), pp. 1854–1856.

Enroth, C. *et al.* (2000) 'Crystal structures of bovine milk xanthine dehydrogenase and xanthine oxidase: structure-based mechanism of conversion', *Proceedings of the National Academy of Sciences of the United States of America*, 97(20), pp. 10723–10728.

Erchova, I., Sun, S. and Votruba, M. (2021) 'A Perspective on Accelerated Aging Caused by the Genetic Deficiency of the Metabolic Protein, OPA1', *Frontiers in Neurology*, 12, p. 538.

- Favero, G. *et al.* (2014) 'Endothelium and Its Alterations in Cardiovascular Diseases: Life Style Intervention', *BioMed Research International*, 2014.
- Feng, S. *et al.* (2016) 'H₂S inhibits pulmonary arterial endothelial cell inflammation in rats with monocrotaline-induced pulmonary hypertension', *Laboratory Investigation* 2017 97:3, 97(3), pp. 268–278.
- Feng, X. *et al.* (2020) 'Toxic effects of hydrogen sulfide donor NaHS induced liver apoptosis is regulated by complex IV subunits and reactive oxygen species generation in rats', *Environmental Toxicology*, 35(3), pp. 322–332.
- Ferrer-Sueta, G. *et al.* (2011) 'Factors affecting protein thiol reactivity and specificity in peroxide reduction', *Chemical research in toxicology*, 24(4), pp. 434–450.
- Filipovic, M. R. (2015) 'Persulfidation (S-sulfhydration) and H₂S', *Handbook of Experimental Pharmacology*, 230, pp. 29–59.
- Filipovic, M. R. *et al.* (2018) 'Chemical Biology of H₂S Signaling through Persulfidation', *Chemical reviews*, 118(3), pp. 1253–1337.
- Fink, B. D. *et al.* (2005) 'Respiratory uncoupling by UCP1 and UCP2 and superoxide generation in endothelial cell mitochondria', *American Journal of Physiology - Endocrinology and Metabolism*, 288(1 51-1).
- Finkel, T. (1998) 'Oxygen radicals and signaling', *Current opinion in cell biology*, 10(2), pp. 248–253.
- Finkel, T. (2011) 'Signal transduction by reactive oxygen species', *The Journal of Cell Biology*, 194(1), p. 7.
- Fishman, A. P. (1982) 'Endothelium: a distributed organ of diverse capabilities', *Annals of the New York Academy of Sciences*, 401(1), pp. 1–8.
- Forman, H. J., Zhang, H. and Rinna, A. (2009) 'Glutathione: Overview of its protective roles, measurement, and biosynthesis', *Molecular aspects of medicine*, 30(1–2), p. 1.
- Foster, M. W., Hess, D. T. and Stamler, J. S. (2009) 'Protein S-nitrosylation in health and disease: a current perspective', *Trends Mol Med*, 15(9), pp. 391–404.
- Foster, M. W., McMahon, T. J. and Stamler, J. S. (2003) 'S-nitrosylation in health and disease', *Trends in molecular medicine*, 9(4), pp. 160–168.
- Fratantonio, D. *et al.* (2018) 'Alpha-lipoic acid, but not di-hydrolipoic acid, activates Nrf2 response in primary human umbilical-vein endothelial cells and protects against TNF- α induced endothelium dysfunction', *Archives of Biochemistry and Biophysics*, 655, pp. 18–25.
- Freed, J. K. and Gutterman, D. D. (2013) 'Mitochondrial reactive oxygen species and vascular function: less is more.', *Arteriosclerosis, thrombosis, and vascular biology*. United States, pp. 673–675.

- Fu, L. *et al.* (2020) 'Direct Proteomic Mapping of Cysteine Persulfidation', *Antioxidants & redox signaling*, 33(15), pp. 1061–1076.
- Fu, M. *et al.* (2012) 'Hydrogen sulfide (H₂S) metabolism in mitochondria and its regulatory role in energy production', *Proceedings of the National Academy of Sciences of the United States of America*, 109(8), pp. 2943–2948.
- Fukai, T. and Ushio-Fukai, M. (2011) 'Superoxide dismutases: role in redox signaling, vascular function, and diseases.', *Antioxidants & redox signaling*, 15(6), pp. 1583–606.
- Furchgott, R. F. and Zawadzki, J. V (1980) 'The obligatory role of endothelial cells in the relaxation of arterial smooth muscle by acetylcholine.', *Nature*, 288(5789), pp. 373–6.
- Furne, J., Saeed, A. and Levitt, M. D. (2008) 'Whole tissue hydrogen sulfide concentrations are orders of magnitude lower than presently accepted values', *Am J Physiol Regul Integr Comp Physiol*, 295, pp. 1479–1485.
- Furukawa, M. and Xiong, Y. (2005) 'BTB protein Keap1 targets antioxidant transcription factor Nrf2 for ubiquitination by the Cullin 3-Roc1 ligase.', *Molecular and cellular biology*, 25(1), pp. 162–71.
- Gagat, M. *et al.* (2014) 'Tropomyosin-1 protects endothelial cell–cell junctions against cigarette smoke extract through F-actin stabilization in EA.hy926 cell line', *Acta Histochemica*, 116(4), pp. 606–618.
- Gage, M. C. *et al.* (2013) 'Endothelium-specific insulin resistance leads to accelerated atherosclerosis in areas with disturbed flow patterns: A role for reactive oxygen species', *Atherosclerosis*, 230(1), pp. 131–139.
- Gale, N. W. and Yancopoulos, G. D. (1999) 'Growth factors acting via endothelial cell-specific receptor tyrosine kinases: VEGFs, angiopoietins, and ephrins in vascular development.', *Genes & development*, 13(9), pp. 1055–66.
- Galimov, E. R. (2010) 'The Role of p66shc in Oxidative Stress and Apoptosis', *Acta Naturae*, 2(4), pp. 44–51.
- Galkin, I. I. *et al.* (2016) 'Mitochondria-Targeted Antioxidant SkQR1 Reduces TNF-Induced Endothelial Permeability in vitro.', *Biochemistry. Biokhimiia*, 81(10), pp. 1188–1197.
- Galley, H. F. and Webster, N. R. (2004) 'Physiology of the endothelium', *British Journal of Anaesthesia*, 93(1), pp. 105–113.
- Gao, X.-H. *et al.* (2015) 'Quantitative H₂S-mediated protein sulfhydration reveals metabolic reprogramming during the integrated stress response.', *eLife*, 4, p. e10067.
- Gapizov, S. S. *et al.* (2018) 'The Effect of TNF and VEGF on the Properties of Ea.hy926 Endothelial Cells in a Model of Multi-Cellular Spheroids.', *Acta naturae*, 10(1), pp. 34–42.

Gardiner, S. M. *et al.* (1994) 'Effects of an ET1-receptor antagonist, FR139317, on regional haemodynamic responses to endothelin-1 and [Ala^{11,15}]Ac-endothelin-1 (6-21) in conscious rats', *British journal of pharmacology*, 112(2), pp. 477–486.

Gaur, U. and Aggarwal, B. B. (2003) 'Regulation of proliferation, survival and apoptosis by members of the TNF superfamily', *Biochemical pharmacology*, 66(8), pp. 1403–1408.

Gavazzi, G. and Faury, G. (2021) 'NOX- and ROS-Driven Hypertension in Elastin Insufficiency', *Function (Oxford, England)*, 2(4).

George, A. K. *et al.* (2019) 'Hydrogen sulfide intervention in cystathionine- β -synthase mutant mouse helps restore ocular homeostasis', *International Journal of Ophthalmology*, 12(5), p. 754.

Geró, D. *et al.* (2016) 'The novel mitochondria-targeted hydrogen sulfide (H₂S) donors AP123 and AP39 protect against hyperglycemic injury in microvascular endothelial cells in vitro', *Pharmacological Research*, 113(Pt A), pp. 186–198.

Giovinazzo, D. *et al.* (2021) 'Hydrogen sulfide is neuroprotective in Alzheimer's disease by sulfhydrating GSK3 β and inhibiting Tau hyperphosphorylation', *Proceedings of the National Academy of Sciences of the United States of America*, 118(4), p. e2017225118.

Go, Y. M. *et al.* (2013) 'Selective targeting of the cysteine proteome by thioredoxin and glutathione redox systems', *Molecular & cellular proteomics : MCP*, 12(11), pp. 3285–3296.

Govers, R. and Rabelink, T. J. (2001) 'Cellular regulation of endothelial nitric oxide synthase', *American Journal of Physiology-Renal Physiology*, 280(2), pp. F193–F206.

Gowans, J. L. (1959) 'The recirculation of lymphocytes from blood to lymph in the rat', *Journal of Physiology*, 146, pp. 54–69.

Grambow, E. *et al.* (2020) 'Hydrogen sulfide reduces the activity of human endothelial cells', *Clinical hemorheology and microcirculation*, 76(4), pp. 513–523.

Greaney, J. L. *et al.* (2017) 'Impaired hydrogen sulfide-mediated vasodilation contributes to microvascular endothelial dysfunction in hypertensive adults HHS Public Access', *Hypertension*, 69(5), pp. 902–909.

Gregory, J. F. *et al.* (2016) 'Vitamin B6 nutritional status and cellular availability of pyridoxal 5'-phosphate govern the function of the transsulfuration pathway's canonical reactions and hydrogen sulfide production via side reactions', *Biochimie*. Elsevier B.V., pp. 21–26.

Greiner, R. *et al.* (2013) 'Polysulfides link H₂S to protein thiol oxidation.', *Antioxidants & redox signaling*, 19(15), pp. 1749–65.

Griendling, K. K. *et al.* (2016) 'Measurement of Reactive Oxygen Species, Reactive Nitrogen Species, and Redox-Dependent Signaling in the Cardiovascular System: A Scientific Statement From the American Heart Association', *Circulation research*, 119(5),

pp. e39–e75.

Griffin, G. K. *et al.* (2012) 'IL-17 and TNF- α Sustain Neutrophil Recruitment during Inflammation through Synergistic Effects on Endothelial Activation', *The Journal of Immunology*, 188(12), pp. 6287–6299.

Guan, L. *et al.* (2019) 'MCU Up-regulation contributes to myocardial ischemia-reperfusion Injury through calpain/OPA-1-mediated mitochondrial fusion/mitophagy Inhibition', *Journal of cellular and molecular medicine*, 23(11), pp. 7830–7843.

Guan, Q. *et al.* (2012) 'Hydrogen sulfide protects against high-glucose-induced apoptosis in endothelial cells', *Journal of Cardiovascular Pharmacology*, 59(2), pp. 188–193.

Guan, R. *et al.* (2019) 'Hydrogen sulfide attenuates mitochondrial dysfunction-induced cellular senescence and apoptosis in alveolar epithelial cells by upregulating sirtuin 1', *Aging*, 11, pp. 11844–11864.

Hahn, W. S. *et al.* (2014) 'Proinflammatory cytokines differentially regulate adipocyte mitochondrial metabolism, oxidative stress, and dynamics', *American Journal of Physiology - Endocrinology and Metabolism*, 306(9), p. E1033.

Hajjar, D. P. and Gotto, A. M. (2013) 'Biological Relevance of Inflammation and Oxidative Stress in the Pathogenesis of Arterial Diseases', *The American Journal of Pathology*, 182(5), pp. 1474–1481.

Halliwell, B. (2014) 'Cell culture, oxidative stress, and antioxidants: avoiding pitfalls', *Biomedical journal*, 37(3), pp. 99–105.

Hameister, R. *et al.* (2020) 'Reactive oxygen/nitrogen species (ROS/RNS) and oxidative stress in arthroplasty', *Journal of Biomedical Materials Research Part B: Applied Biomaterials*, pp. 1–15.

Han, W. *et al.* (2011) 'Hydrogen Sulfide Ameliorates Tobacco Smoke-Induced Oxidative Stress and Emphysema in Mice', *Antioxidants & Redox Signaling*, 15(8), pp. 2121–2134.

Handy, D. E. *et al.* (2009) 'Glutathione peroxidase-1 regulates mitochondrial function to modulate redox-dependent cellular responses', *Journal of Biological Chemistry*, 284(18), pp. 11913–11921.

Hanschmann, E. M. *et al.* (2013) 'Thioredoxins, glutaredoxins, and peroxiredoxins-molecular mechanisms and health significance: From cofactors to antioxidants to redox signaling', *Antioxidants and Redox Signaling*. Mary Ann Liebert, Inc., pp. 1539–1605.

Hao, Y. *et al.* (2019) 'Diallyl trisulfide attenuates hyperglycemia-induced endothelial apoptosis by inhibition of Drp1-mediated mitochondrial fission', *Acta Diabetologica*, 56(11), pp. 1177–1189.

Hara, M. R. *et al.* (2005) 'S-nitrosylated GAPDH initiates apoptotic cell death by nuclear translocation following Siah1 binding', *Nature cell biology*, 7(7), pp. 665–674.

Hartsfield, C. L. (2002) 'Cross talk between carbon monoxide and nitric oxide', *Antioxidants & redox signaling*, 4(2), pp. 301–307.

Hass, D. T. and Barnstable, C. J. (2019) 'Mitochondrial Uncoupling Protein 2 Knock-out Promotes Mitophagy to Decrease Retinal Ganglion Cell Death in a Mouse Model of Glaucoma', *Journal of Neuroscience*, 39(18), pp. 3582–3596.

Hayashida, R. *et al.* (2017) 'Diallyl trisulfide augments ischemia-induced angiogenesis via an endothelial nitric oxide synthase-dependent mechanism', *Circulation Journal*, 81(6), pp. 870–878.

Hayes, J. D. and Dinkova-Kostova, A. T. (2014) 'The Nrf2 regulatory network provides an interface between redox and intermediary metabolism', *Trends in biochemical sciences*, 39(4), pp. 199–218.

He, F., Antonucci, L. and Karin, M. (2020) 'NRF2 as a regulator of cell metabolism and inflammation in cancer', *Carcinogenesis*, 41(4), pp. 405–416.

He, Y. *et al.* (2014) 'Inhibition of high glucose-induced apoptosis by uncoupling protein 2 in human umbilical vein endothelial cells', *International Journal of Molecular Medicine*, 33(5), pp. 1275–1281.

He, Y. *et al.* (2016) 'Overexpression of uncoupling protein 2 inhibits the high glucose-induced apoptosis of human umbilical vein endothelial cells', *International Journal of Molecular Medicine*, 37(3), pp. 631–638.

He, Y. *et al.* (2021) 'SIRT6 inhibits inflammatory response through regulation of NRF2 in vascular endothelial cells', *International Immunopharmacology*, 99, p. 107926.

Held, J. M. (2020) 'Redox Systems Biology: Harnessing the Sentinels of the Cysteine Redoxome', *Antioxidants and Redox Signaling*, 32(10), pp. 659–676.

Henderson, P. W. *et al.* (2010) 'Hydrogen Sulfide Protects Against Ischemia-Reperfusion Injury in an In Vitro Model of Cutaneous Tissue Transplantation¹', *Journal of Surgical Research*, 159(1), pp. 451–455.

Hess, D. T. *et al.* (2005) 'Protein S-nitrosylation: purview and parameters', *Nature Reviews Molecular Cell Biology* 2005 6:2, 6(2), pp. 150–166.

Hildebrandt, T. M. and Grieshaber, M. K. (2008) 'Three enzymatic activities catalyze the oxidation of sulfide to thiosulfate in mammalian and invertebrate mitochondria', *FEBS Journal*, 275(13), pp. 3352–3361.

Ho, C.-Y. *et al.* (2012) 'Effect of diallyl sulfide on in vitro and in vivo Nrf2-mediated pulmonary antioxidant enzyme expression via activation ERK/p38 signaling pathway.', *Journal of agricultural and food chemistry*, 60(1), pp. 100–107.

Hoeben, A. *et al.* (2004) 'Vascular endothelial growth factor and angiogenesis', *Pharmacological reviews*, 56(4), pp. 549–580.

Hou, C.-L. *et al.* (2016) 'Protective Effects of Hydrogen Sulfide in the Ageing Kidney.', *Oxidative medicine and cellular longevity*, 2016, p. 7570489.

Hu, H. *et al.* (2017) 'Protective effects of hydrogen sulfide against angiotensin II-induced endoplasmic reticulum stress in HUVECs', *Molecular Medicine Reports*, 15(4), pp. 2213–2222.

Huang, P. *et al.* (2000) 'Superoxide dismutase as a target for the selective killing of cancer cells', *Nature*, 407(6802), pp. 390–395.

Huang, Y. *et al.* (2013) 'Myeloperoxidase, paraoxonase-1, and HDL form a functional ternary complex', *Journal of Clinical Investigation*, 123(14), pp. 3815–3828.

Hughes, G., Murphy, M. P. and Ledgerwood, E. C. (2005) 'Mitochondrial reactive oxygen species regulate the temporal activation of nuclear factor κ B to modulate tumour necrosis factor-induced apoptosis: evidence from mitochondria-targeted antioxidants', *Biochemical Journal*, 389(Pt 1), p. 83.

Iciek, M. *et al.* (2016) 'S-sulfhydration as a cellular redox regulation', *Bioscience Reports*, 36, p. 304.

Ighodaro, O. M. and Akinloye, O. A. (2018) 'First line defence antioxidants-superoxide dismutase (SOD), catalase (CAT) and glutathione peroxidase (GPX): Their fundamental role in the entire antioxidant defence grid', *Alexandria Journal of Medicine*, 54(4), pp. 287–293.

Incalza, M. *et al.* (2018) 'Oxidative stress and reactive oxygen species in endothelial dysfunction associated with cardiovascular and metabolic diseases', *Vascular Pharmacology*, 100, pp. 1–19.

Inoue, A. *et al.* (1989) 'The human endothelin family: three structurally and pharmacologically distinct isopeptides predicted by three separate genes', *Proceedings of the National Academy of Sciences of the United States of America*, 86(8), pp. 2863–2867.

Ishigami, M. *et al.* (2009) 'A source of hydrogen sulfide and a mechanism of its release in the brain.', *Antioxidants & redox signaling*, 11(2), pp. 205–214.

Islam, R. K. *et al.* (2021) 'Circulating Hydrogen Sulfide (H₂S) and Nitric Oxide (NO) Levels Are Significantly Reduced in HIV Patients Concomitant with Increased Oxidative Stress Biomarkers', *Journal of Clinical Medicine* 2021, Vol. 10, Page 4460, 10(19), p. 4460.

Ito, F., Sono, Y. and Ito, T. (2019) 'Measurement and Clinical Significance of Lipid Peroxidation as a Biomarker of Oxidative Stress: Oxidative Stress in Diabetes, Atherosclerosis, and Chronic Inflammation', *Antioxidants* 2019, Vol. 8, Page 72, 8(3), p. 72.

Itoh, K. *et al.* (1999) 'Keap1 represses nuclear activation of antioxidant responsive elements by Nrf2 through binding to the amino-terminal Neh2 domain', *Genes &*

development, 13(1), pp. 76–86.

Ivanova, I. G. and Perkins, N. D. (2019) 'Hypoxia induces rapid, STAT3 and ROS dependent, mitochondrial translocation of RelA(p65) and I κ B α ', *Bioscience Reports*, 39(9), p. 20192101.

Jaffe, E. A. *et al.* (1973) 'Culture of human endothelial cells derived from umbilical veins. Identification by morphologic and immunologic criteria', *Journal of Clinical Investigation*, 52(11), pp. 2745–2756.

Jain, S. K. *et al.* (2010) 'Low levels of hydrogen sulfide in the blood of diabetes patients and streptozotocin-treated rats causes vascular inflammation?', *Antioxidants and Redox Signaling*. Mary Ann Liebert, Inc., pp. 1333–1338.

Jain, S. K., Huning, L. and Micinski, D. (2014) 'Hydrogen sulfide upregulates glutamate-cysteine ligase catalytic subunit, glutamate-cysteine ligase modifier subunit, and glutathione and inhibits interleukin-1 β secretion in monocytes exposed to high glucose levels', *Metabolic syndrome and related disorders*, 12(5), pp. 299–302.

Jastroch, M. *et al.* (2010) 'Mitochondrial proton and electron leaks', *Essays in Biochemistry*, 47, pp. 53–67.

Jha, S. *et al.* (2008) 'Hydrogen sulfide attenuates hepatic ischemia-reperfusion injury: role of antioxidant and antiapoptotic signaling.', *American journal of physiology. Heart and circulatory physiology*, 295(2), pp. H801-6.

Jhee, K.-H. and Kruger, W. D. (2005) 'The Role of Cystathionine β -Synthase in Homocysteine Metabolism', *Antioxidants & Redox Signaling*, 7(5–6), pp. 813–822.

Jiang, B. *et al.* (2010) 'Molecular mechanism for H₂S-induced activation of K(ATP) channels.', *Antioxidants & redox signaling*, 12(10), pp. 1167–1178.

Jiang, C. *et al.* (2016) 'TNF- α induces vascular endothelial cells apoptosis through overexpressing pregnancy induced noncoding RNA in Kawasaki disease model.', *The international journal of biochemistry & cell biology*, 72, pp. 118–124.

JIANG, F. *et al.* (2020) 'Monotropein alleviates H₂O₂-induced inflammation, oxidative stress and apoptosis via NF- κ B/AP-1 signaling', *Molecular medicine reports*, 22(6), pp. 4828–4836.

Ju, Y. *et al.* (2017) 'H₂S-Mediated Protein S-Sulfhydration: A Prediction for Its Formation and Regulation', *Molecules*, 22(8), p. 1334.

Kabil, O. *et al.* (2011) 'The Quantitative Significance of the Transsulfuration Enzymes for H₂S Production in Murine Tissues', *ANTIOXIDANTS & REDOX SIGNALING*, 15(2).

Kabil, O. and Banerjee, R. (2010) 'Redox biochemistry of hydrogen sulfide.', *The Journal of biological chemistry*, 285(29), pp. 21903–7.

Kabil, O. and Banerjee, R. (2014) 'Enzymology of H₂S biogenesis, decay and signaling',
250

L. Diaz Sanchez, PhD Thesis, Aston University 2022

Antioxidants and Redox Signaling. Antioxid Redox Signal, pp. 770–782.

Kabil, O., Motl, N. and Banerjee, R. (2014) 'H₂S and its role in redox signaling.', *Biochimica et biophysica acta*, 1844(8), pp. 1355–66.

Kaczara, P. *et al.* (2016) 'Carbon monoxide shifts energetic metabolism from glycolysis to oxidative phosphorylation in endothelial cells', *FEBS letters*, 590(20), pp. 3469–3480.

Kadenbach, B. (2003) 'Intrinsic and extrinsic uncoupling of oxidative phosphorylation', *Biochimica et Biophysica Acta (BBA) - Bioenergetics*, 1604(2), pp. 77–94.

Kaludercic, N. *et al.* (2010) 'Monoamine oxidase a-mediated enhanced catabolism of norepinephrine contributes to adverse remodeling and pump failure in hearts with pressure overload', *Circulation Research*, 106(1), pp. 193–202.

Kalyanaraman, B. *et al.* (2012) 'Measuring reactive oxygen and nitrogen species with fluorescent probes: challenges and limitations', *Free radical biology & medicine*, 52(1), pp. 1–6.

Karala, A. R. and Ruddock, L. W. (2007) 'Does S-Methyl Methanethiosulfonate Trap the Thiol–Disulfide State of Proteins?', <https://home.liebertpub.com/ars>, 9(4), pp. 527–531.

Karunya, R. *et al.* (2019) 'Rapid measurement of hydrogen sulphide in human blood plasma using a microfluidic method', *Scientific Reports*, 9(1).

Kaspar, J. W., Niture, S. K. and Jaiswal, A. K. (2009) 'Nrf2:INrf2 (Keap1) signaling in oxidative stress.', *Free radical biology & medicine*, 47(9), pp. 1304–9.

Kastl, L. *et al.* (2014) 'TNF- α mediates mitochondrial uncoupling and enhances ROS-dependent cell migration *via* NF- κ B activation in liver cells', *FEBS Letters*, 588(1), pp. 175–183.

Katsuoka, F. and Yamamoto, M. (2016) 'Small Maf proteins (MafF, MafG, MafK): History, structure and function.', *Gene*, 586(2), pp. 197–205.

Khan, S. Y. *et al.* (2017) 'Premature senescence of endothelial cells upon chronic exposure to TNF α can be prevented by N-acetyl cysteine and plumericin', *Scientific Reports*, 7.

Khatri, J. J. *et al.* (2004) 'Vascular Oxidant Stress Enhances Progression and Angiogenesis of Experimental Atheroma', *Circulation*, 109(4), pp. 520–525.

Kim, J. J. *et al.* (2010) 'TNF- α -induced ROS production triggering apoptosis is directly linked to Romo1 and Bcl-XL', *Cell Death & Differentiation* 2010 17:9, 17(9), pp. 1420–1434.

Kimura, H. (2002) 'Hydrogen sulfide as a neuromodulator', *Molecular Neurobiology*. Humana Press, pp. 13–19.

Kimura, H. (2013) 'Physiological role of hydrogen sulfide and polysulfide in the central

nervous system', *Neurochemistry International*, 63(5), pp. 492–497.

Kimura, H. (2014) 'Production and physiological effects of hydrogen sulfide', *Antioxidants and Redox Signaling*, 20(5), pp. 783–793.

Kimura, H. (2015) 'Hydrogen sulfide and polysulfides as signaling molecules', *Proceedings of the Japan Academy Series B: Physical and Biological Sciences*. Japan Academy, pp. 131–159.

Kimura, H. and Hideo (2014) 'Hydrogen Sulfide and Polysulfides as Biological Mediators', *Molecules*, 19(10), pp. 16146–16157.

Kleinbongard, P., Heusch, G. and Schulz, R. (2010) 'TNF α in atherosclerosis, myocardial ischemia/reperfusion and heart failure', *Pharmacology and Therapeutics*. Pharmacol Ther, pp. 295–314.

Kobayashi, M. and Yamamoto, M. (2006) 'Nrf2–Keap1 regulation of cellular defense mechanisms against electrophiles and reactive oxygen species', *Advances in Enzyme Regulation*, 46(1), pp. 113–140.

Kolluru, G. K. *et al.* (2013) 'Hydrogen sulfide chemical biology: pathophysiological roles and detection.', *Nitric oxide : biology and chemistry*, 35, pp. 5–20.

Kolluru, G. K., Shen, X. and Kevil, C. G. (2020) 'Reactive Sulfur Species', *Arteriosclerosis, Thrombosis, and Vascular Biology*, 40, pp. 874–884.

Kondo, K. *et al.* (2013) 'H₂S protects against pressure overload-induced heart failure via upregulation of endothelial nitric oxide synthase.', *Circulation*, 127(10), pp. 1116–1127.

Korthuis, R. J. (2011) 'Regulation of Vascular Tone in Skeletal Muscle', in *Skeletal Muscle Circulation*. San Rafael (CA): Morgan & Claypool Life Sciences.

Krajewski, W. A. (2019) 'Ubiquitylation: How Nucleosomes Use Histones to Evict Histones', *Trends in Cell Biology*, 29(9), pp. 689–694.

Kraus, D. W. and Wittenberg, J. B. (1990) 'Hemoglobins of the *Lucina pectinata*/bacteria symbiosis. I. Molecular properties, kinetics and equilibria of reactions with ligands.', *Journal of Biological Chemistry*, 265(27), pp. 16043–16053.

Krishnan, N. *et al.* (2011) 'H₂S-Induced sulphydration of the phosphatase PTP1B and its role in the endoplasmic reticulum stress response.', *Science signaling*, 4(203), p. ra86.

Krüger-Genge, A. *et al.* (2019) 'Vascular endothelial cell biology: An update', *International Journal of Molecular Sciences*. MDPI AG.

Kundu, S. *et al.* (2012) 'Oxidative stress as a potential biomarker for determining disease activity in patients with Rheumatoid Arthritis', *Free Radical Research*, 46(12), pp. 1482–1489.

Kushnareva, Y. E. *et al.* (2012) 'Loss of OPA1 disturbs cellular calcium homeostasis and

sensitizes for excitotoxicity', *Cell Death & Differentiation* 2013 20:2, 20(2), pp. 353–365.

Landmesser, U. *et al.* (2003) 'Oxidation of tetrahydrobiopterin leads to uncoupling of endothelial cell nitric oxide synthase in hypertension', *Journal of Clinical Investigation*, 111(8), pp. 1201–1209.

Latorre, E. *et al.* (2018) 'Mitochondria-targeted hydrogen sulfide attenuates endothelial senescence by selective induction of splicing factors HNRNPD and SRSF2', *Aging*, 10(7), pp. 1666–1681.

Lau, N. and Pluth, M. D. (2019) 'Reactive sulfur species (RSS): persulfides, polysulfides, potential, and problems', *Current Opinion in Chemical Biology*, 49, pp. 1–8.

Laviola, L. *et al.* (2013) 'TNF α Signals via p66Shc to Induce E-Selectin, Promote Leukocyte Transmigration and Enhance Permeability in Human Endothelial Cells', *PLoS ONE*. Edited by M. Ushio-Fukai, 8(12), p. e81930.

Lee, J. *et al.* (2017) 'Interaction of IL-6 and TNF- α contributes to endothelial dysfunction in type 2 diabetic mouse hearts.', *PloS one*, 12(11), p. e0187189.

Lee, K. U. *et al.* (2005) 'Effects of recombinant adenovirus-mediated uncoupling protein 2 overexpression on endothelial function and apoptosis', *Circulation Research*, 96(11), pp. 1200–1207.

Lee, TI *et al.* (2019) 'Sodium hydrosulphide restores tumour necrosis factor- α -induced mitochondrial dysfunction and metabolic dysregulation in HL-1 cells', *Journal of cellular and molecular medicine*, 23(11), pp. 7641–7650.

Lermant, A. and Murdoch, C. E. (2019) 'Cysteine Glutathionylation Acts as a Redox Switch in Endothelial Cells', *Antioxidants*, 8(8), pp. 1–25.

Lertkiatmongkol, P. *et al.* (2016) 'Endothelial functions of platelet/endothelial cell adhesion molecule-1 (CD31)', *Current opinion in hematology*, 23(3), pp. 253–259.

Leskova, A. *et al.* (2017) 'Role of thiosulfate in hydrogen sulfide-dependent redox signaling in endothelial cells', *American Journal of Physiology - Heart and Circulatory Physiology*, 313(2), pp. H256–H264.

Levitt, M. D. *et al.* (1999) *Introduction Detoxification of hydrogen sulfide and methanethiol in the cecal mucosa*, *J. Clin. Invest.*

Levitt, M. D., Abdel-Rehim, M. S. and Furne, J. (2011) 'Free and acid-labile hydrogen sulfide concentrations in mouse tissues: Anomalously high free hydrogen sulfide in aortic tissue', *Antioxidants and Redox Signaling*, 15(2), pp. 373–378.

Ley, K. *et al.* (2007) 'Getting to the site of inflammation: the leukocyte adhesion cascade updated', *Nature Reviews Immunology* 2007 7:9, 7(9), pp. 678–689.

Li, J. *et al.* (2019) 'Hydrogen sulfide improves endothelial dysfunction by inhibiting the vicious cycle of NLRP3 inflammasome and oxidative stress in spontaneously

hypertensive rats', *Journal of Hypertension*, 37(8), pp. 1633–1643.

Li, L. *et al.* (2008) 'Characterization of a Novel, Water-Soluble Hydrogen Sulfide-Releasing Molecule (GYY4137) New Insights Into the Biology of Hydrogen Sulfide', *Circulation*, 117(18), pp. 2351–2360.

Li, Q., Lancaster, J. R. and Jr. (2013) 'Chemical foundations of hydrogen sulfide biology.', *Nitric oxide : biology and chemistry*, 35, pp. 21–34.

Li, S. and Yang, G. (2015) 'Hydrogen Sulfide Maintains Mitochondrial DNA Replication via Demethylation of TFAM', *Antioxidants and Redox Signaling*, 23(7), pp. 630–642.

Li, Xinyuan *et al.* (2020) 'Anti-inflammatory cytokines IL-35 and IL-10 block atherogenic lysophosphatidylcholine-induced, mitochondrial ROS-mediated innate immune activation, but spare innate immune memory signature in endothelial cells', *Redox Biology*, 28, p. 101373.

Li, Xia *et al.* (2020) 'Interplay of TNF- α , soluble TNF receptors and oxidative stress in coronary chronic total occlusion of the oldest patients with coronary heart disease', *Cytokine*, 125.

Liao, B.-C. *et al.* (2010) 'The Glutaredoxin/Glutathione System Modulates NF- κ B Activity by Glutathionylation of p65 in Cinnamaldehyde-Treated Endothelial Cells', *Toxicological Sciences*, 116(1), pp. 151–163.

Libby, P. (2017) 'Interleukin-1 Beta as a Target for Atherosclerosis Therapy: Biological Basis of CANTOS and Beyond', *Journal of the American College of Cardiology*, 70(18), pp. 2278–2289.

Lidington, E. *et al.* (1999) 'A comparison of primary endothelial cells and endothelial cell lines for studies of immune interactions', *Transplant Immunology*, 7(4), pp. 239–246.

Lieber, M. *et al.* (1976) 'A continuous tumor-cell line from a human lung carcinoma with properties of type II alveolar epithelial cells.', *International journal of cancer*, 17(1), pp. 62–70.

Lin, F. *et al.* (2020) 'Hydrogen sulfide protects against high glucose-induced human umbilical vein endothelial cell injury through activating PI3K/Akt/eNOS pathway', *Drug Design, Development and Therapy*, 14, pp. 621–633.

Lin, J. *et al.* (2018) 'Exogenous hydrogen sulfide protects human umbilical vein endothelial cells against high glucose-induced injury by inhibiting the necroptosis pathway', *International Journal of Molecular Medicine*, 41(3), pp. 1477–1486.

Lin, V. S., Lippert, A. R. and Chang, C. J. (2013) 'Cell-trappable fluorescent probes for endogenous hydrogen sulfide signaling and imaging H₂O₂-dependent H₂S production', *Proceedings of the National Academy of Sciences of the United States of America*, 110(18), p. 7131.

Lind, L. (2006) 'Impact of ageing on the measurement of endothelium-dependent

vasodilation.', *Pharmacological reports : PR*, 58 Suppl, pp. 41–46.

Lippert, A. R. (2014) 'Designing reaction-based fluorescent probes for selective hydrogen sulfide detection', *Journal of Inorganic Biochemistry*, 133, pp. 136–142.

Lippert, A. R., Van De Bittner, G. C. and Chang, C. J. (2011) 'Boronate Oxidation as a Bioorthogonal Reaction Approach for Studying the Chemistry of Hydrogen Peroxide in Living Systems', *Accounts of chemical research*, 44(9), p. 793.

Lisa, F. Di *et al.* (2009) 'Mitochondria and vascular pathology', *Pharmacological Reports*, 61, pp. 123–130.

Liu, B. *et al.* (2018) 'Protective effect of KLF15 on vascular endothelial dysfunction induced by TNF- α ', *Molecular Medicine Reports*, 18, pp. 1987–1994.

Liu, C. *et al.* (2011) 'Capture and visualization of hydrogen sulfide by a fluorescent probe', *Angewandte Chemie (International ed. in English)*, 50(44), pp. 10327–10329.

Liu, J. *et al.* (2011) 'Vascular bed-specific regulation of the von Willebrand factor promoter in the heart and skeletal muscle', *Blood*, 117(1), p. 351.

Liu, L. L. *et al.* (2014) 'A role for diallyl trisulfide in mitochondrial antioxidative stress contributes to its protective effects against vascular endothelial impairment', *European Journal of Pharmacology*, 725(1), pp. 23–31.

Liu, N. *et al.* (2017) 'Hydrogen Sulphide modulating mitochondrial morphology to promote mitophagy in endothelial cells under high-glucose and high-palmitate.', *Journal of cellular and molecular medicine*, 21(12), pp. 3190–3203.

Liu, T. *et al.* (2017) 'NF- κ B signaling in inflammation', *Signal Transduction and Targeted Therapy*, 2, p. 17023.

Liu, Y. *et al.* (2003) 'Mitochondrial sources of H₂O₂ generation play a key role in flow-mediated dilation in human coronary resistance arteries', *Circulation Research*, 93(6), pp. 573–580.

Liu, Y. *et al.* (2014) 'Hydrogen sulfide maintains mesenchymal stem cell function and bone homeostasis via regulation of Ca(2+) channel sulfhydration.', *Cell stem cell*, 15(1), pp. 66–78.

Liu, Z. *et al.* (2013) 'The hydrogen sulfide donor, GYY4137, exhibits anti-atherosclerotic activity in high fat fed apolipoprotein E-/- mice', *British Journal of Pharmacology*, 169(8), pp. 1795–1809.

Liu, Z. *et al.* (2020) 'Hydrogen Sulfide Protects against Paraquat-Induced Acute Liver Injury in Rats by Regulating Oxidative Stress, Mitochondrial Function, and Inflammation.', *Oxidative medicine and cellular longevity*, 2020, p. 6325378.

Livak, K. J. and Schmittgen, T. D. (2001) 'Analysis of relative gene expression data using real-time quantitative PCR and the 2(-Delta Delta C(T)) Method', *Methods (San Diego*,

Calif.), 25(4), pp. 402–408.

Losó n, O. C. *et al.* (2013) 'Fis1, Mff, MiD49, and MiD51 mediate Drp1 recruitment in mitochondrial fission', *Molecular biology of the cell*, 24(5), pp. 659–667.

Lu, C. *et al.* (2013) 'S-sulfhydration/desulfhydration and S-nitrosylation/ denitrosylation: A Common Paradigm for Gasotransmitter Signaling by H₂S and NO', *Methods*, 62(2), pp. 177–181.

Lugrin, J. *et al.* (2014) 'The role of oxidative stress during inflammatory processes', *Biological Chemistry*, 395(2), pp. 203–230.

Ma, L. *et al.* (2014) 'Anti-peroxynitrite treatment ameliorated vasorelaxation of resistance arteries in aging rats: involvement with NO-sGC-cGKs pathway', *PloS one*, 9(8).

Madamanchi, N. R. and Runge, M. S. (2007) 'Mitochondrial dysfunction in atherosclerosis', *Circulation Research*. Circ Res, pp. 460–473.

Madurga, A. *et al.* (2015) 'The H₂S-generating enzymes cystathionine β-synthase and cystathionine γ-lyase play a role in vascular development during normal lung alveolarization.', *American journal of physiology. Lung cellular and molecular physiology*, 309(7), pp. L710-24.

Mahajan, S. D. *et al.* (2015) 'C5a alters blood-brain barrier integrity in a human in vitro model of systemic lupus erythematosus', *Immunology*, 146(1), pp. 130–143.

Malone Rubright, S. L., Pearce, L. L. and Peterson, J. (2017) 'Environmental toxicology of hydrogen sulfide', *Nitric Oxide - Biology and Chemistry*. Academic Press Inc., pp. 1–13.

Manning, J. E. *et al.* (2021) 'Insights Into Leukocyte Trafficking in Inflammatory Arthritis – Imaging the Joint', *Frontiers in Cell and Developmental Biology*, 9, p. 427.

Martinez-Carreres, L., Nasrallah, A. and Fajas, L. (2017) 'Cancer: Linking powerhouses to suicidal bags', *Frontiers in Oncology*, 7(SEP), p. 204.

Marutani, E. *et al.* (2015) 'Thiosulfate Mediates Cytoprotective Effects of Hydrogen Sulfide Against Neuronal Ischemia.', *Journal of the American Heart Association*, 4(11).

Marutani, E. and Ichinose, F. (2020) 'Emerging pharmacological tools to control hydrogen sulfide signaling in critical illness', *Intensive Care Medicine Experimental*, 8(1), pp. 1–14.

Marzetti, E. *et al.* (2009) 'Cellular Mechanisms of Cardioprotection by Calorie Restriction: State of the Science and Future Perspectives', *Clinics in Geriatric Medicine*. Clin Geriatr Med, pp. 715–732.

Mauch, L. *et al.* (2007) 'Chronic granulomatous disease (CGD) and complete myeloperoxidase deficiency both yield strongly reduced dihydrorhodamine 123 test signals but can be easily discerned in routine testing for CGD', *Clinical chemistry*, 53(5),

256

pp. 890–896.

Mazzuca, M. Q. and Khalil, R. A. (2012) 'Vascular endothelin receptor type B: structure, function and dysregulation in vascular disease', *Biochemical pharmacology*, 84(2), pp. 147–162.

McDonnell, M. A. *et al.* (2003) 'Caspase-9 is activated in a cytochrome c-independent manner early during TNF α -induced apoptosis in murine cells', *Cell Death & Differentiation* 2003 10:9, 10(9), pp. 1005–1015.

McNally, J. S. *et al.* (2003) 'Role of xanthine oxidoreductase and NAD(P)H oxidase in endothelial superoxide production in response to oscillatory shear stress', *American Journal of Physiology - Heart and Circulatory Physiology*, 285(6 54-6).

Meade, E. A. *et al.* (1996) 'Prostaglandins and Related Compounds Lipid Messengers with Many Actions', *Lipid Second Messengers*, pp. 285–305.

Meininger, G. A. and Davis, M. J. (1992) 'Cellular mechanisms involved in the vascular myogenic response', <https://doi.org/10.1152/ajpheart.1992.263.3.H647>, 263(3 32-3).

Meng, G. *et al.* (2018) 'Protein S-sulfhydration by hydrogen sulfide in cardiovascular system', *British Journal of Pharmacology*, 175(8), pp. 1146–1156.

Meng, W. *et al.* (2017) 'Neglected role of hydrogen sulfide in sulfur mustard poisoning: Keap1 S-sulfhydration and subsequent Nrf2 pathway activation', *Scientific Reports*, 7, p. 9433.

Meo, S. Di *et al.* (2016) 'Role of ROS and RNS Sources in Physiological and Pathological Conditions', *Oxidative Medicine and Cellular Longevity*, 2016.

Michiels, C. (2003) 'Endothelial cell functions', *Journal of Cellular Physiology*, 196(3), pp. 430–443.

Mir, S., Sen, T. and Sen, N. (2014) 'Cytokine-induced GAPDH sulfhydration affects PSD95 degradation and memory', *Molecular cell*, 56(6), pp. 786–795.

Módis, K. *et al.* (2013) 'Hydrogen sulfide-mediated stimulation of mitochondrial electron transport involves inhibition of the mitochondrial phosphodiesterase 2A, elevation of cAMP and activation of protein kinase A', *Biochemical Pharmacology*, 86(9), pp. 1311–1319.

Moncada, S. and Higgs, E. A. (2006) 'The discovery of nitric oxide and its role in vascular biology', *British journal of pharmacology*, 147 Suppl(Suppl 1).

Moreno, J. C. *et al.* (2002) 'Inactivating mutations in the gene for thyroid oxidase 2 (THOX2) and congenital hypothyroidism', *The New England journal of medicine*, 347(2), pp. 95–102.

Mukherjee, T. K., Mukhopadhyay, S. and Hoidal, J. R. (2005) 'The role of reactive oxygen species in TNF α -dependent expression of the receptor for advanced glycation

end products in human umbilical vein endothelial cells', *Biochimica et Biophysica Acta - Molecular Cell Research*, 1744(2), pp. 213–223.

Muller, W. A. (2003) 'Leukocyte–endothelial-cell interactions in leukocyte transmigration and the inflammatory response', *Trends in Immunology*, 24(6), pp. 326–333.

Munke, M. *et al.* (1988) *The Gene for Cystathionine P-Synthase (CBS) Maps to the Subtelomeric Region on Human Chromosome 21q and to Proximal Mouse Chromosome 17*, *Am. J. Hum. Genet.*

Munro, D. *et al.* (2016) 'The thioredoxin and glutathione-dependent H₂O₂ consumption pathways in muscle mitochondria: Involvement in H₂O₂ metabolism and consequence to H₂O₂ efflux assays', *Free Radical Biology and Medicine*, 96, pp. 334–346.

Münzel, T. *et al.* (2017) 'Impact of Oxidative Stress on the Heart and Vasculature Part 2 of a 3-Part Series HHS Public Access PATHOPHYSIOLOGICAL ROLE OF OXIDATIVE STRESS IN HEART FAILURE', *J Am Coll Cardiol*, 70(2), pp. 212–229.

Murphy, M. P. (2009) 'How mitochondria produce reactive oxygen species', *Biochemical Journal*, 417(Pt 1), p. 1.

Mustafa, A. K. *et al.* (2009) 'H₂S Signals Through Protein S-Sulfhydration', *Sci Signal*, 2(96), p. ra72.

Mustafa, A. K. *et al.* (2011) 'Hydrogen Sulfide as Endothelial Derived Hyperpolarizing Factor Sulfhydrates Potassium Channels', *Circ Res*, 109(11), pp. 1259–1268.

Mustafa, A. K., Gadalla, M. M. and Snyder, S. H. (2009) 'Signaling by gasotransmitters', *Science signaling*, 2(68).

Musz, P. *et al.* (2021) 'Non-invasive assessment of endothelial function — a review of available methods', *Medical Research Journal*, 6(1), pp. 53–58.

Myers, J. *et al.* (2005) 'Altered endothelial function in isolated human myometrial vessels induced by plasma from women with pre-eclampsia is not reproducible in isolated mouse vessels', *Clinical science (London, England : 1979)*, 108(5), pp. 457–462.

Mylon, S. E. and Benoit, G. (2001) 'Subnanomolar detection of acid-labile sulfides by the classical methylene blue method coupled to HPLC', *Environmental science & technology*, 35(22), pp. 4544–4548.

Nadar, S., Blann, A. D. and Lip, G. Y. H. (2004) 'Endothelial dysfunction: methods of assessment and application to hypertension.', *Current pharmaceutical design*, 10(29), pp. 3591–605.

Nagahara, N. (2013) 'Regulation of mercaptopyruvate sulfurtransferase activity via intrasubunit and intersubunit redox-sensing switches.', *Antioxidants & redox signaling*, 19(15), pp. 1792–1802.

Nagahara, N. and Katayama, A. (2005) 'Post-translational regulation of

mercaptopyruvate sulfurtransferase via a low redox potential cysteine-sulfenate in the maintenance of redox homeostasis', *Journal of Biological Chemistry*, 280(41), pp. 34569–34576.

Nagy, P. *et al.* (2014) 'Chemical aspects of hydrogen sulfide measurements in physiological samples', *Biochimica et biophysica acta*, 1840(2), pp. 876–891.

Nakamura, H. *et al.* (2012) 'p53 promotes cardiac dysfunction in diabetic mellitus caused by excessive mitochondrial respiration-mediated reactive oxygen species generation and lipid accumulation', *Circulation. Heart failure*, 5(1), pp. 106–115.

Nakano, H. *et al.* (2006) 'Reactive oxygen species mediate crosstalk between NF-kappaB and JNK', *Cell death and differentiation*, 13(5), pp. 730–737.

Nan, J. *et al.* (2017) 'TNFR2 Stimulation Promotes Mitochondrial Fusion via Stat3- and NF-kB-Dependent Activation of OPA1 Expression', *Circulation research*, 121(4), pp. 392–410.

Nazarewicz, R. R. *et al.* (2013) 'Nox2 as a potential target of mitochondrial superoxide and its role in endothelial oxidative stress', *American Journal of Physiology - Heart and Circulatory Physiology*, 305(8), p. H1131.

Newby, D. E. *et al.* (1999) 'Endothelial dysfunction, impaired endogenous fibrinolysis, and cigarette smoking: a mechanism for arterial thrombosis and myocardial infarction', *Circulation*, 99(11), pp. 1411–1415.

Ng, H. H. *et al.* (2017) 'Chronic NaHS treatment decreases oxidative stress and improves endothelial function in diabetic mice', *Diabetes and Vascular Disease Research*, 14(3), pp. 246–253.

Nicholson, C. K. *et al.* (2013) 'Thioredoxin 1 is essential for sodium sulfide-mediated cardioprotection in the setting of heart failure.', *Arteriosclerosis, thrombosis, and vascular biology*, 33(4), pp. 744–751.

Nolfi-Donagan, D., Braganza, A. and Shiva, S. (2020) 'Mitochondrial electron transport chain: Oxidative phosphorylation, oxidant production, and methods of measurement', *Redox Biology*. Elsevier B.V., p. 37:101674.

Nordberg, J. and Arnér, E. S. (2001) 'Reactive oxygen species, antioxidants, and the mammalian thioredoxin system.', *Free radical biology & medicine*, 31(11), pp. 1287–1312.

Nourshargh, S. and Alon, R. (2014) 'Leukocyte migration into inflamed tissues', *Immunity*, 41(5), pp. 694–707.

Nunes, J. P. S. *et al.* (2021) 'Co-Exposure of Cardiomyocytes to IFN- γ and TNF- α Induces Mitochondrial Dysfunction and Nitro-Oxidative Stress: Implications for the Pathogenesis of Chronic Chagas Disease Cardiomyopathy', *Frontiers in Immunology*, 12.

Obeng, E. (2021) 'Apoptosis (programmed cell death) and its signals - A review', *Brazilian journal of biology = Revista brasleira de biologia*, 81(4), pp. 1133–1143.

Oldendorf, W. H., Cornford, M. E. and Brown, W. J. (1977) 'The large apparent work capability of the blood-brain barrier: A study of the mitochondrial content of capillary endothelial cells in brain and other tissues of the rat', *Annals of Neurology*, 1(5), pp. 409–417.

de Oliveira, J. S. S. *et al.* (2018) 'Reactive oxygen species generation mediated by NADPH oxidase and PI3K/Akt pathways contribute to invasion of *Streptococcus agalactiae* in human endothelial cells', *Memórias do Instituto Oswaldo Cruz*, 113(6), pp. 1–8.

Oliver, J. J., Webb, D. J. and Newby, D. E. (2005) 'Stimulated tissue plasminogen activator release as a marker of endothelial function in humans', *Arteriosclerosis, thrombosis, and vascular biology*, 25(12), pp. 2470–2479.

Onyewu, S. C., Coombs, A. T. and Kromah, F. (2021) 'Vascular Endothelial Dysfunction and Inflammatory States', in Scher, C. S. *et al.* (eds) *Essentials of Blood Product Management in Anesthesia Practice*. Cham: Springer International Publishing, pp. 217–232.

Ooi, B. K., Goh, B. H. and Yap, W. H. (2017) 'Oxidative Stress in Cardiovascular Diseases: Involvement of Nrf2 Antioxidant Redox Signaling in Macrophage Foam Cells Formation.', *International journal of molecular sciences*, 18(11).

Ormstad, H. *et al.* (2011) 'Serum cytokine and glucose levels as predictors of poststroke fatigue in acute ischemic stroke patients', *Journal of neurology*, 258(4), pp. 670–676.

De Palma, C. *et al.* (2006) 'Endothelial Nitric Oxide Synthase Activation by Tumor Necrosis Factor Through Neutral Sphingomyelinase 2, Sphingosine Kinase 1, and Sphingosine 1 Phosphate Receptors A Novel Pathway Relevant to the Pathophysiology of Endothelium', *Thromb Vasc Biol*, 26, pp. 99–105.

Palmer, R. M. J., Ferrige, A. G. and Moncada, S. (1987) 'Nitric oxide release accounts for the biological activity of endothelium-derived relaxing factor', *Nature*, 327(6122), pp. 524–526.

Palomer, X. *et al.* (2009) 'TNF- α reduces PGC-1 α expression through NF- κ B and p38 MAPK leading to increased glucose oxidation in a human cardiac cell model', *Cardiovascular Research*, 81(4), pp. 703–712.

Pan, J. and Carroll, K. S. (2013) 'Persulfide Reactivity in the Detection of Protein S - Sulfhydration', *ACS Chemical Biology*, 8(6), pp. 1110–1116.

Pan, L.-L. *et al.* (2011) 'Hydrogen sulfide attenuated tumor necrosis factor- α -induced inflammatory signaling and dysfunction in vascular endothelial cells.', *PLoS one*, 6(5), p. e19766.

Pang, Y. *et al.* (2007) 'IGF-1 protects oligodendrocyte progenitors against TNF α -induced

damage by activation of PI3K/Akt and interruption of the mitochondrial apoptotic pathway', *Glia*, 55(11), pp. 1099–1107.

Paone, S. *et al.* (2018) 'Endothelial cell apoptosis and the role of endothelial cell-derived extracellular vesicles in the progression of atherosclerosis', *Cellular and Molecular Life Sciences* 2018 76:6, 76(6), pp. 1093–1106.

Papapetropoulos, A. *et al.* (2009) 'Hydrogen sulfide is an endogenous stimulator of angiogenesis', *Proceedings of the National Academy of Sciences*, 106(51), pp. 21972–21977.

Park, H.-J. *et al.* (2006) 'Human umbilical vein endothelial cells and human dermal microvascular endothelial cells offer new insights into the relationship between lipid metabolism and angiogenesis', *Stem cell reviews*, 2(2), pp. 93–101.

Park, S. Y. Y. *et al.* (2018) 'Age-related endothelial dysfunction in human skeletal muscle feed arteries: the role of free radicals derived from mitochondria in the vasculature', *Acta Physiologica*, 222(1), p. e12893.

Patel, P. *et al.* (2009) 'The endogenous production of hydrogen sulphide in intrauterine tissues', *Reproductive Biology and Endocrinology*, 7.

Paul, Bindu D and Snyder, S. H. (2015a) 'H₂S: A Novel Gasotransmitter that Signals by Sulfhydration.', *Trends in biochemical sciences*, 40(11), pp. 687–700.

Paul, Bindu D and Snyder, S. H. (2015b) 'Modes of physiologic H₂S signaling in the brain and peripheral tissues.', *Antioxidants & redox signaling*, 22(5), pp. 411–23.

Paul, Bindu D. and Snyder, S. H. (2015) 'Protein Sulfhydration', *Methods in Enzymology*, 555, pp. 79–90.

Paulus, P., Jennewein, C. and Zacharowski, K. (2011) 'Biomarkers of endothelial dysfunction: can they help us deciphering systemic inflammation and sepsis?', *Biomarkers: biochemical indicators of exposure, response, and susceptibility to chemicals*, 16 Suppl 1(SUPPL. 1).

Peña-Blanco, A. and García-Sáez, A. J. (2018) 'Bax, Bak and beyond - mitochondrial performance in apoptosis', *The FEBS journal*, 285(3), pp. 416–431.

Penna, C., Perrelli, M. G. and Pagliaro, P. (2013) 'Mitochondrial pathways, permeability transition pore, and redox signaling in cardioprotection: Therapeutic implications', *Antioxidants and Redox Signaling*, pp. 556–599.

Perry, S. W. *et al.* (2011) 'Mitochondrial membrane potential probes and the proton gradient: a practical usage guide', *BioTechniques*, 50(2), p. 98.

Picton, R. *et al.* (2002) 'Mucosal protection against sulphide: importance of the enzyme rhodanese', *Gut*, 50, pp. 201–205.

Pierelli, G. *et al.* (2017) 'Uncoupling protein 2: A key player and a potential therapeutic

target in vascular diseases', *Oxidative Medicine and Cellular Longevity*, 2017(7348372).

Pober, J. S. and Sessa, W. C. (2007) 'Evolving functions of endothelial cells in inflammation.', *Nature reviews. Immunology*, 7(10), pp. 803–15.

Poda, G. A. (1966) 'Hydrogen sulfide can be handled safely.', *Archives of environmental health*, 12(6), pp. 795–800.

Polhemus, D. J. *et al.* (2015) 'A Novel Hydrogen Sulfide Prodrug, SG1002, Promotes Hydrogen Sulfide and Nitric Oxide Bioavailability in Heart Failure Patients', *Cardiovascular Therapeutics*, 33(4), pp. 216–226.

Pollard, D. A., Pollard, T. D. and Pollard, K. S. (2019) 'Empowering statistical methods for cellular and molecular biologists', *Molecular Biology of the Cell*, 30(12), pp. 1359–1368.

Potenza, D. M. *et al.* (2017) 'Hydrogen sulphide triggers VEGF-induced intracellular Ca²⁺ signals in human endothelial cells but not in their immature progenitors', *CELL CALCIUM*, 56(3), pp. 225–234.

Predmore, B. L. *et al.* (2012) 'The polysulfide diallyl trisulfide protects the ischemic myocardium by preservation of endogenous hydrogen sulfide and increasing nitric oxide bioavailability', *American journal of physiology. Heart and circulatory physiology*, 302(11).

Predmore, B. L., Lefer, D. J. and Gojon, G. (2012) 'Hydrogen sulfide in biochemistry and medicine.', *Antioxidants and Redox Signaling*, 17(1), pp. 119–140.

Qin, G. *et al.* (2015) 'Artesunate induces apoptosis via a ROS-independent and Bax-mediated intrinsic pathway in HepG2 cells.', *Experimental cell research*, 336(2), pp. 308–317.

Qiu, Y. *et al.* (2018) 'GYY4137 protects against myocardial ischemia/reperfusion injury via activation of the PHLPP-1/Akt/Nrf2 signaling pathway in diabetic mice', *Journal of Surgical Research*, 225, pp. 29–39.

Quinlan, C. L. *et al.* (2012) 'Mitochondrial complex II can generate reactive oxygen species at high rates in both the forward and reverse reactions', *Journal of Biological Chemistry*, 287(32), pp. 27255–27264.

Radi, R., Cassina, A. and Hodara, R. (2002) 'Nitric oxide and peroxynitrite interactions with mitochondria', *Biological Chemistry. Biol Chem*, pp. 401–409.

Rafelski, S. M. and Marshall, W. F. (2008) 'Building the cell: design principles of cellular architecture', *Nature Reviews Molecular Cell Biology* 2008 9:8, 9(8), pp. 593–602.

Raghunath, A. *et al.* (2018) 'Antioxidant response elements: Discovery, classes, regulation and potential applications', *Redox Biology*, 17, pp. 297–314.

Rainwater, R. *et al.* (1995) 'Role of cysteine residues in regulation of p53 function',
262

Molecular and cellular biology, 15(7), pp. 3892–3903.

Rajendran, P. *et al.* (2013) 'The Vascular Endothelium and Human Diseases', *Int. J. Biol. Sci.*, 9(10), pp. 1057–1069.

Rao, G. *et al.* (2020) 'Cystathionine beta synthase regulates mitochondrial dynamics and function in endothelial cells', *FASEB journal: official publication of the Federation of American Societies for Experimental Biology*, 34(7), p. 9372.

Ren, X. *et al.* (2017) 'Redox Signaling Mediated by Thioredoxin and Glutathione Systems in the Central Nervous System', *Antioxidants & redox signaling*, 27(13), pp. 989–1010.

Renga, B. (2011) 'Hydrogen Sulfide Generation in Mammals: The Molecular Biology of Cystathionine- β -Synthase (CBS) and Cystathionine- γ -Lyase (CSE)', *Inflammation & Allergy - Drug Targets*, 10(2), pp. 85–91.

Rhee, S. G. (2016) 'Overview on Peroxiredoxin', *Molecules and Cells*, 39(1), p. 1.

Ribatti, D. and Crivellato, E. (2012) "Sprouting angiogenesis", a reappraisal', *Developmental biology*, 372(2), pp. 157–165.

Riederer, I. *et al.* (2010) 'Irradiation-Induced Up-Regulation of HLA-E on Macrovascular Endothelial Cells Confers Protection against Killing by Activated Natural Killer Cells', *PLoS ONE*. Edited by N. Cordes, 5(12), p. e15339.

Robert, K. *et al.* (2003) 'Expression of the Cystathionine β Synthase (CBS) Gene During Mouse Development and Immunolocalization in Adult Brain', *Journal of Histochemistry & Cytochemistry*, 51(3), pp. 363–371.

Romagnoli, M. *et al.* (2010) 'Xanthine oxidase-induced oxidative stress causes activation of NF- κ B and inflammation in the liver of type I diabetic rats', *Free Radical Biology and Medicine*, 49(2), pp. 171–177.

Romaschenko, V. P. *et al.* (2015) 'Low Concentrations of Uncouplers of Oxidative Phosphorylation Prevent Inflammatory Activation of Endothelial Cells by Tumor Necrosis Factor', *Biochemistry. Biokhimiia*, 80(5), pp. 610–619.

Rössig, L. *et al.* (2001) 'Vitamin C Inhibits Endothelial Cell Apoptosis in Congestive Heart Failure', *Circulation*, 104(18), pp. 2182–2187.

Roy, S. and Nicholson, D. W. (2000) 'Cross-Talk in Cell Death Signaling', *The Journal of Experimental Medicine*, 192(8), p. f21.

Rudolph, T. K. and Freeman, B. A. (2009) 'Transduction of redox signaling by electrophile-protein reactions.', *Science signaling*, 2(90), p. re7.

Ryoo, I. geun and Kwak, M. K. (2018) 'Regulatory crosstalk between the oxidative stress-related transcription factor Nfe2l2/Nrf2 and mitochondria', *Toxicology and applied pharmacology*, 359, pp. 24–33.

Saha, S. *et al.* (2016) 'Cystathionine b-synthase regulates endothelial function via protein S-sulfhydration', *The FASEB Journal • Research Communication*, 30(1), pp. 441–456.

Sanchez-Aranguren, L. C., Ahmad, S., *et al.* (2020) 'Bioenergetic effects of hydrogen sulfide suppress soluble Flt-1 and soluble endoglin in cystathionine gamma-lyase compromised endothelial cells', *Scientific Reports*, 10(1), pp. 1–11.

Sanchez-Aranguren, L. C., Rezai, H., *et al.* (2020) 'MZe786 Rescues Cardiac Mitochondrial Activity in High sFlt-1 and Low HO-1 Environment.', *Antioxidants (Basel, Switzerland)*, 9(7).

Sanchez, L. D. *et al.* (2022) 'Exploring mitochondrial hydrogen sulfide signalling for therapeutic interventions in vascular diseases', *Advances in Redox Research*, 4, p. 100030.

Sandoo, A. *et al.* (2010) *The Endothelium and Its Role in Regulating Vascular Tone, The Open Cardiovascular Medicine Journal*.

Sasakura, K. *et al.* (2011) 'Development of a highly selective fluorescence probe for hydrogen sulfide', *Journal of the American Chemical Society*, 133(45), pp. 18003–18005.

Savoia, C. *et al.* (2017) 'Microvascular Alterations in Hypertension and Vascular Aging.', *Current hypertension reviews*, 13(1), pp. 16–23.

Schoors, S. *et al.* (2015) 'Fatty acid carbon is essential for dNTP synthesis in endothelial cells', *Nature 2015 520:7546*, 520(7546), pp. 192–197.

Scialò, F., Fernández-Ayala, D. J. and Sanz, A. (2017) 'Role of mitochondrial reverse electron transport in ROS signaling: Potential roles in health and disease', *Frontiers in Physiology*. Frontiers Media S.A., p. 428.

Scioli, M. G. *et al.* (2020) 'Oxidative Stress and New Pathogenetic Mechanisms in Endothelial Dysfunction: Potential Diagnostic Biomarkers and Therapeutic Targets', *Journal of Clinical Medicine 2020, Vol. 9, Page 1995*, 9(6), p. 1995.

Scrivner, O. *et al.* (2021) 'Expanding the Reactive Sulfur Metabolome: Intracellular and Efflux Measurements of Small Oxoacids of Sulfur (SOS) and H₂S in Human Primary Vascular Cell Culture', *Molecules*, 26(23).

Searcy, D. G. and Peterson, M. A. (2004) 'Hydrogen sulfide consumption measured at low steady state concentrations using a sulfidostat', *Analytical biochemistry*, 324(2), pp. 269–275.

Seki, T. *et al.* (2018) 'd-Cysteine promotes dendritic development in primary cultured cerebellar Purkinje cells via hydrogen sulfide production', *Molecular and Cellular Neuroscience*, 93, pp. 36–47.

Sen, N. *et al.* (2012) 'Hydrogen sulfide-linked sulfhydration of NF- κ B mediates its anti-

apoptotic actions', *Molecular cell*, 45(1), pp. 13–24.

Sen, U. *et al.* (2009) 'Hydrogen sulfide ameliorates hyperhomocysteinemia-associated chronic renal failure', *American Journal of Physiology - Renal Physiology*, 297(2).

Sena, L. A. and Chandel, N. S. (2012) 'Physiological roles of mitochondrial reactive oxygen species', *Molecular Cell*. Cell Press, pp. 158–167.

Shaito, A. *et al.* (2022) 'Oxidative Stress-Induced Endothelial Dysfunction in Cardiovascular Diseases', *Frontiers in Bioscience - Landmark*, 27(3), p. 105.

Shakibaei, M. *et al.* (2005) 'Redox regulation of apoptosis by members of the TNF superfamily.', *Antioxidants & redox signaling*, 7(3–4), pp. 482–496.

Shalini, S. *et al.* (2014) 'Old, new and emerging functions of caspases', *Cell Death & Differentiation* 2015 22:4, 22(4), pp. 526–539.

Sharma, V. S. and Magde, D. (1999) 'Activation of soluble guanylate cyclase by carbon monoxide and nitric oxide: a mechanistic model', *Methods (San Diego, Calif.)*, 19(4), pp. 494–505.

Shen, X. *et al.* (2014) 'Hydrogen sulfide measurement using sulfide dibimane: critical evaluation with electrospray ion trap mass spectrometry', *Nitric Oxide*, 41, pp. 97–104.

Shen, Y. *et al.* (2013) 'Protective Effects of Hydrogen Sulfide in Hypoxic Human Umbilical Vein Endothelial Cells: A Possible Mitochondria-Dependent Pathway', *International Journal of Molecular Sciences*, 14(7), p. 13093.

Shenouda, S. M. *et al.* (2011) 'Altered mitochondrial dynamics contributes to endothelial dysfunction in diabetes mellitus', *Circulation*, 124(4), pp. 444–453.

Sherwood, L. (1997) *Human physiology: from cells to system*. 3rd edn. Belmont, CA: Wadsworth Publishing Company.

Shi, M. *et al.* (2018) 'MSCs protect endothelial cells from inflammatory injury partially by secreting STC1', *International immunopharmacology*, 61, pp. 109–118.

Shibuya, N. *et al.* (2009) '3-Mercaptopyruvate Sulfurtransferase Produces Hydrogen Sulfide and Bound Sulfane Sulfur in the Brain', *Antioxidants & Redox Signaling*, 11(4), pp. 703–714.

Shibuya, N. *et al.* (2013) 'A novel pathway for the production of hydrogen sulfide from D-cysteine in mammalian cells', *Nature Communications*, 4(1), p. 1366.

Siekevitz, P. (1957) 'Powerhouse of the Cell', *Scientific American*, 197(1), pp. 131–144.

Sies, H. (2015) 'Oxidative stress: a concept in redox biology and medicine', *Redox biology*, 4, pp. 180–183.

Silva, M., Videira, P. A. and Sackstein, R. (2018) 'E-selectin ligands in the human

mononuclear phagocyte system: Implications for infection, inflammation, and immunotherapy', *Frontiers in Immunology*, 8(JAN), p. 1878.

Sivandzade, F., Bhalerao, A. and Cucullo, L. (2019) 'Analysis of the Mitochondrial Membrane Potential Using the Cationic JC-1 Dye as a Sensitive Fluorescent Probe', *Bio-protocol*, 9(1).

Sivitz, W. I. and Yorek, M. A. (2010) 'Mitochondrial Dysfunction in Diabetes: From Molecular Mechanisms to Functional Significance and Therapeutic Opportunities', *Antioxidants & Redox Signaling*, 12(4), p. 537.

Small, J. M. and Hintelmann, H. (2007) 'Methylene blue derivatization then LC-MS analysis for measurement of trace levels of sulfide in aquatic samples', *Analytical and bioanalytical chemistry*, 387(8), pp. 2881–2886.

Song, P. and Zou, M.-H. (2014) 'Redox regulation of endothelial cell fate.', *Cellular and molecular life sciences : CMLS*, 71(17), pp. 3219–39.

Spasov, S. G. *et al.* (2022) 'Profiling Distinctive Inflammatory and Redox Responses to Hydrogen Sulfide in Stretched and Stimulated Lung Cells', *Antioxidants*, 11(5), p. 1001.

Srinivasan, B. *et al.* (2015) 'TEER measurement techniques for in vitro barrier model systems', *Journal of laboratory automation*, 20(2), pp. 107–126.

Starkov, A. A. and Fiskum, G. (2003) 'Regulation of brain mitochondrial H₂O₂ production by membrane potential and NAD(P)H redox state', *Journal of neurochemistry*, 86(5), pp. 1101–1107.

Steinhubl, S. R. (2008) 'Why Have Antioxidants Failed in Clinical Trials?', *The American Journal of Cardiology*, 101(10), pp. S14–S19.

Steyers, C. *et al.* (2014) 'Endothelial Dysfunction in Chronic Inflammatory Diseases', *International Journal of Molecular Sciences*, 15(7), pp. 11324–11349.

Stroes, E. *et al.* (1997) 'Tetrahydrobiopterin restores endothelial function in hypercholesterolemia.', *The Journal of Clinical Investigation*, 99(1), pp. 41–46.

Sue, G. R., Ho, Z. C. and Kim, K. (2005) 'Peroxiredoxins: A historical overview and speculative preview of novel mechanisms and emerging concepts in cell signaling', *Free Radical Biology and Medicine*, 38(12), pp. 1543–1552.

Suen, D. F., Norris, K. L. and Youle, R. J. (2008) 'Mitochondrial dynamics and apoptosis', *Genes and Development*. *Genes Dev*, pp. 1577–1590.

Sun, L. *et al.* (2014) 'Potential biomarkers predicting risk of pulmonary hypertension in congenital heart disease: the role of homocysteine and hydrogen sulfide.', *Chinese medical journal*, 127(5), pp. 893–899.

Sun, N. *et al.* (2007) 'Plasma hydrogen sulfide and homocysteine levels in hypertensive patients with different blood pressure levels and complications.', *Zhonghua xin xue guan*

bing za zhi, 35(12), pp. 1145–1148.

Sun, W. H. *et al.* (2012) 'Hydrogen sulfide decreases the levels of ROS by inhibiting mitochondrial complex IV and increasing SOD activities in cardiomyocytes under ischemia/reperfusion', *Biochemical and Biophysical Research Communications*, 421(2), pp. 164–169.

Sun, Y. *et al.* (2019) 'Exogenous H₂S reduces the acetylation levels of mitochondrial respiratory enzymes via regulating the NAD⁺-SIRT3 pathway in cardiac tissues of db/db mice', *American Journal of Physiology - Endocrinology and Metabolism*, 317(2), pp. E284–E297.

Suzuki, K. *et al.* (2011) 'Hydrogen sulfide replacement therapy protects the vascular endothelium in hyperglycemia by preserving mitochondrial function.', *Proceedings of the National Academy of Sciences of the United States of America*, 108(33), pp. 13829–13834.

Suzuki, Y. J., Carini, M. and Butterfield, D. A. (2010) 'Protein carbonylation', *Antioxidants & redox signaling*, 12(3), pp. 323–325.

Szabo, C. *et al.* (2014) 'Regulation of mitochondrial bioenergetic function by hydrogen sulfide. Part I. Biochemical and physiological mechanisms.', *British journal of pharmacology*, 171(8), pp. 2099–2122.

Szabo, C. (2018) 'A timeline of hydrogen sulfide (H₂S) research: From environmental toxin to biological mediator', *Biochemical Pharmacology*. Elsevier Inc., pp. 5–19.

Szczesny, B. *et al.* (2014) 'AP39, a novel mitochondria-targeted hydrogen sulfide donor, stimulates cellular bioenergetics, exerts cytoprotective effects and protects against the loss of mitochondrial DNA integrity in oxidatively stressed endothelial cells in vitro', *Nitric Oxide - Biology and Chemistry*, 41, pp. 120–130.

Taddei, S. *et al.* (1996) 'Defective L-arginine-nitric oxide pathway in offspring of essential hypertensive patients.', *Circulation*, 94(6), pp. 1298–303.

Tafari, M. *et al.* (2000) 'Cytochrome c-dependent activation of caspase-3 by tumor necrosis factor requires induction of the mitochondrial permeability transition', *The American journal of pathology*, 156(6), pp. 2111–2121.

Tahrir, F. G. *et al.* (2019) 'Mitochondrial Quality Control in Cardiac Cells: Mechanisms and Role in Cardiac Cell Injury and Disease', *Journal of cellular physiology*, 234(6), p. 8122.

Tang, X. *et al.* (2014) 'Mitochondria, endothelial cell function, and vascular diseases', *Frontiers in Physiology*, 5 MAY, p. 175.

Tang, Y. *et al.* (2015) 'The role of miR-19b in the inhibition of endothelial cell apoptosis and its relationship with coronary artery disease', *Scientific Reports 2015 5:1*, 5(1), pp. 1–11.

- Taylor, S. G. and Weston, A. H. (1988) 'Endothelium-derived hyperpolarizing factor: a new endogenous inhibitor from the vascular endothelium', *Trends in pharmacological sciences*, 9(8), pp. 272–274.
- Tennant, J. R. (1964) 'Evaluation of the trypan blue technique for determination of cell viability', *Transplantation*, 2, pp. 685–694.
- Thannickal, V. J. and Fanburg, B. L. (2000) 'Reactive oxygen species in cell signaling', *American Journal of Physiology-Lung Cellular and Molecular Physiology*, 279(6), pp. L1005–L1028.
- Thomas, S. R., Witting, P. K. and Drummond, G. R. (2008) 'Redox Control of Endothelial Function and Dysfunction: Molecular Mechanisms and Therapeutic Opportunities', *Antioxidants & Redox Signaling*, 10(10), pp. 1713–1766.
- Tilokani, L. *et al.* (2018) 'Mitochondrial dynamics: overview of molecular mechanisms', *Essays in biochemistry*, 62(3), pp. 341–360.
- Tong, M. *et al.* (2020) 'Elevated Expression of Serum Endothelial Cell Adhesion Molecules in COVID-19 Patients', *The Journal of infectious diseases*, 222(6), pp. 894–898.
- Torres, D. *et al.* (2005) 'Membrane tumor necrosis factor confers partial protection to Listeria infection', *The American journal of pathology*, 167(6), pp. 1677–1687.
- Tsuboi, T., Maeda, M. and Hayashi, T. (2018) 'Administration of L-arginine plus L-citrulline or L-citrulline alone successfully retarded endothelial senescence', *PLoS ONE*, 13(2).
- Tucureanu, M. M. *et al.* (2017) 'Lipopolysaccharide-induced inflammation in monocytes/macrophages is blocked by liposomal delivery of G_i-protein inhibitor', *International Journal of Nanomedicine*, 13, pp. 63–76.
- Turrens, J. F. (2003) 'Mitochondrial formation of reactive oxygen species', *The Journal of Physiology*, 552(2), pp. 335–344.
- Twig, G. *et al.* (2008) 'Fission and selective fusion govern mitochondrial segregation and elimination by autophagy', *The EMBO journal*, 27(2), pp. 433–446.
- Twig, G., Hyde, B. and Shirihai, O. S. (2008) 'Mitochondrial fusion, fission and autophagy as a quality control axis: The bioenergetic view', *Biochimica et Biophysica Acta - Bioenergetics*. *Biochim Biophys Acta*, pp. 1092–1097.
- Unger, R. E. *et al.* (2002) 'In vitro expression of the endothelial phenotype: Comparative study of primary isolated cells and cell lines, including the novel cell line HPMEC-ST1.6R', *Microvascular Research*, 64(3), pp. 384–397.
- Untereiner, A. A. *et al.* (2016) 'Stimulatory effect of CSE-generated H₂S on hepatic mitochondrial biogenesis and the underlying mechanisms.', *Nitric oxide: biology and chemistry*, 58, pp. 67–76.

- Vadivel, A. *et al.* (2014) 'Exogenous hydrogen sulfide (H₂S) protects alveolar growth in experimental O₂-induced neonatal lung injury', *PLoS ONE*, 9(3).
- Valente, A. . *et al.* (2017) 'A simple ImageJ macro tool for analyzing mitochondrial network morphology in mammalian cell culture', *Acta histochemica*, 119(3), pp. 315–326.
- Valko, M. *et al.* (2007) 'Free radicals and antioxidants in normal physiological functions and human disease', *International Journal of Biochemistry and Cell Biology*. Int J Biochem Cell Biol, pp. 44–84.
- Vandiver, M. S. *et al.* (2013) 'Sulphydration mediates neuroprotective actions of parkin', *Nature Communications*, 4(1), p. 1626.
- Vaughan, R. A. *et al.* (2013) 'Tumor necrosis factor alpha increases aerobic glycolysis and reduces oxidative metabolism in prostate epithelial cells', *Prostate*, 73(14), pp. 1538–1546.
- Videm, V. and Albrigtsen, M. (2008) 'Soluble ICAM-1 and VCAM-1 as markers of endothelial activation', *Scandinavian Journal of Immunology*, 67(5), pp. 523–531.
- Vito, R. P. and Dixon, S. A. (2003) 'Blood vessel constitutive models-1995-2002', *Annual review of biomedical engineering*, 5, pp. 413–439.
- Vitvitsky, V., Kabil, O. and Banerjee, R. (2012) 'High turnover rates for hydrogen sulfide allow for rapid regulation of its tissue concentrations', *Antioxidants and Redox Signaling*, pp. 22–31.
- Wagner, D. D., Olmsted, J. B. and Marder, V. J. (1982) 'Immunolocalization of von Willebrand protein in Weibel-Palade bodies of human endothelial cells.', *The Journal of cell biology*, 95(1), pp. 355–60.
- Wallace, J. L. *et al.* (2018) 'Hydrogen Sulfide-Releasing Therapeutics: Translation to the Clinic', *Antioxidants & redox signaling*, 28(16), pp. 1533–1540.
- Wallace, J. L. *et al.* (2020) 'A proof-of-concept, Phase 2 clinical trial of the gastrointestinal safety of a hydrogen sulfide-releasing anti-inflammatory drug', *British Journal of Pharmacology*, 177(4), pp. 769–777.
- Walterscheid, J. P., Ullrich, S. E. and Nghiem, D. X. (2002) 'Platelet-activating Factor, a Molecular Sensor for Cellular Damage, Activates Systemic Immune Suppression', *The Journal of Experimental Medicine*, 195(2), p. 171.
- Wang, B. *et al.* (2020) 'A comparative study unraveling the effects of TNF- α stimulation on endothelial cells between 2D and 3D culture', *Biomedical Materials*, 15(6), p. 065018.
- Wang, C. *et al.* (2018) 'Endogenous H₂S resists mitochondria-mediated apoptosis in the adrenal glands via ATP5A1 S-sulphydration in male mice', *Molecular and Cellular Endocrinology*, 474, pp. 65–73.

Wang, R. (2012) 'Physiological Implications of Hydrogen Sulfide: A Whiff Exploration That Blossomed', *Physiological Reviews*, 92(2), pp. 791–896.

Wang, S. *et al.* (2018) 'TNF- α -induced oxidative stress and endothelial dysfunction in EA.hy926 cells is prevented by mate and green coffee extracts, 5-caffeoylquinic acid and its microbial metabolite, dihydrocaffeic acid', <https://doi.org/10.1080/09637486.2018.1505834>, 70(3), pp. 267–284.

Wang, Y. *et al.* (2009) 'Role of Hydrogen Sulfide in the Development of Atherosclerotic Lesions in Apolipoprotein E Knockout Mice', *Arteriosclerosis, Thrombosis, and Vascular Biology*, 29(2), pp. 173–179.

Wang, Y. *et al.* (2012) 'ROS-induced mitochondrial depolarization initiates PARK2/PARKIN-dependent mitochondrial degradation by autophagy', *Autophagy*, 8(10), pp. 1462–1476.

Wang, Z.-J. *et al.* (2017) 'Atherosclerosis and the Hydrogen Sulfide Signaling Pathway - Therapeutic Approaches to Disease Prevention.', *Cellular physiology and biochemistry: international journal of experimental cellular physiology, biochemistry, and pharmacology*, 42(3), pp. 859–875.

Watanabe, T. *et al.* (2014) 'Roles of mitochondrial fragmentation and reactive oxygen species in mitochondrial dysfunction and myocardial insulin resistance', *Experimental Cell Research*, 323(2), pp. 314–325.

Wei Lee, Z. *et al.* (2011) 'The Slow-Releasing Hydrogen Sulfide Donor, GYY4137, Exhibits Novel Anti-Cancer Effects In Vitro and In Vivo', *PLoS ONE*, 6(6), p. 21077.

Wei, W. Bin *et al.* (2014) 'GYY4137, a novel hydrogen sulfide-releasing molecule, likely protects against high glucose-induced cytotoxicity by activation of the AMPK/mTOR signal pathway in H9c2 cells', *Molecular and Cellular Biochemistry*, 389(1–2), pp. 249–256.

Wen, Y. D. *et al.* (2013) 'Hydrogen Sulfide Protects HUVECs against Hydrogen Peroxide Induced Mitochondrial Dysfunction and Oxidative Stress', *PLoS ONE*, 8(2).

Westermann, B. (2010) 'Mitochondrial fusion and fission in cell life and death', *Nature Reviews Molecular Cell Biology* 2010 11:12, 11(12), pp. 872–884.

Wetzel, M. D. and Wenke, J. C. (2019) 'Mechanisms by which hydrogen sulfide attenuates muscle function following ischemia-reperfusion injury: Effects on Akt signaling, mitochondrial function, and apoptosis', *Journal of Translational Medicine*. BioMed Central Ltd., pp. 1–13.

Winterbourn, C. C. (2008) 'Reconciling the chemistry and biology of reactive oxygen species', *Nature Chemical Biology* 2008 4:5, 4(5), pp. 278–286.

Wong, B. W. *et al.* (2016) 'The role of fatty acid β -oxidation in lymphangiogenesis', *Nature* 2016 542:7639, 542(7639), pp. 49–54.

Wong, C. M. *et al.* (2008) 'Protein carbonylation as a novel mechanism in redox signaling', *Circulation research*, 102(3), pp. 310–318.

Wu, B. *et al.* (2012) 'Hydrogen sulfide inhibits the translational expression of hypoxia-inducible factor-1 α ', *British Journal of Pharmacology*, 167(7), p. 1492.

Wu, D. *et al.* (2017) 'Hydrogen sulfide ameliorates chronic renal failure in rats by inhibiting apoptosis and inflammation through ROS/MAPK and NF- κ B signaling pathways', *Scientific Reports*, 7(1).

Wu, L. and Wang, R. (2005) 'Carbon monoxide: endogenous production, physiological functions, and pharmacological applications', *Pharmacological reviews*, 57(4), pp. 585–630.

Xia, Z. *et al.* (2006) 'N-acetylcysteine attenuates TNF- α -induced human vascular endothelial cell apoptosis and restores eNOS expression', *European Journal of Pharmacology*, 550(1–3), pp. 134–142.

Xiao, Z. *et al.* (2017) 'Triggered and Tunable Hydrogen Sulfide Release from Photogenerated Thiobenzaldehydes', *Chemistry (Weinheim an der Bergstrasse, Germany)*, 23(47), pp. 11294–11300.

Xie, L., Gu, Y., *et al.* (2016) 'Hydrogen sulfide induces Keap1 S-sulfhydration and suppresses diabetes-accelerated atherosclerosis via Nrf2 activation', *Diabetes*, 65(10), pp. 3171–3184.

Xie, L., Feng, H., *et al.* (2016) 'SIRT3 Mediates the Antioxidant Effect of Hydrogen Sulfide in Endothelial Cells', *Antioxidants & Redox Signaling*, 24(6), pp. 329–343.

Xie, Z.-Z., Liu, Y. and Bian, J.-S. (2016) 'Hydrogen Sulfide and Cellular Redox Homeostasis.', *Oxidative medicine and cellular longevity*, 2016, p. 6043038.

Xin, T. and Lu, C. (2020) 'Irisin activates Opa1-induced mitophagy to protect cardiomyocytes against apoptosis following myocardial infarction', *Aging (Albany NY)*, 12(5), p. 4474.

Xu, C. *et al.* (2015) 'TNF causes changes in glomerular endothelial permeability and morphology through a Rho and myosin light chain kinase-dependent mechanism', *Physiological Reports*, 3(12), p. e12636.

Xu, S. *et al.* (2011) 'Rosiglitazone attenuates endothelial progenitor cell apoptosis induced by TNF- α via ERK/MAPK and NF- κ B signal pathways', *Journal of pharmacological sciences*, 117(4), pp. 265–274.

Xu, S. *et al.* (2021) 'Endothelial Dysfunction in Atherosclerotic Cardiovascular Diseases and Beyond: From Mechanism to Pharmacotherapies', *Pharmacological Reviews*, 73(3), pp. 924–967.

Xu, W. *et al.* (2015) 'Exogenous H₂S protects H9c2 cardiac cells against high glucose-induced injury and inflammation by inhibiting the activation of the NF- κ B and IL-1 β

- pathways.', *International journal of molecular medicine*, 35(1), pp. 177–186.
- Yadav, P. K. *et al.* (2016) 'Biosynthesis and Reactivity of Cysteine Persulfides in Signaling', *Journal of the American Chemical Society*, 138(1), pp. 289–299.
- Yamagata, K., Suzuki, S. and Tagami, M. (2016) 'Docosahexaenoic acid prevented tumor necrosis factor alpha-induced endothelial dysfunction and senescence', *Prostaglandins, Leukotrienes and Essential Fatty Acids*, 104, pp. 11–18.
- Yamamoto, T. *et al.* (2008) 'Physiological significance of reactive cysteine residues of Keap1 in determining Nrf2 activity.', *Molecular and cellular biology*, 28(8), pp. 2758–70.
- Yan, Y. *et al.* (2020) 'S-adenosylmethionine administration inhibits levodopa-induced vascular endothelial growth factor-A expression.', *Aging*, 12(21), pp. 21290–21307.
- Yang, G. *et al.* (2004) 'Cystathionine γ -lyase overexpression inhibits cell proliferation via a H₂S-dependent modulation of ERK1/2 phosphorylation and p21 Cip/WAK-1', *Journal of Biological Chemistry*, 279(47), pp. 49199–49205.
- Yang, G. *et al.* (2008a) 'H₂S as a physiologic vasorelaxant: hypertension in mice with deletion of cystathionine gamma-lyase.', *Science (New York, N. Y.)*, 322(5901), pp. 587–590.
- Yang, G. *et al.* (2008b) 'H₂S as a Physiologic Vasorelaxant: Hypertension in Mice with Deletion of Cystathionine γ -Lyase', *Science*, 322(5901), pp. 587–590.
- Yang, G. *et al.* (2011) 'Specificity protein-1 as a critical regulator of human cystathionine γ -lyase in smooth muscle cells', *Journal of Biological Chemistry*, 286(30), pp. 26450–26460.
- Yang, G. *et al.* (2013a) 'Hydrogen sulfide protects against cellular senescence via s-sulfhydration of keap1 and activation of Nrf2', *Antioxidants and Redox Signaling*, 18(15), pp. 1906–1919.
- Yang, G. *et al.* (2013b) 'Hydrogen Sulfide Protects Against Cellular Senescence via S -Sulfhydration of Keap1 and Activation of Nrf2', *Antioxidants & Redox Signaling*, 18(15), pp. 1906–1919.
- Yang, G., Sun, X. and Wang, R. (2004) 'Hydrogen sulfide-induced apoptosis of human aorta smooth muscle cells via the activation of mitogen-activated protein kinases and caspase-3', *The FASEB Journal*, 18(14), pp. 1782–1784.
- Yang, H., Zhao, P. and Tian, S. (2016) 'Clopidogrel Protects Endothelium by Hindering TNF α -Induced VCAM-1 Expression through CaMKK β /AMPK/Nrf2 Pathway.', *Journal of diabetes research*, (9128050).
- Yang, J. *et al.* (2019) 'Non-enzymatic hydrogen sulfide production from cysteine in blood is catalyzed by iron and vitamin B6', *Communications Biology*, 2(1).
- Yang, R. *et al.* (2018) 'NaHS inhibits the release of TNF- α and IL-6 from peripheral blood

lymphocytes in rats and down-regulates the expression of connexin 40 and connexin 43', *Xi bao yu fen zi mian yi xue za zhi = Chinese journal of cellular and molecular immunology*, 34(8), pp. 684–689.

Yang, S. *et al.* (2020) 'Leptin mediates protection of hydrogen sulfide against 6-hydroxydopamine-induced Parkinson's disease: Involving enhancement in Warburg effect', *Neurochemistry international*, 135.

Yao, Z. *et al.* (2011) 'Cell metabolism affects selective vulnerability in PINK1-associated Parkinson's disease', *Journal of Cell Science*, 124(24), p. 4194.

Ye, X. *et al.* (2022) 'Endogenous Hydrogen Sulfide Persulfidates Caspase-3 at Cysteine 163 to Inhibit Doxorubicin-Induced Cardiomyocyte Apoptosis', *Oxidative Medicine and Cellular Longevity*, 2022.

Young, B. C., Levine, R. J. and Karumanchi, S. A. (2010) 'Pathogenesis of Preeclampsia', *Annual Review of Pathology: Mechanisms of Disease*, 5(1), pp. 173–192.

Yu, X. H. *et al.* (2014) 'Hydrogen sulfide as a potent cardiovascular protective agent', *Clinica Chimica Acta*. Elsevier, pp. 78–87.

Yuan, S. *et al.* (2016) 'Hydrogen sulfide metabolism regulates endothelial solute barrier function', *Redox Biology*, 9, pp. 157–166.

Yuan, Y. *et al.* (2019) 'S-Sulfhydration of SIRT3 by Hydrogen Sulfide Attenuates Mitochondrial Dysfunction in Cisplatin-Induced Acute Kidney Injury.', *Antioxidants & redox signaling*, 31(17), pp. 1302–1319.

Yuan, Z. N., Zheng, Y. Q. and Wang, B. H. (2020) 'Prodrugs of hydrogen sulfide and related sulfur species: recent development', *Chinese Journal of Natural Medicines*, 18(4), pp. 296–307.

Zakhary, R. *et al.* (1997) *Targeted gene deletion of heme oxygenase 2 reveals neural role for carbon monoxide*, *Neurobiology*.

Zanardo, R. *et al.* (2006) 'Hydrogen sulfide is an endogenous modulator of leukocyte-mediated inflammation.', *FASEB journal: official publication of the Federation of American Societies for Experimental Biology*, 20(12), pp. 2118–2120.

Zhang, C. Y. *et al.* (2006) 'Genipin inhibits UCP2-mediated proton leak and acutely reverses obesity- and high glucose-induced beta cell dysfunction in isolated pancreatic islets', *Cell metabolism*, 3(6), pp. 417–427.

Zhang, D. D. and Hannink, M. (2003) 'Distinct Cysteine Residues in Keap1 Are Required for Keap1-Dependent Ubiquitination of Nrf2 and for Stabilization of Nrf2 by Chemopreventive Agents and Oxidative Stress', *MOLECULAR AND CELLULAR BIOLOGY*, 23(22), pp. 8137–8151.

Zhang, D. X. and Gutterman, D. D. (2007) 'Mitochondrial reactive oxygen species-

mediated signaling in endothelial cells', *American Journal of Physiology-Heart and Circulatory Physiology*, 292(5), pp. H2023–H2031.

Zhang, F. *et al.* (2001) 'Vasoregulatory function of the heme-heme oxygenase-carbon monoxide system', *American Journal of Hypertension*, 14(6 II), pp. 62S-67S.

Zhang, H. *et al.* (2012) 'Hydrogen Sulfide Inhibits the Development of Atherosclerosis with Suppressing CX3CR1 and CX3CL1 Expression', *PLoS ONE*. Edited by C. Schulz, 7(7), p. e41147.

Zhang, H. X. *et al.* (2016) 'H₂S Attenuates LPS-Induced Acute Lung Injury by Reducing Oxidative/Nitrative Stress and Inflammation', *Cellular Physiology and Biochemistry*, 40(6), pp. 1603–1612.

Zhang, J. *et al.* (2011) 'Regulation of endothelial cell adhesion molecule expression by mast cells, macrophages, and neutrophils', *PLoS one*, 6(1).

Zhang, J. *et al.* (2020) 'Hydrogen sulfide restores sevoflurane postconditioning mediated cardioprotection in diabetic rats: Role of SIRT1/Nrf2 signaling-modulated mitochondrial dysfunction and oxidative stress', *Journal of Cellular Physiology*, p. jcp.30214.

Zhang, L. *et al.* (2007) 'TNF α induces apoptosis through JNK/Bax-dependent pathway in differentiated, but not naïve PC12 cells.', *Cell cycle (Georgetown, Tex.)*, 6(12), pp. 1479–1486.

Zhang, Y. (2018) 'Cell toxicity mechanism and biomarker.', *Clinical and translational medicine*, 7(1), p. 34.

Zhao, H. *et al.* (2009) 'Effect of Heme oxygenase-1 deficiency on placental development', *Placenta*, 30(10), p. 861.

Zhao, K. *et al.* (2014) 'S-sulfhydration of MEK1 leads to PARP-1 activation and DNA damage repair', *EMBO reports*, 15(7), pp. 792–800.

Zhao, W. (2001) 'The vasorelaxant effect of H₂S as a novel endogenous gaseous KATP channel opener', *The EMBO Journal*, 20(21), pp. 6008–6016.

Zhao, W. *et al.* (2017) 'Danshenol A inhibits TNF- α -induced expression of intercellular adhesion molecule-1 (ICAM-1) mediated by NOX4 in endothelial cells', *Scientific Reports 2017 7:1*, 7(1), pp. 1–13.

Zhao, Y. and Pluth, M. D. (2016) 'Hydrogen Sulfide Donors Activated by Reactive Oxygen Species', *Angewandte Chemie (International ed. in English)*, 55(47), pp. 14638–14642.

Zhao, Y., Steiger, A. K. and Pluth, M. D. (2018) 'Cysteine-Activated Hydrogen Sulfide (H₂S) Delivery through Caged Carbonyl Sulfide (COS) Donor Motifs', *Chemical communications (Cambridge, England)*, 54(39), p. 4951.

Zheng, J. *et al.* (2015) 'Hydrogen sulfide (H₂S) attenuates uranium-induced acute

nephrotoxicity through oxidative stress and inflammatory response via Nrf2-NF- κ B pathways', *Chemico-Biological Interactions*, 242, pp. 353–362.

Zheng, Y. *et al.* (2015) 'Hydrogen sulfide prodrugs—a review', *Acta Pharmaceutica Sinica B*, 5(5), pp. 367–377.

Zhou, P. *et al.* (2017) 'Attenuation of TNF- α -Induced Inflammatory Injury in Endothelial Cells by Ginsenoside Rb1 via Inhibiting NF- κ B, JNK and p38 Signaling Pathways', *Frontiers in Pharmacology*, 8(AUG).

Zhou, P. *et al.* (2019) 'Protective Effects of Total Saponins of *Aralia elata* (Miq.) on Endothelial Cell Injury Induced by TNF- α via Modulation of the PI3K/Akt and NF- κ B Signalling Pathways', *International Journal of Molecular Sciences*, 20(1).

Zhu, M. L. *et al.* (2021) 'The antihypertension effect of hydrogen sulfide (H₂S) is induced by activating VEGFR2 signaling pathway', *Life Sciences*, 267, p. 118831.

Zhu, X. Y. *et al.* (2007) 'Simvastatin prevents coronary microvascular remodeling in renovascular hypertensive pigs', *Journal of the American Society of Nephrology: JASN*, 18(4), pp. 1209–1217.

Zielonka, J. and Kalyanaraman, B. (2010) 'Hydroethidine- and MitoSOX-derived red fluorescence is not a reliable indicator of intracellular superoxide formation: another inconvenient truth', *Free radical biology & medicine*, 48(8), pp. 983–1001.

Zivanovic, J. *et al.* (2019) 'SELECTIVE PERSULFIDE DETECTION REVEALS EVOLUTIONARILY CONSERVED ANTI-AGING EFFECTS OF S-SULFHYDRATION', *Cell metabolism*, 30(6), p. 1152.

Zmijewski, J. W. *et al.* (2010) 'Exposure to hydrogen peroxide induces oxidation and activation of AMP-activated protein kinase', *The Journal of biological chemistry*, 285(43), pp. 33154–33164.

Zong, Y. *et al.* (2015) 'Downregulation of Endogenous Hydrogen Sulfide Pathway Is Involved in Mitochondrion-Related Endothelial Cell Apoptosis Induced by High Salt', *Oxidative Medicine and Cellular Longevity*, 2015, p. 754670.

Zorov, D. B., Juhaszova, M. and Sollott, S. J. (2014) 'Mitochondrial reactive oxygen species (ROS) and ROS-induced ROS release', *Physiological Reviews*. American Physiological Society, pp. 909–950.

9 Appendices

9.1 Appendix a. Consumables

To address the aims of this project, a series of equipment (Table 9-1), chemicals (Table 9-2) and commercial kits (Table 9-3) were used. Endothelial cell models required specific reagents, as described in Table 9-4. Exogenous H₂S donors and their chemical structure used throughout this thesis are described in Table 9-5.

Table 9-1. Laboratory equipment and software

Equipment	Supplier
Agilent software	Agilent Technologies, INC., California, USA
Automated ELISA wash plate	ASYS Atlantis Biochrom Ltd, Cambridge, UK
Agilent Seahorse 24 XF	Agilent Technologies, INC., California, USA
Automated plate shaker	Stuart® SSM3, # SSL5, Staffordshire, UK
Automated water bath	Grant instrument, Cambridge, UK
Bio-render software	OHSU, Canada
Cell culture flasks 75 cm² cellstar® (# 658175)	Greiner Bio-one, Stonehouse, UK
Cryo-freezing container NALGENE	Thermo Fisher Scientific, Warrington, UK
Confocal lighting microscopy TCS SP8 system	Leica Microsystems Ltd, UK
Electrophoresis apparatus and Western blot semi-dry transfer system	BIO-RAD, Watford, UK
Falcon round polystyrene test tube	SLS, Lonza, Basel, Switzerland
Fluorescence microscope	Nikon Eclipse Tii, Nikon instrument Ltd., Shanghai, CH
Flow cytometer BD Accuri™ C6 Plus	BD Biosciences, Accuri Cytometers, Inc., USA
Flow cytometric analysis software	Accuri™ Cytometers, Inc., USA
Graph Prism v.8 software	GraphPad, California, USA
Homogenizer Crushing	Jencons-PLS T8.01, IKA®, Deutschland, Germany
Hybridisation incubator	HB-1D, Techne, Staffordshire, UK
Image Processing and Analysis in Java software	ImageJ, USA
Mr Frosty™ (# 5100-0001)	ThermoFisher Scientific, Gloucester, UK
Nikon Eclipse T s 2 inverted routine microscope	Nikon, CH

Nikon Ti -S Inverted fluorescence phase contrast microscope Pred Ti2	Nikon, CH
Neubauer haemocytometer chamber	Marienfeld Superior™ , Lauda-Königshofen, Germany
Multimode Microplate Reader Spark®	TECAN Group Ltd., Männedorf, Switzerland
Nanodrop 1000 spectrophotometer	Thermo Fisher Scientific, Warrington, UK
Odyssey® CLx Imaging system	LI-COR Biosciences Ltd., Cambridge, UK
PCR LightCycler 480 II platform	Roche Diagnostic Ltd, Burgess Hill, UK
TransBlot® Turbo Transfer system	Bio-Rad Laboratories, Watford, UK
Seahorse Extracellular Flux Analyzer XF24	Agilent Technologies, Cheadle, UK
Tabletop Centrifuge	Centrifuges # 5418; # 5702; # 5424; # 5424-R, Eppendorf, Hamburg, Germany
TECAN plate reader	Spark-TECAN Trading AG, Switzerland.
Thermal Labcycler SensoQuest Basic	# T3-0140, Geneflow Ltd., Staffordshire, UK
Unidirectional Laminar airflow cabinet	# VCS2-4, Envair Ltd., Lancashire, UK

Table 9-2. Laboratory Reagents and Chemicals

Reagent		Supplier
Acrylamide/Bis-acrylamide (#A3574)	30% solution	Sigma-Aldrich, Poole, Dorset, UK
Alexa Fluor™ 647 C₂ Maleimide (#A20347)		ThermoFisher Scientific, Gloucester, UK
Amersham™ Hybond P Western blotting membrane, nitrocellulose (#GE10600004)		Millipore Sigma-Aldrich, Poole, Dorset, UK
Alexa Fluor 680 C₂-Maleimide (#A20344)		ThermoFisher Scientific, Gloucester, UK
Bovine serum albumin (BSA) (#66-1252)		Fisher Scientific, Loughborough, UK
Biotin-HPDP (#ab145614)		Abcam, Cambridge, UK
Bradford Protein assay Reagent A (#500-0113)		Bio-Rad Laboratories, Watford, UK
Bradford Protein assay Reagent S (#500-0115)		Bio-Rad Laboratories, Watford, UK
Bradford Protein assay Reagent B (#500-0114)		Bio-Rad Laboratories, Watford, UK

β-mercaptoethanol (#444203)	Sigma-Aldrich, Poole, Dorset, UK
CellTiter-Blue® Cell viability assay (#G8080)	Promega, GmbH, Southampton, UK
CM-H2DCFDA™ (#C6827)	ThermoFisher Scientific, Gloucester, UK
DAPI staining solution (#ab228549)	Abcam, Cambridge, UK
DAPI-SlowFade Diamond Antifade Mountant (#s36968)	ThermoFisher Scientific, Gloucester, UK
Deferoxamine mesylate salt powder (D9533)	Sigma-Aldrich, Poole, Dorset, UK
Dimethyl sulfoxide (DMSO) (#D2650)	Sigma-Aldrich, Poole, Dorset, UK
Dithiothreitol (DTT) (#15326322)	Roche diagnostics Ltd. West Sussex, UK
Ethanol (absolute)	Sigma-Aldrich, Poole, Dorset, UK
Ethylenediaminetetraacetic acid (EDTA) (#E9884)	Sigma-Aldrich, Poole, Dorset, UK
Flow cytometer BD Accuri C6 plus buffers	BD Biosciences, Accuri Cytometers, Inc., USA
Goat serum (#S-1000)	2BScientific, Oxfordshire, UK
Glycine (#G8898)	Sigma-Aldrich, Poole, Dorset, UK
Glycerol (#G5516)	Sigma-Aldrich, Poole, Dorset, UK
Glutaraldehyde solution (#G5882)	Sigma-Aldrich, Poole, Dorset, UK
4-(2-Hydroxyethyl)piperazine-1-ethanesulfonic acid (HEPES) (#H3375)	Sigma-Aldrich, Poole, Dorset, UK
Intercept™ Blocking buffer (#P927-60001)	LI-COR Biosciences, Nebraska, USA
JC-1 (#T3168)	ThermoFisher Scientific, Gloucester, UK
Laemmli SDS sample buffer 6X (#J61337)	Alfa Aesar, ThermoFisher Scientific, Gloucester, UK
Laemmli SDS sample buffer 4x (#1610747)	Bio-Rad Laboratories, Watford, UK
Matrigel matrix (#354230)	Corning, UK
Milk-dried skimmed powder	Marvel, DSDelta, Ltd., UK
MitoSox™ Red (#M36008)	ThermoFisher Scientific, Gloucester, UK

MitoTracker™ Red (#M7512)	ThermoFisher Scientific, Gloucester, UK
MMTS (#208795)	Sigma-Aldrich, Poole, Dorset, UK
Neutr-Avidin Agarose Resin (#29200)	ThermoFisher Scientific, Gloucester, UK
N, N, N', N' -tetraacetythylenediamine (#T9281)	Sigma-Aldrich, Poole, Dorset, UK
N,N-Dimethylformamide (#D4551)	Sigma-Aldrich, Poole, Dorset, UK
Paraformaldehyde (PFA) solution (#158127)	Sigma-Aldrich, Poole, Dorset, UK
Potassium ferricyanide (III) powder (#702587)	Sigma-Aldrich, Poole, Dorset, UK
Potassium hexacyanoferrate (II) trihydrate (#P9387)	Sigma-Aldrich, Poole, Dorset, UK
Precision plus Protein™ Kaleidoscope™ Prestained Protein (#1610375)	Bio-Rad Laboratories, Watford, UK
Pierce™ Protein A/G agarose beads (#20421)	ThermoFisher Scientific, Gloucester, UK
Phalloidin Alexa Fluor 488 (#A12379)	ThermoFisher Scientific, Gloucester, UK
Restore Western Blot Stripping Buffer (#21059)	ThermoFisher Scientific, Gloucester, UK
Revert 700 Total protein stain kit (#926-11010)	LI-COR Biosciences, Nebraska, USA
RIPA Lysis buffer (#89900)	ThermoFisher Scientific, Gloucester, UK
Seahorse medium XF Base (#102353)	Agilent Technologies, Cheadle, UK
Seahorse XF Calibrant solution (#100840-000)	Agilent Technologies, Cheadle, UK
Sodium chloride (#S7653)	Sigma-Aldrich, Poole, Dorset, UK
Sodium dodecyl sulfate (#L3771)	Sigma-Aldrich, Poole, Dorset, UK
Sodium pyruvate solution (#s8636)	Sigma-Aldrich, Poole, Dorset, UK
Thin Blot paper (#1620118)	Bio-Rad Laboratories, Watford, UK
Tris-HCL (#T5941)	Sigma-Aldrich, Poole, Dorset, UK
Trizma base (#T6066)	Sigma-Aldrich, Poole, Dorset, UK

Triton X-100 (#T8787)	Sigma-Aldrich, Poole, Dorset, UK
Tween-20 (#63158)	Sigma-Aldrich, Poole, Dorset, UK
X-Gal, 5-bromo-4-chloro-3-indolyl-beta-D-galactopyranosie (#11680293001)	Sigma-Aldrich, Poole, Dorset, UK

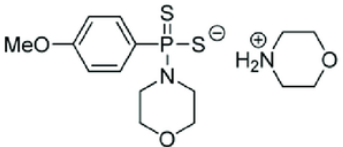
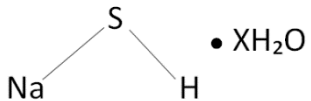
Table 9-3. Assays Kits

Kit	Supplier
Annexin V-FITC / Propidium iodide staining assay kit (#040914)	BioLegend®, California, USA
BCA Protein Assay kit (#23227)	ThermoFisher Scientific, Gloucester, UK
GSH/GSSG-Glo™ Assay kit (#V6611)	Promega, GmbH, Southampton, UK
Human Interleukin 6 (IL-6) ELISA assay kit (#DY206-05)	R&D Systems, Bio-Techne, Inc., Oxford, UK
Revert™ Total Protein Stain assay kit (#P/N 926-11010)	LI-COR Biosciences, Nebraska, USA
SF-Cell LINE 4D-Nucleofector X kit L (#V4XC-2012)	Lonza (SLS), Basel, Switzerland
Seahorse XF Cell Mito Stress Test kit (#103015-100)	Agilent Technologies, INC., California, USA
Caspase-Glo 3/7 3D Assay kit (#G8981)	Promega, GmbH, Southampton, UK

Table 9-4. Cell Culture Reagents

Reagent	Supplier
Dulbecco's Modified Eagle's Medium (#D6429)	Sigma-Aldrich, Poole, Dorset, UK
Endothelial Cell Growth Medium 2 (#C22111)	PromoCell, GmbH, Heidelberg, Germany
EA.hy926 Human endothelial cell line (ATCC® CCL-2922™)	LGC Standards, Teddington, UK
Fetal Bovine Serum Gibco (#11550356)	Fisher Scientific, Loughborough, UK
Human Umbilical Vein Endothelial Cells (#C12203)	PromoCell, GmbH, Heidelberg, Germany
Hydrogen peroxide solution (H₂O₂) 30% (w/w) in H₂O	Sigma-Aldrich, Poole, Dorset, UK
L-glutamine (#G3126)	Sigma-Aldrich, Poole, Dorset, UK
Media 199 with EBSS (#LZBE12-119F)	Lonza (SLS), Basel, Switzerland
Penicillin-Streptomycin solution (#P4333)	Sigma-Aldrich, Poole, Dorset, UK
Phosphate-buffered saline (PBS) 1X (#806552)	Sigma-Aldrich, Poole, Dorset, UK
Human Tumour necrosis factor-alpha (#210-TA-005)	R&D Systems, Bio-Techne, Inc., Oxford, UK
Trypsin-EDTA solution 10X (#LZBE02-007E)	Lonza (SLS), Basel, Switzerland
Trypan blue solution (#T8157)	ThermoFisher Scientific, Gloucester, UK

Table 9-5. H₂S donors

Compound	Chemical structure
<p>GY4137 (morpholin-4-ium 4-methoxyphenyl(morpholino) phosphinodithioate) (#SML2470), Sigma-Aldrich, Poole, Dorset, UK</p>	
<p>NaHS (sodium hydrosulfide) (#161527), Sigma-Aldrich, Poole, Dorset, UK</p>	

9.2 Appendix b. Supplementary material

List of Figures

Figure S3.1. Metabolic capacity of viable HUVECs cells in increasing doses of GYY4137 [0, 50, 100, 200, 400 μM].

Figure S4.1. Angiogenesis capacity of HUVECs in the presence of TNF- α and GYY4137 post-treatment setting by tube formation assay.

Figure S4.2. Senescence analysis of HUVECs in the presence of TNF- α and GYY4137 post-treatment setting by senescence-associated β -galactosidase (SA- β -Gal).

Figure S4.2. Actin cytoskeleton in HUVECs with and without GYY4137 (100 μM) using F-actin phalloidin staining.

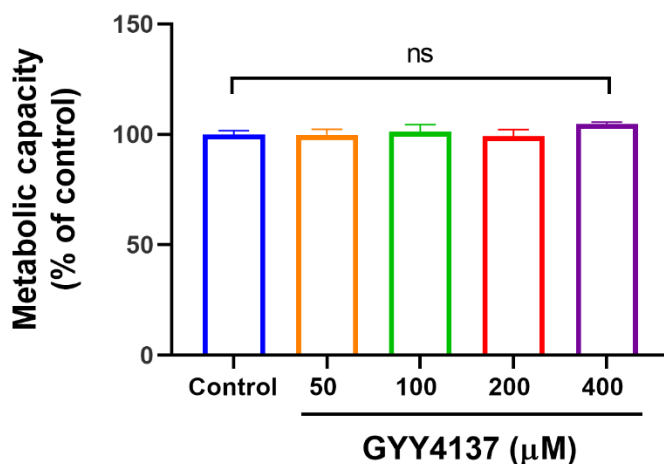


Figure S.3.1. Metabolic capacity of HUVECs in the presence of increasing GYY4137 doses. Cells were treated with increasing GYY4137 concentration [50 μM , 100 μM , 200 μM and 400 μM] in comparison to the control group [0 μM] for 24 hours. Data are represented as mean \pm SEM (n=3) and analysed by one-way ANOVA, followed by a Dunnett's multiple comparison test. ns. represents non-significant vs. control group. (n=3).

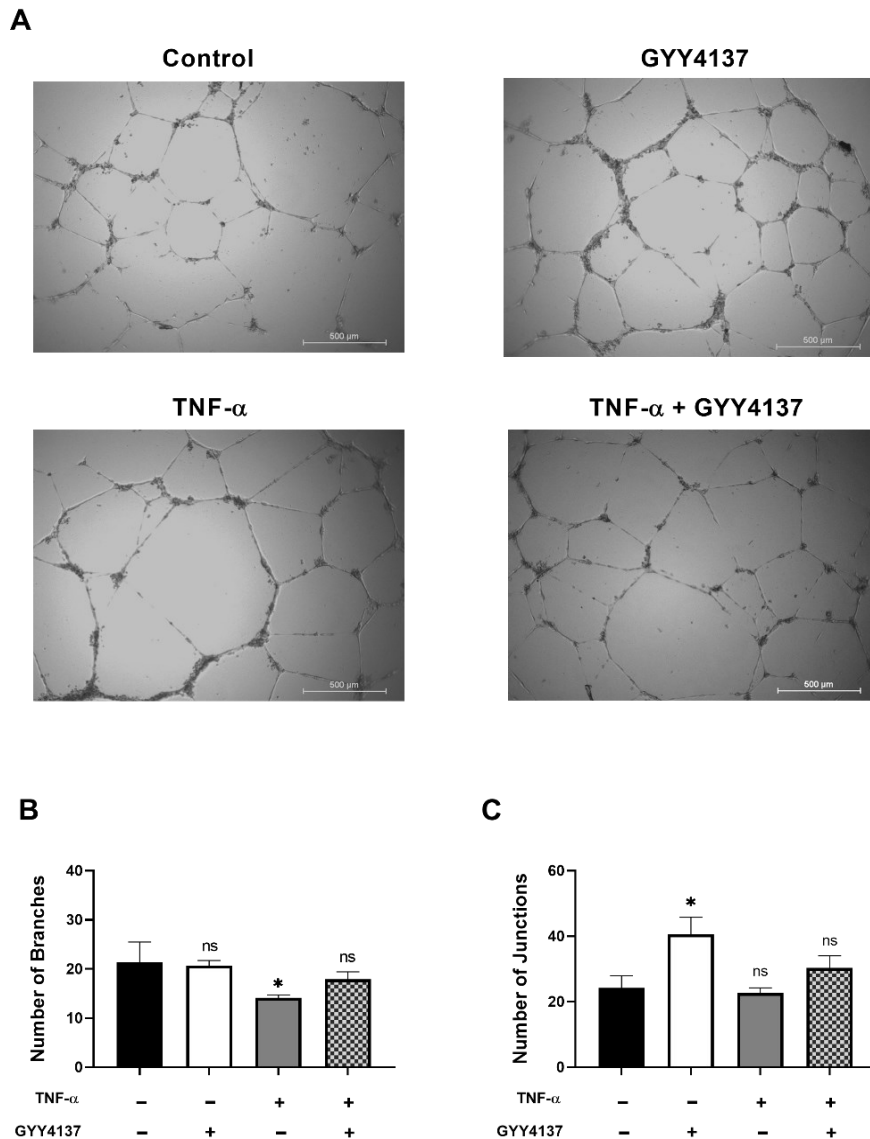


Figure S.4.1. Effects of TNF- α and GYY4137 in endothelial angiogenesis. HUVECs were treated with TNF- α (1ng/ml, 3h) followed by GYY4137 (100 μ M, 21 h). Matrigel HUVECs tube-forming assay was conducted to study the tubulogenesis function of untreated and treated ECs. **(A)** Representative images of vessel formation by ECs. A Nikon microscope captured images using 4x objective magnification (scale bar: 500 μ m). **(B)** The number of branches and **(C)** the number of junctions was analysed by ImageJ software. Results were shown as mean \pm SEM, (n=3). Significance was determined by a one-way ANOVA test followed by Sidak's post-test comparing treatments to control, whereby ns. and (*) represent non-significant, p<0.05, respectively vs. control. (n=3).

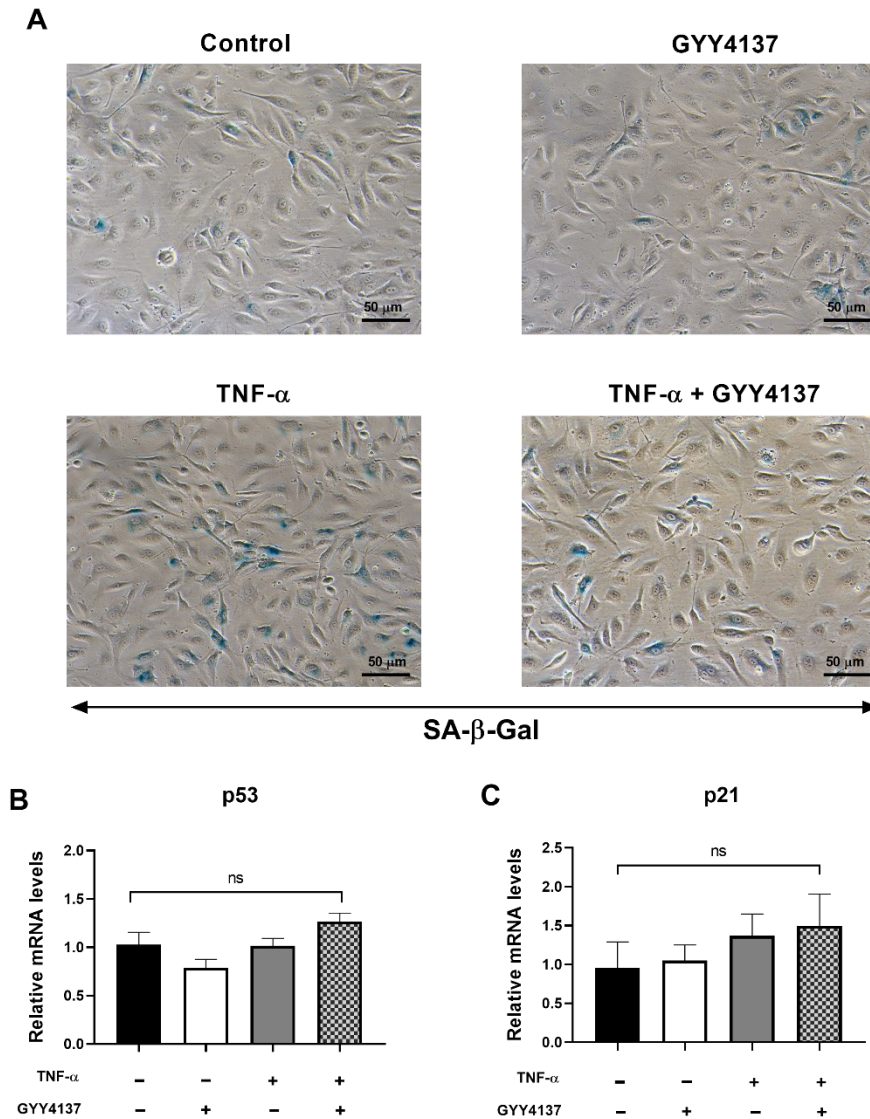


Figure S.4.2. Senescence-associated β -galactosidase (SA- β -Gal) in TNF- α and GYY4137 treated ECs.

HUVECs seeded in a 96-well plate were treated with TNF- α (1ng/ml, 3h), followed by GYY4137 (100 μ M, 21 h). Cells were incubated with stained with SA- β -Gal. **(A)** Representative immunohistochemical images showing SA- β -Gal (blue stain) in untreated and treated ECs (scale bar: 50 μ m). Relative p53 **(B)** and **(C)** p21 mRNA expressions were analysed by RT-qPCR and calculated using the $\Delta\Delta$ Ct value method. YWHAZ and EEF2 were used as housekeeper genes. Significance was determined by ANOVA test followed by Sidak's post-test comparing treatments to control (untreated cells), whereby ns. represents non-significant vs. to control. (n=3)

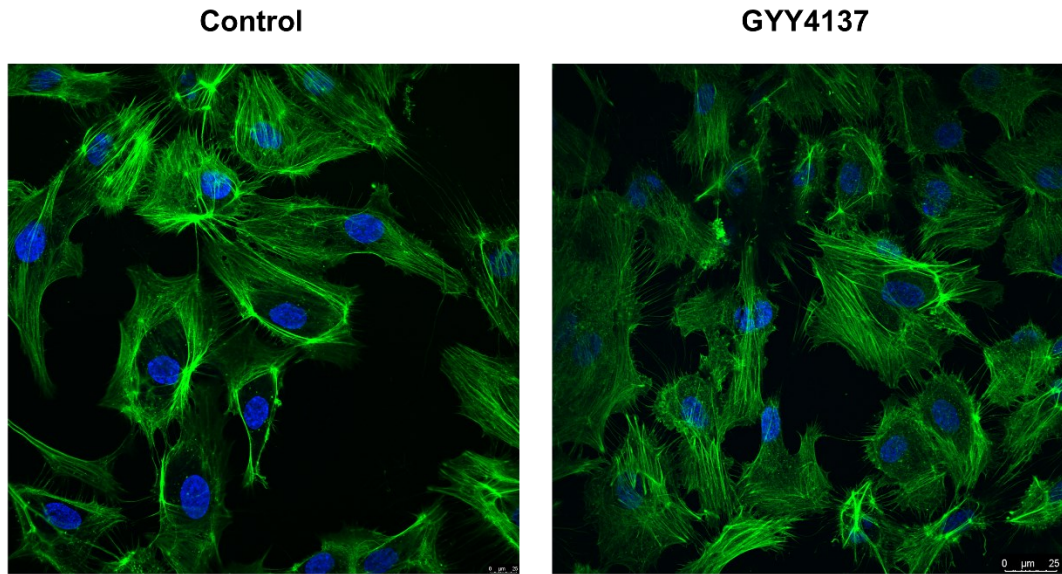


Figure S.6.1. Preliminary fluorescence analysis of the organisation of F-actin in HUVECs.

The effects of GYY4137 on the actin cytoskeleton. Cells were stimulated with or without 100 μM GYY4137 for 24 hours. After that, immunofluorescence analysis was performed using Alexa Fluor 687 Phalloidin (green spectrum) to stain F-actin and DAPI to stain the nucleus (blue spectrum) by confocal microscopy (scale bar: 25 μm) (n=1).

9.3 Appendix c. Uncropped western blot images

List of Figures

Uncropped images of all immunoblots reported in the current project are displayed below. Each blot is labelled, and targeted presented protein bands have been emphasized (orange square).

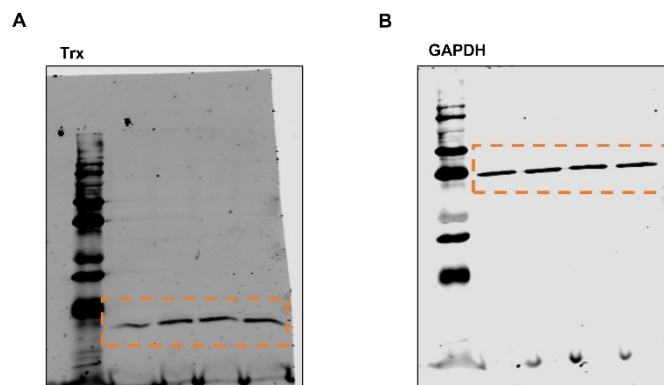


Figure i. Uncropped immunoblotting images corresponding to Trx (A) relative to GAPDH (B) are described in Figure 4.3 (see Chapter 4).

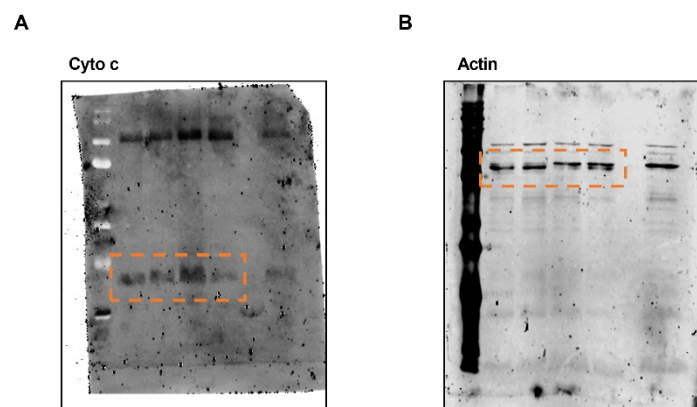


Figure ii. Uncropped immunoblotting images corresponding to cytosolic cyto c (A) relative to actin (B) are described in Figure 5.11 A (see Chapter 5).

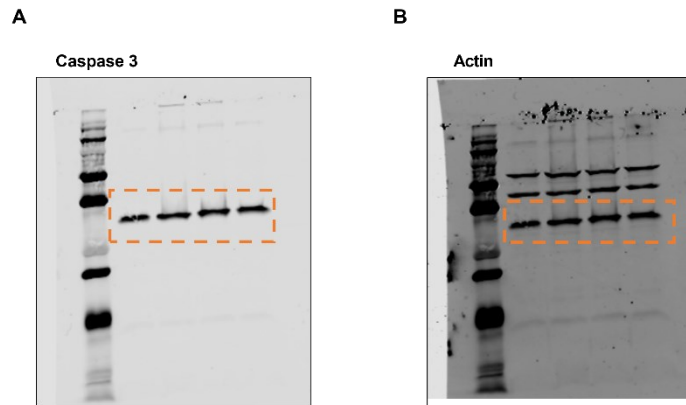


Figure iii. Uncropped immunoblotting images corresponding to caspase 3 (A) relative to actin (B) are described in Figure 5.11 A (see Chapter 5).

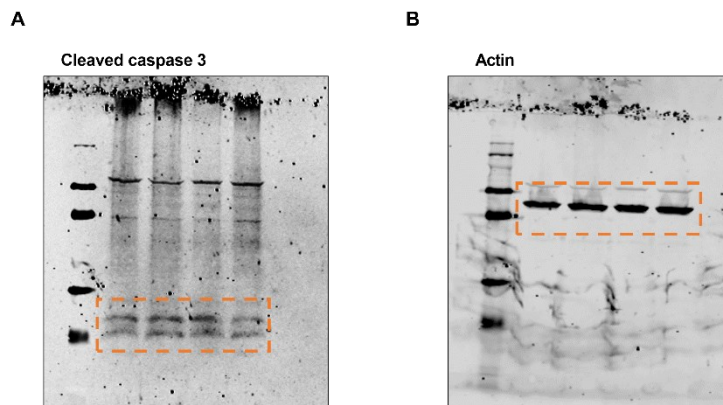


Figure iv. Uncropped immunoblotting images corresponding to cleaved caspase 3 (A) relative to actin (B) described in Figure 5.11 A (see Chapter 5).

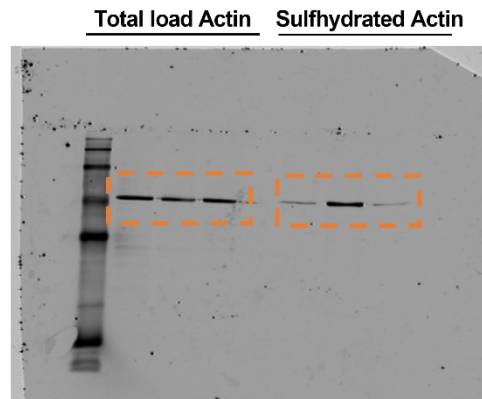


Figure v. Uncropped immunoblotting images corresponding to sulfhydrated actin relative to total load actin described in Figure 6.3 (see Chapter 6).

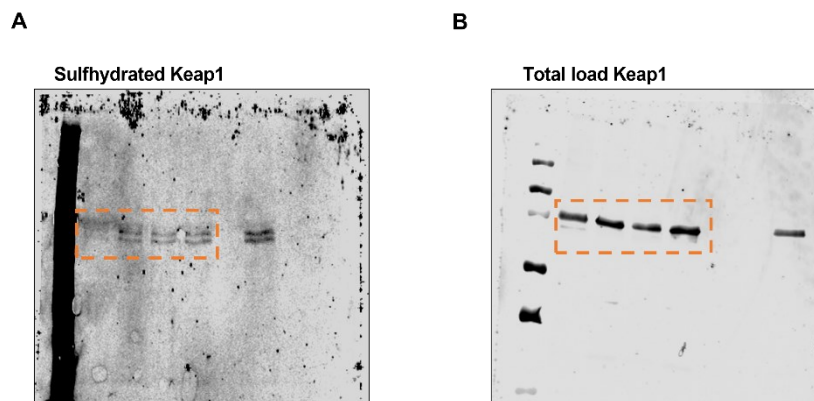


Figure vi. Uncropped immunoblotting images corresponding to sulfhydrated Keap1 (A) relative to total load Keap1 (B) are described in Figure 6.5 (see Chapter 6).

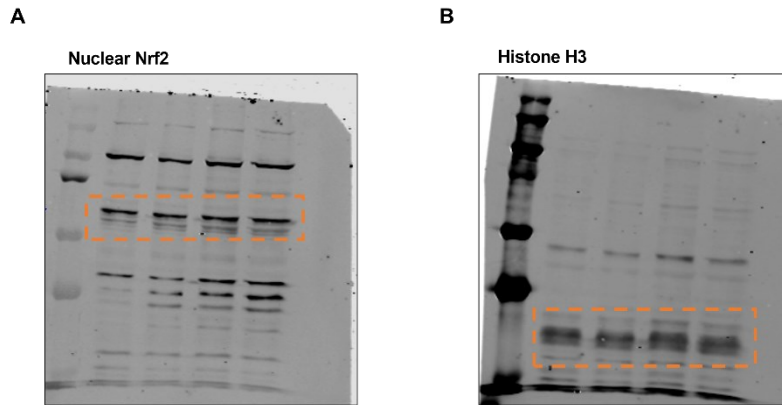


Figure vii. Uncropped immunoblotting images corresponding to nuclear Nrf2 (A) relative to Histone H3 (B) are described in Figure 6.7 (see Chapter 6).

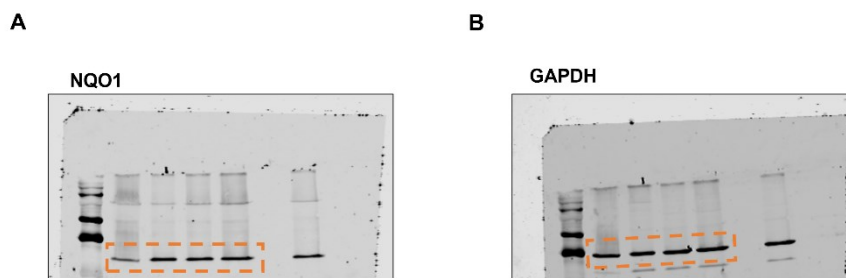


Figure viii. Uncropped immunoblotting images corresponding to NQO1 (A) relative to GAPDH (B) are described in Figure 6.8 (see Chapter 6).

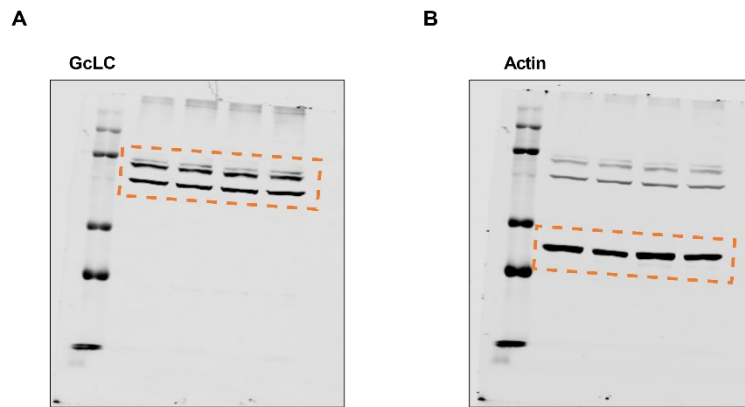


Figure ix. Uncropped immunoblotting images corresponding to GcLC (A) relative to actin (B) are described in Figure 6.8 (see Chapter 6).

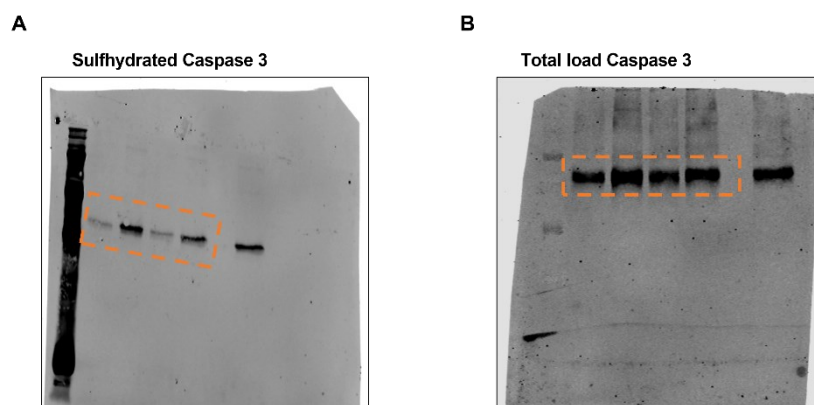


Figure x. Uncropped immunoblotting images corresponding to sulphydrated caspase 3 (A) relative to total load caspase 3 (B) are described in Figure 6.9 (see Chapter 6).

10 Publications

10.1 Published study 1

Advances in Redox Research 4 (2022) 100030



Contents lists available at ScienceDirect

Advances in Redox Research

journal homepage: www.elsevier.com/locate/arres



Review Paper

Exploring mitochondrial hydrogen sulfide signalling for therapeutic interventions in vascular diseases

Lorena Diaz Sanchez^a, Lissette Sanchez-Aranguren^a, Mandeep Marwah^a, Keqing Wang^a, Corinne M Spickett^b, Helen R Griffiths^c, Irundika HK Dias^{a,*}

^a Aston Medical School, College of Health and Life Sciences, Aston University, UK

^b School of Biosciences, College of Health and Life Sciences, Aston University, UK

^c Swansea University Medical School, Swansea University, Swansea, UK



ARTICLE INFO

Keywords:

Hydrogen Sulfide
Mitochondria
Endothelial cells
Sulphydration
Vascular disease
Signalling

ABSTRACT

Hydrogen sulfide (H₂S), a gaseous signalling molecule, is important in numerous physiological and pathophysiological processes. Despite its initial identification as an environmental toxin, H₂S is now well described as an essential physiological molecule that is finely balanced to maintain cellular functions, especially in modulating mitochondrial activity. Mitochondria are responsible for the oxidation of H₂S and its safe elimination while maintaining mitochondrial biogenesis. H₂S oxidation in mitochondria generates various reactive sulfur species that could post-translationally modify proteins by sulphydration. Sulphydrated proteins participate in many regulatory activities either by direct interactions in the electron transport chain or indirect regulation by epigenetics. These investigations explain the importance of research of H₂S as a therapeutic molecule beyond the traditional understanding as a protective role through its anti-inflammatory and antioxidant properties. This review focuses on highlighting the significant involvement of the H₂S pathway in vascular diseases and current H₂S donors for therapeutic use under development.

1. Introduction

The endothelium is formed by a monolayer of endothelial cells located in the inner layer of the vascular wall and continuously exposed to hemodynamic shearing forces, circulating molecules in the blood and mediators released from underlying smooth muscle cells. Disturbances

to the physiological status of the endothelium lead to activated endothelial cells that culminate in vascular dysfunction [1]. Dysfunctional endothelium contributes to a pro-inflammatory and pro-thrombotic phenotype, which causes disturbances to endothelial homeostasis and impair vasodilation-vasocontraction [1,2]. Consequently, endothelial dysfunction has been described as a hallmark for developing several patho-

Abbreviations: AR, androgen receptor; AMPK, 5'-adenosine monophosphate-activated protein kinase; Akt, protein kinase B; ATP5A1, α -subunit of ATP synthase; ATP, adenosine triphosphate; b.End3 cells, brain-derived microvascular endothelial cells; Bax, apoptosis regulator BAX; Bcl-2, B-cell lymphoma 2; Ca²⁺, calcium; CDKN2A, cyclin-dependent kinase inhibitor 2A; CAT, catalase; CSE KO, cystathionine γ -lyase knockout; COX, cyclooxygenase; Cys, cysteine residues; DADS, diallyl disulfide; DATS, diallyl trisulfide; DNA, deoxyribonucleic acid; DJ-1, known as Parkinson disease protein 7 (PARK7); Drp1, dynamin related protein 1; eNOS, endothelial nitric oxide synthase; EA.hy926 cells, human umbilical vein cell line; Fis1, mitochondrial fission 1 protein; GAPDH, glyceraldehyde 3-phosphate dehydrogenase; GATA3, GATA binding protein 3; GSH, glutathione; GYY4137, mor-pholin-4-ium 4-methoxyphenyl-morpholino-phosphinodithioate; HEK293 cells, human embryonic kidney 293 cells; HUVECs, human umbilical vein endothelial cells; HO-1, heme oxygenase-1; ILs, interleukins; IFN γ , interferon gamma; IRF-1, interferon regulatory factor-1; Keap1, Kelch-like ECH-associated protein 1; KATP, ATP, sensitive potassium channel; KLF5, krüppel-like factor 5; LDH, lactate dehydrogenase; MAPK, mitogen-activated protein kinase; Mn-SOD, manganese-dependent superoxide dismutase; MEK1, map kinase-1; MitoROS, mitochondrial reactive oxygen species; mPTP, mitochondrial permeability transition pore; Na₂S, sodium sulfide; NaHS, sodium hydrosulfide; Nrf1, nuclear respiratory factor 1; Nrf2, nuclear factor erythroid 2-related factor 2; NMDAR1 subunit, N-methyl-D-aspartate receptor; NOX4, NADPH oxidase 4; NF-KB, nuclear factor-kappa beta cells; NR, not reported; ox-LDL, oxidised low-density lipoprotein; PARP, Poly (ADP-ribose) polymerase; PPAR γ , peroxisome proliferator-activated receptor- γ ; PI3K, phosphoinositide 3-kinase; PINK1, PTEN-induced kinase 1; PGC, peroxisome proliferator-activated receptor- γ coactivator; PP1c, protein phosphatase-1; PC, pyruvate carboxylase; PTEN, phosphatase and tensin homolog deleted on chromosome ten; PTP1B, protein tyrosine phosphatase 1B; PP2A, protein phosphatase 2A; PPRC, peroxisome proliferator-activated receptor- γ coactivator-related protein; RAGE, receptor for advanced glycation end-products; Runx2, runt-related transcription factor 2; Sp-1, specificity protein 1; VEGFR, receptor of vascular endothelial growth factor; TRPV6, transient receptor potential cation channel subfamily V member 6; BMMS, bone marrow mesenchymal; SIRT1, sirtuin 1; SIRT3, sirtuin 3; USP8, ubiquitin specific peptidase 8 USP8.

* Corresponding author.

E-mail address: diashki1@aston.ac.uk (I.H. Dias).

10.2 Published study 2

Received: 23 April 2020 | Revised: 1 July 2020 | Accepted: 20 July 2020
DOI: 10.1111/bph.15227

REVIEW ARTICLE THEMED ISSUE



Cholesterol and oxysterol sulfates: Pathophysiological roles and analytical challenges

Lorena Diaz Sanchez¹ | Lorenzo Pontini² | Maura Marinuzzi² |
Lissette Carolina Sanchez-Aranguren¹ | Ana Reis³ | Irundika H.K. Dias¹

¹Aston Medical School, Aston University, Birmingham, UK

²Department of Pharmaceutical Sciences, University of Perugia, Perugia, Italy

³LAQV/REQUIMTE, Departamento de Química e Bioquímica, Faculdade de Ciências, Universidade do Porto, Porto, Portugal

Correspondence

Ana Reis, LAQV/REQUIMTE, Departamento de Química e Bioquímica, Faculdade de Ciências, Universidade do Porto, Rua do Campo Alegre 687, 4169-007, Porto, Portugal.
Email: anereis@fc.up.pt

Irundika H. K. Dias, Aston Medical School, Aston University, Birmingham, B4 7ET, UK.
Email: h.k.dias1@aston.ac.uk

Funding information

FCT/MCTES, Grant/Award Number: UIDB/50006/2020; Royal Society, Grant/Award Number: RGS/R1\201135

Cholesterol and oxysterol sulfates are important regulators of lipid metabolism, inflammation, cell apoptosis, and cell survival. Among the sulfate-based lipids, cholesterol sulfate (CS) is the most studied lipid both quantitatively and functionally. Despite the importance, very few studies have analysed and linked the actions of oxysterol sulfates to their physiological and pathophysiological roles. Overexpression of sulfotransferases confirmed the formation of a range of oxysterol sulfates and their antagonistic effects on liver X receptors (LXRs) prompting further investigations how are the changes to oxysterol/oxysterol sulfate homeostasis can contribute to LXR activity in the physiological milieu. Here, we aim to bring together for novel roles of oxysterol sulfates, the available techniques and the challenges associated with their analysis. Understanding the oxysterol/oxysterol sulfate levels and their pathophysiological mechanisms could lead to new therapeutic targets for metabolic diseases.

KEYWORDS

cholesterol sulfate, mass spectrometry, oxysterols, oxysterol sulfate

Abbreviations: 24HC, 24(S)-hydroxycholesterol; 24HC3S, 24(S)-hydroxycholesterol-3-sulfate; 24HCDS, 24(S)-hydroxycholesterol-3,24-disulfate; 25HC, 25-hydroxycholesterol; 25HC3S, 25-hydroxycholesterol-3-sulfate; 25HCDS, 25-hydroxycholesterol-3,25-disulfate; 26HC, (25R)-26-hydroxycholesterol; 26HC26S, (25R)-26-hydroxycholesterol-26-sulfate; 26HC3S, (25R)-26-hydroxycholesterol-3-sulfate; 27HC, 27-hydroxycholesterol; 5,6aECS, 5,6a-epoxycholesterol-3-sulfate; 5-LO, 5-lipoxygenase; 7KC, 7-ketocholesterol; 7KCS, 7-ketocholesterol-3-sulfate; ACN, acetonitrile; CS, cholesterol sulfate; DHEA, dehydroepiandrosterone; DHEAS, dehydroepiandrosterone sulfate; DOCK2, dock2 of cytokinesis protein 2; HMG-CoA reductase, 3-hydroxy 3-methylglutaryl-CoA reductase; LLE, liquid-liquid extraction; LXRI, liver X receptor α ; LXRII, liver X receptor β ; Minde, macrophage inducible Ca^{2+} -dependent lectin receptor; MRM, multiple reaction monitoring; PAPS, 3'-phosphoadenosine 5'-phosphosulfate; PIP₂, phosphatidylinositol diphosphate; PIP₃, phosphatidylinositol (3,4,5)-trisphosphate; PregS, pregnenolone sulfate; RLXI, recessive X-linked ichthyosis; RO α , retinoid acid-related orphan receptor α ; SL, sulfate-based lipids; SPE, solid phase extraction; SREBP-1, sterol regulatory element-binding protein-1; STS, sterol sulfatase; SULTs, sulfotransferases; TCR, T-cell receptor.

1 | INTRODUCTION

Sulfate-based lipids (SL) represent a wide range of lipid classes, from low to high molecular weight compounds (Dias et al., 2019) with key functions in many aspects of human health and disease (Hu et al., 2007; Merten, 2001; Suzuki et al., 2003). The biotransformation of lipids by sulfation and desulfation reactions is fundamental to many cellular pathways. SL represent a diverse class of lipids including sulfate-, sulfonate-, and thiol- or thioether-based lipids (Dias, Ferreira, et al., 2019). In humans, steroid sulfates represent a highly abundant and extensively studied lipid class among the other glycerol-, sphingosine-, or taurine-derived lipids (Mueller, Gilligan, Idkowiak, Arit, & Foster, 2015). Steroid sulfates were traditionally viewed as inactive precursors as they require active transport into cells via organic anion transporters. However, recent research suggests that

10.3 Published study 3

> [J Alzheimers Dis. 2020;74\(1\):113-126. doi: 10.3233/JAD-190923.](#)

Partial Mitigation of Oxidized Phospholipid-Mediated Mitochondrial Dysfunction in Neuronal Cells by Oxocarotenoids

Opeyemi S Ademowo¹, Irundika H K Dias¹, Lorena Diaz-Sanchez¹, Lissette Sanchez-Aranguren¹, Wilhelm Stahl², Helen R Griffiths^{1,3}

Affiliations + expand

PMID: 31985464 DOI: [10.3233/JAD-190923](#)

Abstract

Mitochondria are important (patho)physiological sources of reactive oxygen species (ROS) that mediate mitochondrial dysfunction and phospholipid oxidation; an increase in mitochondrial content of oxidized phospholipid (OxPL) associates with cell death. Previously we showed that the circulating OxPL 1-palmitoyl-2-(5'-oxo-valeroyl)-sn-glycero-3-phosphocholine (POVPC) increases in patients with Alzheimer's disease (AD), and associates with lower plasma antioxidant oxocarotenoids, zeaxanthin, and lutein. Since oxocarotenoids are metabolized in mitochondria, we propose that during AD, lower concentrations of mitochondrial zeaxanthin and lutein may result in greater phospholipid oxidation and predispose to neurodegeneration. Here, we have investigated whether non-toxic POVPC concentrations impair mitochondrial metabolism in differentiated (d)SH-SY5Y neuronal cells and whether there is any protective role for oxocarotenoids against mitochondrial dysfunction. After 24 hours, glutathione (GSH) concentration was lower in neuronal cells exposed to POVPC (1-20 μ M) compared with vehicle control without loss of viability compared to control. However, mitochondrial ROS production (determined by MitoSOX oxidation) was increased by 50% only after 20 μ M POVPC. Following delivery of lutein (0.1-1 μ M) and zeaxanthin (0.5-5 μ M) over 24 hours in vitro, oxocarotenoid recovery from dSH-SY5Y cells was > 50%. Co-incubation with oxocarotenoids prevented loss of GSH after 1 μ M but not 20 μ M POVPC, whereas the increase in ROS production induced by 20 μ M POVPC was prevented by lutein and zeaxanthin. Mitochondrial uncoupling increases and ATP production is inhibited by 20 μ M but not 1 μ M POVPC; carotenoids protected against uncoupling although did not restore ATP production. In summary, 20 μ M POVPC induced loss of GSH and a mitochondrial bioenergetic deficit in neuronal cells that was not mitigated by oxocarotenoids.